A cost-benefit analysis of the inclusion of polyimide in fabric filter bags

JH Fourie

orcid.org/0000-0003-1882-7543

Dissertation submitted in fulfilment of the requirements for the degree *Master of Engineering in Chemical Engineering* at the North-West University

Supervisor:	Dr DJ Branken
Co-supervisor:	Prof HWJP Neomagus
Co-supervisor:	Prof CJ Greyling

Graduation ceremony: May 2019

Student number: 28368185

DECLARATION

I, Jeanne H Fourie, hereby declare that this dissertation, submitted in fulfilment of the requirements for the degree Master of Engineering in Chemical Engineering to the North-West University, is my own work, except where acknowledged in the text. It has not been submitted to any other tertiary institution as a whole or in part.

Jeanne H Fourie (Pr. Eng)

Date: 5 March 2019

ACKNOWLEDGEMENTS

I would like to thank and acknowledge the contributions of the following individuals, all of whom have assisted in various aspects of this study.

North-West University: I am sincerely grateful for the constant guidance and encouragement provided by my supervisor, Dr Dawie Branken and co-supervisor, Prof Hein Neomagus. I appreciate all the effort made with guiding my scientific thinking, explaining chemical concepts and reviewing long dissertation drafts. I would also like to acknowledge the assistance of Dr Johan Jordaan with the TGA analysis of yarn.

Cocos Solutions Technology: I am also infinitely thankful for the guidance and encouragement provided by my co-supervisor, Prof Corinne Greyling. I am grateful for the many discussions on polymer behaviour, sharing a wealth of filtration fabric knowledge and lugging a large suitcase full of industrial reports across the country.

Eskom: I would like to express my gratitude to Mr Leon van Wyk and Mr Ebrahim Patel for industrial guidance and assistance with obtaining information. I am also grateful to Mr Irish Piri, Mr Helgardt Müller and Mr Lihle Siphungu from Eskom Research, Testing and Development for assistance with obtaining unused filter bags for samples and allowing me to use the Eskom textile lab for sample analysis.

Evonik Fibres: I would like to thank Mr Florin Popovici, Mr Franz Pesendorfer and Mr Günter Gasparin. I am grateful to Mr Popovici for introducing me to the intriguing field of the electrostatic properties of filtration fabrics, extensive discussion on the topic and for supplying polyimide yarn samples. I would also like to express my thanks to Mr Pesendorfer and Mr Gasparin for hosting me at the Evonik Fibres plant, assisting with conducting triboelectric experiments and sharing their extensive knowledge of polymeric fibre behaviour.

I would like to acknowledge the assistance of Mr Posh Moodley (**Beier Envirotec)** and Ms Yolandi Serfontein (**BWF Envirotec)** in providing needle felt and yarn samples, respectively.

This study was funded by the **Eskom Power Plant Engineering Institute**.

Finally, I would like to express my special thanks to my dearest Malcolm for his unwavering support and hours spent cutting needle felt tensile samples.

ABSTRACT

Electric energy is central to modern society. Although there is a global shift towards renewable energy sources, coal-fired power production remains a widespread electricity generation method. Coal-fired power production, however, results in particulate matter (PM) emissions. These PM emissions hold significant implications for the environment and human health. Consequently, effective reduction of PM emissions from coal-fired power plants is of great importance, especially in developing countries that rely heavily on coal as primary energy source.

Baghouses are a popular choice for abatement of PM emissions from coal-fired electricity generation. Baghouses capture PM in the flue gas exhausted from the electricity producing boiler system by means of numerous cylindrical bags constructed of specialised filtration fabric. This fabric, made from polymeric fibres, is integral to baghouse efficiency and cost.

South African coal-fired power station baghouses typically use either polyacrylonitrile (PAN) or polyphenylene sulphide (PPS) based filtration fabrics, depending on the operating temperature of the baghouse. Both filtration fabrics types have the option of including polyimide (PI) in a blended surface layer of the fabrics. The inclusion of polyimide, however, increases the cost of the bags.

In this study, the inclusion of PI in PAN- and PPS-based filtration fabrics has been comparatively evaluated. The evaluation was based on the triboelectric properties of the fabrics as well as fabric resistance to acid attack by sulphuric and nitric acids. The latter was assessed through tensile strength analysis of the fabrics following acid exposure. The triboelectric properties of filtration fabrics hold implications for the filtration efficiency and pressure drop experienced in a baghouse. The chemical resistance of the filtration fabrics impacts the durability of the fabrics during operation and greatly influences the bag life. In order to comparatively evaluate the costs associated with bag choices, a cost-benefit analysis (CBA) method is proposed which considers all life cycle costs associated with filtration fabric selection. The triboelectric and chemical resistance results were incorporated in the proposed CBA model.

The experimental findings indicated that fabrics with PI incorporation developed a positive surface charge polarity after triboelectric contact. PAN- and PPS-based fabrics, however, were found to develop a negative polarity after triboelectric contact. Subsequently, a correlation between ash interaction with charged filtration fabric and

fabric polarity was found. It was discovered that ash particles penetrate more deeply into fabric volumes with an increasingly negative surface charge. A filtration and pressure drop benefit may therefore be achieved through the incorporation of PI in PAN and PPS surface layers.

From the acid exposure investigations, it was found that combined sulphuric and nitric acid has severely degradative effects on all fabrics considered. The inclusion of PI in PAN-based fabrics was found to be beneficial when nitric acid exposure was experienced and where combined nitric and sulphuric acid exposure was experienced. When PI was incorporated in PAN, however, the fabric was found to be highly susceptible to degradation after exposure to sulphuric acid. PPS-based fabrics were not significantly affected by sulphuric acid, but were severely degraded by nitric acid. Thermogravimetric analysis revealed a fundamental change in polymer degradation behaviour after nitric acid exposure. PI incorporation in PPS based fabrics was found to offer an advantage in sulphuric acid conditions, but was not beneficial when nitric or combined nitric and sulphuric acid exposure was experienced.

To evaluate the cost-implications of the experimental findings, a CBA method is proposed which considers initial bag capital cost as well as costs associated with induced draught (ID) fan power and production losses due to early bag failure. Assumptions were made based on the technical investigations conducted as part of this study, however are not reflective of actual baghouse operation; the results are therefore only exploratory in nature. High-level application of the CBA to PAN-based fabrics revealed that incorporation of PI could offer a cost-benefit in operating scenarios where nitric acid or simultaneous nitric and sulphuric acid exposure are expected. Application of the CBA to PPS-based fabrics revealed that PI incorporation could offer a cost advantage in environments where sulphuric acid exposure is experienced. Finally, except in extreme cases of chemical degradation, it was found that PI incorporation in PAN- or PPS-based fabrics offers a cost advantage if a filtration benefit due to triboelectric interactions with the ash facilitates a reduction in pressure drop.

Keywords:

Baghouse, FFP, polyacrylonitrile (PAN), polyphenylene sulphide (PPS), polyimide (PI), triboelectric properties of filtration fabric, chemical resistance of filtration fabric, cost-benefit analysis

TABLE OF CONTENTS

LIST OF FIGURES

LIST OF TABLES

ABBREVIATIONS

°C	degrees Celsius
Al	aluminium
Al_2O_3	aluminium oxide
Al_2O_3	aluminum oxide
B.C.	before Christ
Ba	barium
Ca	calcium
CBA	cost-benefit analysis
cm	centimetre
Cr	chromium
CRS	confocal Raman spectroscopy
CTA	cellulose triacetate
DSC	differential scanning calorimetry
dtex	decitex
ECTFE	ethylene chlorotrifluoroethylene
ESP	electrostatic precipitator
Fe	iron
Fe_2O_3	ferric oxide
FFP	fabric filter plant
FTIR	Fourier-transform infrared spectroscopy
g	gram
h	hour
H_2O	water
HCl	hydrochloric acid
HOMO	highest occupied molecular orbital
ID	induced draught
Int$	international dollar
K	potassium
kg	kilogram
kPa	kilopascal
KPFM	Kelvin probe force micrograph
kt	kilotonne
LCC	life cycle costing
LUMO	lowest occupied molecular orbital
m	metre
M	molar
m^2	square metre
Mg	magnesium
mg	milligram
min	minute
mm	millimetre
Mn	manganese
Mt	Megatonne
MW	megawatt
Na	sodium
Na_2O	sodium oxide
NEMAQA	National Environmental Management: Air Quality Act
Nm	metric number
Nm^3	normalised cubic metre
NO	nitric oxide
NO_2	nitrogen dioxide
NO_x	nitrogen oxides
NPV	net present value
O_2	oxygen
O_3	ozone
P	phosphorous
P.A.	per annum
PA	polyamide
PAI	polyamide-imide

PAN	polyacrylonitrile
PBT	polybutylene terephthalate
PDMS	polydimethylsiloxane
PE	polyethylene
PET	polyethylene terephthalate
PI	polyimide
PJFF	pulse jet fabric filter
PM	particulate matter
PMMA	poly methyl methacrylate
PP	polypropylene
PPS	polyphenylene sulphide
PS	polystyrene
PTFE	polytetrafluoroethylene
PU	polyurethane
PVA	polyvinyl alcohol
PVC	polyvinyl chloride
PVDC	polyvinylidene chloride
R	rand
rpm	revolutions per minute
s	second
S	sulphur
Si	silicone
SiO_2	silicone dioxide
SO_2	sulphur dioxide
SO_3	sulphur trioxide
SO_x	sulphur oxides
Sr	strontium
T/m	yarn twist
TGA	thermogravimetric analysis
Ti	titanium
TiO_2	titanium dioxide
TOE	ton of oil equivalent
UTS	ultimate tensile strength
V	vanadium
wt	weight
XPS	x-ray photoelectron spectroscopy
XRF	x-ray fluorescence
Zn	zinc
Zr	zirconium
µm	micrometre
µV	microvolt

SYMBOLS

%	percentage	L_{ID}	ID fan operational power consumption (MW)
C_B	bag capital investment (R)	L_R	capacity reduction due to continued operation (MW)
C_{BA}	annual bag cost (R/year)		
C_C	capacity loss cost (R)		
C_f	final charge (kV)	L_T	total unit capacity (MW)
C_i	initial charge (kV)	n	study period (years)
c_i	inlet dust concentration (kg/m^3)	n_a	actual bag life (years)
		n_b	bag life (years)
C_{ID}	ID fan power cost (R)	n_e	early bag failure time (years)
C_t	cost at defined time (R)		
d	discount rate (%)	P	electricity price (R/MWh)
D_{BR}	duration of bag replacement outage (h)	PD	change in pressure drop (%)
dC	discharge rate (%)	S	drag (kPa.s/m)
D_O	duration of operation with reduced capacity (h)	S_e	specific resistance of filter bag (kPa.s/m)
F_{CR}	capital recovery factor	S_R	strength retained after acid exposure (%)
H	operational hours in a year (h)	t	time (s)
		TAC	total annual cost (R)
i	interest rate (%)	v	filtration velocity (m/s)
K	specific resistance of ash cake (s^{-1})	W_0	aerial density of freshly deposited ash (kg/m^2)
K_0	specific resistance of freshly deposited ash (s^{-1})	W_c	aerial density of redeposited ash (kg/m^2)
K_c	specific resistance of recycling ash (s^{-1})	ΔP	pressure drop (kPa)

CHAPTER 1: INTRODUCTION

1.1 BACKGROUND

1.1.1 GLOBAL ENERGY USE AND ELECTRICITY DEMAND

Energy is central to modern society. Whether it is the life-sustaining energy from food sources or the electric and transportation fuel at the core of global industry and daily life, modern society devours energy at a steadily increasing rate. Global domestic and industrial energy requirements have increased radically during the past two and a half centuries. The Industrial Revolution sparked the development and exploitation of various previously unrecognised forms of energy and triggered the socio-economic development that lead to the dependence of modern society on electricity (Barca, 2011).

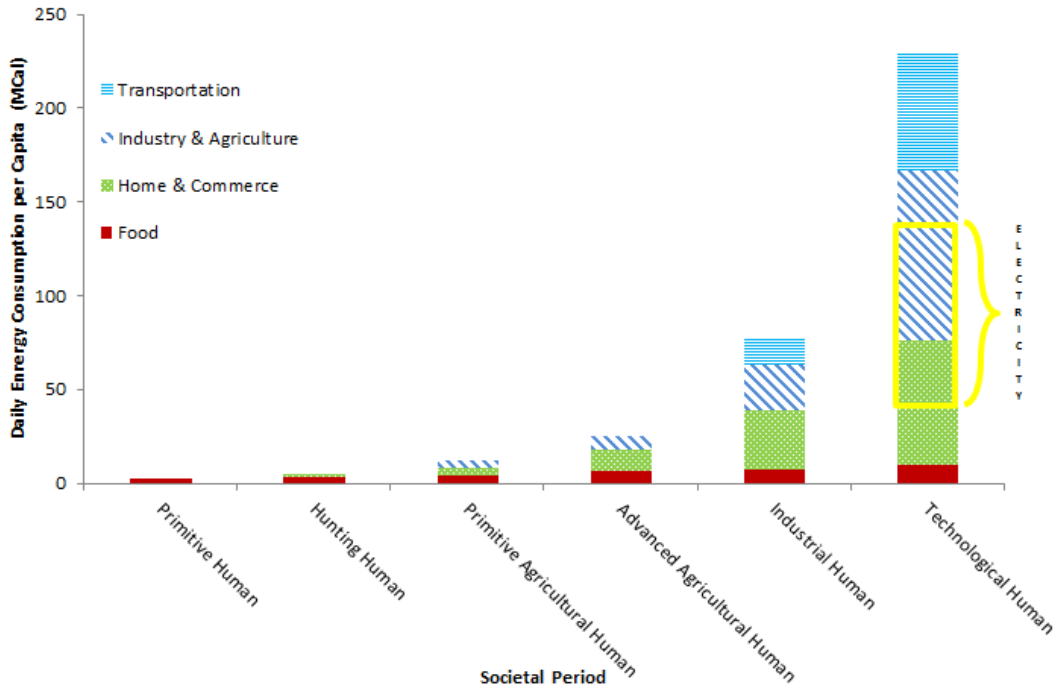

Figure 1-1: Historical Global Daily Energy Consumption per Capita (Cook, 1971)

The increased energy availability resulting from the Industrial Revolution during the late 1700s to early 1900s fed energy demand, causing an exponential increase in energy consumption per capita for technological human[1] (Cook, 1971). This is illustrated in Figure 1-1, which highlights the large portion of daily energy consumption which is electrical.

[1] *Technological human* refers to society alive during the period from 1950 to today (Cook, 1971).

A major driver of electricity demand is the rapidly expanding global population. Population growth and continuing global industrialisation share a symbiotic relationship: population growth contributes to technological progress by providing the requisite labour force, while technological progress stimulates population growth through improved living standards and medical advances (Markandya & Wilkinson, 2007). Therefore, despite a downward trend in international energy intensity[2], due mainly to improvements in industrial efficiency (Ruhl, et al., 2012), electricity demand for sustaining the growing global population is likely to remain significant.

1.1.2 COAL FOR ELECTRICITY PRODUCTION: THE SOUTH AFRICAN CONTEXT

Various primary energy sources for electricity production have been explored. Coal is a major source of primary energy that has been successfully exploited since the Industrial Revolution (Clark & Jacks, 2007) and remains the most prevalent source of primary energy for global electrical power generation (Burnard, et al., 2014). Coal is predicted to continue to play a prominent role on the future global energy stage (Ruhl, et al., 2012), as illustrated in Figure 1-2 below.

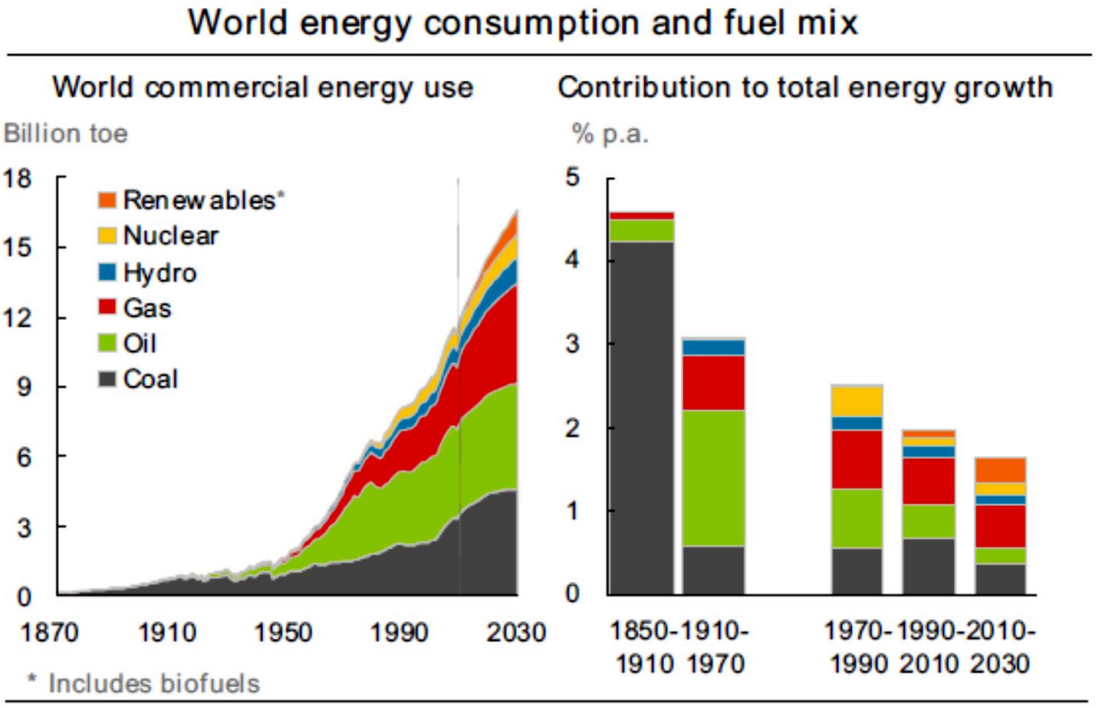

Figure 1-2: World Energy Consumption and Fuel Mix (Ruhl, et al., 2012)

[2] Here, *energy intensity* refers to the energy consumed per unit of gross domestic product (Ruhl, et al., 2012).

The electricity generation landscape of South Africa is dominated by coal. The chief South African power producer, Eskom[3], relies heavily on coal deposits abundant in the nation for electricity generation. Coal fuelled power generation accounted for 82.6% of Eskom's total generating capacity of 44 134MW in 2017 (Figure 1-3) (Eskom Holdings SOC Ltd, 2017).

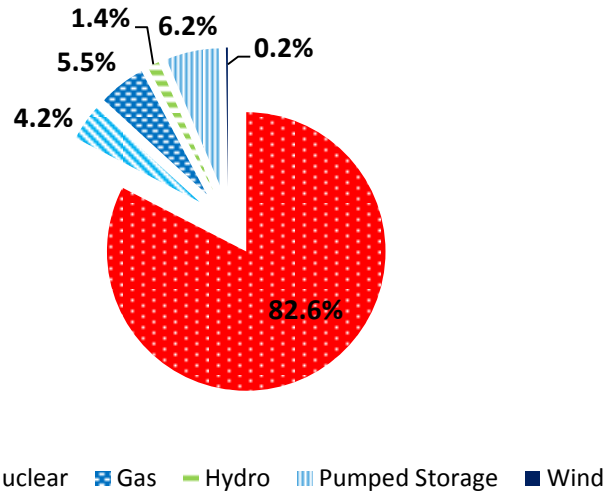

Figure 1-3: Eskom's Power Generation Mix (Eskom Holdings SOC Ltd, 2017)

With Eskom currently constructing two new large coal-fired power stations, it is not expected that South Africa's reliance on coal for electricity generation will change in the coming decades, despite international pressure to take steps towards 'clean'[4] energy production.

South Africa, a developing nation ranked among the world's fifteen most energy intensive economies (Holgate, 2007), is in a position where the relative abundance and affordability of its coal reserves preserves coal as an attractive primary energy source. This is true for liquid fuel production, via coal-to-petroleum-liquefaction, as well as electrical power generation (Jeffrey, 2005). The social cost of power generation from coal, however, includes various human health and environmental impacts.

The coal-fired power production process produces various harmful by-products, including pollutant gases and particulate emissions, often referred to smoke, ash or

[3] Eskom Holdings SOC Ltd (referred to as *Eskom*) is a state-owned South African power utility, producing approximately 90% of South Africa's electricity, as well as supplying electricity to neighbouring countries in the Southern African Development Community. Eskom generates approximately 40% of the total electricity consumed by Africa as a whole (Eskom Holdings SOC Ltd, 2017).

[4] *Clean energy* typically refers to renewable electricity generation, where the process of energy production itself produces little or no emissions. In some instances, biomass, nuclear and waste energy are included. This term does not refer to low-emissions fossil fuel energy (Sklar, 2012).

dust. Eskom burnt 113.74 Mt of coal during the 2016/2017 financial year, producing 32.6 Mt of ash, of which 65.1 kt was exhausted to the atmosphere as particulate emissions (Eskom Holdings SOC Ltd, 2017).

1.1.3 HEALTH AND ENVIRONMENTAL IMPACTS OF PARTICULATE EMISSIONS

The effects of particulate and gaseous emissions from coal-fired electricity generation on the environment and human health have been extensively studied. The release of particulate matter (PM)[5] has been found to be a major cause for concern. Adverse effects are aggravated by the tendency of PM to disperse at atmospheric levels (World Health Organization, 2013). PM emissions therefore have the potential to affect ambient air quality not only in areas surrounding the source of the emissions, but on a regional level (Ebi & McGregor, 2008).

PM can impact the environment through water and soil contamination and impaired visibility due to haze. PM emissions also pose an aesthetic threat due to the potential for damage to stone and other materials. This could lead to the ruin of culturally important landmarks, such as monuments (United States Environmental Protection Agency, 2016).

Apart from destructive environmental impacts, PM emissions hold serious implications for human health. The health effects of exposure to PM are diverse and severe, and have been reported following short and long term exposure. Effects of short-term exposure include the aggravation of respiratory disorders such as asthma. Mortality trends have been observed with long term exposure (Pelucchi, et al., 2009). Long term exposure to PM in children has been linked to stunted lung development. PM has been shown to cause cardiopulmonary diseases and lung cancer as well as contributing to the development of diabetes mellitus and adverse birth outcomes (Feng, et al., 2016). No safe exposure level has been identified (World Health Organization, 2013).

It is notable that PM related mortality rates attributed to large scale energy generation are significantly lower than those attributed to the domestic use of fossil fuels for heating and cooking (Markandya & Wilkinson, 2007). It is, however, estimated that 10% of the South African population do not have access to domestic electricity or burn fossil fuels domestically due to cost reasons (Gaunt, et al., 2012). South Africa is

[5] $PM_{2.5}$ (particulate matter with an aerodynamic diameter of < 2.5 µm) has been shown to be most harmful, although PM_{10} (particulate matter with an aerodynamic diameter of < 10 µm but > 2.5 µm) also poses significant dangers to human health (United States Environmental Protection Agency, 2016). Note that *PM* in this study refers to all emitted particulate matter.

therefore faced with the challenge of providing sufficient, affordable electricity to support economic development and the growing population. While coal-fired power generation is suitable for this in the South African context, it comes with the challenge of ensuring minimal environmental and human health impact.

1.1.4 PARTICULATE EMISSIONS LEGISLATION

In light of the serious health and environmental concerns associated with PM emissions, legislation has steadily dictated stricter PM emission limits worldwide (World Health Organization, 2013). South Africa follows the trend set by developed nations. The South African Department of Environmental Affairs enforces the applicable limits in accordance with the National Environmental Management: Air Quality Act (NEMAQA) of 2004. This act dictates that particulate emissions of existing power stations must be maintained below 100 mg/Nm^3 by 2015 and conform to the new power station limit of 50 mg/Nm^3 by 2020[6] (Department of Environmental Affairs, 2010).

Power stations are forced to reduce generation load in order to operate within the prescribed emissions levels should limits be exceeded. This not only translates to lost revenue, but is a major concern for the socio-economic development of South Africa (Khobai, et al., 2017).

In order to ensure compliance and limit their environmental footprint, coal-fired power stations invest in equipment to reduce particulate emissions to within acceptable limits. Technology is often selected with the view of further reduction, in anticipation of increasingly stringent limits. This necessitates research and development of cost effective, sustainable PM emissions reduction solutions.

1.2 MOTIVATION

1.2.1. PARTICULATE EMISSIONS REDUCTION: BAGHOUSES VS ELECTROSTATIC PRECIPITATORS

The two most popular particulate emissions abatement technologies for coal-fired power stations are the baghouse, also referred to as fabric filter plants (FFP), and the electrostatic precipitator (ESP) (McKenna, et al., 1974).

Baghouses remove PM from the flue gas stream in a manner similar to a domestic vacuum cleaner. Long, typically cylindrical fabric bags capture the PM prior to exhausting filtered flue gas to the atmosphere. The pressure drop across the baghouse

[6] *mg/Nm^3* refers to milligrams per normalised cubic metre, normalised to 101.3 kPa and 0°C.

increases steadily as the captured PM collects on the surface of the bags. Therefore, the bags are periodically cleaned; either by mechanical shaking, reverse air, which entails relatively gentle flow of clean air in the opposite direction to filtration, or a pulse of compressed air (Wu, 2001).

ESPs work on the principle of electrostatic attraction. PM in the flue gas stream are charged by corona discharge from high voltage, shaped wires known as discharge electrodes and subsequently collected on grounded collection plates. Collection plates are periodically rapped to remove the PM build-up (Lavely & Ferguson, 2003).

If correctly designed, both technologies offer high collection efficiencies exceeding 99%. To meet current emissions limits, however, even higher efficiencies are required. The major advantage that baghouses hold over ESPs is that they are able to collect the very fine particles in the range of 0.05 µm – 1 µm that escape ESP capture (Wu, 2001). Furthermore, since ESP efficiency is dependent on ash resistivity, ESP performance is highly susceptible to changes in coal supply and operating parameters. This makes the less sensitive baghouse an attractive choice for applications where consistent coal supply cannot be guaranteed (Sloat, et al., 1993).

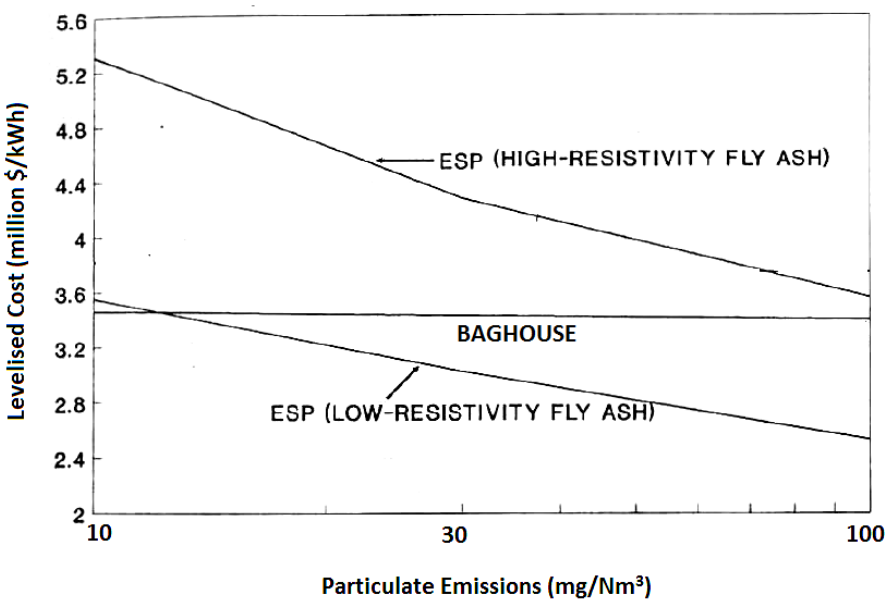

Figure 1-4: ESP vs FFP levelised cost (Sloat, et al., 1993)

Apart from efficiency, capital and operational costs are a deciding factor when selecting a PM abatement technology. Compared to ESPs, baghouses pose relatively high operational costs for low collection efficiency applications. This is owing to periodic filter bag replacements and increased auxiliary power consumption by the induced draught

(ID) fan due to baghouse pressure drop. For higher collection efficiencies, however, baghouses are more economical than ESPs (Wu, 2001). This is reflected in Figure 1-4, where capital, operating and maintenance costs, in 1993 US dollars, are shown for a range of particulate emissions. From Figure 1-4 it can be seen that, for high resistivity coal fly ash such as that typical in South Africa (Lloyd, 1987), ESPs are more expensive than baghouses. This cost differential grows rapidly as particulate emissions decrease.

1.2.2. BAGHOUSES AND ASSOCIATED COSTS

For application where fluctuations in coal supply are expected and low emissions are required, baghouses are popular choice at coal-fired power stations in South Africa and internationally (Popovici, 2010). Various types of baghouses exist, including reverse-air, shaker and pulse jet fabric filters (PJFF). PJFFs are commonly selected for power utility application due to their ease of operation, ability to perform online bag cleaning and lower cost compared to other baghouse types (Wu, 2001). A schematic of a PJFF is shown in Figure 1-5.

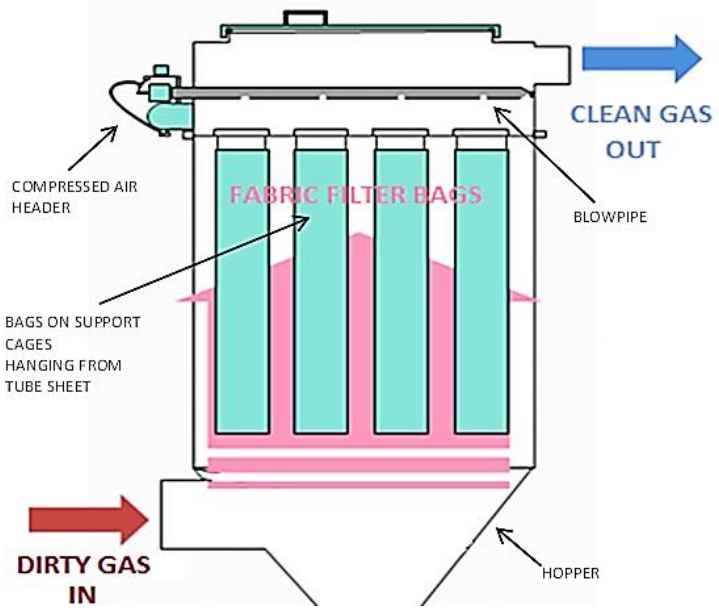

Figure 1-5: Baghouse schematic (Neundorfer, 2016)

A key design parameter for a baghouse is the air-to-cloth ratio[7]. This parameter is selected based on the type of PM being filtered and the type of filtration fabric used. An optimally designed baghouse selects an air-to-cloth ratio that balances pressure drop (operational costs) and baghouse footprint (initial capital outlay and bag replacement

[7] The *air-to-cloth ratio*, or filtration velocity, is defined as the volume of flue gas being filtered divided by the total filtration cloth area, in m/s (Wang, et al., 2004).

costs). For typical coal-fired utility applications, suitable air-to-cloth ratios dictate that thousands of bags are required (Turner, et al., 1998).

Bag fabric selection is at the core of baghouse efficacy. The bag acts as the basis on which the ash cake, which is vital for filtration, forms. Various fabric properties affect the filtration efficiency, pressure drop and ultimately the lifetime of the bag. These three factors drive baghouse cost. For cost effective power production, it is essential that these bag performance factors are balanced with bag costs.

In order to maintain costs at profitable levels, it is desirable that bag life is extended as long as practical. Bag life is defined as the time during which bag failures (due to blinding[8] or physical failure) do not limit the operation of the boiler units (Greyling, 1998). As indicated by Figure 1-6, effective baghouse cost decreases with increased bag life. Appropriate bag fabric selection is therefore essential for a cost optimised system, both for ID fan power consumption and reduction of production losses (Mycock, 1999).

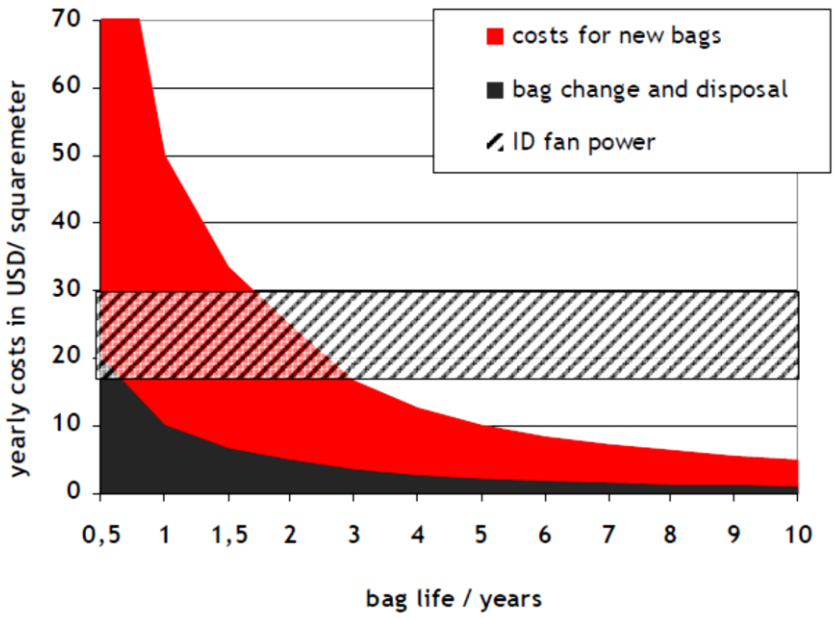

Figure 1-6: Major baghouse operational costs (Rathwallner, 2008)

1.2.3. FILTRATION FABRICS

Different types of fabrics for filtration exist, including woven fabrics, membranes and non-woven, needle felt fabrics. Various natural and polymeric fibres for fabric

[8] *Blinding* refers to the undesirable phenomenon of needle felt filtration fabric being saturated with particulate as a result of depth filtration. The material is thus unable to be cleaned effectively, leading to unacceptably high pressure drop (Neundorfer, 2016).

production are available, suitable for specific applications and limited by operating conditions (Davis, et al., 1990).

Historically, natural fabrics were used for filtration. Records from 1852 detailing a baghouse developed for filtration of zinc oxide dust show that bags of cotton, flax or wool were used (Billings & Wilder, 1970).

Modern pulse jet baghouses typically use non-woven, felted fabrics made of polymeric fibres. Non-woven fabrics are formed by needling randomly oriented fibre mats onto a woven support scrim. Different fibre types can be blended to optimise filtration and bag life properties (Popovici, 2010). Table 1-1 compares the properties of various materials for potential use as baghouse filtration fabrics.

Table 1-1: Typical Fabric Used for Filter Bags (McKenna & Turner, 1989)

Fibre Type	Generic Material Category	Maximum Continuous Temperature (°C)	Maximum Surge Temperature (°C)	Acid Resistance	Alkali Resistance	Flex Abrasion Resistance	Relative Cost
Cotton	Natural fibre cellulose	82	107	Poor	Excellent	Average	0.3
Polypropylene	Polyolefin	88	93	Excellent	Excellent	Good	0.4
Wool	Natural fibre protein	93	121	Good	Poor	Average	--
Nylon	Polyamide	93	121	Poor to fair	Excellent	Excellent	--
Orlon® (PAN)	Acrylic	116	127	Very good	Fair	Average	0.4
Dacron®	Polyester	135	163	Good	Fair	Excellent	0.4
Nomex® (aramid)	Aromatic polyamide	204	218	Fair	Very good	Very good	0.9
Teflon®	Fluorocarbon	232	260	Excellent except poor for fluorine	Excellent except for trifluoride, chlorine and alkaline metals	Fair	4.7
Fiberglas®	Glass	260	288	Good	Poor	Poor to fair	0.8
Ryton® (PPS)	Polymer	191	232	Excellent	Excellent	Good	1.0
P84® (PI)	Polymer	232	260	Good	Fair	Fair	1.7

Traditionally, filtration fabric is selected based primarily on temperature resistance and cost. Further important, and often neglected, factors to consider when establishing the suitability of a chosen filtration fabric are resistance to chemical attack from the flue gas stream and compatibility with the ash particles (Mycock, 1999).

In modern South African coal-fired power station baghouses, filtration fabric is primarily of the polymeric, non-woven variety. Two fibre types are commonly used: polyacrylonitrile (PAN) for low temperature[9] applications and polyphenylene sulphide (PPS) for high temperature[10] applications. Both fabrics may incorporate a blended surface layer containing polyimide (PI) (Patel, 2016). The intention of the blended surface layer is to improve filtration characteristics and bag life. Blended fabrics are, however, more expensive than bags of the base fibre (PAN or PPS) only. Furthermore, uncertainty exists as to under which conditions PI incorporation is beneficial.

1.3 PROBLEM STATEMENT

Due to the growing energy demand and South Africa's continued reliance on coal for electricity production, high efficiency PM emissions reduction technology is required to cost effectively maintain emissions below legislated limits. Baghouses, offering effective capture of ultrafine PM from variable coal supplies, are an attractive choice.

The heart of a baghouse is the filtration fabric from which filter bags are constructed. In order to achieve increasingly higher PM capture efficiency requirements while simultaneously reducing operating costs and extending bag life, an improved understanding of bag selection criteria is required. Specifically, scenarios in which the incorporation of expensive surface blends will offer benefits must be better defined.

1.4 AIM AND OBJECTIVES

This study aims to comparatively evaluate the benefits of the incorporation of PI in low and high temperature filtration fabrics commonly used in baghouses at South African coal-fired power plants, namely PAN and PPS. The aim is to establish whether the cost of incorporating PI is warranted.

The objectives of this study include:

- Developing improved understanding of the electrostatic properties of the selected filtration fabrics, including charge polarity and charge dissipation behaviour, and ranking the fabrics on a triboelectric series
- Suggesting models for the characteristic discharge curves of the filtration fabrics considered

[9] *Low temperature* baghouses operate between approximately 120°C and 130°C (Patel, 2016).
[10] *High temperature* baghouses operate between approximately 130°C and 150°C (Patel, 2016).

- Investigating the impact of moisture on the electrostatic behaviour of the filtration fabrics
- Investigating the electrostatic interactions of the charged fabrics with various ash types using optical microscopy
- Evaluating the resistance of the filtration fabrics to acid attack through evaluation of tensile properties after exposure to sulphuric and nitric acids
- Evaluating the impact of acid attack on the individual polymeric fibre types considered by completing thermogravimetric analysis (TGA) and differential scanning calorimetry (DSC) of yarn samples before and after acid exposure
- Developing a method of conducting cost-benefit analyses (CBA) for filtration fabric selection for bags that is reflective of costs incurred during the operational lifetime of bags
- Applying the CBA method to PAN-based and PPS-based fabrics in order to draw conclusions about the economic impact of incorporating PI surface layers in bags in various acidic operational environments

1.5 SCOPE OF STUDY

This study is limited to the evaluation of PAN, PPS and PI fibre for use in layered, needle felt filtration fabric in pulse jet baghouses. Woven fabrics are not considered. Other fibre types do not form part of the scope of this study, but are included in the literature discussion where research is relevant to this study. Fabric of 100% PI construction is considered where behaviour related specifically to PI is investigated, but is not considered a fabric option for baghouse application in this study. The scope is limited to individual fabric and yarn samples in laboratory environments and does not consider complete bags and in situ tests.

This study focuses on two aspects of bag selection which are not currently extensively understood and applied: the electrostatic properties of selected polymers and chemical resistance throughout the operating temperature ranges of the filtration fabrics. Chemical resistance is limited to acid attack and thermal degradation. Alkaline resistance and chemical interaction with ash do not form part of this study. This study does not investigate the role of fibre shape or size in filtration.

The proposed CBA method is for bag selection for a defined baghouse. Costs associated with baghouse construction are thus not included. The CBA economic assumptions consider a baghouse in isolation and do not take opportunity costs associated with energy availability across a power producing fleet into account.

1.6 DISSERTATION STRUCTURE

This dissertation is structured as follows:

Chapter 1: Introduction

This chapter provides background to electricity generation and the need for particulate emissions reduction. It outlines the problem statement and objectives of this dissertation as well as defining the scope of the study.

Chapter 2: Literature Review

The literature review chapter critically analyses selected literature related to fabric filtration. Fabric filtration mechanisms and selection criteria are discussed. Current knowledge of electrostatic phenomena in fabric filtration is examined. The chemical and thermal compatibility of selected fabrics is highlighted. Current bag costing techniques are reviewed.

Chapter 3: Triboelectric Behaviour of PAN, PPS and PI Filtration Fabrics

This chapter describes the methods used for triboelectric analysis of selected filtration fabrics. Results are reported and discussed and conclusions drawn.

Chapter 4: Filtration Fabric Resistance to Acid Attack and Thermal Degradation

In this chapter, the impacts of acid attack and thermal degradation on selected filtration fabrics and corresponding yarns are discussed. Results of investigations into the effects of nitric and sulphuric acids on the fabrics are reported. Furthermore, results of thermogravimetric analysis of the selected polymer types is reported and discussed.

Chapter 5: Cost-Benefit Analysis of Filtration Fabrics

This chapter proposes a new model for the cost-benefit analysis of filtration fabrics in power utility baghouses. Assumptions based on the results discussed in Chapters 3 and 4 are made and input into the cost-benefit analysis in order to evaluate the cost implications of PI incorporation in low and high temperature filtration fabrics. Model sensitivity to various parameters is discussed.

Chapter 6: Conclusions and Recommendations

The final chapter summarises the conclusions that can be drawn from this study and makes recommendations for areas where further research is warranted.

CHAPTER 2: LITERATURE REVIEW

2.1 INTRODUCTION

Efficient baghouse filtration is heavily dependent on the selection of appropriate bag material. Fabric must be selected for filtration properties and to meet various operational demands. Selected literature related to fabric filtration is critically reviewed in the following chapter. Sources include published journals and books, online sources as well as industry reports and discussions with subject matter experts.

2.2 FABRIC FILTRATION BACKGROUND

2.2.1. FILTRATION MECHANISMS

Filtration in a baghouse occurs when an aerosol (in this case ash laden flue gas) is forced to flow through a solid, porous filtration medium (the needle felt filter bags), which captures a certain portion of the particulates (Carr & Smith, 1984). Filtration is driven by a pressure differential created by the ID fan, forcing the particulate laden gas through the physical barrier of the filter medium and the consequently agglomerated ash cake (Koch, 2008).

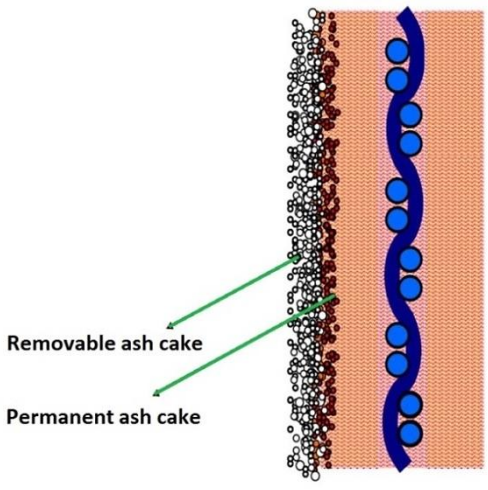

Figure 2-1: Ash cake on filter fabric surface (Di Blasi, et al., 2015)

Baghouses achieve gas filtration by a combination of fabric filtration and, predominantly, ash cake filtration. When filtration commences, fabric filtration at the surface of the bags occurs. Depth filtration, where filtration occurs within the fabric structure, is undesirable as this will result in blinding. The initial fabric surface filtration

forms a permanent ash cake supported by the outer fibre layer of the bags (Figure 2-1). This permanent ash cake is the dominant filtration instrument and also serves to protect the bag from chemical attack. An initial ash cake is often achieved by pre-coating the bags before boiler operation starts. Since bags are periodically pulsed to remove excess ash, a complete model of filter bag filtration includes the initial fabric surface filtration, ash cake filtration varying with time as well as the transition between fabric and cake filtration as the bags are cleaned (Turner, et al., 1998).

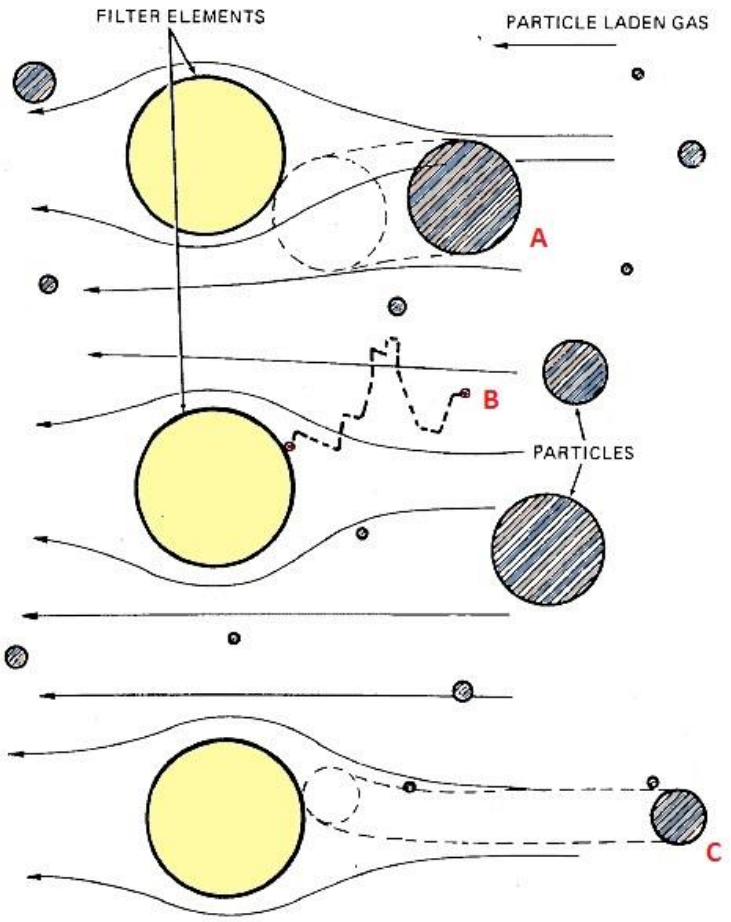

Figure 2-2: Fabric filtration mechanisms (Carr & Smith, 1984)

Since cake filtration is the chief particulate collection mechanism, it is vital that the selected fabric possesses appropriate fibre properties to enable the formation of a stable and porous ash cake (Popovici, 2010). The mechanisms of fabric filtration are described below with reference to Figure 2-2.

- **Inertial impaction** – as fluid flows around a fibre, the flow direction and velocity is affected. Larger particles are more significantly affected by their inertia and cannot follow this diverted gas stream. Particles are thus deposited on the fibre

(Sipes, 2011), as illustrated by A in Figure 2-2. This filtration mechanism is improved by irregularly shaped fibres.

- **Diffusion** – very small particles are affected by the gas molecules in the fluid stream. This molecular interaction results in chaotic, Brownian motion of the particle. Since the erratic motion of the particles does not follow the fluid stream, they are likely to collide with a fibre. For filtration by diffusion it is important that once the particle collides with the fibre it remains captured and does not continue to travel through the filter medium, as its small size allows (Sipes, 2011). This is illustrated by B in Figure 2-2.
- **Interception** – smaller particles that are not significantly affected by their inertia, follow the fluid flow around a fibre. When the particle is within a distance of one radius of itself from the fibre, it makes contact with the fibre and hence becomes attached (Camfil, 2015), as shown by C in Figure 2-2.
- **Sieving** – sieving, or straining, occurs when the ash particle is larger than the space between adjacent fibres. The filter medium thereby poses a physical barrier to the particle (Camfil, 2015).
- **Electrostatic attraction** – particles charged as a result of their interaction with molecules in the gas stream are attracted to oppositely charged fibres (Brosseau & Berry Ann, 2009).
- **Gravity** – a constant downward force is applied to particles during filtration. Under certain circumstances, such as low gas flow velocities and large particle sizes, this can cause particles to fall out of the gas stream. The mutual gravitational attraction of the particles to fibres and each other, however, is negligible (Carr & Smith, 1984).

Fabric filter overall particulate collection efficiency is typically greater than 99%. There are two basic methods through which particles escape capture. Firstly, ash can seep through leaks in the tube sheet, ducting, through bag tears or improperly sewn seams. The second method, relevant to this study, is termed bleed-through where particles move through the ash cake and fabric, evading collection. This is typically a function of ash characteristics. Small particles, near spherical in shape with smooth surfaces are less cohesive and more likely to travel through the filter (Benitez, 1993). This can, however, be significantly reduced by selecting the optimal fabric for the specific application.

2.2.2. FABRIC FILTRATION MODELLING

A tool which could assist in appropriate fabric selection is modelling. Theoretical modelling of fabric filtration, however, is complicated by the interference of neighbouring fibres in the random needle felt structure. A further complication results from the inhomogeneity of the needle felt fibres. Ideal gas flow patterns typically assumed are therefore not applicable in practice. Fuchs and Stechkina (1963) have suggested a model based on viscous fluid flow, taking neighbouring fibre interference into account. Further work completed by Lee and Liu (1982) suggests an efficiency equation based on the combined effects of interception and diffusion, which are the predominant mechanisms in the region of maximum penetrating particle size. While these theoretical models of fabric filtration exist, it is often more fruitful to characterise the filtration characteristics of a fabric experimentally (Koch, 2008).

As the ash cake thickens pressure drop across the bag increases. As mentioned in the preceding section, pressure drop is directly related to the auxiliary power consumption of the plant and is thus an important factor in maintaining costs below a suitable level (Turner, et al., 1998). Once a certain pressure drop or time interval has elapsed, the bags are cleaned by means of a pulse of air. While the removable ash cake is pulsed off, the permanent ash cake remains (Figure 2-1). The ash cake is not necessarily homogeneously cleaned, which may result in non-uniform cake regeneration and consequent variable cake permeability. Due to this, modelling the cake filtration is complex and heavily reliant on empirical data (Koch, 2008).

When analysing ash cake formation in a plant, the average filter cake properties under varying conditions, as empirically determined, can be used to build approximate models. Ash cake formation and growth can be predicted based on ash properties and operating conditions for simplified analysis. Flue gas properties as well as compression due to the operating pressure differential affect the porosity and thickness of the ash cake. Due to the often variable nature of baghouse operating conditions, the development of a reliable model is therefore complicated and often impractical for industrial design applications (Khean, 2003).

A simplified pressure drop equation, based on Darcy's law describing fluid flow through a porous medium, is typically used in the design of baghouses (Benitez, 1993). This relationship, described by Equation (2-1), governs the pressure drop of the combined filter medium and ash cake as a function of the filtration velocity, often referred to as the air-to-cloth ratio. In basic fluid flow terms, this quantity may be described as flux.

$$\Delta P(t) = S(t)v \quad \textbf{(2-1)}$$

where:

$\Delta P(t)$ = pressure drop through the filter as a function of time (kPa)
$S(t)$ = drag through the fabric and the ash cake (kPa.s/m)
v = filtration velocity (m/s)

Providing for the separate pressure drop through the bag and the ash cake the following expression described by Equation (2-2) for fabric filter pressure drop as a function of time is developed:

$$\Delta P(t) = S_e v + K c_i v^2 t \quad \textbf{(2-2)}$$

where:

S_e = specific resistance of clean (dust free, freshly cleaned) filter bag (kPa.s/m)
K = specific resistance of ash cake (s^{-1})
c_i = FFP inlet dust concentration (kg/m^3)
t = operating time (s)

While more complex equations considering pulse cleaning pressure have been suggested by Koehler and Leith (1983) and a fabric specific equation by Dennis and Klemm (1980), both accounting for ash characteristics, it is advisable that S_e and K are determined experimentally (Turner, et al., 1998). S_e is by dependent on the composition, fibre shape and construction of the fabric, while K is affected by ash properties as well as ash interaction with the fabric surface, including the fibre material, shape, electrostatic properties and surface finish (Saleem, et al., 2011).

The difficulty in accurately analysing K is that it is affected by operating conditions. K is affected by fluctuations in coal quality, which result in varying ash particle size, shape and composition, as well as filtration velocity, operating pressure and cleaning methodology. Tests using limestone dust on PPS, PI and polytetrafluoroethylene (PTFE) bags found that, although the specific resistance of the fabric is unaffected by the filtration velocity, the specific resistance of the ash cake showed a linear increase with increased filtration velocity (Saleem, et al., 2012). Furthermore, pulse cleaning does not remove the pulse cake uniformly, resulting in uneven cake regeneration. As the ash cake builds up, it experiences a pressure drop gradient as the ash cake nearest the bag surface is compacted by the subsequently collected ash (Koch, 2008).

It must be noted that when bags are pulse cleaned during operation only a portion of the ash falls into the hopper for removal, with a large portion redeposited on the surrounding bags. The properties of the original ash cake are not the same as the redeposited dust (Benitez, 1993). In order to account for this variance, Dennis and Klemm (1979) suggested a model of filter drag described by Equation (2-3).

$$S(t) = S_e + K_c W_c(t) + K_0 W_0(t) \quad \textbf{(2-3)}$$

where:

K_c = specific ash cake resistance of the redeposited ash (s^{-1})

$W_c(t)$ = aerial density of redeposited ash (kg/m^2)

K_0 = specific ash cake resistance of the freshly deposited ash (s^{-1})

$W_0(t)$ = aerial density of freshly deposited ash (kg/m^2)

The reliance of the factors discussed above on fabric properties and the interactions of dust with the selected filtration fabric highlight the importance of appropriate fabric selection for effective filtration and acceptable pressure drop.

2.3 FILTRATION FABRIC

2.3.1 FABRIC CONSTRUCTION

Non-woven materials used for bag fabrics, often referred to as needle felt materials, consist of a woven support base, called a scrim[11], onto which randomly oriented fibres are joined by a needling process. The non-woven layers are referred to as batts and may consist of more than one layer and more than one fibre type. These various configurations are optimised to find the best design for filtration efficiency, dust release properties, chemical stability and mechanical strength (Popovici, 2010). Cascade™, or layered construction (Figure 2-3), is typically used in baghouses at South African coal-fired power utilities (Patel, 2016).

In order to balance performance and cost, high efficiency and typically more expensive fibres are often employed in the surface layer only, with coarser, less expensive fibres used for the inner batts. By limiting finer fibres to the surface layer, lower pressure drop can be maintained (Mukhopadhyay & Choudhary, 2013). Fibre selection is therefore central to bag selection.

[11] The *scrim* may be woven to various degrees of tightness and combinations of warp and weft yarns for increased strength or porosity (Saad & Alkadey, 2010).

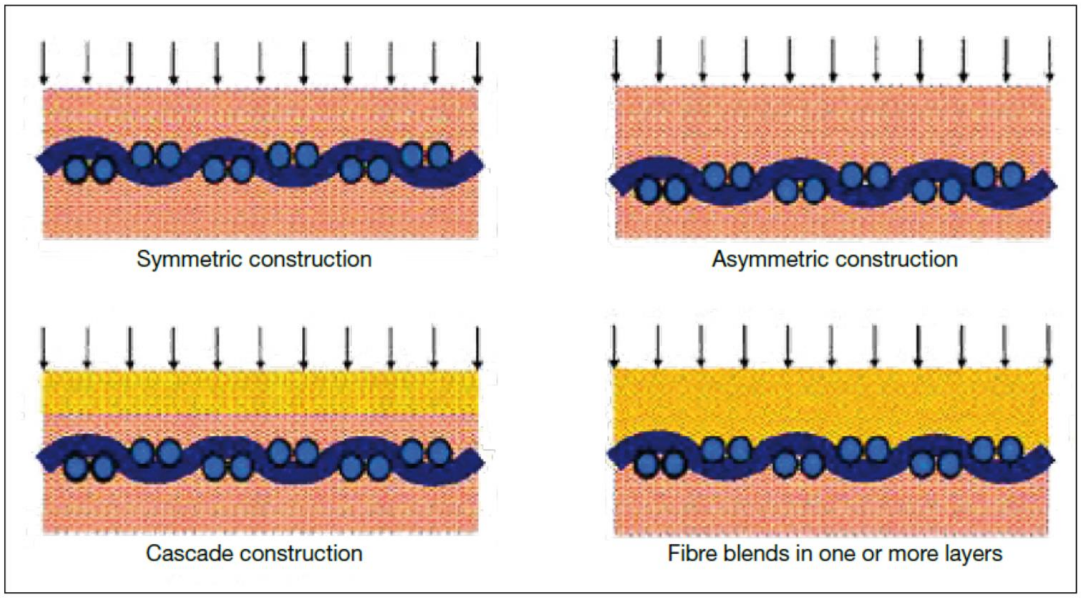

Figure 2-3: Needle felt fabric construction types (Popovici, 2010)

2.3.2 FABRIC SELECTION CRITERIA

When selecting filtration fabric for bags for a particular baghouse application, a good understanding of the operational conditions of the specific baghouse is vital. The baghouse inlet flue gas conditions, including temperature, moisture content and flue gas constituents as well as ash loading, ash morphology and ash chemistry all impact the performance of the selected fabric (Mycock, 1999). Suitability of fabric options can be evaluated based on the following considerations (Davis, et al., 1990):

- **Filtration efficiency**. Since the bags are chosen for the purpose of filtering harmful particulates from the flue gas, filtration efficiency is a key consideration.
- **Mechanical strength**. Fabrics experience mechanical stresses from the weight of the ash cake it holds, cyclic pulse cleaning as well as the negative pressure maintained across the bag house. Bags therefore experience forces in various directions as well as abrasion against the support cage, making mechanical tenacity an important factor.
- **Dust release characteristics**. In order for the baghouse to function effectively, bags must be periodically cleaned. While it is desirable for some ash to remain on the bag, the ability to release the removable ash cake effectively is paramount to extending bag life and maintaining pressure drop within acceptable limits.
- **Temperature resistance**. Baghouses, especially those used for coal-fired boilers, operate at elevated temperatures. The chosen fabric must be capable

of operation throughout the expected temperature range, which may include high temperature excursions as well as temperature drops and operation below acid dew point.

- **Chemical resistance**. Flue gas chemistry necessitates bag resistance to a range of chemical constituents. These may be acidic or alkaline and potentially accelerate the chemical degradation of the chosen fabric. Temperature fluctuations and the introduction of excess oxygen through ducting leaks/attemperation systems or chemical additives for various emissions reduction purposes may affect the chemical composition of the flue gas entering the baghouse.

These criteria are affected by fabric construction, surface finishing techniques and fibre type. This study focuses on fabric of the layered construction type, as discussed in the proceeding section. The impact of fibre polymer type on fabric filtration properties, specifically electrostatic interactions and thermal and chemical resistance is extensively discussed in subsequent sections. Fabric surface finish options and fibre morphology are briefly discussed below.

2.3.3 FABRIC SURFACE TREATMENTS

Various forms of fabric pre-treatment exist, all of which are aimed at improving fabric dimensional and mechanical stability and cleanability. Surface treatments are applied after the fabric needling process is complete, prior to bag manufacture. Treatment options include (Neundorfer, 2016):

- **Singeing.** Singeing is performed in order to create a uniform fabric surface. Needle felt is passed over an open flame in order to singe off any protruding surface fibres.
- **Calendering.** Calendering is performed to achieve a uniform surface area as well as improve dimensional stability. The needle felt is passed through rollers at high pressure, pushing any protruding fibres into the felt body and thereby achieving a smooth surface.
- **Napping.** Napping is performed when protruding surface fibres are desirable. The needle felt is scraped across metal burrs, creating a fuzzy surface for increased particle collection.
- **Glazing.** Glazing reduces bag shrinkage by pre-exposing the fabric to elevated temperatures during a high pressure pressing process.

- **Coating and membranes.** Various coating options are available on the market. Needle felts are immersed in the coating material in order to lend it better chemical or temperature resistance, altered triboelectric properties, cleanability or abrasion resistance.

Coatings and membranes are available for various purposes. Surface coatings can be applied by spraying a chemical coating onto the filtration surface or applying a foam layer (Mukhopadhyay, 2009). PTFE membranes can be applied to the filtration surface of the fabric. PTFE membranes are reported to offer significant efficiency advantages due to micro-pores allowing gas to pass through but trapping fine particles. These advantages, however, come at the cost of higher pressure drop (Mukhopadhyay, 2009). The improved efficiency for small particulate capture is illustrated in Figure 2-4.

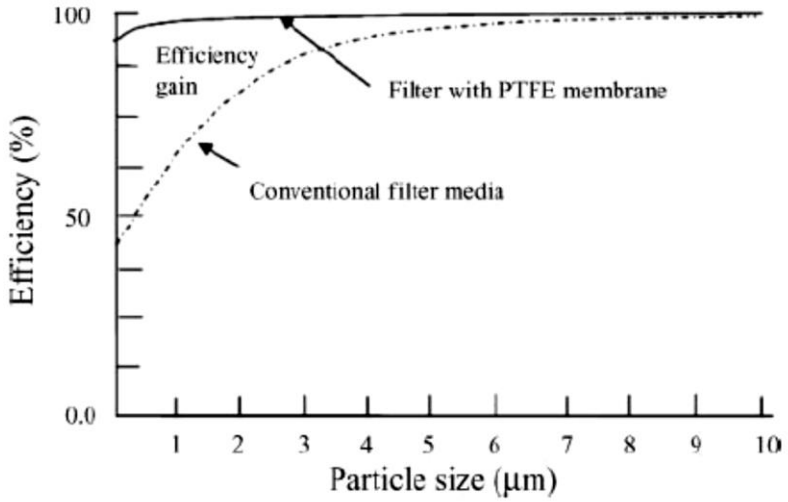

Figure 2-4: Efficiency comparison of filter media without and without PTFE membrane (Mukhopadhyay, 2009)

Fabric surface treatment is selected based on the fibre types used in the fabric construction and the baghouse application. For application in coal-fired power utility baghouses in South Africa, fabrics are typically singed and calendared but no coatings are applied. Fibre morphology is selected in order to achieve the filtration benefits offered by membranes and coatings (Patel, 2016).

2.3.4 FIBRE MORPHOLOGY

Due to differing fibre manufacturing processes, fibres possess different morphologies. Themmel (2006) and later Popovici (2010) state that fibres with irregular, multilobal cross-sectional shapes offer improved filtration characteristics when used in needle felt

fabrics. These improvements are due to the relative increase in surface area of the multilobal fibres when compared to round fibres. The higher fibre surface area results in improved fabric porosity which enhances ash capture. This case is analogous to membrane application discussed above.

Particle capture is further improved by the flow dynamics of the multilobal fibres. Local low velocity areas are formed in between the lobes which effectively capture ash without creating additional pressure drop due to the gas flow paths remaining unchanged (Themmel, 2006). The comparison of round versus irregular fibre cross sections and relevant flow characteristics is shown in Figure 2-5.

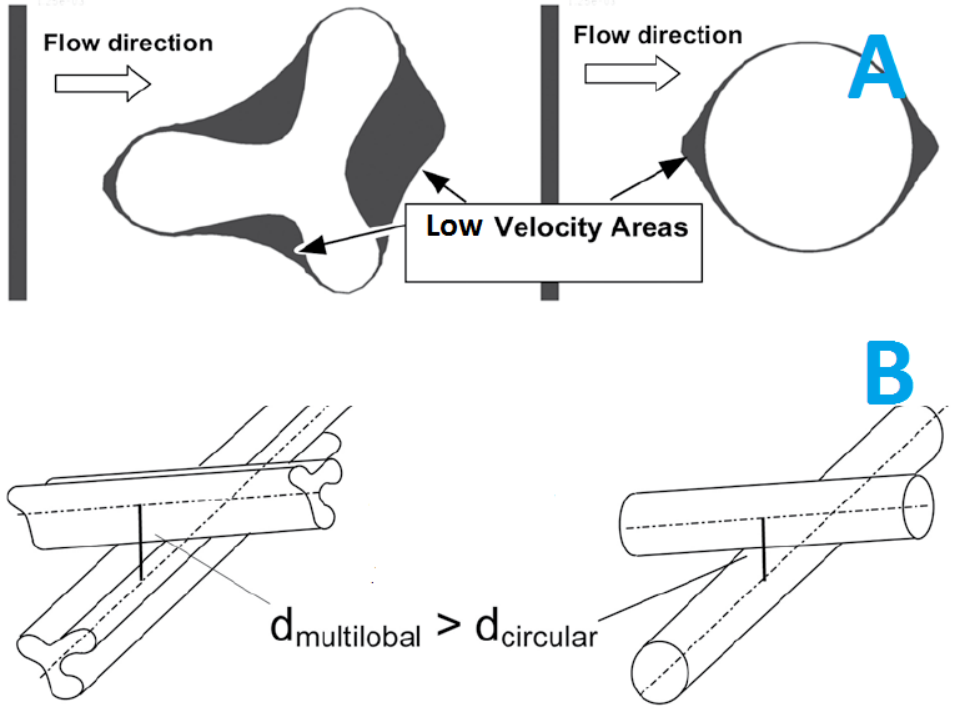

Figure 2-5: Comparison of round and multilobal fibre cross sections: A – flow dynamics, B – distance between fibres (Themmel, 2006)

The multilobal fibre shape shown in Figure 2-5 is proprietary to P84® type PI produced by Evonik Industries. Other fibre types are also available in a variety of shapes. The shapes of fibres relevant to this study are discussed here. Toyobo's Procon® offers a trilobal product in addition to the traditional round PPS fibre. The morphology differences between round, trilobal and multilobal fibres are illustrated in Figure 2-6. PAN fibres for filtration applications are typically kidney-shaped or dog bone shaped, as shown in the cross sectional views of fibres produced by Polyacryl Iran illustrated in Figure 2-7. Trilobal PAN is also available, such as the AKSA AT203 shown in Figure 2-8.

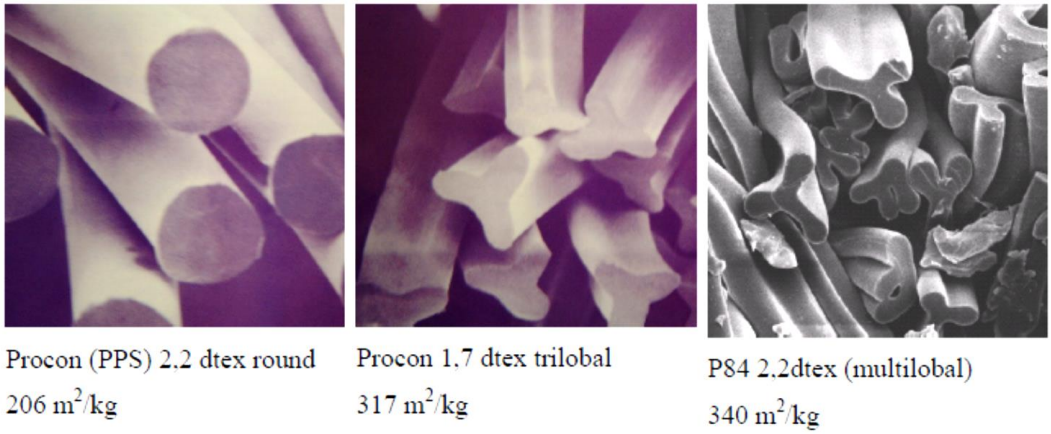

Figure 2-6: Different fibre shapes: Procon® PPS (round, left and trilobal, centre) and P84® PI (multilobal, right) (Rathwallner, 2009)

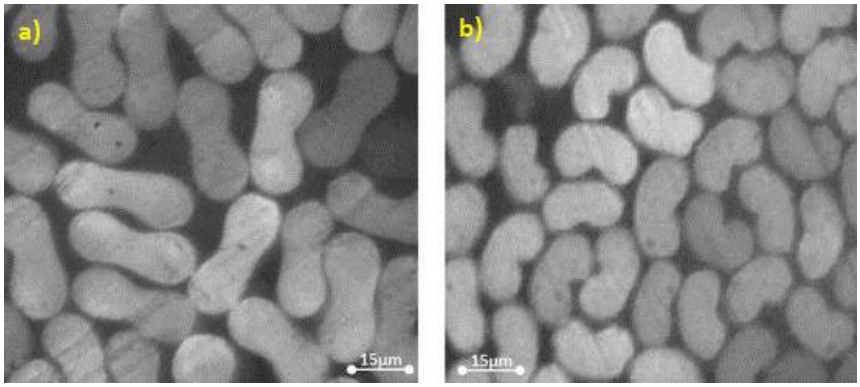

Figure 2-7: PAN fibre cross sections: a) dry spun dog bone shape, b) wet spun kidney shape (Pakravan, et al., 2012)

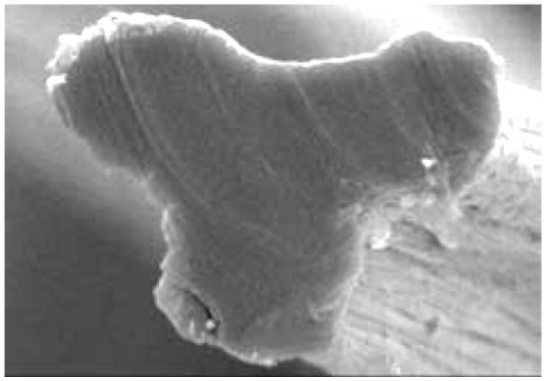

Figure 2-8: Trilobal PAN fibre cross section (AKSA, 2010)

All fibres are available in various fibre sizes where fineness, or titre[12], affects the filtration properties and pressure drop of the needle felt fabric in which it is used. Finer

[12] *Titre* is a measure of fibre fineness, defined as its mass per unit length. This is useful for fibre comparison since it takes the differences in material density into account (Steinmann & Saelhoff, 2016).

fibres have larger surface areas than less fine fibres, which, as with irregularly shaped fibres, results in smaller pores (Popovici, 2010; Mukhopadhyay, 2009). Research conducted by Mukhopadhyay and Choudhary (2013) on polyester needle felt bags found that higher filtration efficiencies are possible with more fine fibres due to the higher surface area, smaller pore sizes and the higher level of fibre consolidation (during material manufacture the needle barb punches more fibres at the same time). Pressure drop, however, was observed to increase with fibre fineness.

2.4 ELECTROSTATIC PHENOMENA IN BAG FILTER FILTRATION

Selection of appropriate fibres for fabric construction can have an impact on the electrostatic phenomena at play in baghouse filtration. A review of pertinent literature follows.

2.4.1 BACKGROUND: ELECTROSTATIC FORCES IN FABRIC FILTRATION

The electrostatic interaction of filter fabrics with ash has often been observed and reported in industry and several literary sources, including Frederick (1974; 1980; 1996), Carr and Smith (1984) and, more recently, Kazyuta (2013). The various phenomena at play, however, are not well understood. Electrostatic interactions may be either beneficial or detrimental, depending on the specific scenario (Frederick, 1974). For instance, electrostatic forces in appropriately selected fabrics may improve the adhesion and agglomeration of the ash particles, aiding the formation of a stable ash cake. This reduces pressure drop because effective cake filtration is maintained and, consequently, ID fan power consumption and the related cost is reduced (Topkin, 2000). Unfavourable interactions, however, could lead to decreased pulse cleaning efficiency, bag blinding and the reduced filtration effectiveness of the ash cake (Kazyuta, 2013).

In order to establish the impact of the electrostatic characteristics of filtration fabrics on in situ ash cake formation, Topkin (2000) completed a series of tests whereby samples of sixteen selected filtration fabrics (PAN and PPS from different suppliers) were

The unit of titre is *tex,* where filtration fabrics are most commonly defined using *decitex* (dtex), which refers to the mass of the fibres in grams per 10 000 metres.
Note that another term often used is *denier*, specifically *microdenier*, to refer to very fine fibres. Similar to titre, it is also a measure of the linear mass density of the fibres, however it based on typical silk weights where a 1 g strand is approximately 9000 m long (Haynes, 1946).

triboelectrically[13] charged by rubbing with polyethylene terephthalate (PET) in a laboratory environment. The charge polarity, charge magnitude and discharge rate of the fabrics were recorded. Later, bags of the selected fabric types were installed in an industrial baghouse and evaluated for permeability after operation for 6000 hours. Topkin concluded that bags made of fabrics with more negative charges recorded during laboratory charging experiments result in lower permeability after operation for 6000 hours than fabrics with less negative or positive charges. This result implies that for Topkin's application, negatively charged bags were more prone to high pressure drop and potential blinding. Furthermore, a correlation between higher discharge rates (the rate at which charge decays from the fabric surface after initial charging) recorded in the laboratory and higher air permeability after operation in situ was observed. This correlation supports the statement that appropriately selected filtration fabrics improve the ease of bag cleaning, subsequently reducing pressure drop and possibly extending bag life due to a decreased propensity for bag blinding, previously suggested by Frederick (1974).

The electrostatic phenomenon observed in baghouses is due to the interaction of charged ash with charged bag fibres. Therefore, in order to understand how a fabric type will behave in a certain application, the nature of the ash must be understood. Due to movement within the flue gas stream, ash particles are always electrostatically charged to some extent. The magnitude of ash charge depends on a variety of factors, including turbulence of the flue gas, collision with surfaces and other particles as well as particle size and mineralogy (Kunkel, 1950).

Apart from the natural electrostatic charge present on particles due to their dispersion and transport in the flue gas stream, artificial charge augmentation has been investigated in various baghouse applications. Favourable results for pressure drop reduction have been obtained by pre-charging ash particles with corona discharge prior to collection in a baghouse. Frederick (1980) concluded that this is due to the formation of a more porous and uniformly distributed ash cake. At increasing flue gas filtration velocities (which, as previously discussed, drive pressure drop), Frederick reported that a review of available results showed significant reductions in overall pressure drop for a variety of ash types and varying flue gas moisture content. Humphries et al. (1984) reached a similar conclusion after tests conducted with corona pre-charged lead smelter dust achieved baghouse pressure drop reductions of up to 60%. Kwetkus (1997) later conducted laboratory tests with corona pre-charged fly ash and recorded

[13] *Triboelectric charging* refers to the contact electrification of two materials (Diaz & Felix-Navarro, 2004).

similar pressure drop reductions and efficiency improvements. Humphries et al. and Kwetkus both found that although baghouse enhancement is possible with particle pre-charging, the use of a corona pre-charger was problematic for sustainable implementation due to sensitivity to particle resistivity.

Further positive results with charge augmented baghouses have been reported when the bags themselves are charged. Greiner et al. (1981) found higher collection efficiency, reduced pressure drop and improved operation at higher filtration velocity in a pilot plant by charging the bags using stainless steel wire electrodes in contact with the filtration side of the fabric bags. Many novel fabric charging methods and fibrous fabric constructions for effective charging, known as electret filters, have been developed in the past sixty years (Thankur, et al., 2013). Harnessing the electrostatic charge effects present in fabric filtration is therefore an area of significant interest, although the phenomenon is not conclusively understood.

For traditional baghouse applications where ash or fabric charge augmentation is not used, filter fabric is charged during operation by the friction between the flue gas molecules and the fabric. Furthermore, the deposition of naturally charged ash particles on the fabric influences the fabric charge (Kazyuta, 2013). It is also known that contact charging occurs between metals and polymers (Lowell & Rose-Innes, 1980), implying the potential for charging via bag and cage contact. In practice, however, this contact may serve to dissipate bag charges due to the contact of the cages with the earthed baghouse structure.

Polymer characteristics, as well as fabric structure and condition, influence the intensity of the charge generated. The surface texture of the fabric is reported as a pertinent factor in charge strength, with increased surface roughness corresponding with higher intensity of generated charge. Surface roughness is a function of the fibre type and production method as well as fabric construction and surface treatment (Frederick, 1974).

It must be noted, however, that triboelectric charges can be generated through static contact: friction need not be present. Contact electrification is a surface phenomenon that occurs when dissimilar objects are brought into contact and then separated (Williams, 2012). Charge of opposite polarity develops on the two materials, the polarity and magnitude of which is a function of the composition of the materials, the environment in which contact occurs and the contact process itself (Diaz & Felix-Navarro, 2004). This finding implies that inherent fabric charges could be present in

fabric filter bags due to the manufacturing process of the fibre or material and bag installation and operation. Pertinently, for the filtration fabrics under consideration, dissimilar materials are in contact in the blended layered type filtration fabrics used in baghouses. It is thus possible that charge within the fabric volume is developed due to the blended composition.

2.4.2 ELECTROSTATIC CHARACTERISTICS OF FILTRATION FABRICS

2.4.2.1 THE TRIBOELECTRIC SERIES

Filtration fabric types can be classed on a triboelectric series according to the magnitude and polarity of their intrinsic charge, established through frictional tests (Kazyuta, 2013). Figure 2-9 illustrates the range in static charge of selected filtration fabrics investigated by means of rubbing tests, as described by Frederick (1974). Fabric samples were tensioned in a support frame and rubbed using a motorised wheel covered in reference fabric. It was found that a fabric may vary in terms of polarity and charge intensity depending on inherent fibre properties and specific polymer characteristics. This variability is evident from Figure 2-9 where fabrics of the same polymer but different fabric forming methods or tradenames occupy different positions in the series.

Diaz and Felix-Navarro (2004) conducted a literature survey collating results from four previous triboelectric studies of a variety of metallic and polymeric materials, conducted between 1898 and 1987. Subsequently, a semi-quantitative triboelectric series was developed, ranking materials after contact charging with metal probes reported by three laboratories. Examination of the experimental and literary results lead the authors to conclude that hydrocarbons develop negligible charge, polymers containing nitrogen develop the most positive charge and halogenated polymers the most negative charge.

Gas absorption on the polymer surface is also known to have an impact on charge development (Jasti, 2011). Charging method and material also impacts results. Liu and Seyam (2013) found that increased contact force increased charge magnitude on polypropylene (PP) and PTFE after triboelectric contact with steel, but did not impact nylon.

There is no widely accepted conclusive triboelectric series. Due to the many factors influencing polymer charge development, results are largely irreproducible (Charlson,

et al., 1992; Diaz & Felix-Navarro, 2004; Hutton, 2007). Consequently, developing a definitive triboelectric series characterising fabric types is a complex exercise and positions within the triboelectric series are often debateable (Burgo, et al., 2012).

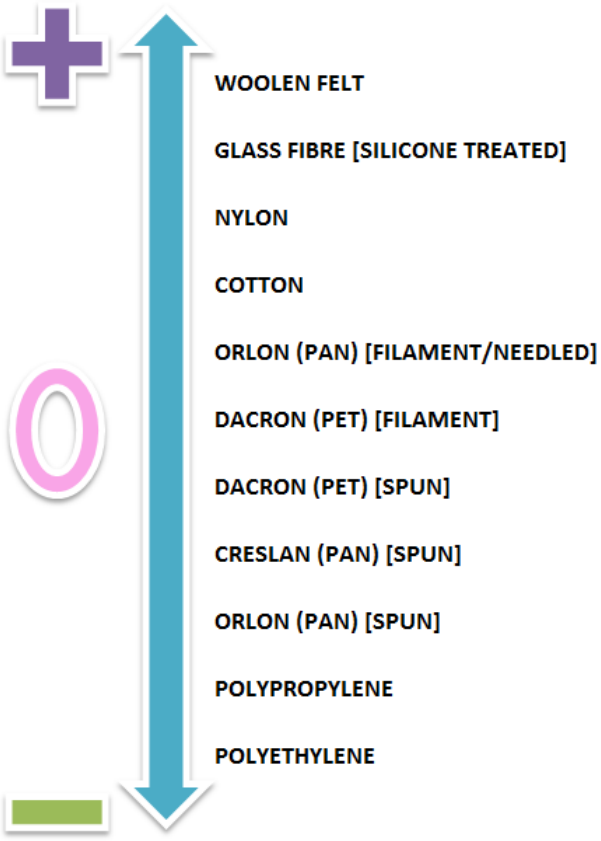

Figure 2-9: Triboelectric Series of Selected Fabrics (Frederick, 1974)

Triboelectric series described in eight literature sources are compared in Table 2-1. Since triboelectric series are relative and absolute charge magnitude is not consistently reported, this comparison is indicative of polarity only. It can, however, be seen that although there is variation in positions, the reported polarities are consistent in most cases.

Specific to the filtration materials considered in this study, PAN is reported to obtain negative polarity after triboelectric charging except in the case of Frederick (1974), where both positive and negative polarities were recorded. In Frederick's (1999) later work, however, PAN is reported to obtain negative charge. The triboelectric properties of PPS are not widely studied and contradictory reports of positive and negative charge polarity are made by Frederick (1999) and Zhu et al. (2018). PI is studied by only one author included in the comparison: Charlson et al. (1992) reports negative charge polarity.

Table 2-1: Comparison of Triboelectric Series from Literature

Series Position	Frederick (1974)	Adams (1987)	Charlson et al. (1992)	Frederick (1999)	Purchas & Sutherland (2002)	Diaz & Felix-Navarro (2004)	Hutton (2007)	Zhu et al. (2018)
More Positive						PA		
+						Wool		
						Silk		
						Cellulose		
		Asbestos				Cotton		
		Rabbit Fur				PU		
		Glass				Wood		
	Wool felt	Mica				Hard rubber		
	Glass	Human Hair		Wool	Wool	Acetate		
	PA (Nylon, spun)	Nylon		PPS (Ryton)	PA (Nylon 66)	PMMA		Glass
	Cotton	Wool		PA (Nylon)	PA (Nylon 6)	PVA		Human hair
	PAN (Orlon, needled)	Fur		Fiberglass	Silk	PET (Dacron)	Fiberglass	PA (Nylon)
	CTA (Arnel, filament)	Lead		PET (Dacron A)	Cellulose	Natural rubber	Wool	Wool
	PET (Dacron, filament)	Silk		PET (Kodel)	Cotton	PAN	PA (Nylon)	Cat fur
0	PAN (Creslan)	Aluminum	PA (Nylon)	Aramid (Nomex)	PVA	PAN (Orlon)	Viscose	Silk
	PAN (Orlon, spun)	Paper	PMMA	PAN (Orlon)	CTA	PVDC (Saran)	Cotton	Paper
	PET (Dacron, needled)	Cotton	PS	PAN (Dralon-T)	Calcium alginate	PS	Wood pulp	Cotton
	PP	Steel	PP	PTFE (Teflon)	PAN	PVC	PET	Steel
	PET (Kodel)	Wood	PI (Kapton)	ECTFE (Halar)	Cellulose diacetate	PTFE (Teflon)	Acetate	PPS
	PE	Amber	PET	Aramid (Kevlar)	PTFE		PAN	PET
		Sealing Wax	PTFE		PE		PE	PE
		Hard Rubber			PP		PP	PP
		Nickel, Copper			PET		PTFE	Silicon
		Brass, Silver			PBT			PTFE
		Gold, Platinum			Modacrylic			
		Sulphur			Chlorofibre			
		Acetate, Rayon						
		PET						
		PS						
		PAN (Orlon)						
		PVDC (Saran)						
		PU						
		PE						
-		PP						
		PVC						
More Negative		Silicon						
		PTFE (Teflon)						

Abbreviations:
Cellulose triacetate (CTA)
Polybutylene terephthalate (PBT)
Polyethylene (PE)
Polypropylene (PP)
Polyurethane (PU)
Polyvinyl alcohol (PVA)
Polyvinylidene chloride (PVDC)
Polystyrene (PS)
Polyvinyl chloride (PVC)
Ethylene Chlorotrifluoroethylene (ECTFE)

2.4.2.2 CHARGE DISSIPATION

The position of a filtration fabric on a triboelectric series, however, is not the only consideration when characterising the electrostatic properties of a fabric. The charge dissipation rate is a critical factor as it affects the ability of the fabric to be suitably pulse cleaned (Frederick, 1974), as shown by Topkin's (2000) in situ results.

Charge decay depends on the resistance of the flow path to earth, which is affected by various environmental factors as well as the capacitance of the fabrics (Jasti, 2011). While static charging is a surface phenomenon, the nature of needle felt fabrics results in many fibre surfaces being in contact to varying degrees within the fabric volume. Charge may thus dissipate throughout the bulk volume of the fabric, across the fabric surface or directly to the environment (Frederick, 1974). The nature of polymeric fabric charge dissipation is consequently complex and affected to a large degree by the following parameters, which are further discussed below:

- Fabric and polymer characteristics
- Initial generated charge
- Discharge environment

Kazyuta (2013) noted that the charge dissipation rate varies for the same material with different fabric structures. It was observed on PET fabrics that charge dissipated rapidly on smooth, calendared filament type fabric, while PET with a rough surface retained charge longer. While the structure of a fabric has an impact on charge decay, the fibre (or polymer) characteristics are of importance. Through experiments with nylon, cotton, polypropylene and polyester, Jasti (2011) noted a significant correlation between fibre resistivity and charge dissipation. Fibres with low resistivity allowed rapid charge dissipation due to fibres allowing charge to be conducted to surrounding fibres/their environment.

Ieda et al. (1967) noted a significant relationship between initial charge magnitude, or the strength of the applied electric field, and charge dissipation rate through investigations with polyethylene (PE) film. The surface of the PE film was uniformly charged with varying intensities of corona discharge from a screen electrode prior to surface charge decay measurement with an electrometer. For low initial electric field strengths, exponential charge decay was observed. However, for higher initial electric field strengths, the decay no longer fits an exponential curve with considerably more rapid charge dissipation observed, described more accurately by double exponential

decay (Figure 2-10). This observation of initial charge intensity affecting charge dissipation rate of polyethylene was later supported by Zhang et al. (2008).

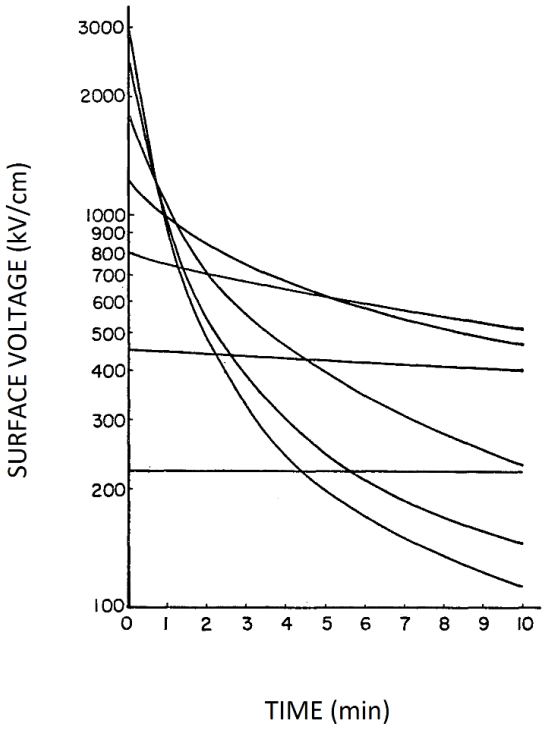

Figure 2-10: Natural logarithmic Curve for discharge of Polyethylene Films (Ieda, et al., 1967)

A major parameter to consider when evaluating discharge characteristics is the environment that the fabric is in. As previously noted, the resistivity, conductivity or dielectric constant of the atmosphere surrounding the materials or contact items impacts the charge dissipation rate (Jonassen, 1998). Pressure has been shown to affect charge decay, with ion desorption occurring more effectively at low pressure, resulting in faster charge decay (Mekishev, et al., 2005). It has further been observed that the volume[14] resistivity of polymers decreases with increasing temperature (Liu, 2010). This observation implies more rapid charge dissipation at higher temperatures as charge is better conducted through the bulk of the fibres in the fabric. This is corroborated by Du and Li (2016) who found that the volume conductivity of heat shrink polymers increases with increasing ambient temperature and consequently charge decays more rapidly. This behaviour was observed regardless of charge polarity. It was, however, observed that negative charges consistently decay more slowly than positive charges.

[14] *Volume resistivity* is the bulk resistivity of a three dimensional volume of a sample, as opposed to the surface resistivity which refers to the resistance to current flow across a surface (Liu, 2010).

The same observation regarding charge dissipation rate and polarity was made by Burgo et al. (2011); however, tests were aimed at investigating polyethylene charge dissipation at increased humidity. A pronounced relationship between increased relative humidity and charge dissipation rate was reported. Similar effects of humidity on polymer triboelectric charge have been reported by many authors (Park, et al., 2008; McCarty & Whitesides, 2008; Liu, 2010; Kazyuta, 2013) after testing various polymeric substances. Humidity is thus a vital environmental factor significantly affecting charge dissipation to atmosphere.

Moisture impacts electrostatic charge decay through both the polymer bulk for hydrophilic polymers and the polymer surface for hydrophobic polymers. Moisture from the atmosphere does, however, settle locally even on hydrophobic polymer surfaces, thereby affecting surface charge decay by providing charge carriers (Jasti, 2011). The marked impact of humidity has also been noted with polymer powder coatings (Sharma, et al., 2003).

Pertinent to charge decay on filtration fabrics, the impact of humidity on fabric surface resistivity and subsequent more rapid charge decay at increased relative humidities (at constant temperature) has been observed by various researchers, including Ramer and Richards (1968) and later Frederick (1974) and Mishra (1982). Furthermore, the high dielectric constant of water has been observed to dampen all electrostatic interaction (Brown & Cox, 2017). Frederick found that at relative humidities below 35%, no significant impact on discharge rate or charge intensity can be observed. Ramer and Richards, however, while reporting the notable impact of humidity on charge decay, noted no impact on initial charge intensity across the range of humidities considered.

2.4.3 POLYMER CHARGING MECHANISMS

At the crux of fabric charging and discharging, lies in the fundamental question of charging mechanism. It is known that when two dissimilar materials, including insulators, come into frictional contact, one adopts an electronegative charge while the other becomes electropositive (Frederick, 1974). The mechanism, through which this occurs, however, is controversial. While it is known that static charging between two metal objects occurs due to the transfer of electrons, there is as of yet no consensus on the charging mechanism between electrically insulating materials such as the polymeric fibres considered in this study.

When considering metal-polymer or polymer-polymer charging, theories suggest that either a transfer of electrons, similar to metal-metal charging, or transfer of ions[15] occurs. The electron exchange theory raises questions because by definition an insulator inhibits electron flow. It has been suggested that a transfer of physical surface material may be the cause. Furthermore, it has been suggested that mechanical stresses introduced during material manufacture breaks the polymer chains to produce free radicals which facilitate electron transfer (Henniker, 1962). No definitive theory has yet been accepted, and it is generally supposed that a combination of these mechanisms, shown in Figure 2-11, is at play (Williams, 2012).

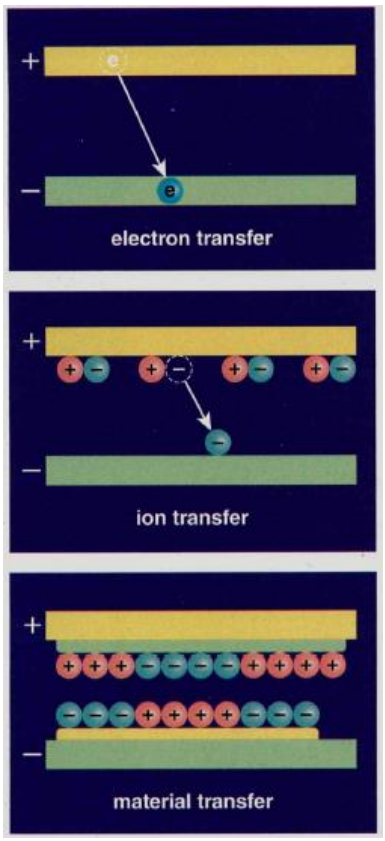

Figure 2-11: Triboelectric charging mechanisms of polymers (Williams, 2012)

Conflicting theories of dielectric polymer charging have been presented by Liu and Bard (2009) and Piperno, et. al. (2012). Liu and Bard suggest that 'cryptoelectrons', defined as electrons existing in a material but with significantly different energies than expected from typical molecular states in the material, on poly methyl methacrylate (PMMA) surfaces are available for redox reactions and may be responsible for PMMA becoming positively charged and PTFE negatively charged after triboelectric contact.

[15] While an electron is a negatively charged subatomic particle, an ion is a charged molecule, atom or polymer fragment that carries either a positive (cation) or negative (anion) charge (Williams, 2012).

Piperno, et. al., however, refute the electron transfer model and suggest that polymer fragments are transferred when two materials are charged by rubbing, resulting in a change in the surfaces' physical properties.

In support of Piperno et. al.'s theory, Burgo et al. (2012) published findings based on experiments with PTFE and PMMA, charged with PE, illustrating the material transfer charging mechanism. It was found that surfaces are not uniformly charged. Both positive and negative charges are present on the surface, forming macroscopic 'charge mosaics'. It was suggested that during frictional contact local high temperatures at the surface contact points causes polymer plasticisation. The shear forces as a result of the relative motion of the surfaces then causes these molecular chains to break, resulting in polymer-fragment free radicals. Due to an imbalance in electronegativity, hydrocarbon free radicals transfer electrons to fluorocarbon free radicals. This tribochemical reaction results in anions and cations being present on the surfaces in varying domains.

These mosaics of random nano-scopic charge regions could explain the counterintuitive triboelectric charging of materials of identical chemical composition. Typical Kelvin probe force micrograph (KPFM)[16] maps of a polymer before and after contact charging, as tested by Baytekin et al. (2011) in order to test the charge mosaic theory are illustrated by Figure 2-12. Through tests with various materials, including PTFE, polydimethylsiloxane (PDMS), silicone, polycarbonate and aluminium, it was found that nano-scopic regions of random charge polarity are formed, independent of charging contact time, pressure and removal speed. Further tests using x-ray photoelectron spectroscopy (XPS)[17] and confocal Raman spectroscopy (CRS)[18] confirmed that material was transferred from one surface to the other during contact electrification. This work again corroborates the earlier study suggesting the theory of material transfer. Consequent chemical changes and resulting electron transfer cause nonhomogeneous surface charge patterns, the average of which results in the nett electrostatic charge of the fabric surface. It is further suggested that this explains the inconsistencies between various researchers' attempts at defining a triboelectric series as it is the fluctuating nano-scopic surface structure of materials that defines triboelectric charging characteristics and not the average surface properties.

[16] *Kelvin probe force microscopy (KPFM)* is a scanning probe microscopy technique that obtains imaging of surface potential with nanometer resolution. This non-contact scanning method measures the electrostatic forces between the sample surface and the probe (Glatzel, et al., 2007).
[17] *X-ray photoelectron spectroscopy (XPS)* is an analysis method used to obtain the elemental composition and chemical state of surfaces (Kratos Analytical Ltd, 2018)
[18] *Confocal Raman spectroscopy (CRS)* is a technique used to identify the molecules present in a sample (Pålsson, 2003).

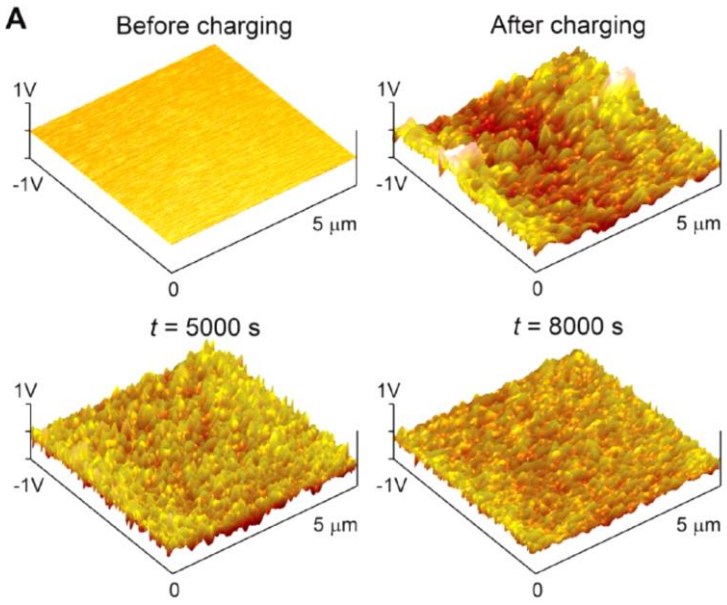

Figure 2-12: Typical KPFM map of polymer surface before charging, after charging and during charge dissipation (Baytekin, et al., 2011)

2.4.4 POLYMER CHARGE AND CHEMICAL STRUCTURE

Understanding polymer charging can be taken a step further. Accepting the theory that nano-scopic charge mosaics form during charging, the question is raised of which materials will charge positively and which negatively based on chemical characteristics. Sakaguchi et al. (2014) completed a study to identify polymers on a triboelectric series based on their chemical composition. Reiterating the theory developed by Baytekin et al. (2011), Piperno et al. (2012) and Burgo et al. (2012), it was found that nano-scopic charge mosaics of opposite polarity are formed on polymer surfaces, with anions and free radicals (HOMO[19]) donating electrons to cations and free radicals (LUMO[20]). The materials can thus be classified as either donors or acceptors, depending on their behaviour during electron transfer.

Free radicals, anions and cations are formed when covalent bonds in polymer chains are broken during the material transfer phenomenon that is observed during frictional contact. Depending on the number of electron paths created, the nett relative polarity of polymers can be theoretically deduced (Sakaguchi, et al., 2014).

Triboelectric charging of polymers is a complex matter, further complicated by the inhomogeneities present in polymer structures, resulting in charging between two

[19] 'HOMO' is an acronym for *Highest Occupied Molecular Orbital* and refers to a molecule's frontier orbital with weakly held electrons, which are easily excitable and available for bonding (Hunt, n.d.).
[20] 'LUMO' is an acronym for *Lowest Unoccupied Molecular Orbital* and is a molecule's frontier orbital with the lowest energy available. The LUMO accepts electrons (Hunt, n.d.).

materials of seemingly identical composition (Williams, 2012). Although various researchers have attempted to further the understanding of the electrostatic properties of polymers, no commonly accepted theories currently exist to conclusively explain the observed phenomena. Furthermore, materials for the specific application of coal ash filtration have not been extensively researched for their beneficial or detrimental electrostatic properties in baghouses.

2.4.5 RESULTS OF PREVIOUS FILTRATION FABRIC ELECTROSTATIC CHARACTERISTIC TESTS

2.4.5.1 PESENDORFER (2014): DISCHARGE RATES OF VARIOUS FILTRATION FABRICS

Previous experiments to develop the characteristic charge polarity of various filter fabrics were carried out by Pesendorfer (2014) (Table 2-2). Note that the reported results are industrial research and have not yet been peer reviewed. Samples were charged by rubbing the filtration side of the fabrics with a PET reference wheel for 5 minutes. Charge was measured immediately after charging ceased and again after discharging for 2 minutes.

The results presented in Table 2-2 are arranged according to triboelectric ranking after initial 5 minutes charging. For materials of interest in this study, it is therefore apparent that, based on this test, PAN and PI were positively charged, while PPS was negatively charged. The relatively high standard deviation of charge dissipation could be due to the importance of environmental factors in fabric discharging. It is possible that humidity, temperature, or other environmental factors may have changed from one test to the next.

Tests were repeated with a slower rotational speed of 100 rpm. Similar initial charge and discharge behaviour was observed for all fabrics except PET, which was observed to be positive (+1.9 kV). This may be due to differences in sample construction and supports Burgo et. al.'s (2012) theory of charge mosaics, as the same material oscillates between relatively low positive and negative charges. The similar behaviour of the other fabrics suggests that charging characteristics are independent of rubbing speed. This theory was corroborated by tests at reference wheel rotational speeds varying between 50 rpm and 300 rpm in 50 rpm intervals. This corresponds with Liu and Seyam's (2013) finding that rotational speed does not affect triboelectric charging of nylon, PTFE or PP.

Table 2-2: Discharge characteristics of filter fabrics – PET reference material, 200rpm charging speed (Pesendorfer, 2014)

Sample type	Average charge after 5 min rubbing (kV)	Average charge after 2 min discharge (kV)	Average charge dissipation (%)
Polyamide-imide (PAI)/PAI	$\bar{x} = +12.7$ $s = 1.6$	$\bar{x} = +11.4$ $s = 0.9$	$\bar{x} = 10.1$ $s = 5.3$
PAN/PAN	$\bar{x} = +9.5$ $s = 1.3$	$\bar{x} = +4.7$ $s = 0.1$	$\bar{x} = 49.4$ $s = 8.3$
PI/PI P84 polyimide	$\bar{x} = +5.4$ $s = 0.4$	$\bar{x} = +2.5$ $s = 1.1$	$\bar{x} = 54.6$ $s = 17.1$
PI/PTFE scrim Yilun polyimide	$\bar{x} = +5.3$ $s = 2.2$	$\bar{x} = +2.4$ $s = 0.7$	$\bar{x} = 49.4$ $s = 12.7$
PET/PET	$\bar{x} = -2.7$ $s = 1.1$	$\bar{x} = -1.7$ $s = 0.8$	$\bar{x} = 39.5$ $s = 4.3$
PTFE/PTFE	$\bar{x} = -14.8$ $s = 3.5$	$\bar{x} = -12.1$ $s = 2.6$	$\bar{x} = 17.2$ $s = 6.9$
PPS/PPS	$\bar{x} = -15.8$ $s = 3.4$	$\bar{x} = -8.8$ $s = 3.3$	$\bar{x} = 45.4$ $s = 10.5$

Test data are also reported where the fabric samples were charged using a reference wheel of the same fabric. Intuitively, as triboelectric charging is a phenomenon that causes opposite charge between dissimilar materials, rubbing with the same material would not be expected to result in electrostatic charging. However, as indicated in Table 2-3, charging does occur. This is possibly due to the fabric construction and potential inclusion of impurities in the polymer, surface treatments or the blended nature of certain materials. The charge polarities match those reported in Table 2-2, with the exception of PAN/PAN, which obtained a marginally negative charge. This charge, however, is insignificant and PAN/PAN can be viewed as being neutral when rubbed on itself. This neutral state may be an indication of fabric purity; however sufficient data are not available to draw conclusions.

Differences in the charge developed on the clean gas and filtration side of the PPS/PI samples is due to the fabric construction. The clean gas surface is made purely of PPS, while the filtration side is a blend of PPS and PI fibres. The surface roughness is also a factor to consider as the filtration surface of the fabric is subject to surface finishes for improved filtration.

Table 2-3: Discharge characteristics of selected filter fabrics charged with various reference materials, 200rpm charging speed (Pesendorfer, 2014)

Sample type	Reference wheel material	Charge after 5 min rubbing (kV)	Charge after 2 min discharge (kV)	Charge dissipation (%)
PPS/PI Filtration surface	PET	1.2	0.16	87
PPS/PI Filtration surface	PPS/PI	3.8	2.8	26
PPS/PI Clean gas surface	PET	-16.0	-10.2	36
PPS/PI Clean gas surface	PPS/PI	-6.1	-3.5	43
PPS/PPS	PPS/PPS	-5.3	-1.4	74
PAN/PAN	PAN/PAN	-0.12	-0.05	58

2.4.5.2 PESENDORFER (2015; 2016): ASH INTERACTION WITH CHARGED FILTRATION FABRICS

Subsequent to the tests establishing discharge characteristics, Pesendorfer expanded on previous findings by comparing fabric samples that had been exposed to dust during charging. The fabric samples were triboelectrically charged by rubbing with a PET wheel on the clean gas surface of the fabric while 0.5 g of dust was applied to the filtration surface of the fabric. Initially, standard test dust Pural NF[21] was used (Pesendorfer, 2015) and later iron oxide (Fe_2O_3) (Pesendorfer, 2016).

Similar observations were made during both test campaigns. Dramatic dust motion was observed on the PPS and PTFE fabrics during charging while the dust appeared not to move on the PI samples during charging. Cross sections of the samples were studied under a microscope to establish the extent of dust penetration caused by triboelectric charging. Cross sections of PI, PPS, PPS/PI, PTFE and PTFE/PI needle felt fabrics after triboelectric charging with Pural NF dust exposure are shown in Figure 2-13. It can be seen that the PPS- and PTFE-based fabrics experience significant dust penetration into the fabric volume while dust penetration on the PI samples is minimal. Results of tests with Fe_2O_3 dust are similar (Figure 2-14).

[21] *Pural NF* is a standard test dust of aluminium oxide (Al_2O_3) with a known particle size distribution and conforms to ISO 11057, VDI 3926-1, GB/T 6719 and ASTM D6830. Pural NF is commonly used for baghouse filter media performance tests (Standard International Group, Ltd., n.d.).

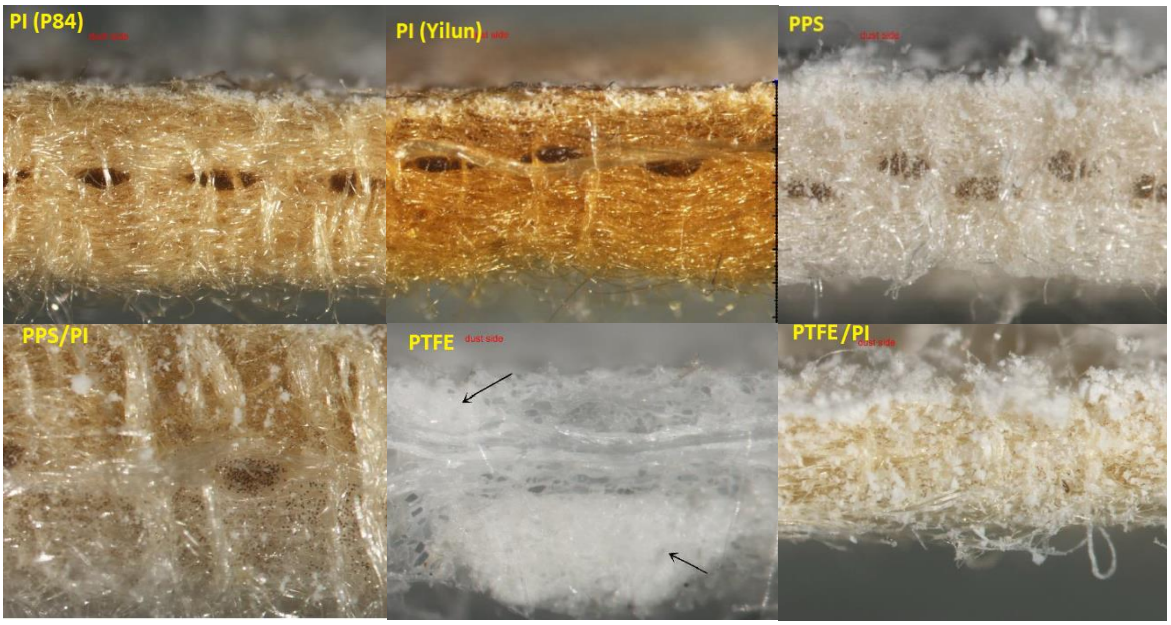

Figure 2-13: Cross sections of triboelectrically charged filtration fabrics exposed to Pural NF dust (Pesendorfer, 2015)

Figure 2-14: Cross sections of triboelectrically charged filtration fabrics exposed to Fe_2O_3 dust (Pesendorfer, 2016)

By comparing the results of Pesendorfer's 2014 study of filtration fabric charge polarity and magnitude to that of the later dust interaction studies, it can be noted that the fabrics that obtained significantly negative charges after triboelectric charging showed the most significant ash penetration through the sample cross sections. Frederick (1974) previously reported that fabrics most distant from particulates in a triboelectric series attract the most particulates.

Although Pesendorfer's industrial studies provide insight into the electrostatic properties of selected filtration fabric samples, the test was not expanded to include fly ash from a coal-fired power station. There thus remains a significant gap in the accepted understanding of the triboelectric properties and ash interactions of filtration fabric.

2.5 CHEMICAL COMPATIBILITY OF FILTRATION FABRICS

2.5.1 FLUE GAS CHEMISTRY

Due to economic factors, coal-fired boilers increasingly rely on variable coal sources. This necessitates flexibility of particulate collection plants and, in the case of a baghouse, the selection of filtration fabric that is suitable for a full range of expected operating conditions (Wu, 2001; Nguyen, et al., 2008; Popovici, 2010).

The nature of the coal burnt and the boiler's combustion process dictate both the flue gas and ash properties, which ultimately affect the baghouse downstream. Apart from the ash (the particulate removed by the baghouse), flue gas contains various gases, including carbon dioxide, carbon monoxide, water vapour and various other chemical components (Zevenhoven & Kilpinen, 2001). Apart from oxygen (O_2) and water vapour, flue gas constituents which are known to be particularly detrimental to filtration fabrics are sulphur oxides (SO_x) and nitrogen oxides (NO_x).

The two main components of SO_x in flue gas are sulphur dioxide (SO_2) and sulphur trioxide (SO_3). For South African coal-fired power stations, SO_x concentrations are typically in the range of 2000 – 3500mg/Nm^3 at 10% O_2 concentration (Govindsamy, 2018; Rampiar, 2018).

SO_2 is the main species. It reacts with excess O_2 in the flue gas stream to form SO_3 as described by (2-4) below (Klotz & Haug, 2006). Excess O_2 may be introduced through ducting leaks or, in the case of low temperature bags, the attemperation system upstream from the baghouse. This conversion is catalysed by the iron oxide content of the fly ash (Marier & Dibbs, 1974; Belo, et al., 2014).

$$2SO_2 + O_2 \rightarrow 2SO_3 \quad \textbf{(2-4)}$$

In combination with water, SO_2 and SO_3 form sulphurous acid (H_2SO_3) and sulphuric acid (H_2SO_4) respectively. Sulphurous acid, however, is rarely experienced in great quantities as SO_2 reacts with O_2 at elevated temperature to form SO_3, which ultimately forms corrosive sulphuric acid, as shown in Equation (2-5). This acid not only attacks the bags but also corrodes the baghouse's metal internals (Klotz & Haug, 2006).

$$SO_3 + H_2O \rightarrow H_2SO_4 \quad \textbf{(2-5)}$$

When selecting suitable filtration fabric, the frequency of fuel oil combustion support must be considered since heavy fuel oil contains significant amounts of sulphur which converts to sulphurous oxides during combustion (Klotz & Haug, 2006).

At the high temperatures present in the coal combustion process, nitrogen molecules from the combustion air splits and combines with oxygen to form nitric oxide (NO) and nitrogen dioxide (NO_2). For South African coal-fired power stations, NO_x concentrations typically range between 750mg/Nm^3 at stations fitted with low-NO_x burners and 1400mg/Nm^3 at stations with traditional firing systems, referenced at 10% O_2 (Rampiar, 2018; Govindsamy, 2018).

Although NO_x is comprised of various species, NO is the most prevalent species present in flue gas, with highly oxidative NO_2 accounting for typically only 5% of the NO_x in coal-fired boiler flue gas (Zevenhoven & Kilpinen, 2001). Excess O_2, however, will increase NO_2 production at low temperature. As cautioned with SO_x above, it is thus important to limit ingress air – and consequent excess O_2 - from ducting leaks and baghouse attemperation systems as far as practicable as the low temperature air introduced will increase NO_2 production.

It is important to note, however, that increased moisture levels in flue gas reduce the oxidative effect of NO_2 (Weber, et al., 1988). This effect is due to its reaction with H_2O at high temperature breaking it down to NO, shown in Equation (2-6) and Equation (2-7).

$$2NO_2 + H_2O \rightarrow HNO_3 + HNO_2 \quad \textbf{(2-6)}$$

At elevated temperature:

$$HNO_2 \rightarrow HNO_3 + 2NO + H_2O \quad \textbf{(2-7)}$$

Note, however, that while oxidative NO_2 is reduced, corrosive nitric acid (HNO_3) is produced.

2.5.2 FLY ASH CHEMISTRY

Fly ash impacts the performance of filtration fabrics in various ways. Morphology, particle size distribution, hygroscopicity and electrostatic properties affect the likelihood of particulate capture and manageable pressure drop. Ash chemical composition affects the ability of the permanent ash cake to neutralise acid in the flue gas (Aleksandrov, et al., 2010).

The elemental analysis of fly ash does not give sufficient indication of the propensity of fly ash for acid neutralisation. Mineralogy must be considered in order to ascertain whether neutralising elements such as calcium oxide are present as free ions available for reaction or in the glassy phase, such as quartz or calcium aluminium silicates, which are less soluble and more abrasive. Furthermore, as mentioned above, the presence of certain metal ions in fly ash, such as Fe^{3+} and Al^{3+}, results in the catalysis of SO_2 to SO_3 and consequent acid formation on the bag surface (Greyling, 1998).

Further considerations include ash abrasiveness, which impacts bag wear. In localised high velocity flue gas areas, abrasive ash will significantly increase bag wear. Ash abrasiveness, which can be characterised by an experimentally determined abrasiveness factor, is a function of particle hardness, density, shape and size. The most abrasive dusts are typically aluminium dust, cement, coke, dolomite and quartz and not necessarily fly ash from coal-fired boilers (Aleksandrov, et al., 2010).

2.5.3 FABRIC TEMPERATURE CLASSIFICATION AND CHEMICAL RESISTANCE

As discussed above, fabric filter bags are expected to perform in typically harsh environments. Flue gas from coal-fired power production contains many chemical constituents, both acidic and alkaline, that may attack the bags. Additionally, flue gas is typically at high temperature. Furthermore, periodic bag cleaning introduces mechanical wear through material flexing. The main bag failure modes therefore include thermal degradation, chemical degradation, mechanical wear and bag blinding (Wedman & Gore, 2010).

A vital aspect to consider when selecting bags for a chosen application is thus the chemical stability of the fibres used in the bags throughout the operating temperature range. Three types of chemical attack can be experienced by bags, namely hydrolytic damage (or acid attack), alkali attack and thermo-oxidative aging. The former occurs when a reduction in operating temperature or cold spots due to baghouse geometry cause the flue gas to dip below the acid dew point. The latter is caused by oxidation due to chemical constituents in the flue gas at high temperature (Rathwallner, 2009).

The properties of three fibre types considered in the present study are compared in Table 2-4. Descriptions available in commercial brochures for the three fibre types described above follow in the subsequent sections. Reported data are, however, not on similar basis and simple comparison is therefore not possible. A comparative baseline is required in order to assess the relative benefits of the fibres for specific applications.

Table 2-4: Comparison of PAN, PPS and PI fibre properties (Mukhopadhyay, 2009; McKenna, 2013)

Material	Maximum Temperature (°C)		Physical Resistance					Chemical Resistance					Relative Price
	Continuous	Maximum surge	Dry heat	Moist heat	Abrasion	Flexing	Hydrolysis	Mineral acids	Organic acids	Alkalis	Oxidising agents	Organic solvents	
PAN	125	140	F	F	F	G	G	G	G	G	G	G	0.4
PPS	190	232	E	E	G	G	E	G	G	G	P	E	1.0
PI	232	260	E	-	G	G	F	G	G	F	-	-	1.7

P = poor, F = fair, G = good, E = excellent

2.5.3.1 PAN: COMMERCIAL INFORMATION

PAN is a low temperature filtration fibre, suitable for applications up to 140°C, above which significant thermal degradation can be expected. It is recommended that operating temperature for continuous operation is maintained below 130°C (AKSA, 2010).

Copolymer PAN is often used for non-industrial textiles. Homopolymer PAN, used for filtration applications, is superior in terms of chemical resistance and temperature stability (Dolan GmbH, 2013). Homopolymer PAN is reported to have good hydrolysis, alkali and acid resistance, with 90% of original strength retained after dipping in 30% sulphuric acid for fifteen hours at 75°C (AKSA, 2010). Common types of homopolymer PAN used specifically in fabric filtration are described in Table 2-5.

Table 2-5: Common PAN fibre types for filtration (AKSA, 2010; Dolan GmbH, 2013)

Tradename	Producer	Fibre shape	Fibre size (dtex)
AKSA-AT200	AKSA (Turkey)	Kidney-shaped	0.9 / 1.7 / 2.2 / 8.2
AKSA-AT203	AKSA (Turkey)	Trilobal	1.7 / 2.2
Dolanit® 12	Dolan (Germany)	Kidney-shaped	0.9 / 1.7 / 2.2 / 8.2

2.5.3.2 PPS: COMMERCIAL INFORMATION

PPS fibre is commonly used for high temperature particulate filtration. It is insusceptible to hydrolysis and suitable for applications where chemical resistance against alkalis, acids and organic solvents is required between operating temperatures of 150°C and 190°C (Toray Industries, Inc, 2018). These characteristics make it an attractive option for coal-fired power utility application where air heater outlet temperatures are high. Furthermore, it is reported that 80% of its strength is retained when dipped in 7% sulphuric acid for two hours at 200°C (Toyobo Co., Ltd., 2005).

Common types of PPS used for fabric filtration applications are described in Table 2-6.

Table 2-6: Common PPS fibre types for filtration (Toyobo Co., Ltd., 2005; Toray Industries, Inc, 2018; EMS-Griltech, 2018)

Tradename	Producer	Fibre shape	Fibre size (dtex)
Procon®	Toyobo (Japan)	Round	2.2 / 3.0 / 7.8
Procon®	Toyobo (Japan)	Trilobal	1.7
Torcon™	Toray (Japan)	Round	1.0 / 2.2 / 7.8
Nexylene®	EMS-Griltech (Switzerland)	Round	1.0 – 14.0

2.5.3.3 PI: COMMERCIAL INFORMATION

PI is classified as a non-flammable fibre for high temperature applications and can be used for filtration applications up to 260°C. Chemical decomposition begins at 450°C. For dipping in sulphuric and nitric acids, each of 10% strength for a hundred hours at 20°C, loss of strength of less than 15% is stated. Good resistance to oxidation and hydrolysis is further reported (Evonik Fibres GmbH, n.d.).

Although Chinese fibres such as Hipolyking Co. Ltd.'s Yilun® exist, the only PI type commonly used for fabric filtration in South African coal-fired power stations is Evonik Industries' P84®. Properties of P84® are described in Table 2-7.

Table 2-7: Common PI fibre for filtration(Evonik Fibres GmbH, n.d.)

Tradename	Producer	Fibre shape	Fibre size (dtex)
P84®	Evonik (Austria)	Multilobal	0.6 / 1.0 / 1.7 / 2.2 / 3.3 / 5.5 / 8.0

2.5.4 CHEMICAL DEGRADATION OF PAN

PAN, as an affordable and readily available material, has enjoyed popularity in low temperature bag filter applications. Little recent work, however, has been published on PAN chemical compatibility with flue gas constituents.

Two major challenges faced by plants employing PAN relate to its requisite lower operating temperature. Low temperature operation often necessitates attemperation air to maintain the inlet temperature of the baghouse at suitably low levels if the upstream boiler process cannot consistently achieve them. Attemperation, in turn, leads to increased volume flow and consequent filtration velocity (which affects pressure drop) but also, pertinently, could lead to cold spots within the flue gas path and consequent operation below the acid dew point, as well as the introduction of excess O_2 and consequent production of oxidative gaseous species (Popovici, 2010). This is particularly problematic for applications where high sulphur coal is burnt. A further problematic item to note is that PAN is prone to shrinkage, which can affect its long term performance (Bowden, et al., 2006).

Shrinkage is due to the instability of the molecules inherently present in PAN filtration fabrics. Since the molecules in the fibres are not all in their equilibrium state, they are vulnerable to the influence of temperature, chemical attack or mechanical load and flexing. To combat this situation, PAN fabric is commonly heat set. As with PPS described in the preceding sub-section, this treatment increases the crystallinity of the material and consequently stabilizes the fibre (Grobbelaar, 2006).

Oxidation by NO_2 has been observed at temperatures above 100°C, which implies that oxidation is a concern at typical operating temperatures (Klotz & Haug, 2006). This is supported by the previous work completed by Weber et al. (1988), investigating the impact of NO_2 and SO_2 on PAN. PAN fibres were exposed to humid air (100 g/m^3 and 150g/m^3 of H_2O were considered) at 125 °C, containing 2000 ppm of SO_2 or 100 ppm of NO_2 for a contact time of five weeks, during which they were periodically examined.

The fibres exposed to NO_2 were observed to darken in colour from pale yellow to dark yellow and eventually brown, with this change accelerated in the lower moisture content tests. After five weeks fibres were black and brittle. Significant deterioration of mechanical strength was also observed and noted to be more marked at the lower moisture content. After five weeks of exposure at the higher moisture content, a decrease in tensile strength of 40% was recorded. At the lower moisture content, however, it became impossible to measure strength after four weeks of exposure when

fibres disintegrated upon touch. After three weeks of exposure at the lower moisture content a 60% decrease in tensile strength was recorded. As previously mentioned, increased moisture reduces the amount on NO_2 available for oxidation. Weber et al. (1988) explains this fibre degradation and discolouration through the use of Fourier-transform infrared spectroscopy (FTIR), which indicated that treatment of PAN with NO_2 lead to new functional groups forming as a result of the cyclisation of nitrile side chains as well as the oxidation of the polymer backbone.

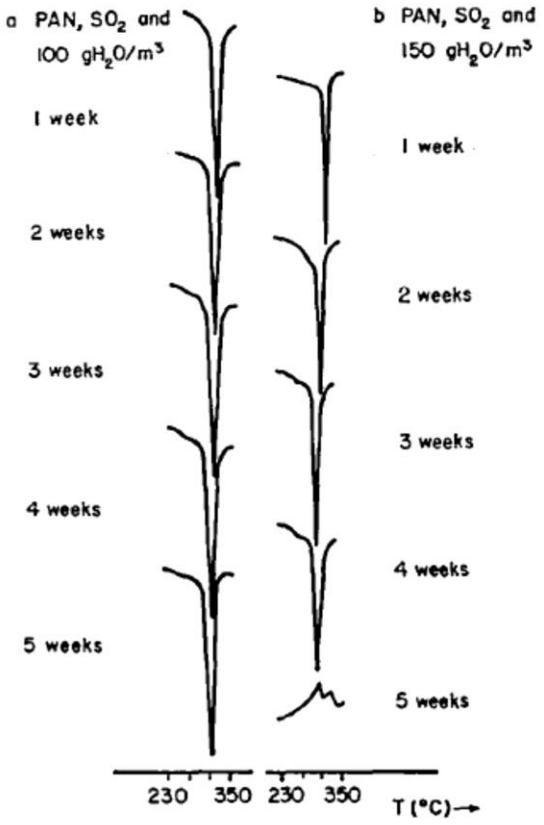

Figure 2-15: DSC thermograms of PAN fibres treated with SO_2 (Weber, et al., 1988)

Weber et al. (1988) observed similar discolouration with treatment of PAN with SO_2. FTIR spectrometry suggests similar degradation mechanisms as described for exposure to NO_2. In contrast to NO_2, however, the higher moisture content caused more rapid degradation when combined with the elevated SO_2 level, due to the onset of hydrolytic attack from the formation of H_2SO_4. Another difference between exposure at the two moisture levels is that at the higher moisture, differential scanning calorimetry (DSC) thermograms reveal that after five weeks the consistently exothermal behaviour of the sample becomes endothermal (Figure 2-15), suggesting that the PAN had degraded/reacted to such an extent as to form a different product.

2.5.5 CHEMICAL DEGRADATION OF PPS

PPS is widely used in filtration applications due to its thermal stability and acid resistant properties. The chemical degradation of PPS and the resistance of PPS to acid attack have been studied by various parties, as discussed below.

A study focusing purely on the thermal decomposition kinetics of PPS found that the thermal decomposition activation energy, established using non-isothermal thermogravimetry, can be used as a key indicator of relative thermal stability of samples from different manufacturers. It was further noted that increasing heating rates resulted in increased initial decomposition temperatures (Deqiang, et al., 2013). While this result is not immediately relatable to the influence of chemical exposure in a baghouse environment, it does present a promising method for targeted analysis and comparison of the fabrics in question.

Cai and Hu (2015) investigated the oxidation of PPS by sulphuric acid (H_2SO_4) by exposing needle felt samples to saturated H_2SO_4 vapour at 90% concentration at varying temperatures. Significant degradation was observed at the various temperatures studied (105°C, 110°C and 130°C). It was found that the degree of oxidative corrosion is increased at higher temperatures, with the melting point and thermal decomposition temperatures, established during TGA and differential thermal analysis, decreasing as temperature increases.

While Cai and Hu's (2015) work provides insight into the chemical degradation of PPS, the high H_2SO_4 concentration makes studying the strength retention impossible as samples were too badly degraded. In practice, lower concentrations of acids in flue gas due to the coal combustion process can be expected. Strength retention, often reported in commercial brochures, is an important factor when analysing bag filter performance as it provides a practical measure of the extent of chemical attack and the likelihood of bag failure. It has been shown that not only temperature, but also exposure time, has an impact on PPS chemical degradation. This can be seen in Table 2-8, where strength retention decreases gradually with prolonged exposure to hydrochloric acid (HCl) and H_2SO_4 and dramatically with prolonged exposure to HNO_3.

Although Table 2-8 indicates that HNO_3 has the most significantly degradative effect on PPS when compared to the other acids studied, the inconsistent concentrations used make this conclusion unconvincing. To this end, Tanthapanichakoon et al. (2006) completed another experiment to establish the strength retention of needle felt PPS at various comparative concentrations of sulphuric, hydrochloric and nitric acids. Samples

were immersed in the diluted acid solutions while maintained at 90°C in an incubator for a set time period. Figure 2-16 summarises the results of this investigation, showing that HNO_3 does indeed have the greatest degradative effect.

Table 2-8: PPS strength retention after short and long term acid exposure at 90°C (Tanthapanichakoon, et al., 2006)

	Strength retention (%)		
	24 hours	**3 months**	**12 months**
37% HCl	72	34	29
10% HNO_3	91	0	0
30% H_2SO_4	94	89	61

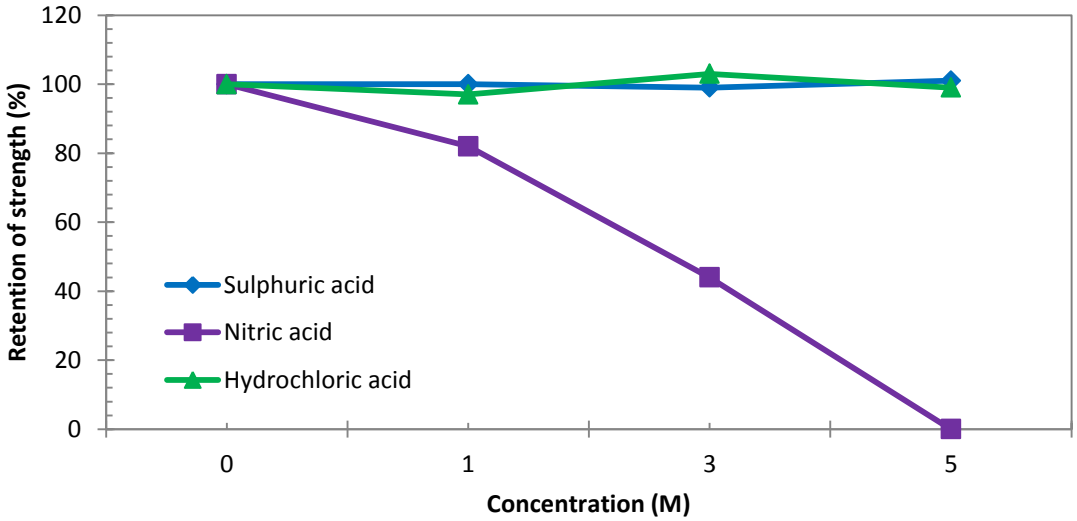

Figure 2-16: PPS strength retention after exposure to various acids at 90°C for 100 hours (adapted from Tanthapanichakoon, et al., 2006)

In order to better understand the degradation mechanisms at play, Tanthapanichakoon et al. (2006) embarked on a further study where PPS needle felt is exposed to known oxidative gases in a temperature controlled test chamber. Samples are exposed to elevated levels of nitric oxide (NO) and oxygen (O_2), as compared to typical operating gas concentrations, at 200°C for 100, 200, 300 and 500 hours. Sample analysis after exposure reveals that the polymer recrystallizes at the high temperatures, which results in fibre shrinkage. Initially, the crystallinity increases due to the annealing effect of the elevated temperature. After the maximum is reached, however, gaseous degradation results in the continued decrease of the crystallinity of the sample, which implies loss of strength (Figure 2-17).

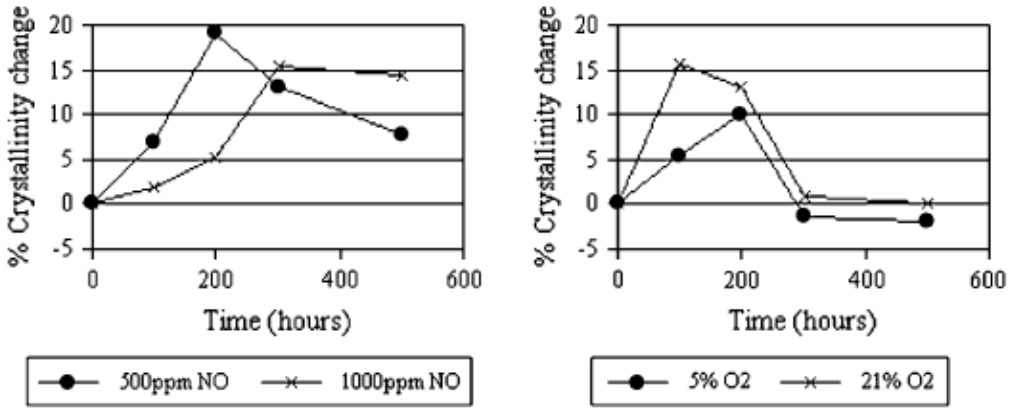

Figure 2-17: PPS crystallinity change with time (Tanthapanichakoon, et al., 2006)

While some level of total mass loss is reported, it is suggested that this is due to the initial vaporisation of impurities and not due to morphological material changes. Fibre strength, however, is affected by the gaseous exposure. Since fabric tensile strength is reliant on two main factors, namely fibre strength and fibre orientation, and fibre orientation is only marginally affected by chemical exposure due to fibre shrinkage, it is concluded that the fibre strength is affected by the gas exposure. During initial exposure the fabric strength increases as a result of the increased crystallinity discussed above. However, at increased test durations, strength began to decrease as crystallinity declined and amorphous polymer regions degraded (Tanthapanichakoon, et al., 2006).

Having suggested an explanation for the strength changes exhibited by the PPS samples due to increasing and decreasing crystallinity, Tanthapanichakoon et al. (2006) stated that NO has a more significant degradative effect than O_2. This is because while exposure to O_2 does accelerate the deterioration process, it also increases the rate of initial crystallinity increase (or annealing process). NO, however, increases only the rate of degradation and has no effect on the initial crystallinity increase. This supports the previous finding during dip tests of the significant strength reduction caused by exposure to HNO_3.

Flue gas from coal combustion is known, however, to contain not only NO but also highly oxidative NO_2. The effect of exposing PPS to NO_2 at different concentrations for varying exposure times and throughout the operational range was studied by Liu et al. (2010). Samples were exposed to mixtures of nitrogen and NO_2 in order to control the concentrations (ranging from moderately elevated at 1000 ppm to highly elevated at 250 000 ppm) in an oven. For constant temperature of 190°C and exposure for 24

hours, it was found that increased NO_2 concentration corresponds to a reduction of material strength retention, although results were significant only above 3000 ppm. Contact time was also found to have a significant impact on strength retention. At a NO_2 concentration of 3000 ppm and temperature of 190°C, a clear trend of strength reduction can be seen as exposure time increases (Figure 2-18). This strength reduction implies that PPS bag life could be significantly reduced should frequent, prolonged operation at high NO_2 levels be experienced.

Liu et al. (2010) drew a further notable conclusion based on PPS tested at an elevated NO_2 concentration of 3000 ppm for 24 hours throughout its operating temperature range (Figure 2-19). It was found that the oxidative effect of NO_2 increases with increasing temperature. This must therefore be taken into consideration for applications where temperature excursions are often experienced. This result is analogous to that found by Tanthapanichakoon et al. (2007) where, in keeping with their previous work, PPS samples were exposed to elevated NO levels. Reduction in strength was noted both with increased temperature as well as increased NO concentration.

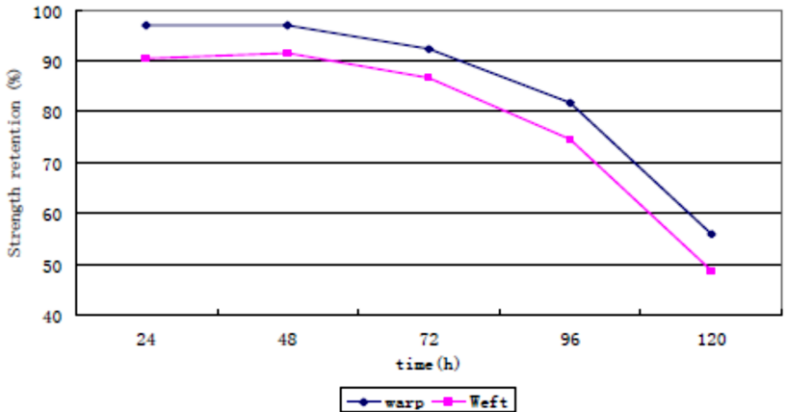

Figure 2-18: Effect of 3000 ppm NO_2 exposure on PPS at 190°C for increasing durations (Liu, et al., 2010)

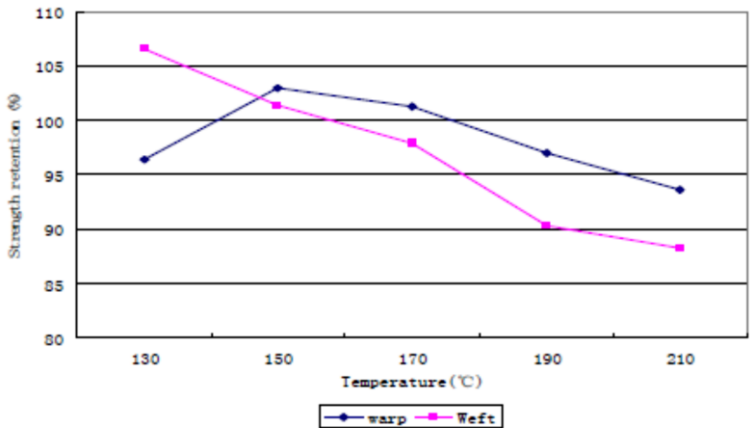

Figure 2-19: Effect of 3000 ppm NO_2 exposure for 24 hours on PPS at various temperatures (Liu, et al., 2010)

Liu et al. (2010) suggests Equation (2-8) as the descriptive model for oxidation of PPS by NO_2. As the reaction occurs, the PPS samples were observed to obtain a brown colour and become brittle as their structure was influenced by the additional oxygen atom.

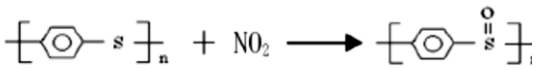

(2-8)

Ozone (O_3) has also been shown to have a degradative effect on PPS. This is of particular interest in applications where an electrostatic precipitator (ESP) is used as a pre-duster prior to the FFP inlet. The corona discharge used to collect ash in the ESP produces O_3 during sparking conditions. At high temperatures, the O_3 reacts with the NO and SO_2 present in the flue gas to produce the more harmful NO_2 and SO_3 species, thereby degrading PPS and causing it to become brittle (Hecen, et al., 2011).

2.5.6 CHEMICAL DEGRADATION OF PI

PI fibre is suitable for very high temperature applications. Its inflammable nature makes it popular for flame-retardant clothing, and widely used in high temperature filtration applications. PI is reported to have superior filtration properties to PPS and PAN, although its chemical compatibility to typical flue gas constituents is not necessarily superior. For this reason, it is often incorporated as a surface layer in bags of PAN or PPS base fabric. For certain applications, PI is used for the entire bag construction, although this is significantly more expensive and only recommended for specific high-efficiency applications where the process conditions are suitable. Process conditions at typical coal-fired power stations are not suitable for the use of 100% PI bags (Popovici, 2010).

Although PI is specified to be suitable for operation at temperatures in the region of 230°C, shrinkage at temperatures of this magnitude has been reported. In an experiment evaluating the performance of very high temperature filter bags in a purpose designed test rig it was found that for operation at 235°C significant shrinkage of the bag length (7.7%) caused substantial baghouse efficiency reduction after operation for five weeks. A temperature reduction to between 200°C and 220°C reduced the shrinkage to 2% after four weeks (Lupión, et al., 2010). This contradicts its typically reported properties of less than 1% thermal shrinkage at 250°C (Weinrotter & Seidl, 1993).

PI has also been observed to be sensitive to hydrolysis at temperatures beyond 140°C. Hydrolysis increases with increasing moisture content. Oxidation by NO_2 has also been experienced (Klotz & Haug, 2006). Furthermore, PI is not suitable for operation in highly alkaline environments (Aleksandrov, et al., 2010).

Davis et al. (1990) investigated the resistance to acid attack by H_2SO_4 of PI and various other fabrics. After immersion in an acid bath of 25% concentration in an oven at 150°C for 75 minutes, it was found that an average of 92.8% strength was retained (where the average considers warp, weft and Mullen burst strength). An apparatus to test the susceptibility of the fabric to fatigue failure was employed to repeatedly flex the fabrics and simulate the repetitive pulse cleaning that they would experience in operation. After a 100 000 load cycles, PI retained 100% of its strength. In order to test whether acid exposure would impact its fatigue resistance, samples were conditioned with acid in the method described above before fatigue loading. Retained strength after subsequent tensile testing was then calculated as a percentage difference from the original strength retained after acid exposure. It was found that fatigue loading after acid exposure caused no further strength reduction, reiterating the insensitivity of PI to fatigue loading. This is a finding of consequence for baghouse application, as the implied result is that if an instance of mild acid attack occurs which does not lead to outright bag failure, continued operation and pulse cleaning will not exacerbate the effect. It must be noted, however, that Davis et al.'s test method does not perfectly replicate baghouse conditions since the acidic environment would be maitained in situ during flexing from pulse cleaning.

Table 2-9: Chemical resistance of PI fibre (Weinrotter & Seidl, 1993)

Chemical	Concentration (%)	Temperature (°C)	Time (hours)	Retained strength (%)
H_2SO_4	5	95	100	55-65
	10	20	100	85-95
	20	50	100	75-85
HNO_3	10	20	100	85-95
	30	20	100	75-85

Weinrotter and Seidl (1993) published further results investigating the resistance of PI to various chemicals; however, exposure time was significantly longer than that considered by Davis et al. The pertinent results for sulphuric and nitric acids are shown in Table 2-9. For nitric acid, it is clear that increasing concentration lowers strength retention. For sulphuric acid, however, the varying of both temperature and

concentration makes drawing conclusions difficult. It can, however, be seen that increasing temperature with acid exposure reduces strength.

2.6 PERFORMANCE OF FABRICS WITH PI BLENDED SURFACE LAYER

As is evident from the preceding sections, each of the fibre types discussed has limitations in terms of chemical compatibility, temperature resistance and fibre properties. In order to combat this and optimise filtration properties, blended fabric compositions are often selected (Mukhopadhyay, 2009; Popovici, 2010).

Advantages of blended fabrics are often not in the area of chemical resistance, but in improved filtration efficiency and pressure drop, as was concluded by Rathwallner (2010). The cleaning efficiency and pressure drop performance of PPS with a PI (specifically P84) surface layer compared to pure PPS and PI samples on a laboratory filtration test rig, conforming to DIN 3926, was presented. Circular felt samples of 15 cm diameter were exposed to air contaminated with Pural NF at a filtration velocity of 0.03 m/s for 10 000 five-second-long cleaning cycles. Samples are described in Table 2-10.

Table 2-10: Filtration test rig sample description (Rathwallner, 2010)

	PPS	**PPS/PI blend**	**PI**
Filtration batt	3 dtex Procon® (singed)	50% 1.7 dtex Procon® 50% 2.2 dtex P84® (singed)	1.0 dtex P84® (singed)
Scrim	Procon®	Procon®	P84®
Inner batt	3 dtex Procon®	3 dtex Procon®	2.2 dtex P84®
Weight per area (g/m^2)	550	480	500

A comparison of the dust emitted through the fabric samples at certain intervals is shown in Figure 2-20. It can be seen that the blended fabric and PI fabric present improved collection efficiency compared to the PPS fabric. It was further found that PI and the blended PPS/PI sample develop pressure drop more slowly than the PPS sample. This may be due to factors such as fibre morphology and electrostatic properties. The practical application of this result is that bags would require less frequent pulsing. Note, however, that the test environment does not consider any chemical aggressors.

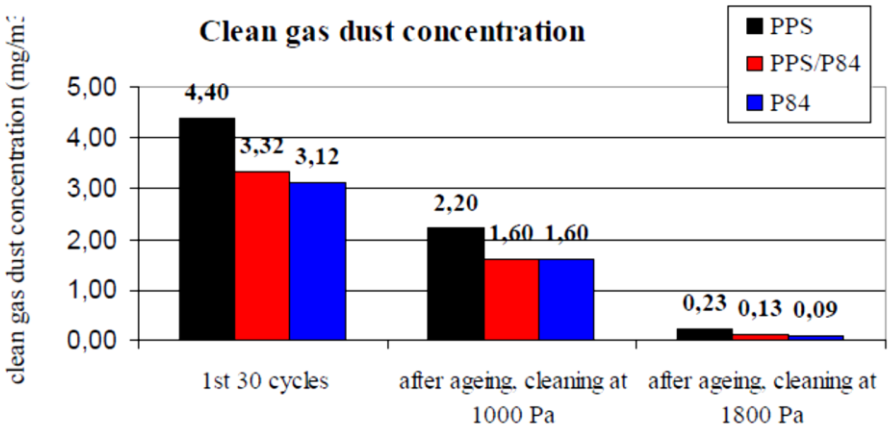

Figure 2-20: PPS, P84 and PPS/P84 test rig emissions (Rathwallner, 2010)

Clayton (2006) reported similar results when comparing filtration fabrics on a VDI/DIN 3926 test rig. Compared to 100% PPS, the Optivel® fabric, which incorporates a blend of PI fibres in the surface of a PPS bag, showed lower residual pressure drop and emissions.

2.7 BAGHOUSE COST-BENEFIT ANALYSES

2.7.1 COST-BENEFIT ANALYSIS BACKGROUND

From the discussion above, it can be seen that appropriate filtration fabric selection is paramount to baghouse function. It affects not only particulate emissions reduction efficiency, but is a major cost driver, as discussed in Section 1.2.2.

Cost-benefit analyses (CBA) are valuable tools for understanding the complete cost impact of technology options. Different approaches to completing a CBA can be taken depending on the goal of the analysis. Differing levels of complexity can be used to evaluate the economic feasibility of different options, investigate cash flow throughout project lifetime or gauge the economic feasibility of a specific project (Lauer, 2008). Typically, capital and operational costs are considered. Costs are reflected on a consistent basis, such as the net present value (Department of Environmental Affairs and Tourism, 2004).

Apart from the purely technical investment costs, there is a trend towards including environmental and health costs in CBAs for projects and scenarios with environmental impacts. These costs, however, are not easily defined and can vary widely between applications (Department of Environmental Affairs and Tourism, 2004; Sterner & Persson, 2008; Mirasgedis, et al., 2008; Farber, 2009).

Approaches for conducting baghouse sizing and the associated costing methods have been presented (Turner, et al., 1987; Turner, et al., 2002). As described below, these methods include ways to calculate financial factors that are used to estimate capital recovery for a baghouse during its expected life and bags at their expected lives. While these methods are adequate for use when embarking on a baghouse construction project, they have major limitations when comparing filtration fabric options since only the initial investment cost for the bags is considered.

2.7.2 TRADITIONAL BAG COST-BENEFIT ANALYSIS APPROACH

Traditional baghouse CBAs focus on overall baghouse costs where bag selection has already been made. Electricity consumption by the ID fan as a result of pressure drop caused by the bags is assumed to be constant for all bag types and included only when making a technology selection between particulate emissions reduction methods (Turner, et al., 1987). Where bag costs are to be included, Turner et al. (1987; 2002) recommends using a method to determine the annualised cost of the selected bags. Annualised bag cost, or capital recovery cost, can be calculated according to Equation (2-9), included in the United States Environmental Protection Agency Air Pollution Control Cost Manual (Turner, et al., 2002).

$$C_{BA} = C_B \times F_{CR} \quad \textbf{(2-9)}$$

where:

C_{BA} = annual bag cost (R/year)
C_B = initial bag cost (R)
F_{CR} = capital recovery factor

The capital recovery factor is a function of the bag life and applicable interest rate for the time period under consideration. It can be calculated according to Equation (2-10) (Turner, et al., 2002).

$$F_{CR} = \frac{i(1+i)^{n_b}}{(1+i)^{n_b}-1} \quad \textbf{(2-10)}$$

where:

i = interest rate (%)
n_b = bag life (years)

The method suggested above is suitable when only the capital costs associated with bag purchase are considered and expected bag life can be accurately estimated. It is, however, limited in terms of including costs associated with early bag failure such as potential production losses and emissions excursions. Furthermore, it does not allow for comparative analysis of bag options unless differences in bag life are definitely known.

2.8 SUMMARY OF REVIEWED LITERATURE

It is clear from the reviewed literature that appropriate bag selection is paramount to economically viable bag life as well as formation of a stable ash cake for filtration efficiency and maintaining appropriate pressure drop.

Studies of the triboelectric effects present in baghouse filtration indicate that the electrostatic interactions between the fibres and the ash play a significant role in stable ash cake formation. Industrial research using dust on charged fabric samples further indicates that undesirable electrostatic interactions can lead to bag blinding. Polymer triboelectric phenomena in general, however, are not well understood. The triboelectric properties of filtration fabrics for baghouse applications, specifically, have not been widely studied.

Appropriate chemical resistance of filtration fabrics is essential for prolonged bag life. While literature exists describing the chemical compatibility of the fabrics considered, results are not on a consistent basis and comparative conclusions regarding the suitability of filtration fabrics for specific applications can therefore not be drawn.

Existing methods for estimating bag costs are suited to inclusion in feasibility studies of baghouse construction projects. The recommended CBA method for bags neglects the cost impacts associated with electrostatic and chemical suitability of the selected filtration fabric. There is therefore scope for the development of an alternative, all-encompassing CBA method, suitable for comparing filtration fabric prior to purchasing bags for an existing baghouse or well defined baghouse project.

CHAPTER 3: TRIBOELECTRIC BEHAVIOUR OF PAN, PPS AND PI FILTRATION FABRICS

3.1 INTRODUCTION

In this chapter, the results of a series of electrostatic and triboelectric evaluations and the discussion thereof are presented. As discussed in Chapter 2, the existence and impact of electrostatic phenomena in fabric filtration is largely anecdotal. The impact on filtration efficiency and pressure drop, however, is known to affect baghouse operation. The results of the experiments described in this chapter investigate the triboelectric properties of fabrics commonly used for flue gas filtration in coal-fired power station baghouses. Better appreciation of these fabric properties will enable further targeted research into filtration applications.

3.2 MATERIALS AND METHODS

Experimental procedures and sample descriptions for results reported in this chapter are described below.

3.2.1 GENERAL DESCRIPTION OF NEEDLE FELT FABRIC SAMPLES

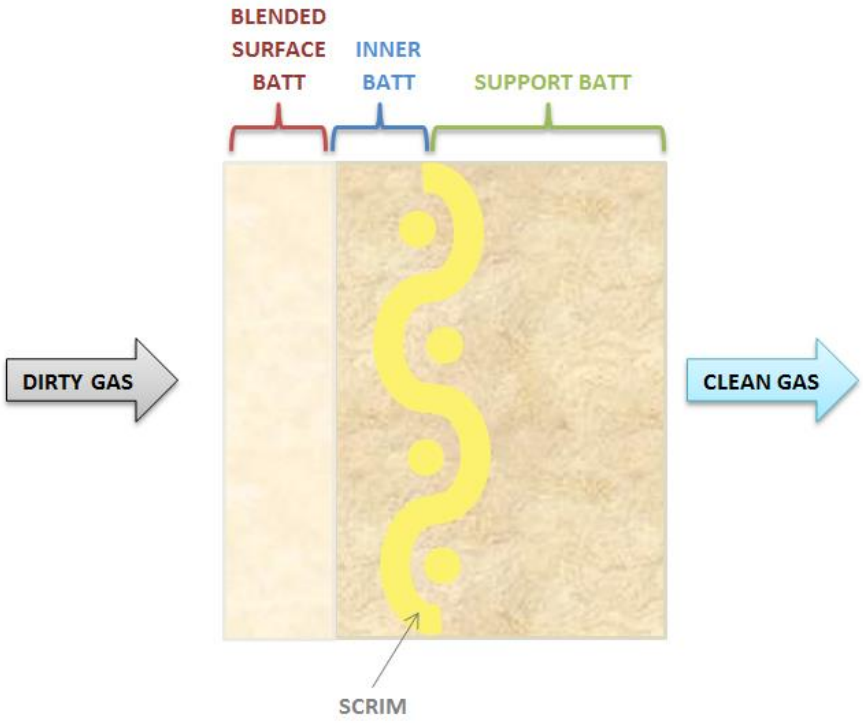

Figure 3-1: Indicative cross-sectional illustration of layered needle felt fabric construction

The fabrics considered in this study are of the layered type, illustrated in Figure 3-1. In subsequent sections, samples are described in the format Material A/Material B. Note that “clean gas” refers to filtered flue gas. This flue gas will still contain gaseous emissions and reduced levels of PM emissions.

For all samples considered, Material A refers to the base material. This material is used for the support batt, woven scrim, inner batt and as part of the possibly blended surface batt. Although the polymer type remains constant, fibre size and shape may vary between layers. The surface batt often uses fibres of a finer size than the other material layers. Material B is used only as a portion of the blended surface batt, in combination with the base material. Therefore, where PI is incorporated in the filtration fabrics, the base material constitutes the bulk of the fabric, with only a minor portion of PI incorporated in the blended surface batt.

3.2.2 TRIBOELECTRIC FILTRATION FABRIC SAMPLES

Five materials, described according to the convention defined in Section 3.2.1, were considered for all triboelectric tests. Needle felt fabric samples were cut to 400 mm long by 80 mm wide test specimens in order to fit appropriately on the test apparatus described in Section 3.2.4 and Section 3.2.5. A description of the samples is given in Table 3-1 and the unexposed samples, prior to testing, are shown in Figure 3-2.

Table 3-1: Triboelectric needle felt fabric sample description

Material	Fabric supplier	Fibre type	Scrim	Filtration Surface Batt	Inner Batt	Support Batt
PAN/PAN	Beier Envirotech	Dolanit®	2.2 dtex PAN	1.7 dtex kidney shaped PAN	2.2 dtex kidney shaped PAN	2.2 dtex kidney shaped PAN
PAN/PI	Beier Envirotech	Dolanit®/P84®	2.2 dtex PAN	1.7 dtex kidney shaped PAN / 1.7 dtex multilobal PI	2.2 dtex kidney shaped PAN	2.2 dtex kidney shaped PAN
PPS/PPS	Beier Envirotech	Procon®	2.2 dtex PPS	1.7 dtex trilobal PPS	2.2 dtex round PPS	2.2 dtex round PPS
PPS/PI	Beier Envirotech	Procon®/P84®	2.2 dtex PPS	1.7 dtex trilobal PPS / 1.7 dtex multilobal PI	2.2 dtex round PPS	2.2 dtex round PPS
PI/PI	BWF	P84®	2.2 dtex PI	2.2 dtex multilobal PI with PTFE coating	2.2 dtex multilobal PI	2.2 dtex multilobal PI

Note that Dolanit® is homopolymer PAN, produced by Dolan GmbH. Procon® and P84® are produced by Evonik Fibres GmbH.

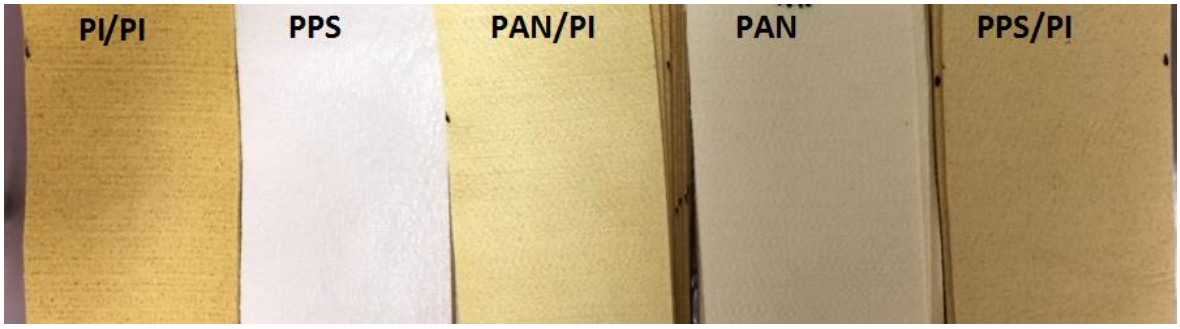

Figure 3-2: Fabric samples used for triboelectric tests

Samples were selected to be representative of the types of filtration fabrics commonly used in baghouses at South African coal-fired power stations (Patel, 2016). Low temperature and high temperature fabrics were considered. The exception is the PI/PI fabric which was included in order to establish which triboelectric effects are due purely to PI when used in a blend with PAN or PPS, and is not considered suitable for use in South African coal-fired baghouses (Popovici, 2010).

3.2.3 DUST SAMPLE DESCRIPTION AND PREPARATION

In order to investigate the electrostatic interaction of the charged fabric samples with ash, three types of dust were used. These are described in Table 3-2.

Table 3-2: Dust sample description

Dust description	Dust type	Sample origin	Typical particle size distribution (d_{50})
Pural® NF	Boehmite. Standard filter test dust.	Supplied by Sasol Germany GmbH	15 µm
Power Station A Ash	Highveld coal field opencast bituminous coal fly ash.	Isokinetically sampled at a power station in Mpumalanga, South Africa.	14 µm
Power Station B Ash	Waterberg coal field underground bituminous coal fly ash.	Isokinetically sampled at a power station in Limpopo, South Africa.	35 µm

The samples were chosen to investigation of a range of dust types. Pural® NF is a standard test dust commonly used in laboratory particulate filtration tests. Power Station A ash and Power Station B ash represent different fly ash types commonly found at South African coal-fired power stations. Ash from combustion of Highveld coal is known to differ from ash produced from Waterberg coal. This is in terms of elemental composition as well as particle size distribution. Furthermore, the Power Station A ash is from an open cast mined source and the Power Station B ash from an underground mined source.

3.2.3.1 ASH SAMPLE PREPARATION METHODS

Three methods of ash sample preparation were employed in order to ensure the representativeness of the samples. These methods are described below (Bumiller, 2012):

1. **Grab sampling**. A sample is removed from the larger batch with a spatula or suitable tool. This method is only suitable for narrow particle distributions.

2. **Coning and quartering**. A small batch mixed sample is placed on a flat surface and divided into quarters using a ruler. Two diagonal sections are discarded and the remaining two reformed. The process is repeated until the desired sample size is reached. This method is depicted in Figure 3-3.

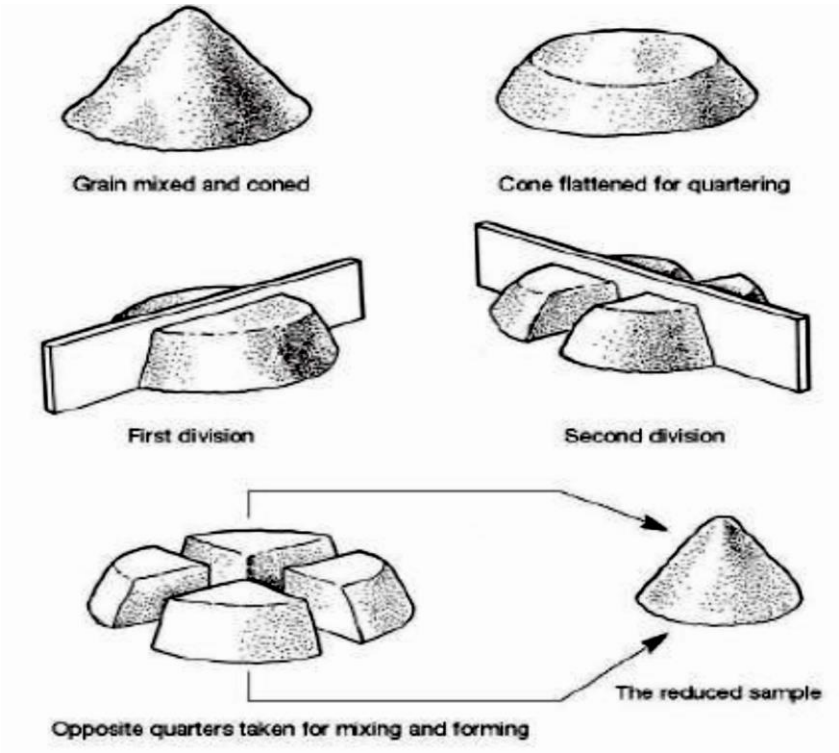

Figure 3-3: Coning and quartering ash sample preparation method (Bumiller, 2012)

3. **Chute riffle sampling**. A batch sample is divided into two by a series of vanes. This process is repeated until the desired sample size is reached. The large and small chute riffle samplers used to prepare the ash samples in this study can be seen in Figure 3-4.

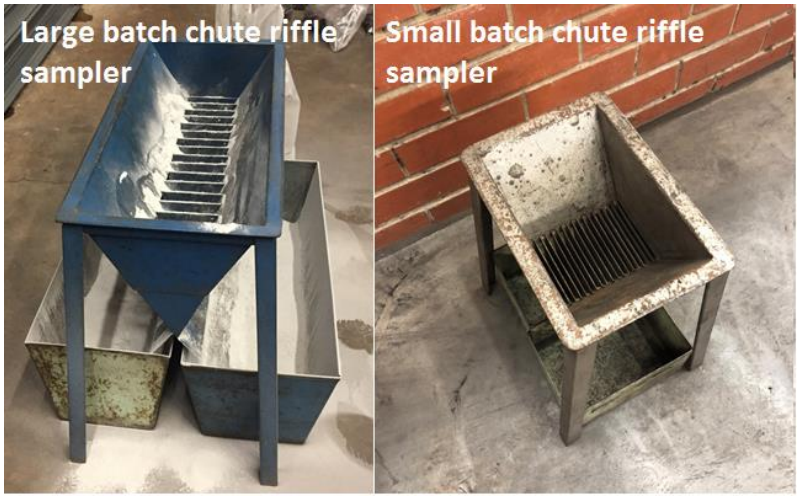

Figure 3-4: Large and small batch chute riffle samplers

3.2.3.2 PURAL® NF

Pural® NF is a standard filter test dust commonly used in particulate emissions reduction tests. It conforms to ISO 112057, VDI 3926-1, GB/T 6719 and ASTM D6830. The chemical composition reported by the Pural NF data sheet is described in Table 3-3.

Table 3-3: Typical Pural™ NF elemental analysis (Sasol, 2003)

Chemical constituent	Composition (wt %)
Al_2O_3	77
Na_2O	0.002
SiO_2	0.01 - 0.015
Fe_2O_3	0.005 – 0.015
TiO_2	0.01 – 0.20

An initial grab sample of approximately 20 g of Pural NF was taken from a 32 kg storage drum (lot number 686). Since the Pural NF is of standard particle distribution and composition, a grab sample posed low risk of poor representativeness. The coning and quartering method, described in Section 3.2.3.1, was used to reduce the initial sample to 0.5 g samples for the ash interaction tests.

3.2.3.3 POWER STATION ASH

The power station ash samples were isokinetically sampled by means of CEGRIT[22] samplers. The elemental composition of the ash, determined from X-ray fluorescence (XRF) analysis and normalised to 100%, is described in Table 3-4.

Table 3-4: Power station ash elemental analysis

Elemental analysis	Normalised Composition (%)	
	Power Station A	**Power Station B**
Al	16,89	14,82
Ba	0,38	0,21
Ca	12,79	3,84
Cr	0,03	0,02
Fe	3,56	6,12
K	0,95	0,89
Mg	2,56	1,36
Mn	0,07	0,20
Na	0,13	0,05
P	0,21	0,09
S	0,54	0,61
Si	59,25	70,00
Sr	0,42	0,06
Ti	2,08	1,54
V	0,01	0,02
Zn	0,00	0,04
Zr	0,12	0,11
Total (%)	100	100

The initial approximately 5 kg bulk sample was riffled down to a 1 kg sample for testing and the remaining sample archived. The 1 kg sample was then divided using the quartering and coning method until reduced to 0.5 g samples for ash interaction tests. The archived sample was further riffled to a 200 g sample for XRF analysis. This method is described in Section 3.2.3.1.

From Table 3-4 it can be seen that Power Station A ash and Power Station B ash differ in terms of composition. Both consist mainly of silicone, as opposed to aluminium based Pural NF® dust. Power Station B ash, however, has higher silicone composition

[22] A CEGRIT fly ash sampler is an isokinetic ash sampling device. It is installed prior to the flue gas side of the air heaters at the power stations in question. The ash is therefore not contaminated by the SO_3 injection system that may be installed at stations with ESPs.

than Power Station A ash. The second most prevalent element in both ashes is aluminium, followed by calcium. Power Station A ash, however, has higher calcium constitution than Power Station B ash.

3.2.4 FABRIC TRIBOELECTRIC CHARACTERISATION TEST METHOD

Triboelectric test apparatus, shown in Figure 3-5, was used to electrostatically charge the filtration fabric samples by rubbing on a reference material. Tests were repeated on four clean, untested samples for each measurement.

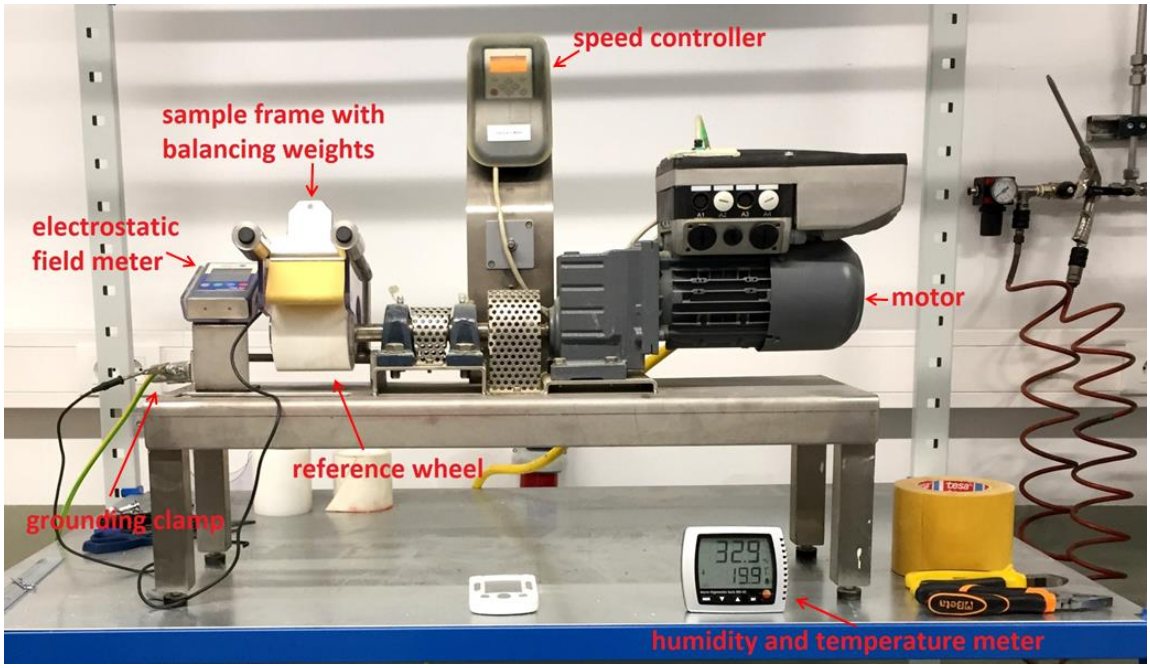

Figure 3-5: Triboelectric test apparatus for fabric discharge characteristics

PET was chosen as the reference material covering the reference wheel used for triboelectric rubbing. This is based on the approximate neutrality of PET on the triboelectric series (Frederick, 1974; Frederick, 1999; Diaz & Felix-Navarro, 2004). Previous studies of electrostatic charge development on filtration fabrics by Topkin (2000) and Pesendorfer (2014; 2015; 2016) also used PET as the reference material. Consequently, the use of PET in the current experiments facilitates comparison of results. The reference wheel itself is made of polyamide (PA) due to the low frictional coefficient between the wheel and shaft.

While PET is used for baseline tests, the wheel was also covered in PAN, PPS and PI fabric in subsequent tests to investigate the electrostatic behaviour of the fabrics when rubbed on themselves.

The electrostatic charge magnitude and polarity is measured using a Simco FMX-003 portable electrostatic field meter with a range of ±22 kV.

The test procedure, adapted from that suggested by Frederick (1996), is described below, with reference to Figure 3-5. Frederick suggested establishing discharge rate based only on an initial charge measurement after five minutes of rubbing and a single charge measurement after two minutes of discharging. This calculation, described by Equation (3-1) (Frederick, 1996), was used for establishing the discharge rate in this study. The discharge measurement frequency, however, was increased in order to better understand the incremental discharge characteristics of the fabrics.

$$\mathrm{dC} = 100 \times \frac{C_i - C_f}{C_i} \qquad \textbf{(3-1)}$$

where:

dC = discharge rate (%)
C_i = initial charge potential after rubbing for 5 minutes (kV)
C_f = charge potential after discharging for 2 minutes (kV)

Prior to testing, a clean sample of the reference material was firmly affixed to the reference wheel and the wheel mounted onto the motor shaft. Test samples, described in Section 3.2.2, of 400 mm length and 800 mm width were prepared. For each test, a fabric sample was secured to the sample frame using the grounded clamps. The sample frame was equipped with balancing weights to ensure even contact force during charging. Prior to each test, it was confirmed that the triboelectric test apparatus was suitably grounded using the grounding clamp. Grounding of the apparatus is important to avoid charge build up which may influence measurement of results.

The grounded electrostatic field meter was zeroed and latent fabric charged dissipated using either the grounding clamp or hands. The sample in the sample frame was then placed a fixed distance of 25 mm from the field meter using the locating pin and the initial fabric charge recorded. The locating pin was then removed and the sample frame placed onto the reference wheel, positioned as shown in Figure 3-5, with the sample

centred on the wheel. The ambient temperature and humidity in the room were recorded.

The speed controller was set at 200 rpm and the motor switched on in order to charge the samples for 5 minutes. After charging, the sample frame was immediately slid into the electrostatic field meter reading position, taking care not to touch the sample or allow any loose fibres to touch the test apparatus as this may cause discharge. The initial electrostatic field reading was recorded and subsequent readings taken at 30 second intervals for 3 minutes.

3.2.5 CHARGED FABRIC AND DUST INTERACTION TEST METHOD

This experiment investigated the interaction of ash with fabric samples during fabric charging. Three repeats of each experiment were carried out on clean, untested samples.

The test apparatus described in Section 3.2.4 was modified to use a different sample frame that kept the Simco FMX-003 electrostatic field meter in a fixed position above the surface of the fabric sample, which is exposed to ash. The fabric sample was charged on the clean gas surface by means of the reference material covered PA wheel. PET was used as the reference material for all dust interaction tests. The modified apparatus is shown in Figure 3-6. The experimental procedure, with reference to Figure 3-6, is described below.

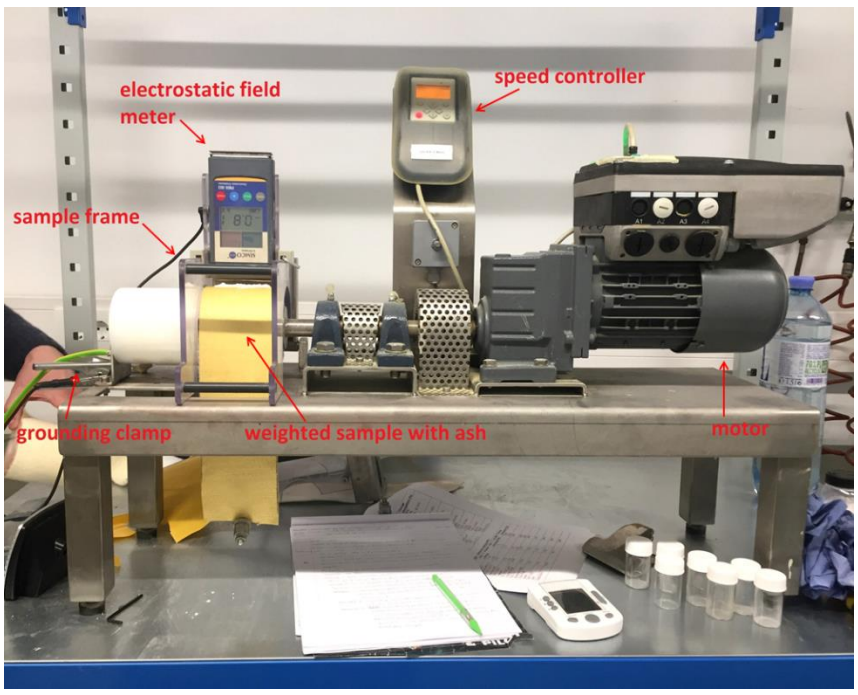

Figure 3-6: Triboelectric test apparatus for fabric and dust interaction

The reference wheel was covered in the reference material and mounted onto the motor shaft. A 400 mm length and 80 mm wide fabric sample, as described in Section 3.2.2., was secured to the top of the sample frame using an insulated clamp and the bottom of the sample placed over the reference wheel and weighted in order to allow even contact force during charging.

The electrostatic field meter was then secured in place, zeroed and grounded to the test apparatus using a crocodile clamp. The test apparatus was grounded and latent charge on the fabric and frame dissipated. 0.5 g of the selected dust was then placed on the sample at the area where it contacted the reference wheel, shown in Figure 3-7.

Figure 3-7: Dust on triboelectric sample in sample frame

After recording the ambient temperature and humidity in the laboratory, the fabric was charged for 5 minutes at 200 rpm. Any ash motion observed during charging was recorded. After charging, the samples were carefully removed from the frame so as not to disturb the ash on the sample surface. Optical microscopy analysis was performed using a Nikon SMZ1000 Stereoscopic Zoom Microscope capable of 10 – 80 times magnification.

3.3 TRIBOELECTRIC CHARACTERISATION OF FILTRATION FABRIC

The results of the discharging experiments described in Section 3.2.4 are subsequently discussed. Results represent the average of four tests. Details of all tests are included in Appendix A.

3.3.1 CHARGING CHARACTERISTICS

The initial charge magnitude of the fabric samples after rubbing were ranked in a triboelectric series in terms of polarity and magnitude, shown in Figure 3-8. This ranking allows comparison of the relative triboelectric potential of all considered fabrics. Clean gas and filtration surfaces are considered separately due to the differing compositions and constructions of the fabric surfaces, discussed in Section 3.2.1.

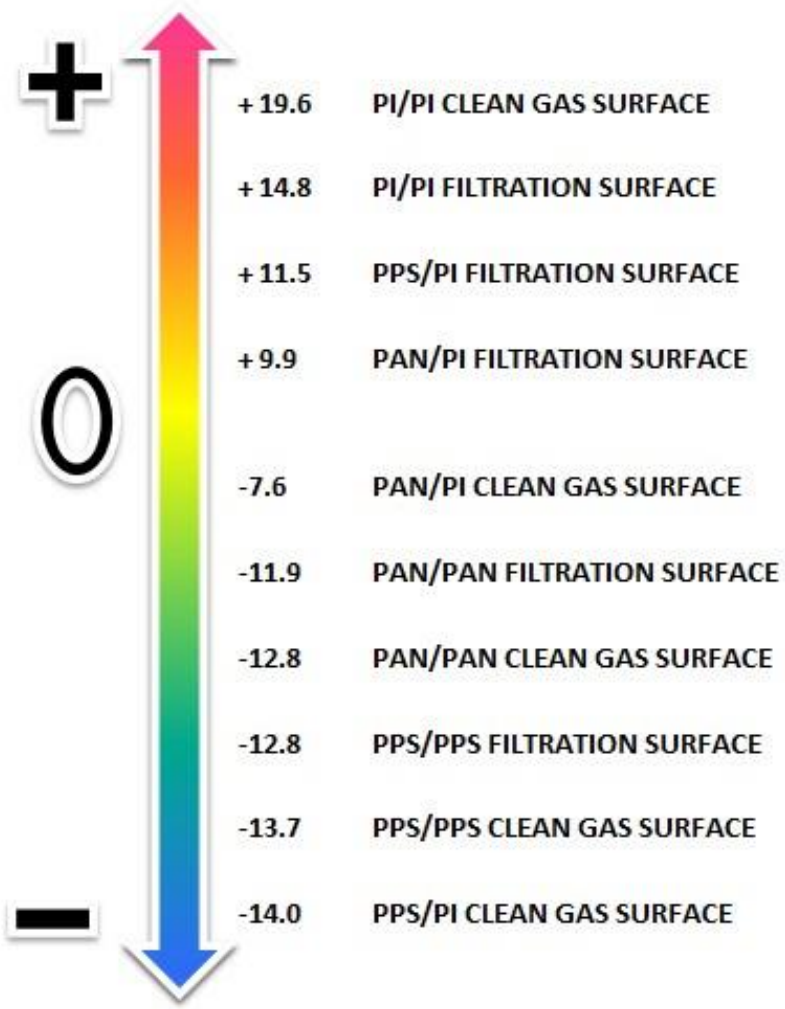

Figure 3-8: Triboelectric series of selected filtration fabrics including average charge magnitude

From the data reported in Figure 3-8 it is apparent that for the fabrics studied, PPS becomes significantly electronegative after triboelectric contact, as does PAN to a lesser extent. PI becomes significantly electropositive. Furthermore, PI dominates charging behaviour when used in a blend with PAN or PPS.

The fabric obtaining the most significant negative charge is the PPS/PI clean gas side, which is 100% PPS, with the PI blend only present on the filtration side surface. It is suggested that this may be due to electrostatic interactions within the fabric volume. Electrostatic theory suggests that the charge generated between dissimilar materials is more intense for materials occupying distant positions on the triboelectric series (Frederick, 1974). Therefore, contact between the highly electronegative PPS and highly electropositive PI in the blended filtration surface layer could result in charge generation between the dissimilar materials in contact. This could result in amplified electron flow to the pure PPS clean gas surface.

It can also be seen that for all fabrics considered the charge magnitude of the clean gas side is greater than the filtration side. This observation supports Frederick's (1974) and later Kazyuta's (2013) observation of the influence of fabric surface roughness on charge magnitude since the clean gas side is significantly more fibrous than the finished filtration side. The selected surface treatment of the filtration surface of filtration fabrics may therefore hold implications for electrostatic phenomena in operational baghouses.

As discussed in Chapter 2, no definitive triboelectric series for polymers has been agreed upon. Although similar results have been reported for some materials, authors differ significantly on a consolidated ranking (Table 2-1). Analysis of the detailed data for all specimens reported in Appendix A reveals a possible reason for this disparity: although polarity is consistent, the standard deviation of charge magnitude between individual samples is large (Table A-1). This large deviation corroborates the statements of the general irreproducibility of triboelectric experiments on polymers made by Charlson et al. (1992), Diaz & Felix-Navarro (2004) and Hutton (2007).

Behaviour that is constant throughout all tests in this study, however, is the polarity of the fabrics. Therefore, although charge magnitudes vary on an individual sample basis, there is confidence in the average relative rankings of filtration fabrics commonly used in South African power plants, as reported in the triboelectric series above.

The polarities recorded after triboelectric charging in this study are compared to those reported in literature in Table 3-5. It can be seen that PAN has been reported to be

positive, negative and neutral. Adams (1987), Frederick (1999), Purchas & Sutherland (2002) and Hutton (2007), however, support the finding of this study that PAN obtains negative polarity. Similarly, PPS has been reported to be both negative and positive. Frederick (1999) findings corroborate the findings of this study, showing the negative polarity of PPS. PI is not extensively studied; however Charlson et al.'s (1992) finding of the negative polarity of PI contradicts the findings of this study. Charge intensity has not been widely reported and is thus not compared.

Table 3-5: Comparison of triboelectric charge polarities of selected fabrics with that reported in literature

	Frederick (1974)	Adams (1987)	Charlson et al. (1992)	Frederick (1999)	Purchas & Sutherland (2002)	Diaz & Felix-Navarro (2004)	Hutton (2007)	Zhu et al. (2018)	This Study
Positive	PAN			PPS					PI
Neutral						PAN			PAN
Negative	PAN	PAN	PI	PAN	PAN		PAN	PPS	PPS

The variance between results reported by the authors mentioned above can be ascribed to variances in test environment and procedure. For the same reason, reliable comparison of the results reported in this study to those in Table 3-5 is problematic. Direct comparison of the results found in this study to the industrial results reported by Pesendorfer (2014) is, however, possible since the same test apparatus described in Section 3.2 was used to perform the experiments, although in a different laboratory. Blended fabrics were not tested by Pesendorfer; however the polarity and charge intensity of PAN/PAN, PPS/PPS and PI/PI filtration surfaces are compared to the results of this study in Table 3-6.

Table 3-6: Comparison of selected filtration fabric triboelectric behaviour: Pesendorfer (2014) vs this study

	Pesendorfer (2014)		Present Study	
Sample type	**Average charge after 5 minutes rubbing (kV)**	**Standard deviation (kV)**	**Average charge after 5 minutes rubbing (kV)**	**Standard deviation (kV)**
PAN/PAN	+9.5	1.3	-11.9	4.7
PPS/PPS	-15.8	3.4	-12.8	1.3
PI/PI	+5.4	0.4	+14.8	3.4

It can be seen that both studies found PPS to exhibit highly negative polarity. Both studies further found that PI exhibits positive polarity; however, Pesendorfer reported significantly lower charge intensity than that found in this study. This study therefore retested Pesendorfer's original 2014 sample, which had been archived. This revealed that the 2014 PI/PI sample now exhibited positive charge magnitude of +14.5 ± 0.5 kV, in keeping with the results of the present study. The same sample was tested twice, allowing discharge time of 4 hours between tests.

Of further notable dissimilarity is the PAN result. While this study found PAN to be consistently negatively charged, Pesendorfer reported positive polarity. As with the archived PI/PI sample, the original PAN/PAN sample was retested. Retesting found it to exhibit negative polarity of -10.2 ± 1.3 kV, in keeping with the current results.

It is theorised that the difference in PI/PI and PAN/PAN results may be due to the specific PET covering on the reference wheel since this was the only part of the test apparatus that had been changed. PET has been reported to obtain charge with minor fluctuations about the neutral point (Table 2-1). It is therefore possible that the PET reference wheel cover in this study had a charge of low magnitude, but opposite polarity to that used in 2014. This may have intensified the positive charge seen on PI/PI which becomes significantly positive and reversed the polarity of the less intensely charged PAN/PAN samples. It must also be noted that, as in Table 3-5, PAN has been observed to be both positive, negative and neutrally charged in various studies (Frederick, 1974; Adams, 1987; Frederick, 1999; Purchas & Sutherland, 2002; Hutton, 2007) and a conclusive, widely repeated polarity has not yet been established.

Environmental considerations, which have been widely reported to affect triboelectric charging (Jonassen, 1998; Mekishev, et al., 2005; Liu, 2010), may also have had an effect on the behaviour of the samples. The 2014 tests were conducted in a different laboratory with generally higher ambient temperature and at a different time of year with potentially different weather conditions affecting temperature and humidity. These environmental factors may have had an effect on the lower standard deviation recorded by Pesendorfer.

Apart from the polarity and initial charge intensity, the charge dissipation behaviour of filtration fabrics is of interest. The discharge rate of a filtration fabric holds potential implications for operational fabric performance. A more rapid discharge rate may imply higher permeability during operation and consequent improvement of pressure drop due to improved fabric cleanability (Frederick, 1974; Topkin, 2000). Although discharge

rates are reported for both the filtration and clean gas surfaces, it is suggested that the discharge rates of the filtration surfaces are of greater importance when considering bag selection. This is because the filtration surface interacts with dust during baghouse operation and must suitably release dust during pulse cleaning in order to maintain appropriate baghouse pressure drop.

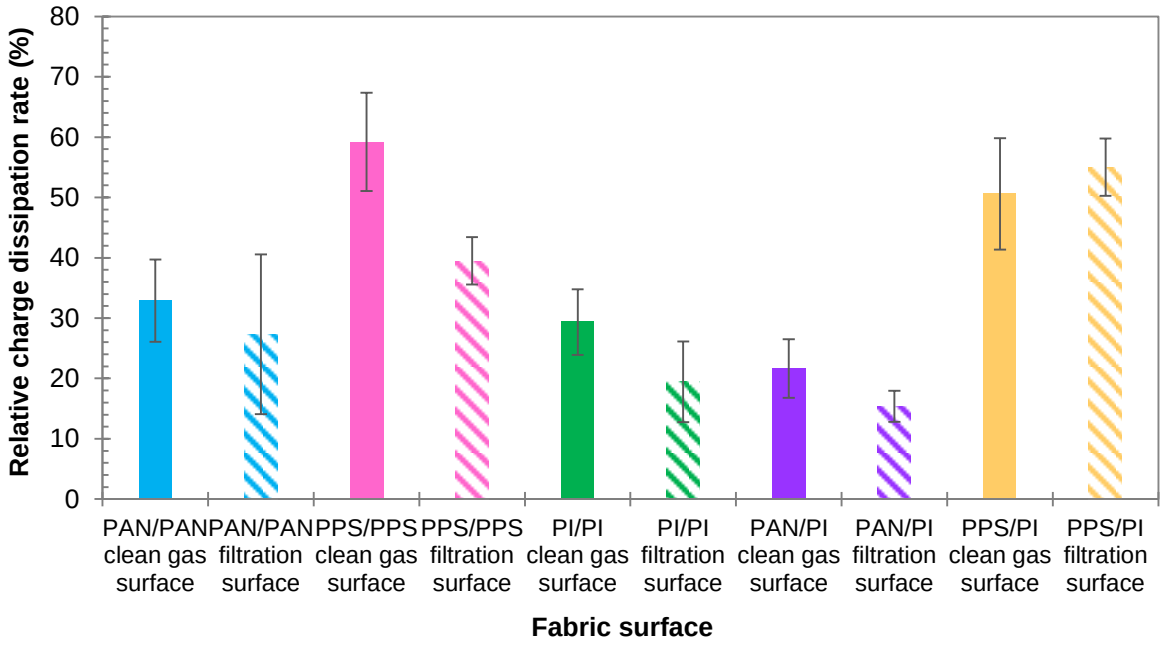

Figure 3-9: Relative charge dissipation rates of selected filtration fabrics

Average relative charge dissipation rates, based on the data reported in Appendix A and calculated using Equation (3-1), can be seen in Figure 3-9. From the data it is apparent that PPS-based fabrics exhibit higher relative charge dissipation rates than PAN- and PI-based fabrics. Furthermore, blended fabrics reveal slower dissipation rates when compared with uniform polymer fabrics. This result may be due to the interaction of dissimilar materials in contact within the fabric constructions. Frederick (1974) suggests that the larger the polarity spread between materials in the triboelectric series, the greater the electrostatic interaction. Therefore, the contact between highly positive PI and negative PAN and PPS could result in localised triboelectric effects within the volume of the blended fabrics, which could hamper charge dissipation to the environment due to continued triboelectric contact between blended fibres. For fabrics of uniform polymer type, however, flow paths to the atmosphere or objects in contact with the fabrics are unobstructed by electron exchange pairs within the fabric depth.

It can also be observed that the average charge dissipation rates are higher for the clean gas sides compared to the filtration sides, with the exception of PPS/PI. While

this agrees with Kazyuta's (2013) finding of fabric surface roughness affecting charge decay, it does not corroborate Kazyuta's report that charge decays more quickly on smooth surfaces. The surface treated filtration surfaces are smoother than the 'woolly', unfinished clean gas surfaces. It is instead suggested that the loose fibres on the clean gas surfaces aid charge dissipation by providing increased surface area on individual fibres exposed to the atmosphere for charge dissipation.

Comparison of Figure 3-9 with the triboelectric series in Figure 3-8 reveals no clear trend between polarity, initial charge intensity and charge dissipation rate. It is therefore suggested that the filtration fabrics in question do not behave analogously to the more widely studied polymer, PE, for which Ieda et al. (1967) and later Zhang et al. (2008) reported that higher initial charge magnitude corresponds with more rapid charge decay. The lack of correlation between polarity and charge dissipation rate is in contradiction to the results of Burgo et al. (2011) and Du and Li (2016), who reported polymer charge dissipation rates to be higher for polymers ranked on the positive polarity side of the triboelectric series.

Comparison of the present results is again made with Pesendorfer's (2014) results in Table 3-7. It can be seen that results differ in various respects. Firstly, the order of charge dissipation rate magnitude does not correspond. Secondly, magnitudes of charge dissipation rate vary significantly. This is most pronounced for PAN and PI where significantly higher charge dissipation rates were reported in 2014. This may be due to various factors. The samples tested in 2014, although of the same material type, were not from the same fabric manufacturers and construction differences as well as polymer differences may exist. Liu (2010) stated that differences in polymer manufacture and impurities may affect textile triboelectric behaviour. Environmental differences, such as humidity and temperature, may also have an effect, as previously discussed.

Table 3-7: Comparison of selected filtration fabric relative charge dissipation rates: Pesendorfer (2014) vs this study

Sample type	Average Charge Dissipation (%)	
	Pesendorfer (2014)	This Study
PAN/PAN	49	30
PPS/PPS	44	48
PI/PI	54	26

Although relative charge dissipation rate provides an indication of the propensity of a polymer towards losing charge, discharge behaviour is not linear. The triboelectric characteristics of the filtration fabrics studied are illustrated in Figure 3-10, where polarity and incremental charge dissipation is shown. Where initial charge exceeded the ±22 kV electric field meter limit, values were extrapolated based on the discharge characteristic models of the fabrics, summarised in Table A-2.

Although large standard deviation of charge measurements is reported, the characteristic discharge curve shapes recorded for repeated tests was found to be fairly constant. The average curves are thus representative of the discharge behaviour of the fabrics (Figure 3-10). Repeatability details are discussed in Appendix A and summarised in Table A-1. Repeated tests of the discharge behaviour of the fabrics considered are described in Figure A-1, Figure A-2, Figure A-4, Figure A-5 and Figure A-6.

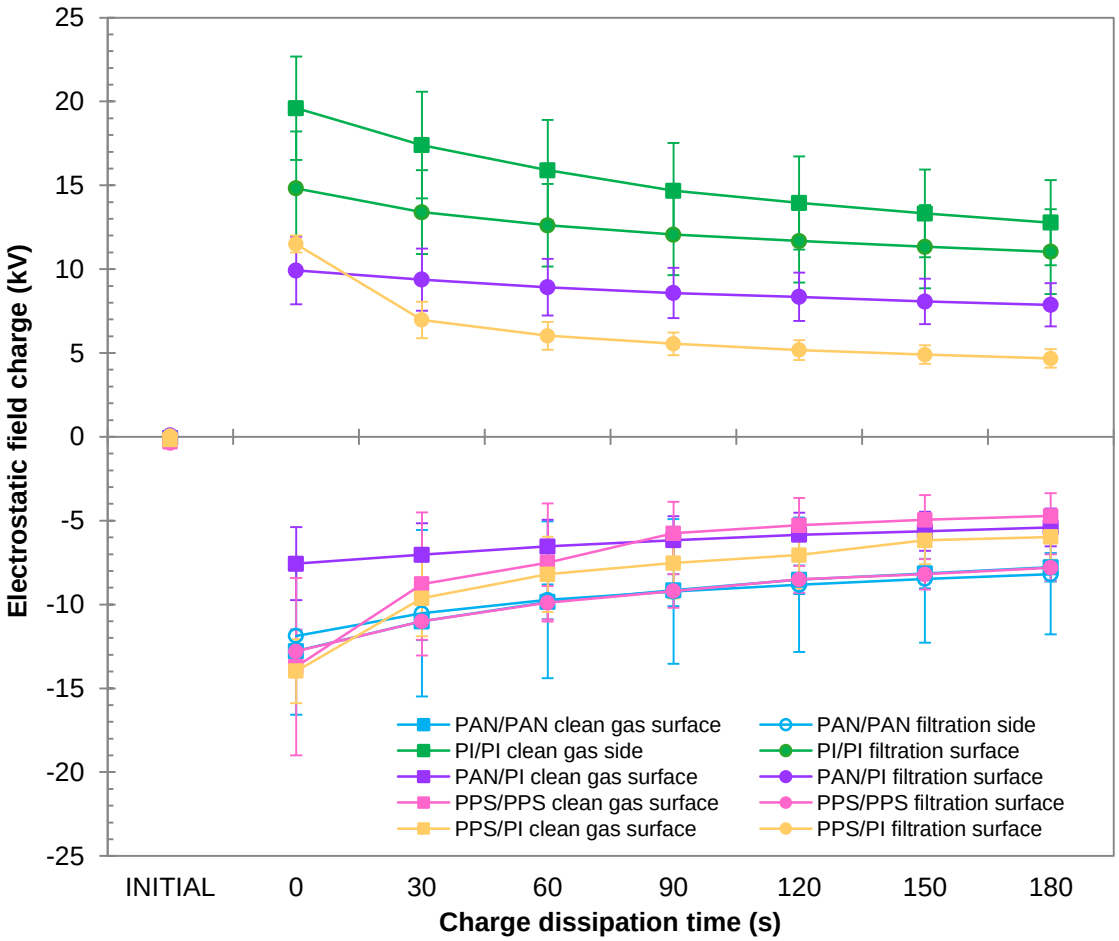

Figure 3-10: Average discharge characteristics of low temperature fabrics, high temperature fabrics and PI

In order to describe the discharge characteristics of the fabrics at time intervals beyond those measured, discharge characteristic models based on the average data discussed

above were developed. These models may be beneficial when considering charge dissipation between bag pulse cleaning during operation. Characteristic equations are described in Table A-2 in Appendix A and illustrated in Figure 3-11.

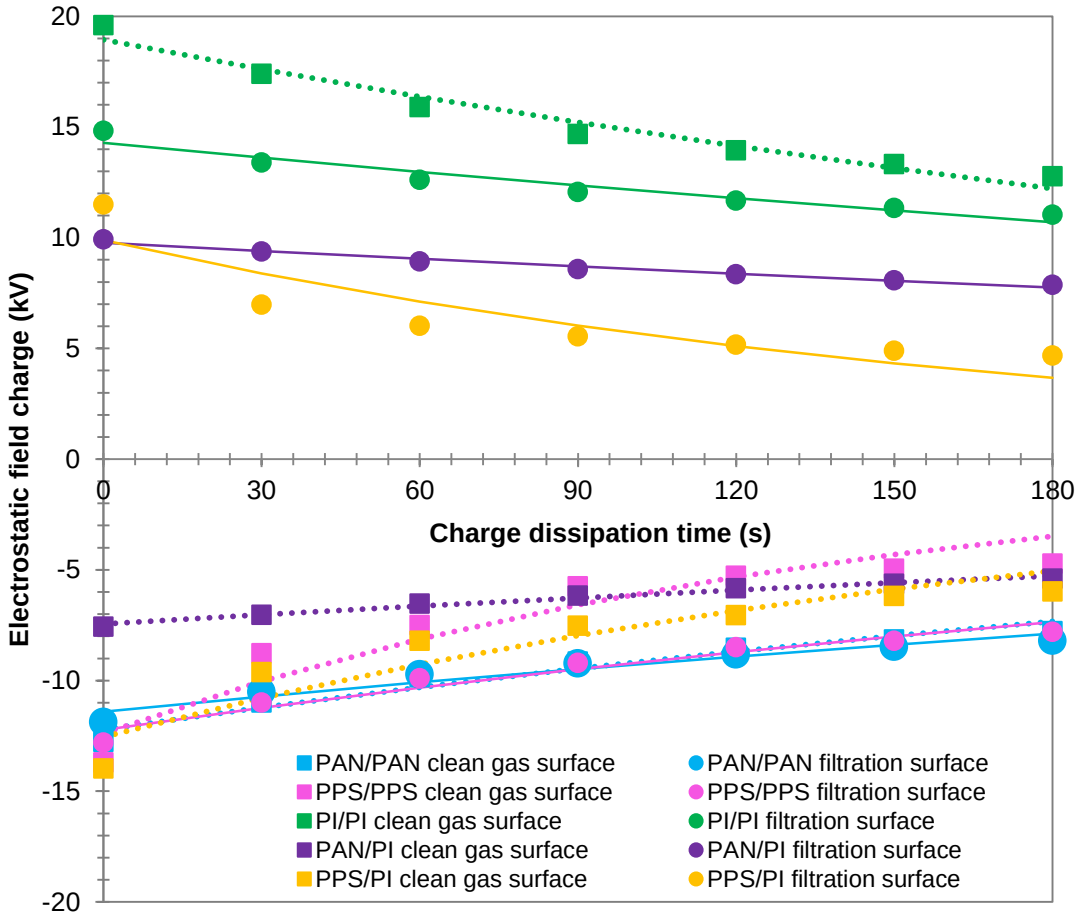

Figure 3-11: Discharge characteristics models of selected filtration fabrics

The discharge characteristics of the fabrics are best described by logarithmic or polynomial functions of the fourth and third order. Such functions, however, have shortcomings. Initial charge is overestimated for polynomials and invalid for logarithmic models. Furthermore, polynomial functions cannot be used to extrapolate beyond the time intervals for which measurements were taken due to the function turning points. It is therefore suggested that the best exponential fits are more appropriate to describe the discharge characteristics of the fabrics, in keeping with the exponential decay reported by Ieda et al. (1967). The results show that although the best fit polynomial and logarithmic functions provide more accurate descriptions of the data, the exponential decay models can still be considered appropriate since the correlation coefficients (R^2-values) range between 0.9771 and 0.9998. The suggested exponential

decay discharge characteristic curves are illustrated in Figure 3-11 along with the measured data. Dashed curves relate to clean gas surfaces and solid curves to filtration surfaces.

3.3.2 IMPACT OF HUMIDITY ON TRIBOELECTRIC BEHAVIOUR

The potential impact of the ambient environment on charge development and decay has been extensively discussed in literature. Environmental factors such as atmospheric pressure (Mekishev, et al., 2005), temperature (Liu, 2010; Du & Li, 2016) and, prominently, humidity (Park, et al., 2008; McCarty & Whitesides, 2008; Liu, 2010; Burgo, et al., 2011; Kazyuta, 2013) have been reported to impact the intensity of triboelectric charge development as well as charge decay. The results reported in Section 3.3.1 are therefore further examined for any correlation with the absolute humidity[23] of the environment in which the charging experiments were performed. The results are shown in Figure 3-12 and Figure 3-13. Multiple data points of the same colour represent repeats of experiments.

It has been reported that the presence of moisture in the air at increased levels dampens all electrostatic interaction (Brown & Cox, 2017). For the tests conducted as part of this study, however, the results do not consistently demonstrate this theory. Although lower initial charge intensity at higher absolute humidity is shown by PI/PI filtration surface, PPS/PPS filtration surface and PAN/PAN clean gas surface (Figure 3-12), this behaviour cannot be conclusively linked to material type or surface. The results of this study are therefore aligned with Ramer and Richards (1968) who, although noting the impact of humidity on charge decay, reported no impact on initial charge intensity.

The impact of humidity on the relative charge dissipation rates of the fabrics reported in this study is investigated in Figure 3-13. Holistically, a trend of higher charge dissipation rate at increased humidity is confirmed by the results presented in Figure 3-13. However, when specific fabric types are considered individually, i.e. the repeat measurements of the individual fabrics, this trend is not apparent. Absolute humidity measurements for individual specimens, however, fall within a narrow range. It is thus possible that if tests were repeated at more widely varying humidity levels, significant results may be observed.

[23] Absolute humidity is a measure of the total moisture present in the air at the local atmospheric pressure, the relative humidity and air temperature that were recorded next to the experimental apparatus.

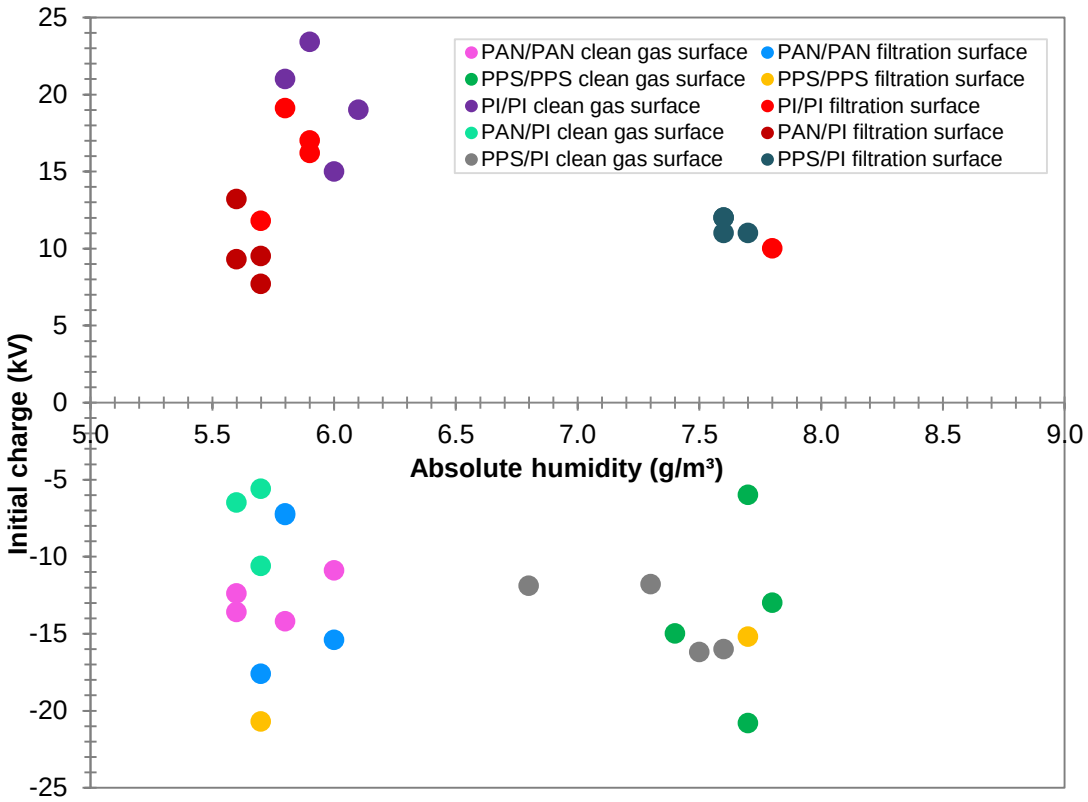

Figure 3-12: Fabric initial triboelectric charge vs absolute humidity

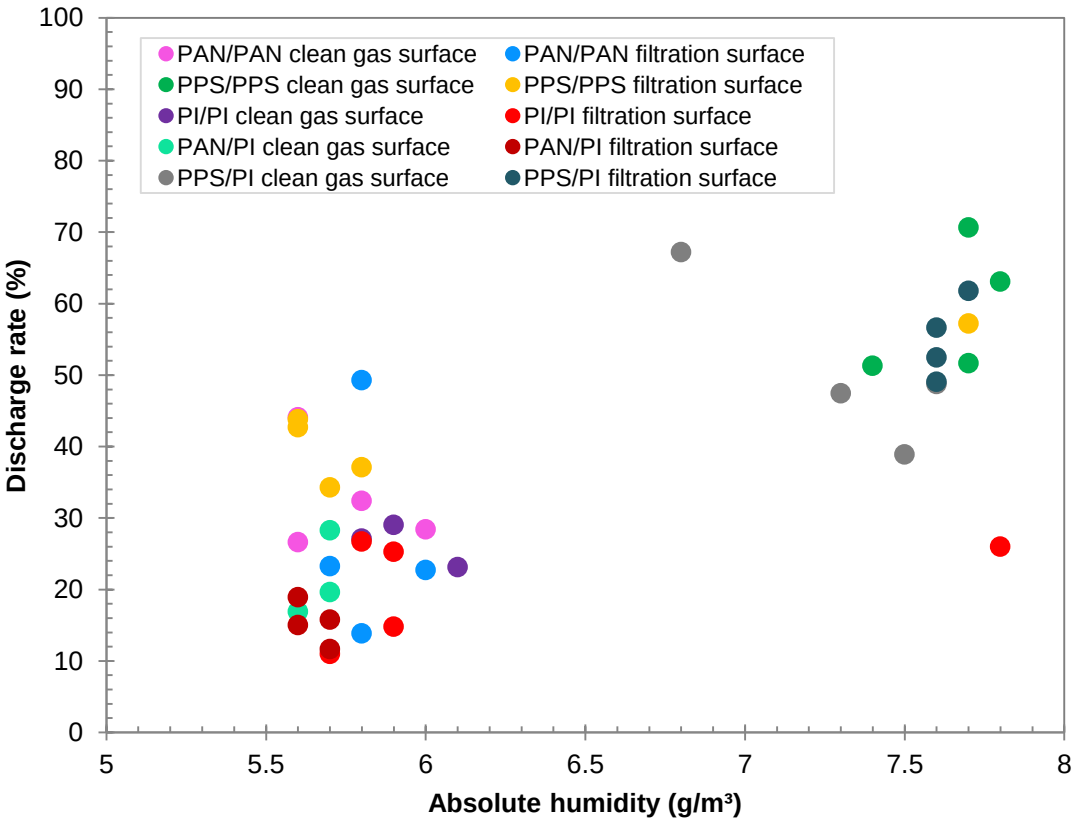

Figure 3-13: Fabric relative charge dissipation rate vs absolute humidity

3.3.3 ELECTROSTATIC INTERACTION OF SIMILAR FABRICS

While the results reported in Section 3.3.1 and 3.3.2 relate to the triboelectric behaviour of high and low temperature fabrics when rubbed on PET, it could be of benefit to understand the behaviour of the fabrics when rubbed on themselves. When installed in a baghouse, it is hypothesised that the rubbing of fibres in contact in the fabric volume during pulse cleaning may result in triboelectric charge generation. For this reason, fabric specimens were rubbed on reference wheels covered in the fabrics relevant to this study according to the method described in Section 3.2.4. The reference material was applied to the reference wheel in a manner such that the filtration surface was rubbed on the test specimens. This experiment was limited to establishing the polarity and initial charge magnitude when specimens are rubbed on like reference material. The data are reported in Table 3-8.

Note that the polarity of the reference wheel after charging was opposite to the test specimens. Charge magnitude, however, was not recorded since the reading was not taken instantly after charging ceased due to the availability of only one electrostatic field meter.

Table 3-8: Triboelectric behaviour of similar fabrics

	PAN/PAN reference wheel	PPS/PPS reference wheel	PI/PI reference wheel
PAN/PAN clean gas side	-0.85	-	-18.00
PAN/PI filtration side	+1.39	-	-16.00
PPS/PPS clean gas side	-	+9.20/-11.43	-22.00
PPS/PI filtration side	-	+15.25	-22.00
PI/PI clean gas side	+10.50	+18.00	+11.00/-12.00

The PAN/PAN reference wheel resulted in low intensity charges developing on specimens, with the polarities corresponding with the triboelectric series (Figure 3-8). When rubbed on itself PAN/PAN developed a negligible charge and can be considered neutral.

The PPS/PPS reference wheel resulted in fabrics containing PI developing positive charges consistent with the previously developed triboelectric series. The interaction of

PPS/PPS with itself, however, showed polarity changes and significant charge generation.

This polarity change was echoed by PI/PI being rubbed on itself. Although the PAN and PPS based fabrics developed negative charges when rubbed on PI/PI as expected from the previously developed triboelectric series, PI/PI rubbed on itself showed both positive and negative polarity.

From the surveyed literature summarised in Table 3-5 it can be seen that PAN has been known to fluctuate between neutral and low positive and negative charges. From Figure 3-8 it can be further seen that PAN develops generally low magnitude charges when rubbed with PET. It is therefore suggested that the negligible negative charge developed when rubbed upon itself is indicative of a low propensity towards charge generation when rubbed with materials occupying a similar space on the triboelectric series (such as PET and itself). This is in keeping with triboelectric theory, as discussed by Frederick (1974) and later Kazyuta (2013).

This theory can be extended to PPS and PI. Both these fabric types developed intense charges when rubbed on the neutral PET reference wheel. From Table 3-8 it is apparent that when materials occupying very different positions in the triboelectric series come into contact, such as PPS which is highly negative and PI which is highly positive, intense charges of the opposite polarity are developed. However, when rubbed upon themselves, it is suggested that the tendency toward intense charge development is still present, however polarity fluctuates since two similar materials are in contact. Therefore, while one surface develops a nett positive charge and the other a nett negative charge, the surfaces are interchangeable. Broken polymer chains may be responsible for the donation and acceptance of electrons resulting in a nett charge (Baytekin, et al., 2011; Burgo, et al., 2012; Piperno, et al., 2012).

Morton and Hearle (2008) further found that charge can occur on surfaces of fibres of the same material when asymmetric frictional rubbing occurs, which generates unequal heat on the contact surfaces. It was suggested that the greater mobile energy of the particles with greater heat will result in increased movement of charge from the hotter to colder surface. Since the fibre orientation in needle felt fabric is random, this theory may explain the fluctuating surface polarity when similar materials come into contact.

3.4 ELECTROSTATIC INTERACTION OF DUST WITH FILTRATION FABRICS

To further investigate the triboelectric behaviour of filtration fabrics while in use in baghouses, the interaction of the filtration fabrics described in Section 3.2.2 with different dust samples, described in Section 3.2.3, was studied using the method described in Section 3.2.5.

Specimens were of clean, unused fabric and the test method did not impose any draught or other mechanical interference on the fabric. It can therefore be assumed that any observed dust interaction was due to electrostatic forces. Only the filtration surfaces of the filtration fabric specimens were exposed to the dust samples since the clean gas surfaces are not designed for ash exposure or filtration. Since small quantities of dust were used in the experiments, significant changes in the fabric permeability after exposure were not expected. Analysis is therefore limited to observations during charging and visual inspection of cross sections of the fabric specimens after exposure.

3.4.1 ENVIRONMENTAL CONDITIONS AND TEST OBSERVATIONS

The charge polarity of specimens after charging while exposed to dust were consistent with those reported in Figure 3-8. Qualitative comparison of dust penetration, discussed in Sections 3.4.2 to 3.4.6, reveals that PPS/PPS and PAN/PAN experienced the most significant dust penetration. Ash penetration was reduced when PI was incorporated into the filtration surfaces, which corresponds with the negligible penetration observed on PI/PI.

It was previously highlighted in Section 3.3.1 that PI dominates the charging behaviour of filtration fabrics in terms of polarity when used in a blend. It is thus suggested that fabric triboelectric polarity is an indicator of whether dust penetration will occur. It is apparent that the most significant dust penetration was observed on the most negatively charged fabric, PPS/PPS. Less negative PAN/PAN experienced less dust penetration. PAN/PI and PPS/PI, which exhibit positive polarity when triboelectrically charged, experienced less dust penetration. The most positively charged filtration fabric studied, PI/PI, experienced negligible dust penetration.

It is suggested that this observed increase in ash penetration into fabrics of negative polarity may be due to the surplus of electrons available on the negatively charged polymers for donation to ash particles. If ash particles obtain mostly positive charges,

then particles would be attracted to the negative fibres and repelled by the positive fibres. This behaviour would explain the ash motion observed during charging where electrostatic interactions occur, however after charging ash remains on positive fabric surfaces and is drawn into the negative fabric volumes.

No correlation with the fabric charge dissipation rates shown in Figure 3-9 and dust penetration can be seen.

The laboratory ambient test conditions for the interaction tests of fabrics with the respective dusts are summarised in Table 3-9. PI/PI dust interaction tests were all carried out at 19.1°C, 30.1% relative humidity and 4.9 g/m^3 absolute humidity.

Table 3-9: Test conditions for dust interaction with PAN/PAN, PAN/PI, PPS/PPS and PPS/PI

Dust	Temperature (°C)	Relative Humidity (%)	Absolute humidity (g/m^3)
Pural NF®	19.8	36.4	6.2
Power Station A Ash	19.1	30.1	4.9
Power Station B Ash	21.3	37.4	7.0

During triboelectric charging of the dust exposed fabric specimens, observations of dust behaviour were recorded. Dust interaction was observed to be similar for the fabrics tested at the same environmental conditions.

For PAN/PAN, PAN/PI, PPS/PPS and PPS/PI, slight initial dust motion was observed when exposed to Pural NF at 6.2 g/m^3 absolute humidity. When exposed to Power Station A ash at the lowest recorded absolute humidity of 4.9 g/m^3, noticeable dust motion was observed. Particles were seen to bounce on the surfaces of the samples, spread across the area contacted by the wheel and became attracted to the electrostatic filed meter. Power Station B ash, however, which was tested at the highest recorded absolute humidity of 7.0 g/m^3, did not exhibit any observable dust motion.

Interaction of PI/PI with all dust types was tested at the lowest recorded absolute humidity of 4.9 g/m^3. Significant dust motion was observed for all dust types. From Figure 3-14 the dust spread across the fabric surfaces after testing can be seen to be most noticeable on the PI/PI surfaces and PPS/PI, PPS/PPS and PAN/PAN surfaces exposed to Power Station A ash. This behaviour suggests that significant ash interaction occurs at low ambient humidity.

Cross-sectional analysis, however, reveals that observed surface motion was not a consistent indication of ash penetration into the fabric volume. The observed dust motion on the surface of the fabric could thus either be due to differences in the charging propensity of dust of different compositions, the electrostatic properties of the fabrics or could be due to the impact of humidity on electrostatic interactions. The latter theory is reinforced by the noticeable dust motion observed on all PI/PI samples, regardless of dust type and the motion observed with all Power Station A ash tests, irrespective of fabric type.

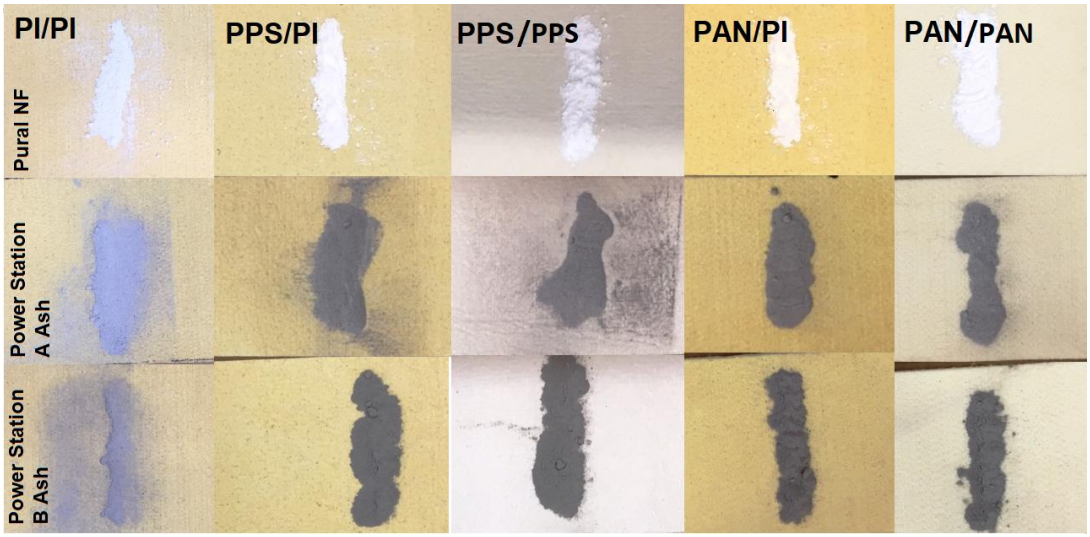

Figure 3-14: Dust on filtration fabric surfaces after triboelectric rubbing

The impact of increased humidity on charge dissipation to the atmosphere has been extensively reported in triboelectric studies of polymers (Ramer & Richards, 1968; Frederick, 1974; Mishra, 1982; Sharma, et al., 2003; Park, et al., 2008; McCarty & Whitesides, 2008; Liu, 2010; Jasti, 2011; Kazyuta, 2013) and it has been suggested that the same mechanism impacts dust charge (Andrabi, et al., 2012). This humidity effect could explain the increased dust motion observed at the lowest tested absolute humidity. At the higher absolute humidity tests, less dust motion may have been observed due to more rapid charge dissipation from the fabric surface and dust particles to the atmosphere.

3.4.2 ELECTROSTATIC INTERACTION OF DUST WITH PAN/PAN

It can be seen from Figure 3-15 that PAN/PAN did not experience significant Pural NF® penetration, with most dust remaining on the filtration surface. Small quantities of particles could be seen to have collected near the scrim.

Similar observations can be made from Figure 3-16, where most Power Station A and B ash can be seen to remain on the surface of PAN with only small black particles penetrating into the fabric volume. This penetration is most noticeable for the Power Station A ash. These particles may be unburnt carbon from the coal firing process from which the ash was produced. It has been reported that unburnt carbon and fly ash have different electrostatic properties (Ban, et al., 1996; Soong, et al., 1999), specifically that unburnt carbon has lower resistivity than fly ash (Neundorfer, 2018). This could explain why the black particles exhibited more interaction with the charged fabric.

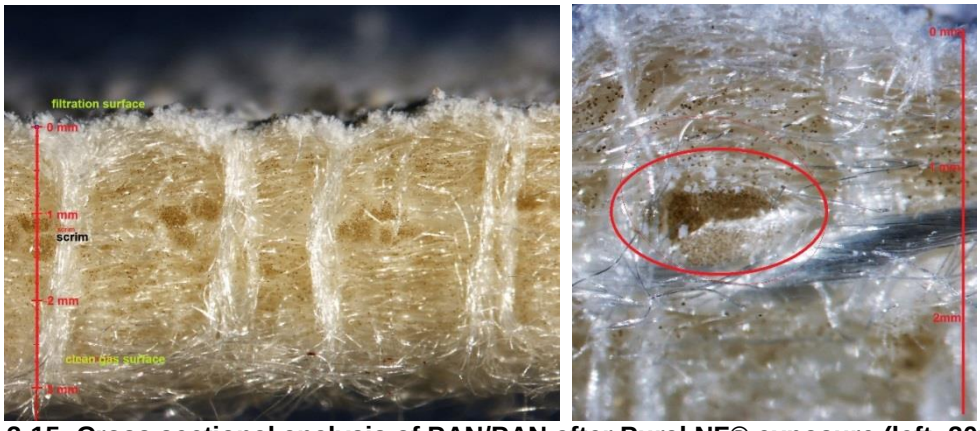

Figure 3-15: Cross sectional analysis of PAN/PAN after Pural NF® exposure (left: 20x magnification, right: 40x magnification)

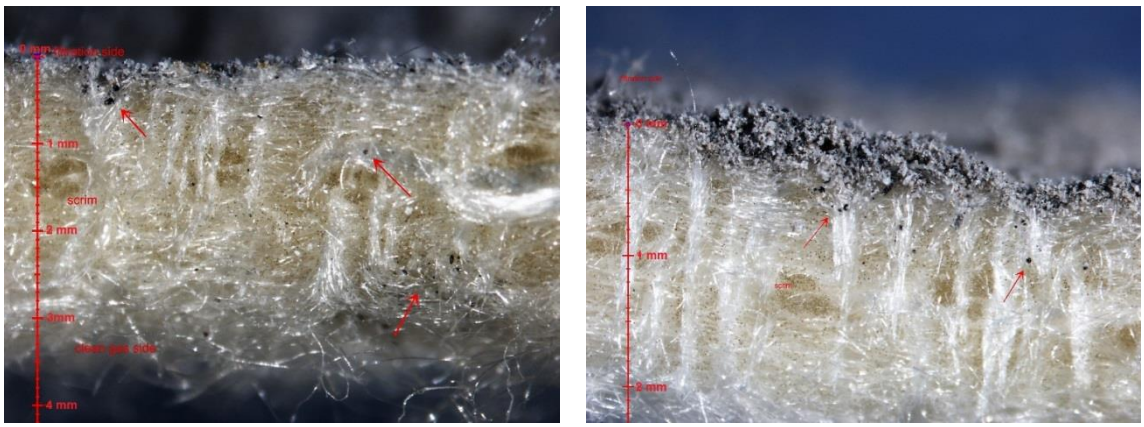

Figure 3-16: Cross sectional analysis of PAN/PAN after Power Station A ash exposure (left, 20x magnification) and Power Station B ash exposure (right, 40x magnification)

3.4.3 ELECTROSTATIC INTERACTION OF DUST WITH PAN/PI

It is apparent from Figure 3-17 and Figure 3-18 that dust does not significantly penetrate PAN/PI during triboelectric charging. Dust can be seen to remain on the

filtration surfaces of the fabric samples. As with PAN/PAN, some black particles in Power Station A ash can be seen to have penetrated to the scrim.

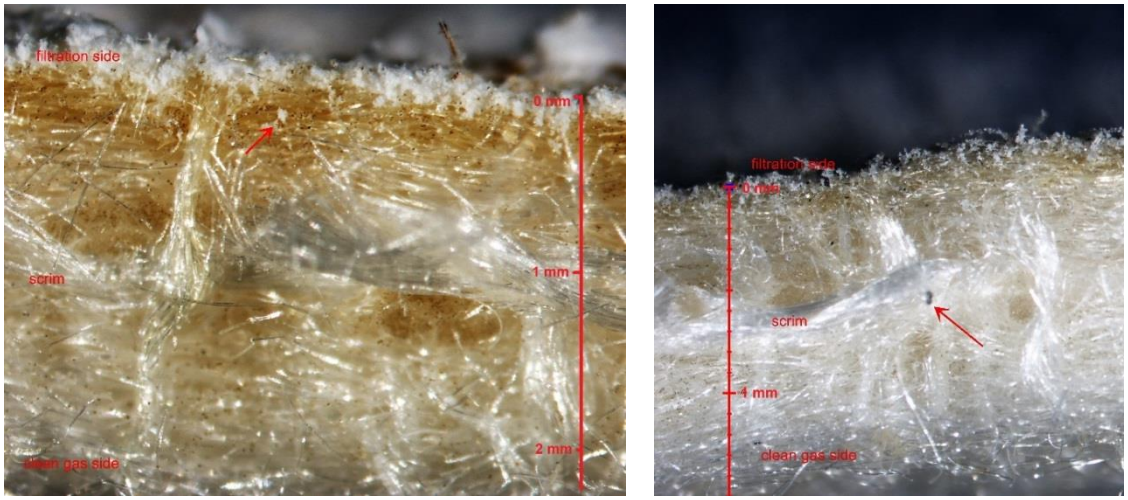

Figure 3-17: Cross sectional analysis of PAN/PI after Pural NF ® (left, 30x magnification) Power Station A ash exposure (right, 20x magnification)

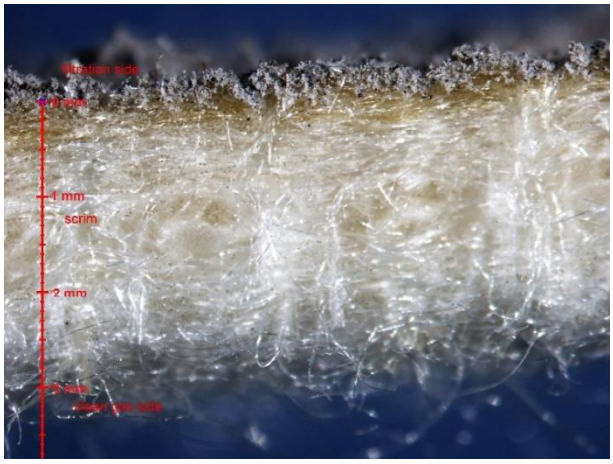

Figure 3-18: Cross sectional analysis of PAN/PI after Power Station B ash exposure (20x magnification)

Visual comparison of PAN/PAN with PAN/PI reveals that less dust penetration is experienced when PI is incorporated into the surface blend.

3.4.4 ELECTROSTATIC INTERACTION OF DUST WITH PPS/PPS

PPS/PPS experienced significant ash penetration by all dusts considered, as can be seen in Figure 3-19 and **Figure** 3-20. These results are in keeping with those reported by Pesendorfer (2015; 2016). Pural NF® penetration was the most significant. From the image on the left in Figure 3-19 Pural NF® dust saturation can be seen throughout the fabric volume to the clean gas surface.

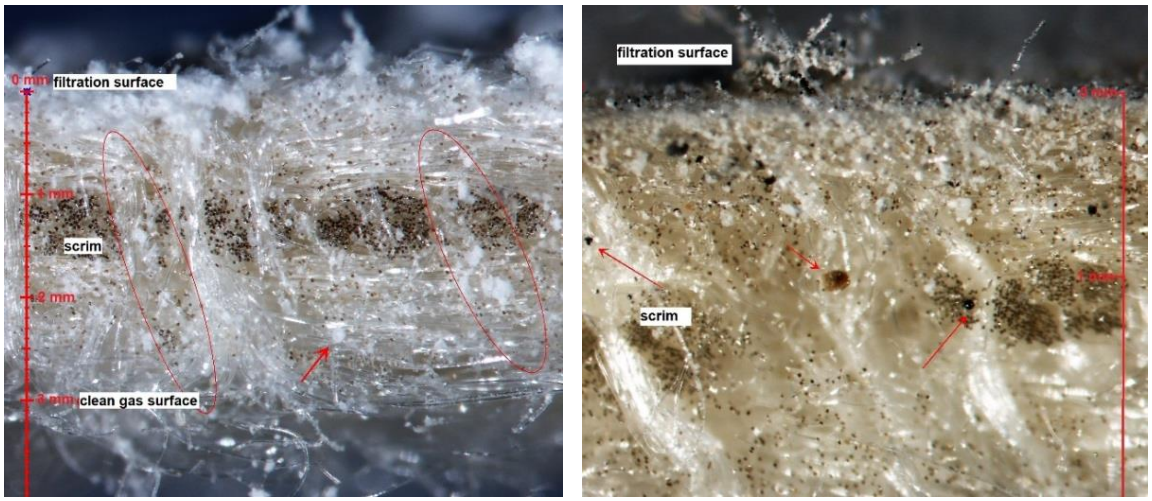

Figure 3-19: Cross sectional analysis of PPS/PPS after Pural NF ® (left, 20x magnification) and Power Station A ash exposure (right, 40x magnification)

Power Station A ash penetrated to the scrim, as can be seen from the image on the right in Figure 3-19. Similar behaviour of Power Station B ash can be seen in **Figure 3-**20. Qualitatively, Power Station A ash appears to have penetrated to a greater extent than Power Station B ash. It is suggested that this is due to the elemental and mineralogical differences between the two dust types, which is known to affect ash resistivity (Yan, 2009; Andrabi, et al., 2012) and would therefore impact electrostatic interaction of the dusts with the triboelectrically charged fabric samples. Similar to results discussed for PAN based samples, small black particles in the power station ashes penetrated further into the fabric than other particles.

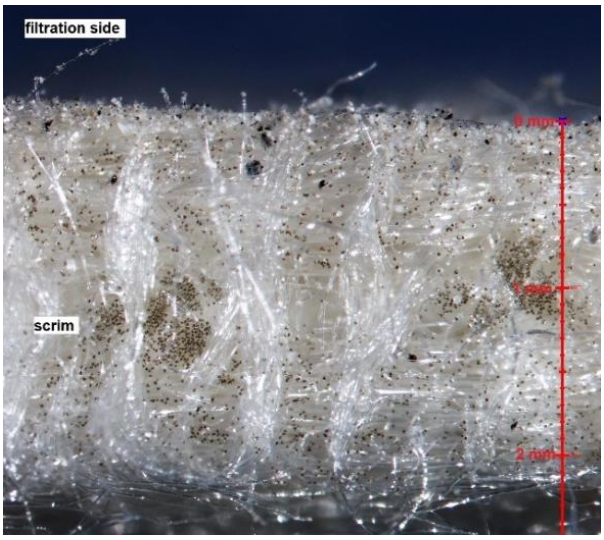

Figure 3-20: Cross sectional analysis of PPS/PPS after Power Station B ash exposure (30x magnification)

3.4.5 ELECTROSTATIC INTERACTION OF DUST WITH PPS/PI

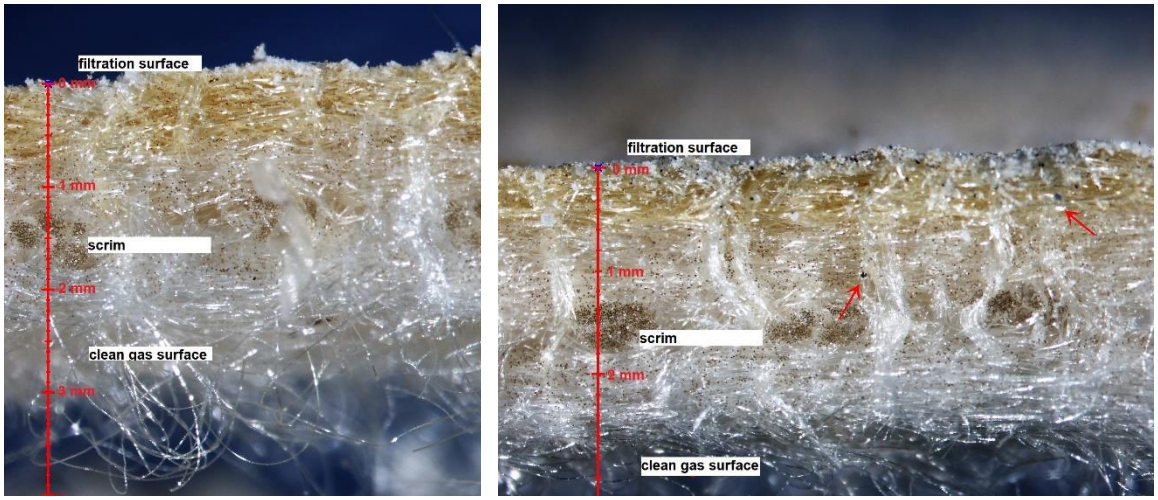

Figure 3-21: Cross sectional analysis of PPS/PI after Pural NF ® (left, 20x magnification) and Power Station A ash exposure (right, 20x magnification)

From Figure 3-21 it is apparent that PPS/PI experienced little penetration by Pural NF® during triboelectric contact. Power Station A ash remained mainly on the filtration surface, with some particles moving into the volume of the filtration batt. Black particles penetrated most deeply. Similar behaviour of Power Station B ash can be seen in **Figure** 3-22. These results are in agreement with Pesendorfer's (2015) results.

Visual comparison of PPS/PPS and PPS/PI dust penetration into the fabric volumes during triboelectric contact reveals that less penetration can be observed when PI is incorporated in the blended filtration surface.

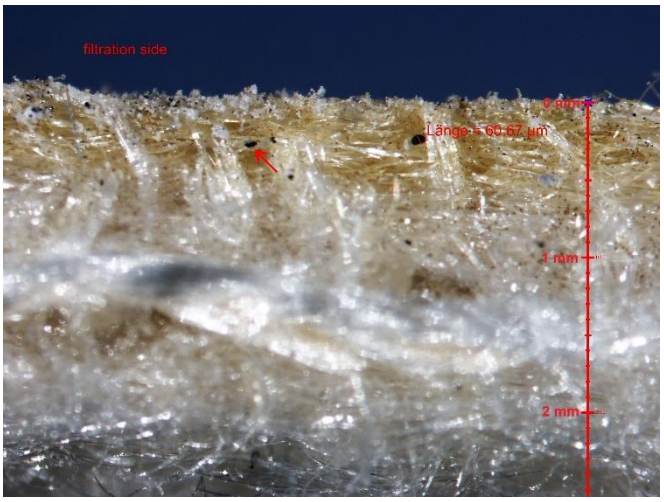

Figure 3-22: Cross sectional analysis of PPS/PI after Power Station B ash exposure (30x magnification)

3.4.6 ELECTROSTATIC INTERACTION OF DUST WITH PI/PI

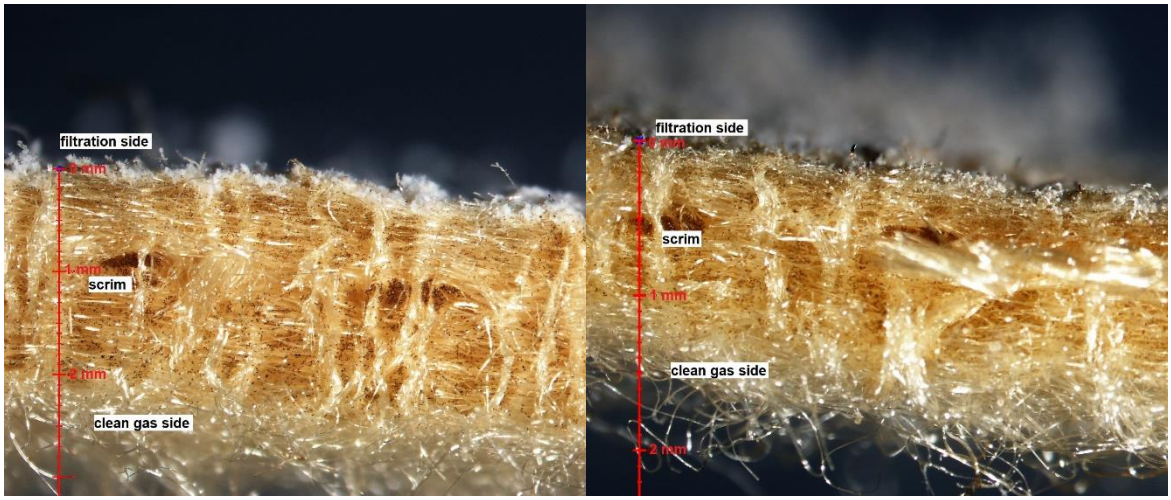

Figure 3-23: Cross sectional analysis of PI/PI after Pural NF ® (left, 20x magnification) and Power Station A ash exposure (right, 20x magnification)

It is apparent from Figure 3-23 and Figure 3-24 that PI/PI experienced negligible dust penetration during triboelectric charging. Dust can be seen to remain on the filtration surfaces of the fabric samples. This lack of penetration corresponds with the results reported by Pesendorfer (2015; 2016).

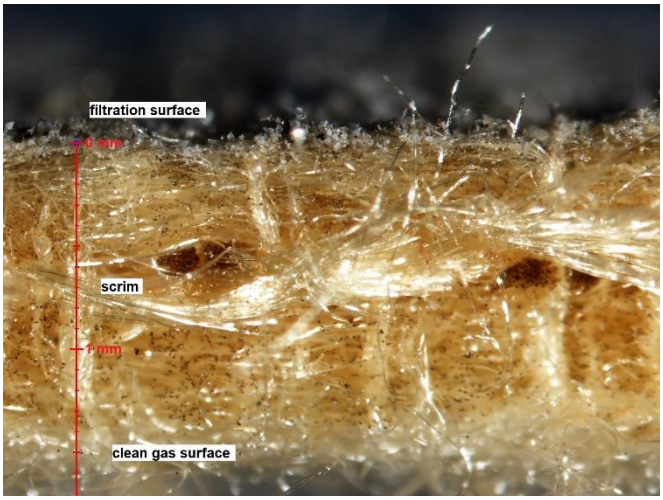

Figure 3-24: Cross sectional analysis of PI/PI after Power Station B ash exposure (30x magnification)

3.5 CONCLUSIONS OF TRIBOELECTRIC BEHAVIOUR OF BAGHOUSE MATERIALS

Conclusions are drawn based on the results of filtration and clean gas surfaces of blended and non-blended filtration fabrics; fibre types are thus considered separately.

PPS exhibits highly negative charge polarities after triboelectric contact. PAN exhibits negative polarity of lower charge magnitude than PPS. PI exhibits highly positive charge polarity. PI, however, dominates the charging behaviour of the fabric surfaces when included in blends with PAN or PPS.

When triboelectric contact between similar filtration fabrics occurs, PAN develops negligible charge while PPS and PI fluctuate between positive and negative polarity of similar magnitudes.

Negative fabric charge of increasing magnitude corresponds with qualitatively increased dust penetration into the fabric cross sections. Positive fabric polarity correlates with reduced dust interaction. Similar dust interaction with fabric occurs regardless of differences in the dust compositions considered in this study.

PPS exhibits the highest relative charge dissipation rate of the filtration fabrics considered, followed by PAN and then PI. Fabrics that are constructed of the same polymer throughout the fabric cross section show higher relative charge dissipation rates than blended fabrics. Relative charge dissipation rates are also greater for the clean gas fabric surfaces than filtration surfaces. It can be further concluded that neither charge magnitude nor polarity correspond conclusively with charge dissipation rate. Charge dissipation rate was not found to affect dust interaction.

It can further be concluded that humidity does not impact initial fabric charge magnitude or charge dissipation rate. Humidity does, however, affect electrostatic interaction between dust and triboelectrically charged fabrics.

CHAPTER 4: FILTRATION FABRIC RESISTANCE TO ACID ATTACK AND THERMAL DEGRADATION

4.1 INTRODUCTION

The results of a series of experiments designed to investigate the potential impact of sulphuric and nitric acid attack on the mechanical strength of selected filtration fabrics are discussed in this chapter. As discussed in Chapter 2, chemical resistance is often not reported on a consistent basis. These results therefore provide a comparative basis for the fabrics considered. Furthermore, the relative thermal stability of the polymeric fibre types used in these fabrics were investigated using TGA and DSC analysis of the corresponding yarns. Results provide insight into the temperature resistance of the fabrics that incorporate these polymers as well as the effect of acid exposure on the individual fibre types used in blended filtration fabrics.

For acid attack, only the effect on tensile properties of the filtration fabrics was considered. However, fabric shrinkage and changes in fabric burst strength and permeability as a result of acid attack, which are beyond the scope of this study, may impact fabric operation.

4.2 MATERIALS AND METHODS

4.2.1 FILTRATION FABRIC AND YARN SAMPLES

The fabric samples considered for this study were cut from unused fabric filter bags and are described using the convention illustrated in Figure 3-1. Only the fabrics chosen for comparison in this study are included, namely PAN/PAN versus PAN/PI and PPS/PPS versus PPS/PI. Since PI/PI fabric is not suitable for South African coal-fired boiler application (Popovici, 2010), it was not considered in this acid attack investigation. Details of the filtration fabric samples used in the study are listed in Table 4-1.

Needle felt fabric tensile strength differs in the machine direction[24] and cross-machine direction[25]. Since the fabric is pre-tensioned in the machine direction during manufacture, tensile analysis results are typically more consistent than those of the cross-machine direction, where increased fibre randomness is present (Maity &

[24] The *machine direction* is the fabric orientation parallel to the movement of the fabric during needling. It is analogous to warp in woven fabrics (Koerner, 1994).
[25] The *cross-machine direction* is the fabric orientation perpendicular to the movement of the fabric during needling. It is analogous to weft in woven fabrics (Koerner, 1994).

Singha, 2012). The objective of this experiment is comparative study; therefore, it was considered sufficient to analyse samples cut in the machine direction only.

Table 4-1: Acid attack needle felt sample description

Material	Supplier	Fibre type	Scrim	Filtration Surface Batt	Inner Batt	Support Batt
PAN/PAN	Metso	Dolanit®	2.2dtex PAN	1.7dtex PAN	2.2dtex PAN	2.2dtex PAN
PAN/PI	Metso	Dolanit®/P84®	2.2dtex PAN	1.7dtex PAN / 1.7dtex multilobal PI	2.2dtex PAN	2.2dtex PAN
PPS/PPS	Metso	Procon®	2.2dtex PPS	1.7dtex trilobal PPS	2.2dtex round PPS	2.2dtex round PPS
PPS/PI	Filtafelt	Procon®/P84®	2.2dtex PPS	1.7dtex trilobal PPS / 1.7dtex multilobal PI	2.2dtex round PPS	2.2dtex round PPS

While the objective was to compare PAN and PPS filtration fabrics to their counterparts with PI incorporation, the different polymeric fibre types were also analysed using TGA to characterise the individual thermal degradation properties of the polymers before and after acid exposure. Yarn was selected for analysis, and the specific types used in this study are summarised in Table 4-2.

Table 4-2: Yarn test sample description

Material	Fibre type	Construction	Fineness (dtex)	Description
PAN	Dolanit®	Staple fibre thread[26], twisted	1350	Nm 25/3
PPS	Torcon®	Multifilament thread, twisted	1440	Nm 25/3
PI	P84®	Multifilament yarn[27], twisted	1060	80 T/m

Dolanit® homopolymer PAN is produced by Dolan GmbH. Procon® and P84® are produced by Evonik Fibres GmbH. Torcon® is produced by Toray Industries, Inc.

[26] A *thread* consists of multiple yarns plied together and can be described by its metric number (Nm): the number of 1km lengths of thread in 1kg of the material, by the number of yarns plied together (Srivani, n.d.).
[27] A *yarn* is a single spun agglomeration of fibres and can be described by its yarn twist (T/m): the number of single fibre filaments per yarn length (Srivani, n.d.)

4.2.2 CHEMICALS

Fabric and yarn exposure to sulphuric and nitric acids, diluted to various concentrations, was considered. The chemicals used are summarised in Table 4-3.

Table 4-3: Acid description

Chemical	Strength	Supplier
Nitric acid (HNO_3)	55%	Saarchem
Sulphuric acid (H_2SO_4)	98%	Associated Chemical Enterprises

4.2.3 ACID EXPOSURE AND TENSILE STRENGTH ANALYSIS OF NEEDLE FELT FABRIC

Samples of the selected filtration fabrics described in Section 4.2.1 were prepared. Test samples were cut to 50 mm x 300 mm in the machine direction of the fabric. Samples were weighed using a Bel Engineering balance, accurate to two decimals measured in grams, prior to chemical and temperature exposure.

Solutions of nitric and sulphuric acids were diluted with deionised water to the required concentrations, ranging between 0.2 M and 3 M. After recording the initial mass and dimensions of the fabric samples, three samples per test were soaked for approximately 5 minutes in the relevant acid solution before being rolled and placed in an autoclave. The autoclave was then filled with the relevant acid solution before being placed in the pre-heated Scientific 9000 Series oven at the required temperature, ranging between 95°C and 190°C.

After the exposure time was complete, samples were removed from the autoclave and thoroughly rinsed with demineralised water before air drying until dry to the touch, for approximately 8 hours. Final drying was then completed in an oven at 60°C for 1 hour. Sample mass and dimensions after acid exposure were recorded.

Tensile properties were analysed using a Zwick Tensile Tester. A 5 kN load cell was used with a pre-load of 20 N. The test speed was 100 mm/min.

4.2.4 ACID EXPOSURE AND THERMAL ANALYSIS OF YARN

Nitric and sulphuric acid solutions, each of 3 M, were prepared. Samples of the yarn described in Section 4.2.1 were cut to lengths of approximately 3 g mass. A sample of each yarn type was individually submerged in the selected acid solution in an

autoclave. The sealed autoclave was then placed in the pre-heated Scientific 9000 Series oven for 4 hours. PAN yarn samples were exposed at 125°C and PPS and PI yarn samples were exposed at 150°C. After exposure, samples were thoroughly rinsed with demineralised water and allowed to dry at room temperature for 24 hours. Final drying was completed in an oven at 60°C for 1 hour.

A Netzsch 449 F3 analytic TGA, capable of both TGA and DSC analysis, was used to conduct the thermal analysis of the yarn samples. Equipment parameters are described in Table 4-4. Samples of approximately 5 mg were grab-sampled from the 3 g bulk samples and loaded into the equipment on the crucible. Yarn that had been exposed to acid as well as unexposed yarn was analysed at heating rates of 10°C/min or 15°C/min throughout the temperature range.

Table 4-4: TGA test parameter details

Parameter	Value
Crucible	Aluminium pan
DSC limit	5000 µV
TGA limit	35000 mg
Test program temperature range	30 – 800°C
Purge gas	helium

4.3 THE EFFECT OF ACID ATTACK ON FILTRATION FABRICS

In this section, the results of the acid exposure tests performed according to the procedure described in Section 4.2.3 are reported and discussed.

4.3.1 FABRIC BASELINE TENSILE PROPERTIES

The objective of this study was to comparatively evaluate the effects of including PI in both low (PAN based) and high (PPS based) temperature fabrics. Since all four fabrics typically have suitable tensile properties for effective function in a baghouse, fabric ultimate tensile properties are of less interest than the change in properties exhibited after exposure to temperature and acidic conditions.

In order to make such a comparison, the baseline tensile properties of the fabrics prior to acid and temperature exposure were defined. The nature of needle felt fabric is inherently variable due to the inhomogeneous orientation of the fibrous felt and variance in tensile properties is expected. This standard variance must be defined in

order to understand when tensile property changes exhibited after experiments are significant. To this end, the tensile properties of ten unexposed samples per fabric type were evaluated to estimate a baseline error. The results are shown in Figure 4-2.

Due to the nature of the needle felt fabric samples there is inherent uncertainty regarding fabric dimensions, particularly thickness. Samples were measured with a Vernier calliper. Since fabric samples are not rigid, minor variations in applied pressure can result in measurement inaccuracy. It is therefore not appropriate to report changes in Young's modulus, which is reliant on fabric dimensions. Force and elongation are thus used to describe the tensile properties of the filtration fabrics considered in this study.

Typical tensile curves, representative of the tensile behaviour of PAN- and PPS-based fabrics, are shown in Figure 4-1. The ultimate tensile strength (UTS), or maximum force that a fabric sample can withstand under tension, is used as an indication of the resistance of the fabric to tearing during operation. After this point, the fabric fails and no longer serves as an effective PM filter.

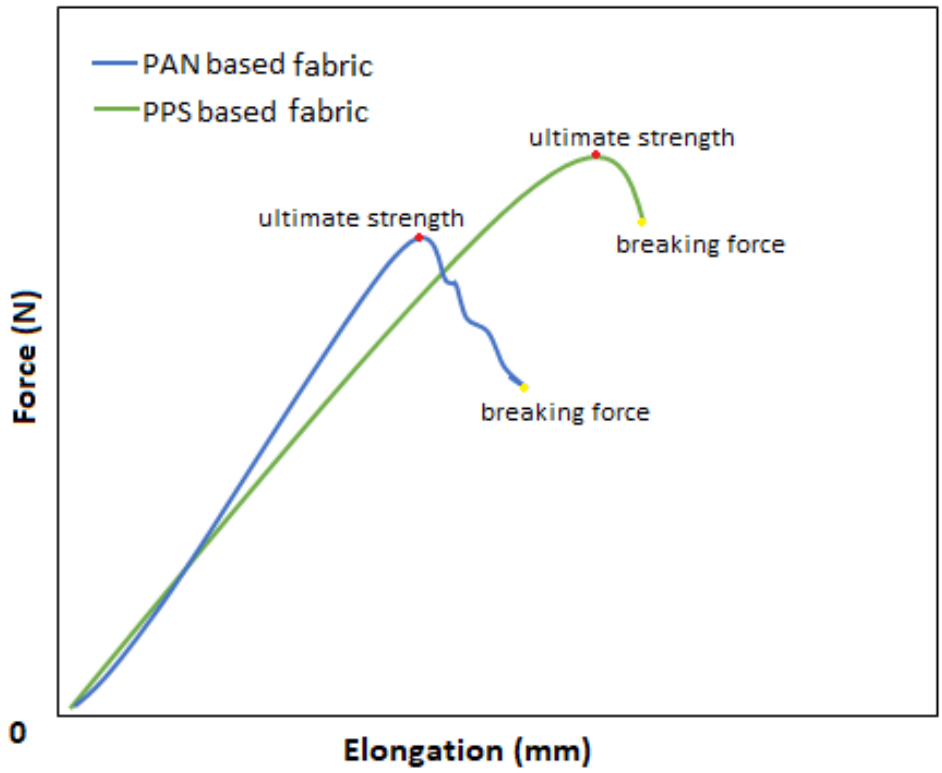

Figure 4-1: Indicative filtration fabric tensile curve

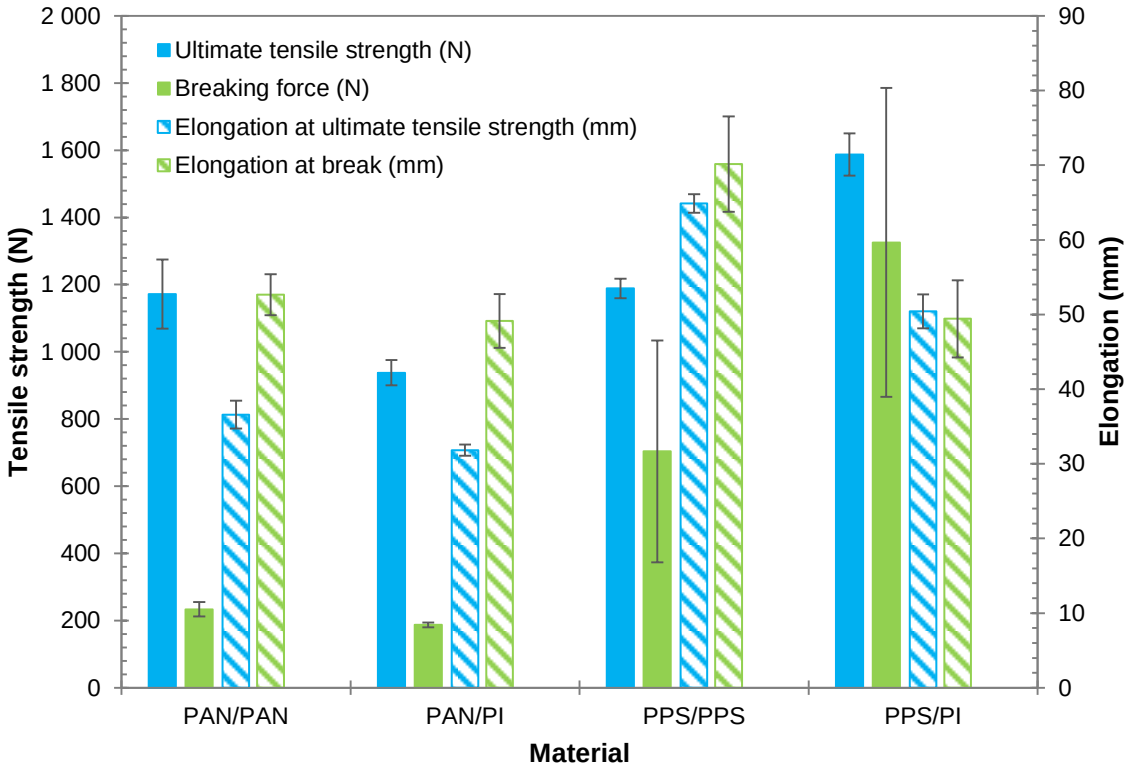

Figure 4-2: Baseline fabric strength and elongation properties

From Figure 4-2 it is apparent that the high temperature fabrics (PPS/PPS and PPS/PI) exhibit higher UTS than the low temperature fabrics (PAN/PAN and PAN/PI). Furthermore, the addition of PI does not consistently offer an UTS advantage. While PPS/PI was found to have higher UTS than PPS/PPS, PAN/PI was found to have lower UTS than PAN/PAN.

However, the incorporation of PI in both low and high temperature fabrics resulted in lower elongation at ultimate tensile strength, implying greater fabric rigidity. It must be noted, however, that since samples are needle felt fabric, elongation is impacted by the fabric manufacturing method and quality as well as the fibre properties since individual fibres unfurl during tension.

While Figure 4-2 provides insight into the ultimate tensile properties of the fabrics under consideration, the purpose of the baseline experiments was to establish reference points against which to evaluate changes in tensile properties after subsequent experiments. The relative standard error was therefore used to establish the percentage change from the baseline which can be considered significant. This is shown in Figure 4-3.

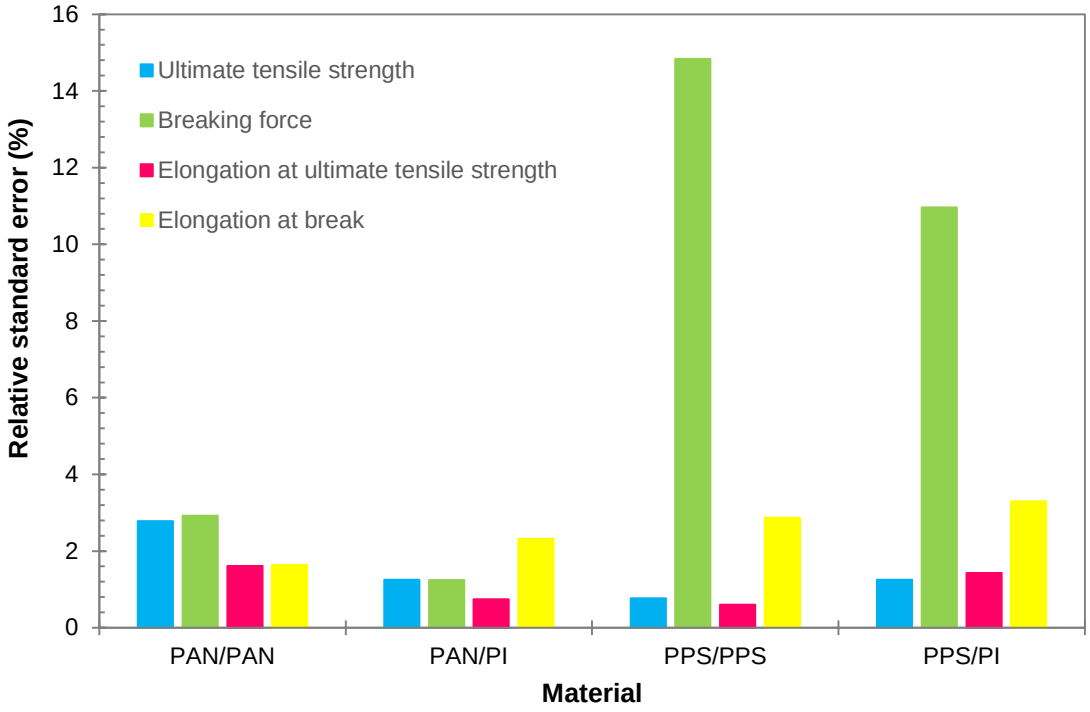

Figure 4-3: Relative standard error of tensile properties

From Figure 4-3 it can be seen that generally deviations of more than 3% can be considered to be significant, with the exception of PPS/PPS and PPS/PI breaking force. The breaking force and associated elongation are largely impacted by the variation inherent to needle felt fabric.

Therefore, only the UTS and the associated elongation were considered for evaluation of the tensile properties of the fabrics following acid exposure. The effects of acid exposure on the low temperature, PAN-based fabrics (PAN/PAN and PAN/PI) are first discussed in Section 4.3.2, followed by a discussion on the effects on the high temperature, PPS-based fabrics (PPS/PPS and PPS/PI) in Section 4.3.3.

4.3.2 COMPARISON OF THE EFFECTS OF ACID ATTACK ON PAN-BASED FABRICS

4.3.2.1 NITRIC ACID

In order to evaluate the inclusion of PI in PAN-based fabric filter material for low temperature baghouse applications under conditions where nitric acid is present, three experiments were conducted. All experiments were conducted according to the method described in Section 4.2.3. All the reported results reflect the average of three samples.

Firstly, the duration of nitric acid exposure required to observe a significant change in the UTS and elongation compared to the relative standard error recorded for the neat PAN-based fabrics was determined. This experiment also gave insight into the impact of increased exposure time on tensile strength retention. The typical operational temperature of 125°C was used, as recommended for PAN/PAN and PAN/PI operation in coal-fired baghouses. Secondly, the impact of increased nitric acid concentration at the established exposure time and operational temperature was investigated. Finally, the impact of exposure at varying temperature was studied, i.e. over the operating temperature range of the PAN-based fabric, while keeping the nitric acid concentration and exposure time constant.

EXPOSURE TIME

Since PAN constitutes the bulk of the fabric in both PAN-based fabrics, only PAN/PAN samples were considered for exposure time establishment. Four time intervals were tested, with results summarised in Table 4-5.

Table 4-5: Effect of 0.8 M nitric acid on PAN at 125°C

Exposure time (h)	Change in Tensile Strength (%)	Baseline Tensile Strength Fluctuation (%)	Change in Mass (%)
2	0.57	±2.8%	-0.13
4	-52	±2.8%	5.7
8	-	±2.8%	-
24	-	±2.8%	-

From Table 4-5 it can be seen that after two hours a significant impact on UTS could not be seen. After four hours, however, a significant decline in tensile strength could be observed as well as an increase in mass. After eight and 24 hours of nitric acid exposure, the samples had degraded to such an extent that tensile strength analysis could not be performed since the material was brittle and blackened (see Figure B-1). This result corresponds with the results reported by Weber et al. (1988), where it was found that PAN fibres yellowed and ultimately blackened when exposed to NO_2 and moisture.

An exposure time of 4 hours was therefore selected as appropriate for further analysis of the effect of nitric acid exposure of the PAN-based fabrics.

EFFECT OF CONCENTRATION

The tensile strength analysis results presented in this section represent those of the PAN-fabrics that were exposed to nitric acid at varying concentrations, while the temperature was kept fixed at 125°C for four hours.

No clear trend in the changes in the UTS of either fabric was observed with increasing nitric acid concentration (Figure B-2). The significant degradation of PAN/PAN in 0.8 M nitric acid appears to be an outlier. However, since samples that were exposed for longer periods at 0.8 M were degraded to such an extent that tensile testing could not be performed (Figure B-1), it would seem that 0.8 M nitric acid has a notable effect on PAN/PAN, but not necessarily PAN/PI. Minor changes in sample mass after exposure, as can be seen in Figure B-3, show some correlation of increased mass with decreased ultimate tensile strength.

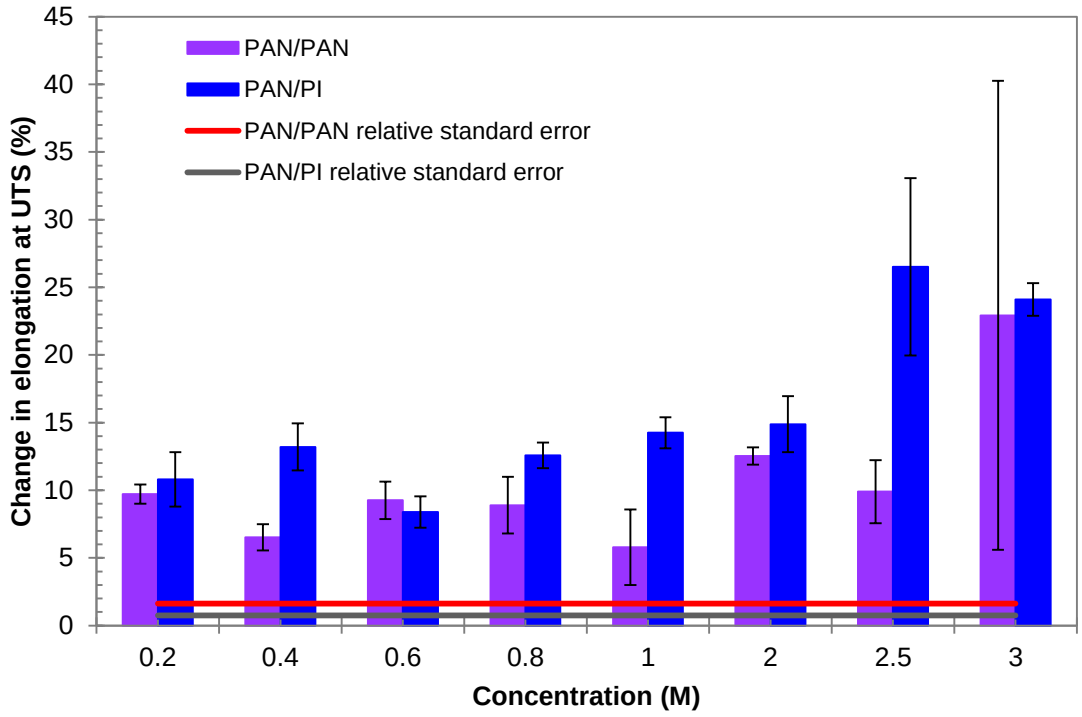

Figure 4-4: Effect of nitric acid exposure for 4 hours at 125°C on PAN/PAN and PAN/PI elongation at ultimate tensile strength

From Figure 4-4, however, it is clear that significant increases in the elongation at the UTS occurred. It can be seen that both fabrics follow a trend of increasing elongation after exposure to increased nitric acid concentrations. Although a large increase in PAN/PAN elongation is reported after exposure to 3 M nitric acid solution, the error is large and a consistent trend of increasing PAN/PAN elongation at UTS is not clear. The

increased elongation at UTS is most notable in PAN/PI. Although the incorporation of PI in PAN-based fabrics therefore improves fabric tensile strength retention, the increased elongation (plasticity) may have adverse effects on bag shape retention after prolonged exposure to nitric acid when the flue gas temperature frequently drops below the acid dew point temperature.

Visually, no change in the PAN/PAN or PAN/PI samples was observed for the fabrics that were exposed to nitric acid solutions with a concentration of up to 2 M, with the exception of PAN/PAN exposed to 0.8 M nitric acid. Observable changes at higher concentrations are pictured in Figure B-4. Instances where hardened edges were observed correspond with the highest increase of elongation. Visual changes also correspond with an increase of between 0.88% and 5.7% in the mass of the samples. Hardened edges in PAN/PAN correspond with decreased tensile strength, although the same is not true for PAN/PI.

EFFECT OF TEMPERATURE

In these experiments, PAN-based fabrics were exposed to nitric acid solutions with a fixed concentration of 2 M for four hours while varying the temperature over the low-temperature operating range (95°C – 140°C). Although baghouses are typically operated above 120°C due to acid dew point concerns, temperatures below this are considered in this study to understand the impact of acid attack on PAN-based fabrics.

For all temperatures considered, a control sample of PAN/PAN was submerged in only water to exclude the possibility that any tensile strength impacts were due purely to temperature effects and/or the absorption of water by the polymers. Since both PAN-based fabrics consist predominantly of PAN, considering PAN/PAN only was deemed reasonable. From Figure 4-5 it can be seen that the control samples exposed to water showed negligible tensile strength changes in most cases, except in two cases where a positive change in the UTS was observed at 110°C and 140°C. It is possible that the slight increase in the UTS in these cases was due to an annealing effect, whereby the degree of crystallinity of the polymers could have been increased (Jung, et al., 2005). It can therefore be concluded that the decrease in the UTS observed for the fabrics that were exposed to nitric acid (Figure 4-5) was due to degradation and not merely temperature effects.

The effect of nitric acid exposure on the tensile strength of PAN/PI was marginally significant at all tested temperatures except the operating temperature of 125°C, while the same was true for PAN/PAN at all temperatures except 110°C and 140°C. At

110°C, a slight increase in the UTS was observed for the PAN/PAN samples although this was not statistically significant, and at 140°C a definite decrease in the UTS was observed, as is clear from Figure 4-5. In terms of nitric acid exposure, it would therefore seem that PI, which is rated for high temperature baghouse applications, offers a slight benefit in terms of strength retention of PAN-based fabrics at the maximum operating temperature, but does not offer any benefit at lower temperatures.

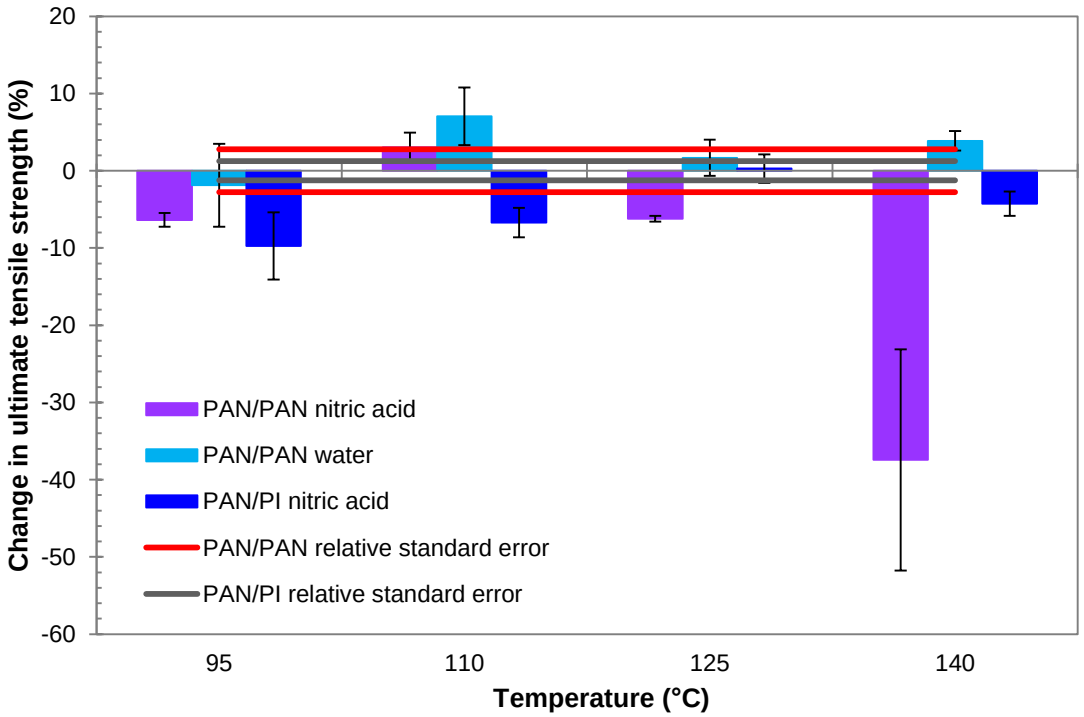

Figure 4-5: Effect and 2 M nitric acid exposure on PAN/PAN and PAN/PI ultimate tensile strength at various temperatures compared to PAN/PAN control samples in water

While the tensile strength was not significantly affected in the control samples that were exposed to varying temperatures while being submerged in deionised water, the elongation at UTS was affected (Figure 4-6). With the exception of the 140°C data point in Figure 4-6, nitric acid exposure appears to have inhibited the increase in elongation experienced by PAN/PAN when heat-treated in deionised water. The increased elongation with increasing temperature, coupled with the slight decrease in the UTS for the samples that were treated with nitric acid at 95°C and 125°C, and the significant decrease in the UTS for the samples treated at 140°C, suggests that nitric acid exposure had the effect of increasing the plasticity of the PAN/PAN samples. The degree to which the plasticity was increased was more pronounced at higher temperatures. However, since the increased plasticity was reduced relative to that of

the samples that were heat-treated only in water, the increase in the plasticity was suppressed by the presence of nitric acid at 2 M except at a temperature of 140°C.

PAN/PI showed a similar trend, with the exception of the data point at 110°C. The increase in the elongation at 140°C after nitric acid exposure, however, was significantly less than that of PAN/PAN; suggesting PI incorporation again offers an advantage at high temperature. This benefit is not clear at the lower temperatures. This advantage is specifically improved strength retention (Figure 4-5) and reduced elongation (Figure 4-6), which translates to improved rigidity at high temperatures and exposure to high nitric acid concentrations.

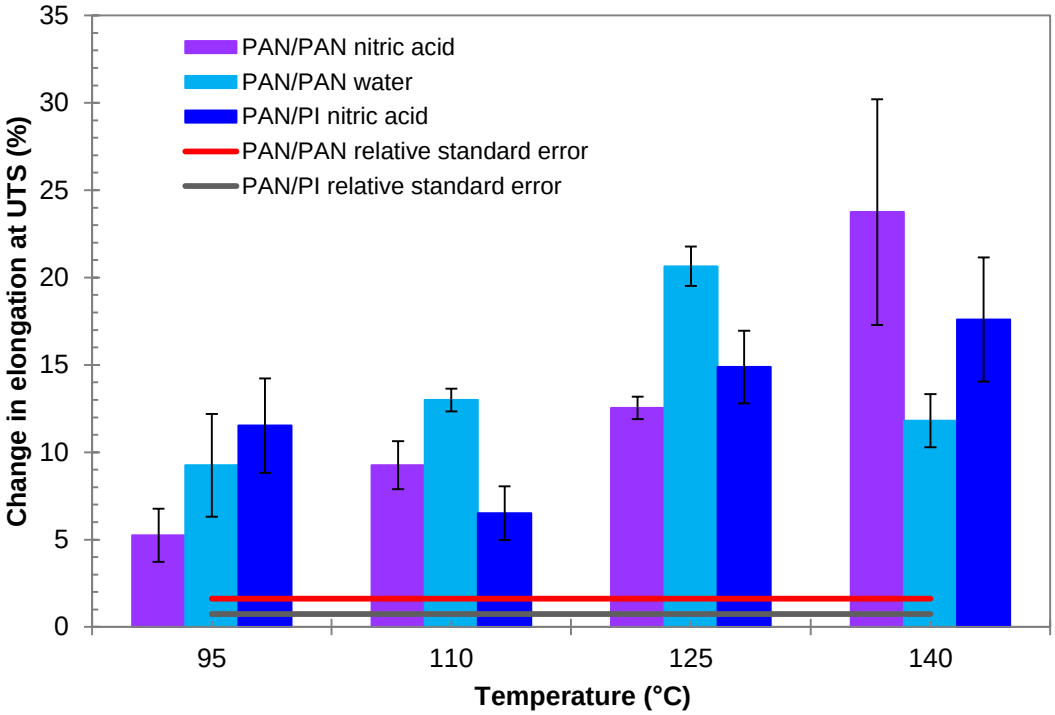

Figure 4-6: Effect of 2 M nitric acid on PAN/PAN and PAN/PI elongation at ultimate tensile strength at various temperatures compared to PAN/PAN control samples in water

The large increase in the elongation after nitric acid exposure at increasing temperatures echoes the discussion in the previous section, where elongation was seen to increase with increasing nitric acid concentration. It is therefore concluded that increasing nitric acid aggressors, namely the nitric acid concentration, exposure time and exposure temperature, results in increased PAN-based fabric elongation at UTS. The incorporation of PI aids in improving the strength retention at extreme conditions. At lower temperatures and nitric acid concentration, PI incorporation does not seem to offer any substantial advantages. The reduced increase in the plasticity of the PAN/PI

samples compared to the PAN/PAN samples at high temperatures might be due to the inhibition of plasticisation of the PI fibre due to charge-transfer complexes formed by thermal annealing or possible thermal or chemical cross-linking of PI (Vanherck, et al., 2013), although further analysis would be required to confirm this hypothesis.

Visually, only the samples exposed at 140°C showed any observable change. This can be seen in Figure B-5. Similar to the concentration analysis discussed above, hardened edges correspond with decreased tensile strength and increased elongation. Mass change does not correspond with strength or elongation.

4.3.2.2 SULPHURIC ACID

Experiments similar to those described for nitric acid above were conducted to establish the impacts of PAN-based fabric exposure to sulphuric acid, of which the results are discussed in the following sections.

EXPOSURE TIME

As with nitric acid, only PAN/PAN samples were considered for establishing the minimum exposure time that was required to observe a statistically significant change in the tensile properties. Samples were thus exposed to sulphuric acid for 2, 4, 8, 12 and 24 hours at concentrations of 0.5 M, 1 M and 3 M sulphuric acid, of which the results are shown in Figure 4-7.

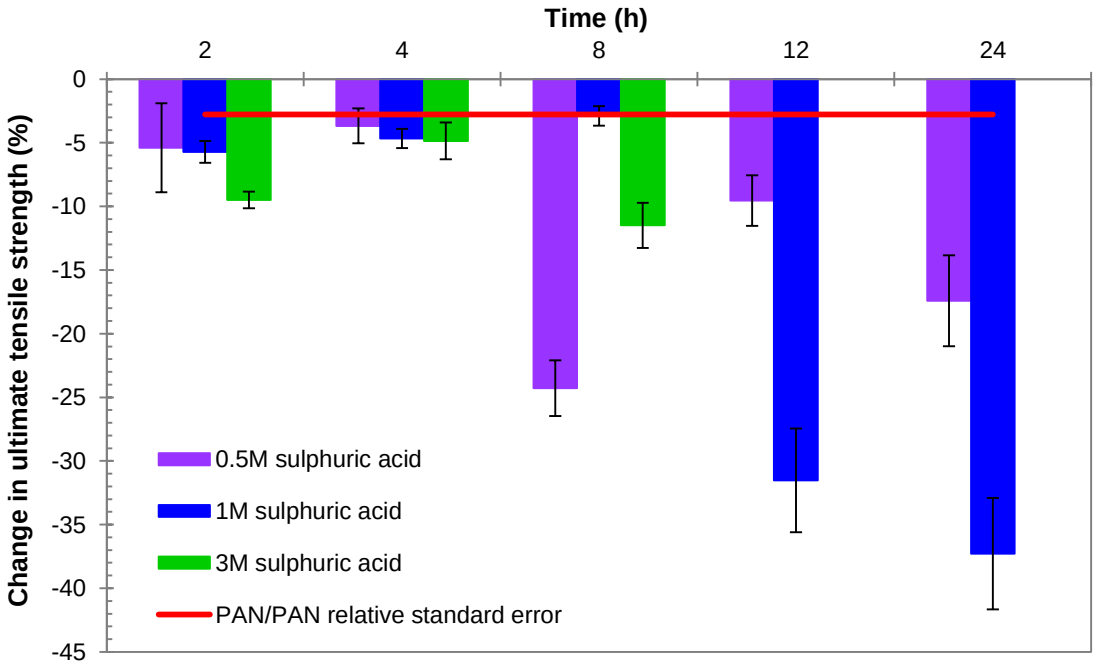

Figure 4-7: Effect of sulphuric acid on PAN/PAN ultimate tensile strength at 125°C

Unlike the nitric acid experiments where a clear trend was observed in terms of the degradation as a function of time, the sulphuric acid experiment results did not yield a conclusive trend.

Tensile strength results indicate that at below 1 M, sulphuric acid did not show any distinct degradative trend. At a sulphuric acid concentration of 3 M and an exposure time of 12 hours, the samples were shrunken and had hardened to the extent that they could no longer be unrolled (Figure B-6) for tensile strength analysis. Therefore, an exposure time of eight hours was selected for further experiments where the effects of sulphuric acid concentration and temperature on the tensile properties of PAN-based fabrics were studied.

EFFECT OF CONCENTRATION

Insight into the effect of increasing sulphuric acid concentration on PAN/PAN can be gained from the exposure time discussion above. However, in order to understand the comparative effect of sulphuric acid exposure on PAN/PI, samples of PAN/PI filtration fabric were exposed to concentrations of sulphuric acid between 0.5 M and 3 M for eight hours at a constant temperature of 125°C.

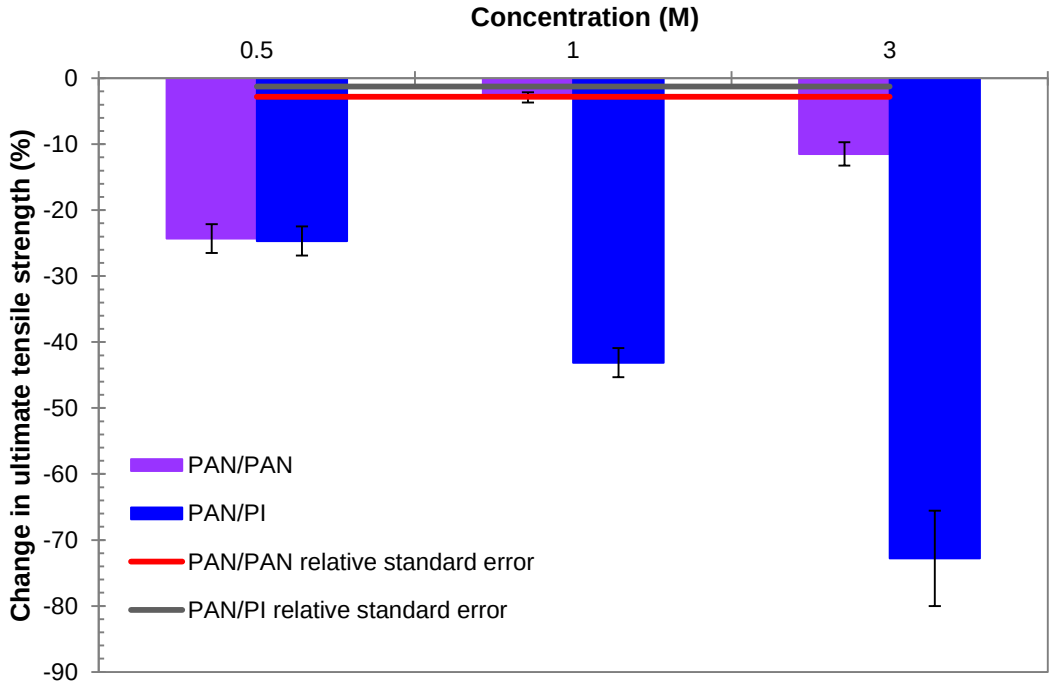

Figure 4-8: Effect of sulphuric acid exposure for 8 hours at 125°C on PAN/PAN and PAN/PI tensile strength

As can be seen from the results reported in Figure 4-8, it was found that increasing sulphuric acid concentration has a lesser impact on PAN/PAN than PAN/PI. Furthermore, PAN/PAN did not show any correlation in terms of the UTS with respect to concentration, whereas the UTS of the PAN/PI fabric samples exhibited a definite trend of decreasing tensile strength with increasing sulphuric acid concentration. As with nitric acid exposure, loss of strength correlated with a mass gain of between 8.8% and 14% (Figure B-7). Changes in the elongation at the UTS, however, did not exhibit any correlation with the tensile strength or mass and were seen to fluctuate between increasing and decreasing elongation, exhibiting no clear trend with sulphuric acid concentration (Figure B-8).

Visually, impact was only noted on PAN/PAN fabric samples after exposure to 0.5 M sulphuric acid for eight hours at 125°C, where dark stains could be seen on the fabric, edges had hardened and the fabric appeared to have lost flexibility (Figure B-9). This appearance corresponds with the greatest loss in tensile strength for the PAN/PAN fabric samples, as well as the largest mass gain and the highest increase in elongation exhibited during the tests of exposure to increasing sulphuric acid concentrations. The increase in elongation when hardened edges were observed was also in keeping with the PAN/PAN results discussed for the nitric acid exposure experiments.

The PAN/PI fabric samples did not exhibit any significant visual changes after sulphuric acid exposure with a concentration of 0.5 M; however, the samples became increasingly hardened, darkened and shrunken when the concentration was further increased (Figure B-10). As with the nitric acid exposure results, PAN/PI fabric samples that had darkened after acid exposure exhibited decreased UTS.

EFFECT OF TEMPERATURE

PAN-based fabrics were exposed to sulphuric acid with a concentration of 1 M for eight hours over the PAN-based fabric operating temperature range. Control samples of PAN/PAN were exposed to deionised water at the various temperatures to exclude effects due solely to temperature and moisture.

From Figure 4-9 it can be seen that UTS of PAN/PAN was only negatively impacted at the maximum operating temperature, whereas PAN/PI was also impacted at the normal operating temperature of 125°C. Elongation at UTS, shown in Figure 4-10, did not correspond with the UTS results. Similar to the results for nitric acid, a trend of increased plasticity with increased temperature can be seen for PAN/PAN. This trend,

however, is not apparent for PAN/PI which alternated between increased and decreased elongation. The decrease of PAN/PI UTS and elongation at UTS at 140°C indicates increased fabric rigidity.

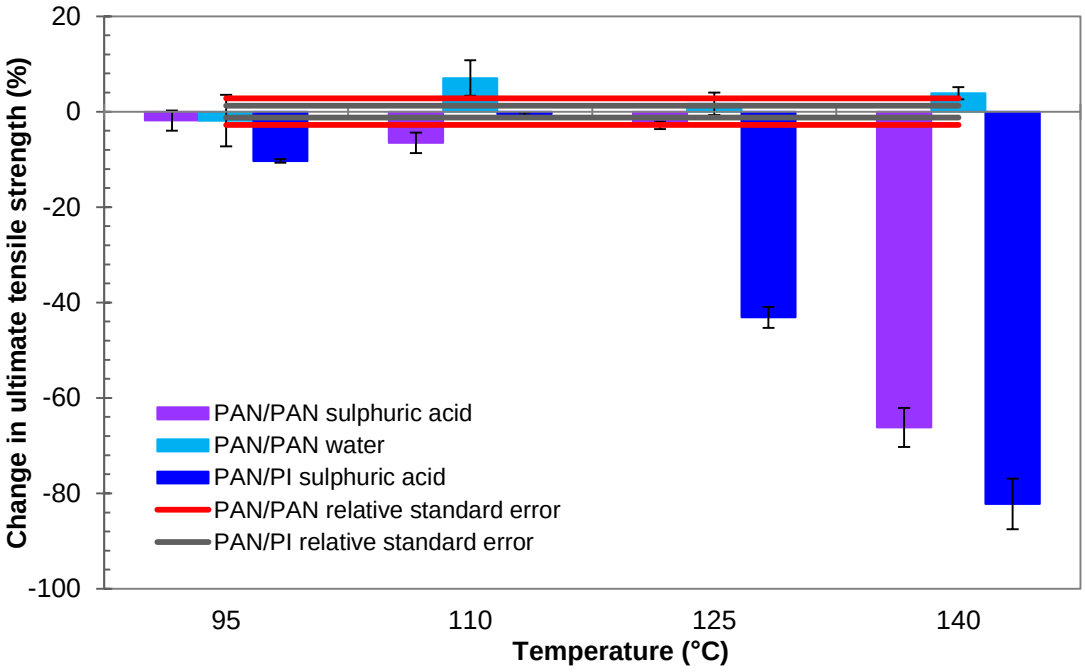

Figure 4-9: Effect 1 M sulphuric acid exposure for 8 hours on PAN/PAN and PAN/PI ultimate tensile strength at various temperatures compared to PAN/PAN control samples in water

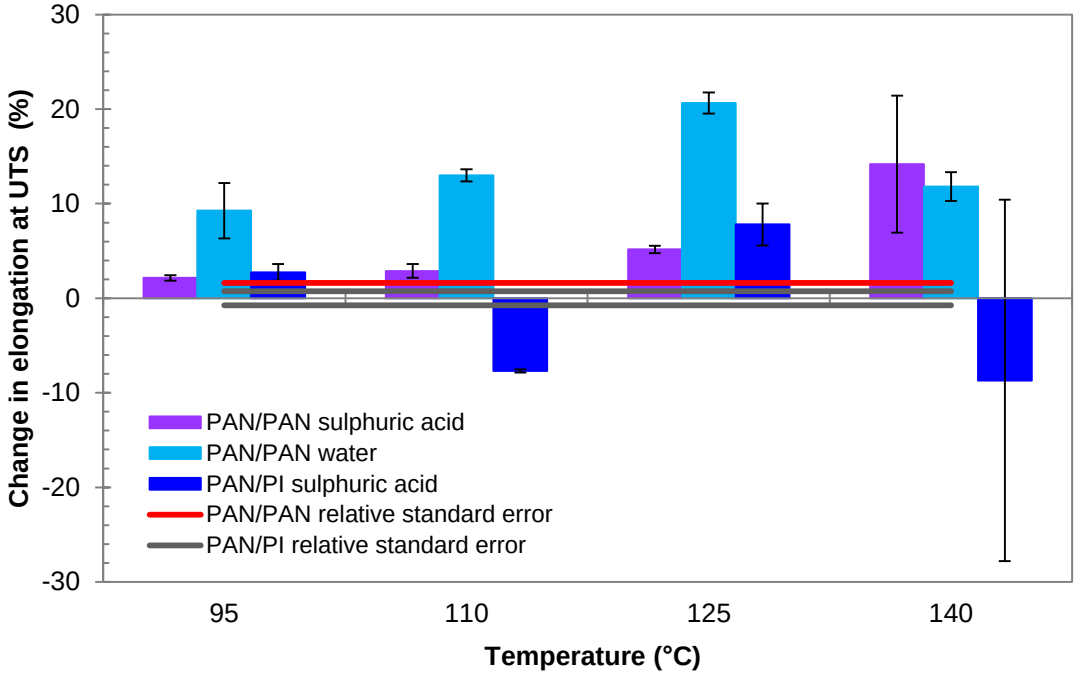

Figure 4-10: Effect of 1 M sulphuric acid exposure for 8 hours on PAN/PAN and PAN/PI elongation at ultimate tensile strength at various temperatures compared to PAN/PAN control samples in water

Visually, little change could be observed in the PAN/PAN or PAN/PI samples exposed to sulphuric acid below temperatures of 140°C. However, at 140°C the samples of both PAN/PAN and PAN/PI were hardened and could not be fully unrolled to perform tensile strength tests (Figure B-11). This hardening corresponds with decreased UTS. The difficulty in sampling handling could be a reason for the large variability of elongation at UTS measurements observed at 140°C.

4.3.2.3 EFFECT OF COMBINED NITRIC AND SULPHURIC ACID

To further understand the impact of nitric and sulphuric acid exposure on PAN-based fabrics, the combined impact of the acids that could be present in flue gas simultaneously was also evaluated. An exposure time of four hours was selected for these experiments, seeing as nitric acid degraded PAN/PAN samples to a point where tensile strength analysis was no longer possible at longer exposure durations. The impact of increasing concentrations of both acids at the typical operating temperature of 125°C was studied.

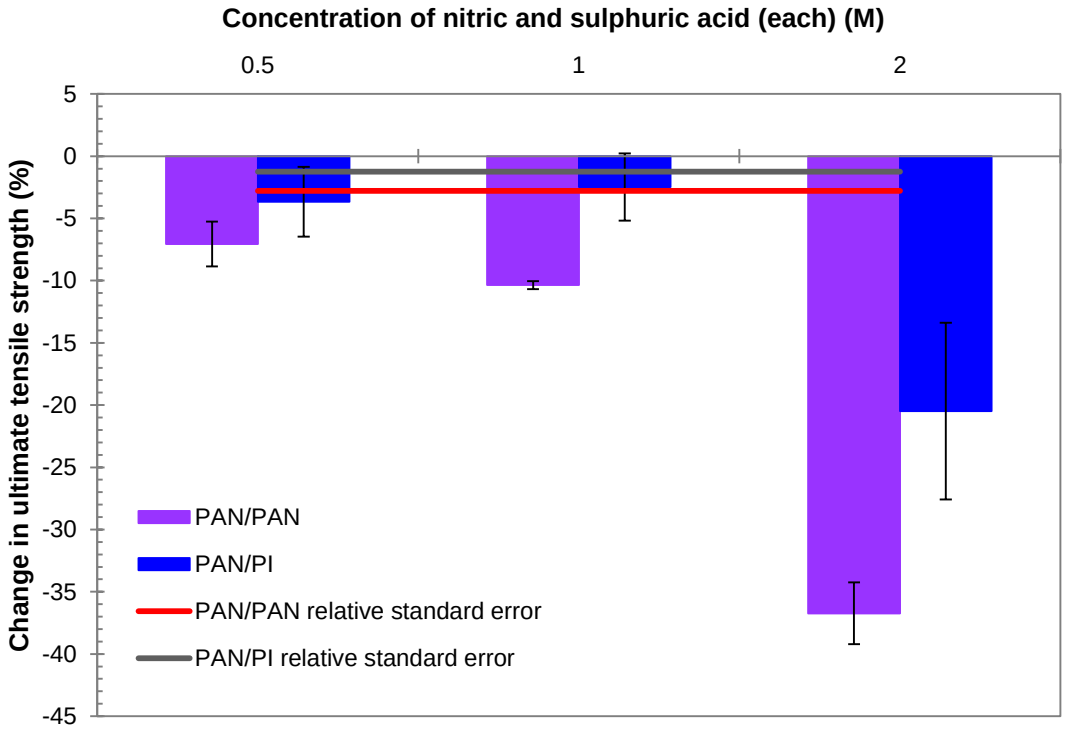

Figure 4-11: Effect of combined nitric and sulphuric acid exposure for 4 hours at 125°C on PAN/PAN and PAN/PI ultimate tensile strength

From the results reported in Figure 4-11, it is evident that combined nitric and sulphuric acid exposure had a significant negative impact on the PAN/PAN UTS. This impact became more significant with increasing acid concentration. It is further evident that PI

incorporation offered an apparent tensile strength retention benefit, since PAN/PI was not significantly affected when exposed to 0.5 M and 1 M concentrations of sulphuric and nitric acid each. However, both fabrics exhibited a significant reduction in UTS after exposure to a mixture of nitric and sulphuric acids with a concentration 2 M of each acid.

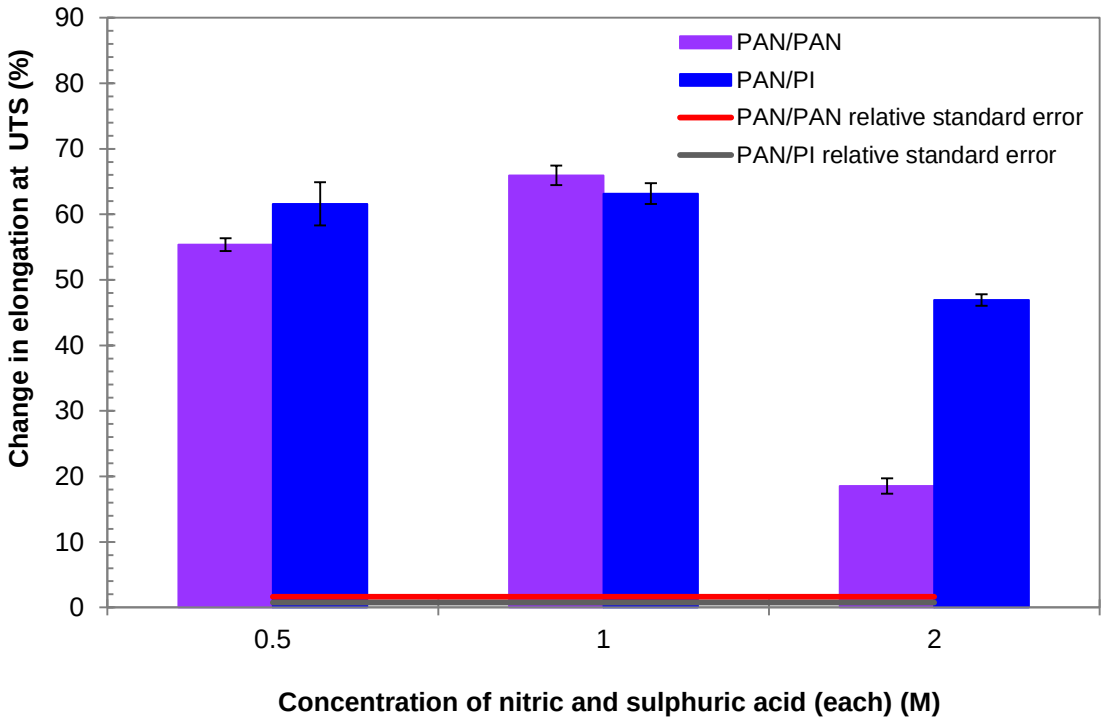

Figure 4-12: Effect of combined nitric and sulphuric acid exposure for 4 hours at 125°C on PAN/PAN and PAN/PI elongation at ultimate tensile strength

The elongation data at UTS after exposure to nitric and sulphuric acid mixtures, shown in Figure 4-12, did not correlate with the trend observed for the UTS results. Nonetheless, both fabrics exhibited a significant increase in elongation (19% - 69% for PAN/PAN and 47% - 63% for PAN/PI) at all of the concentrations studied, in keeping with the results of PAN-based fabrics that were exposed to either nitric or sulphuric acid solutions individually. This increase is elongation, however, was significantly greater than when fabric samples were exposed to nitric acid or sulphuric acid only, where changes in elongation at UTS were less than 27%. In this specific case, however, the increase observed for the PAN-based fabrics did not differ significantly at concentrations of 0.5 M and 1 M, while a marked decrease in the elongation change was observed at the combined nitric and sulphuric acids of concentrations of 2 M, especially for the PAN/PAN fabric samples. This behaviour, coupled with the 35% decrease in the UTS of the PAN/PAN fabrics (Figure 4-11), suggests that a further

increase in the acid concentrations or exposure time would have led to embrittled fabrics. At the conditions that were studied, however, the fabrics experienced an increase in plasticity, which could be due to the absorption of sulphuric acid by the PAN fibres that led to swelling (Śmigiel-Kamińska, 2014). This hypothesis is supported by the fact that, as with exposure of PAN-based fabrics to nitric acid or sulphuric acid only, mass gain correlated with the decreased UTS (Figure 4-13).

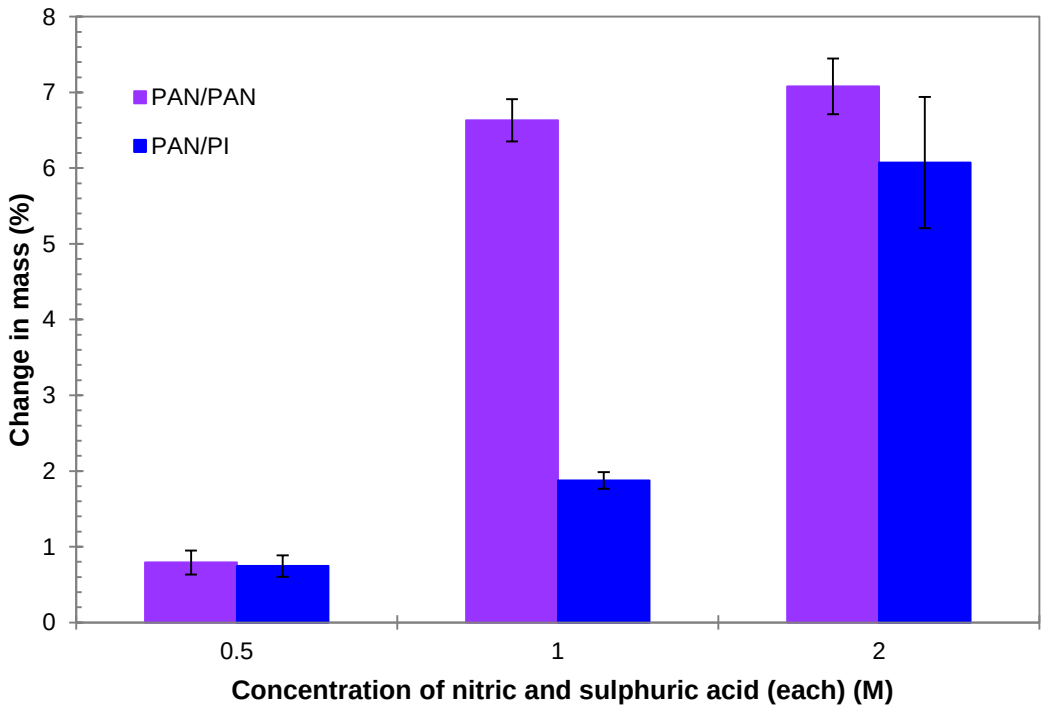

Figure 4-13: Effect of combined nitric and sulphuric acid exposure for 4 hours at 125°C on PAN/PAN and PAN/PI mass

4.3.2.4 SUMMARY OF ACID ATTACK ON PAN-BASED FILTRATION FABRIC

The effects of nitric and sulphuric acid exposure on the UTS of PAN-based fabrics under varying acid concentrations are summarised in Table 4-6. In this table, the data for PAN/PAN and PAN/PI at 125°C and an exposure time of 4 hours at acid concentrations of 0.5 M, 1 M and 2 M are presented. The only exception is the data of PAN/PI exposure to sulphuric acid, where only 8 hour exposure time data are available. Where test data at the specific concentrations were not available, results were interpolated. These conditions were selected to be representative of low, medium and high acidic concentrations.

Table 4-6: Strength retention of low temperature fabrics after acid attack

Acid	Fabric type	Tensile Strength Retention (%)			
		Low Concentration (0.5 M)	Medium Concentration (1 M)	High Concentration (2 M)	Average
Nitric acid	PAN/PAN	95	96	94	95
	PAN/PI	99	103	100	101
Sulphuric acid	PAN/PAN	96	95	95	95
	PAN/PI	75	57	42	58
Nitric & sulphuric acid	PAN/PAN	93	90	63	82
	PAN/PI	96	98	80	91

It is evident from Table 4-6, that PI incorporation in PAN-based fabrics offered a tensile strength retention benefit under the conditions studied when exposure to nitric acid or combined nitric and sulphuric acids was experienced. Nonetheless, the fact that PAN/PAN fabrics did not degrade significantly in these conditions is also noteworthy.

When exposed to sulphuric acid, PAN/PI fabrics underwent significant degradation as is evident from its very poor strength retention (58%), whereas PAN/PAN showed good strength retention (95%). The sensitivity of PI to sulphuric acid attack is in keeping with results reported by Weinrotter and Seidl (1993). Weinrotter and Seidl also reported strength reduction of PI by nitric acid, however this is not corroborated by the present study. This lack of corroboration of results could have been due to the use of PI as a minor portion of a blend of PAN and PI, wherein the negative effects on PI could not be discerned.

4.3.3 COMPARISON OF THE EFFECTS OF ACID ATTACK ON PPS-BASED FABRICS

4.3.3.1 NITRIC ACID

The same approach followed for PAN-based fabrics was applied to PPS-based fabrics. PPS/PPS and PPS/PI were evaluated at the recommended operating temperature of 150°C and fixed concentration to establish an appropriate exposure time for further nitric acid exposure tests. Subsequently, the effect of concentration was investigated. Finally, the effect of exposure to nitric acid of fixed concentration throughout the operating temperature range was investigated.

EXPOSURE TIME

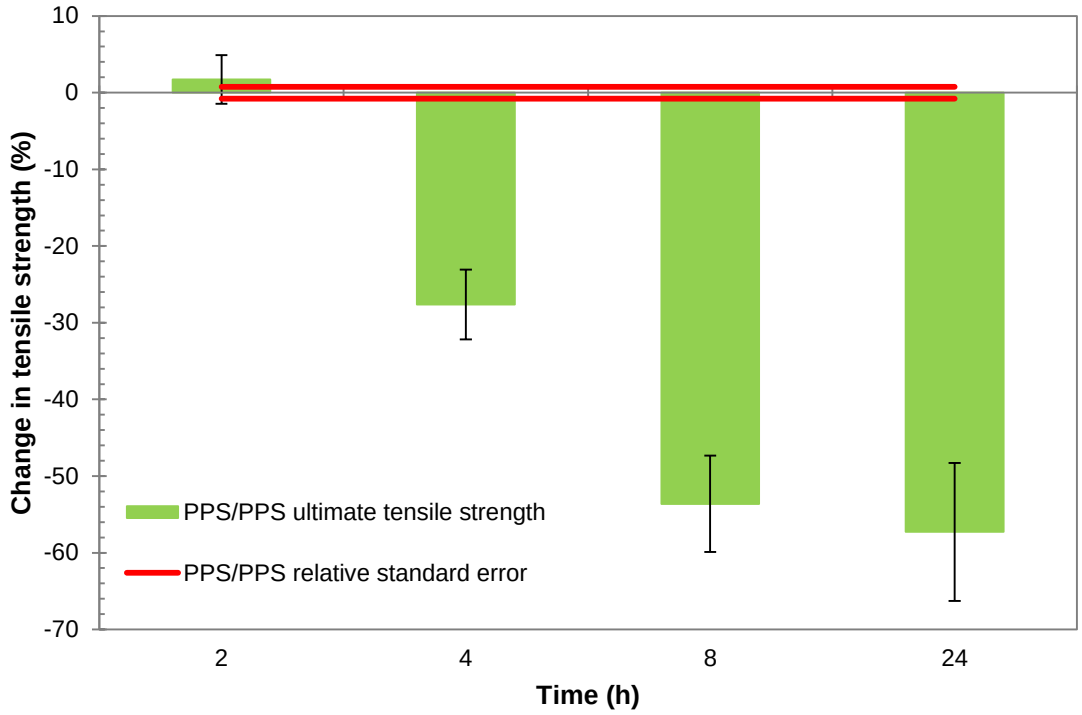

Figure 4-14: Effect of 0.8 M nitric acid exposure at 150°C on PPS/PPS tensile strength over time

Since the bulk of the fabric in both high temperature fabrics is PPS, only PPS/PPS samples were considered when establishing the exposure time for nitric acid exposure. After a marginal strength increase after exposure to nitric acid for two hours, it is clear from Figure 4-14 that a trend of decreasing UTS with increasing exposure time was observed. This corresponds with the results published by Tanthapanichakoon et al. (2006), reporting the significant impact of long term nitric acid exposure on PPS tensile strength. Observed sample yellowing after nitric acid exposure also corresponds with Tanthapanichakoon et al.'s (2006) findings. After four hours the change in strength was significant; therefore, four hours was selected for subsequent test durations.

At exposure times beyond two hours, a correlation between decreased UTS and decreased elongation can be seen when comparing Figure 4-14 with Figure 4-15. This indicates that PPS/PPS became increasingly brittle with exposure to nitric acid for increasing durations. Although mass increase is low, a further correlation of mass increase with UTS decrease was noted (Figure B-12).

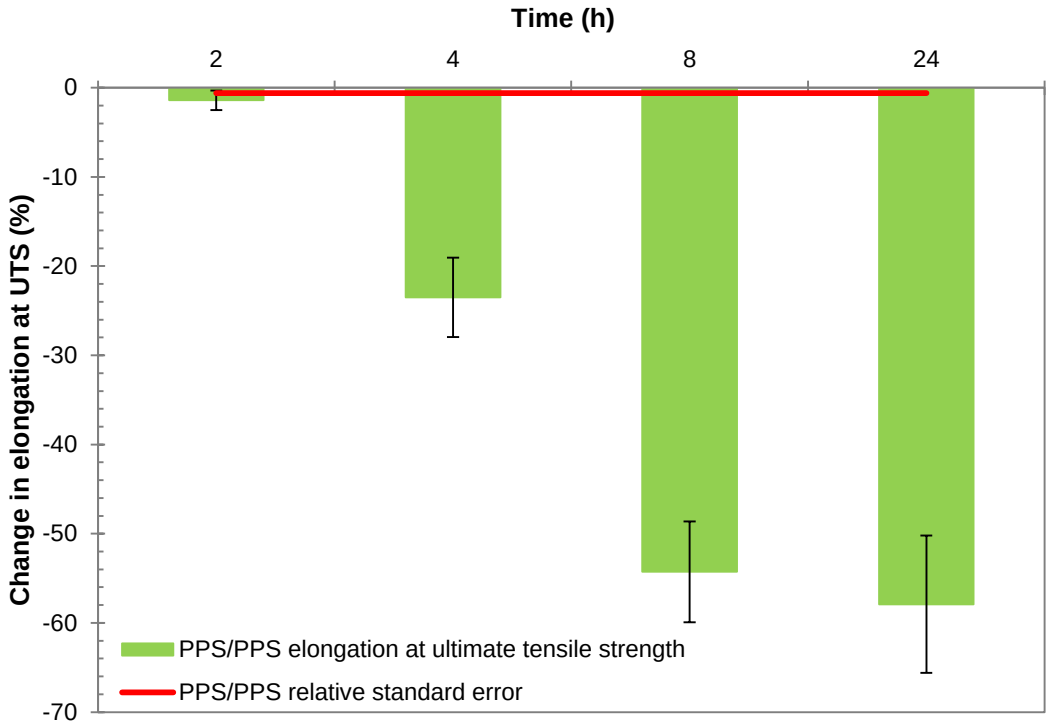

Figure 4-15: Effect of 0.8 M nitric acid exposure at 150°C on PPS/PPS elongation at ultimate tensile strength

EFFECT OF CONCENTRATION

Applying the established exposure time of four hours, the effects of exposure to various nitric acid concentrations on high temperature fabrics were studied. The temperature was fixed at the nominal PPS operating temperature of 150°C.

The results shown in Figure 4-16 indicate that increasing nitric acid concentration led to decreasing UTS for both PPS/PPS and PPS/PI. These results corroborate those of Tanthapanichakoon et al. (2006) and Weinrotter & Seidl's (1993), who found a significant decrease of PPS and PI tensile strength retention, respectively, with increased nitric acid concentration.

Increasing mass of the PPS-based fabrics was noted after nitric acid exposure (Figure B-13), which correlated with decreased PPS/PPS tensile strength. This finding again corroborates Tanthapanichakoon et al.'s (2006) results of PPS mass increase after nitric acid exposure. It can further be seen that the same trend holds true for PPS/PI, except for the marginally reduced PPS/PI mass increase at 1 M, compared to that at 0.8 M.

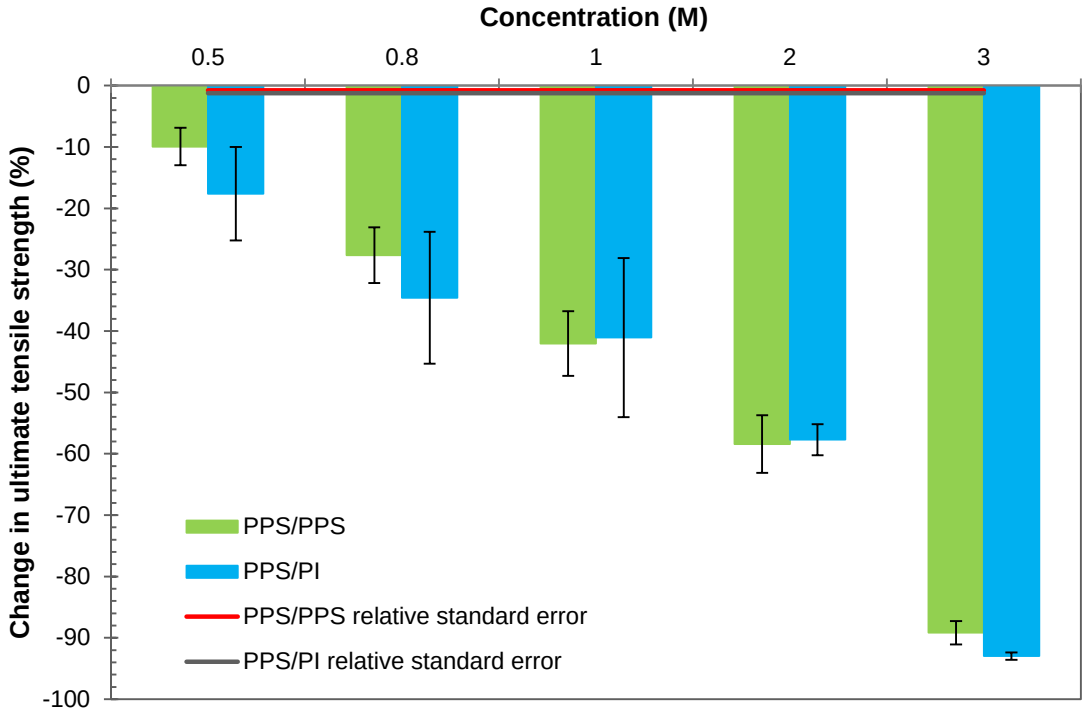

Figure 4-16: Effect of nitric acid exposure for 4 hours at 150°C on PPS/PPS and PPS/PI tensile strength

A similar trend of decreasing elongation with increasing nitric acid concentration for both PPS-based fabrics can be seen in Figure 4-17. The exception to this trend is PPS/PI elongation at 3 M nitric acid, which at -43%, was a smaller decrease than that observed at 2 M, i.e. -49%. Despite this average result, the large standard error indicates, however, that the trend of decreasing elongation was observed for some samples. Nonetheless, the decrease in the elongation relative to the neat fabrics was significant, and it can therefore be concluded that both PPS-based fabrics become increasingly brittle after exposure to nitric acid of increasing concentration.

At tested concentrations of 1 M nitric acid and above, PPS/PPS shows a greater decrease in elongation than PPS/PI. This corresponds with the greater mass increase of PPS/PPS than PPS/PI (Figure B-13). It can thus be concluded that mass increase of PPS-based fabrics after nitric acid exposure corresponds with increased fabric brittleness. Furthermore, PI incorporation in PPS-based fabrics corresponds with lower brittleness after nitric acid exposure.

While acid absorption by the PAN-based fabrics is hypothesised to have led to increased plasticity, it would seem to have the opposite effect on PPS-based fabrics. It is suggested that PPS is less resistant to nitric acid, which initiates chain scission

reactions when absorbed by the polymer matrix (Tanthapanichakoon, et al., 2006). This reaction would explain the increased brittleness of the PPS fabrics when exposed to nitric acid solutions.

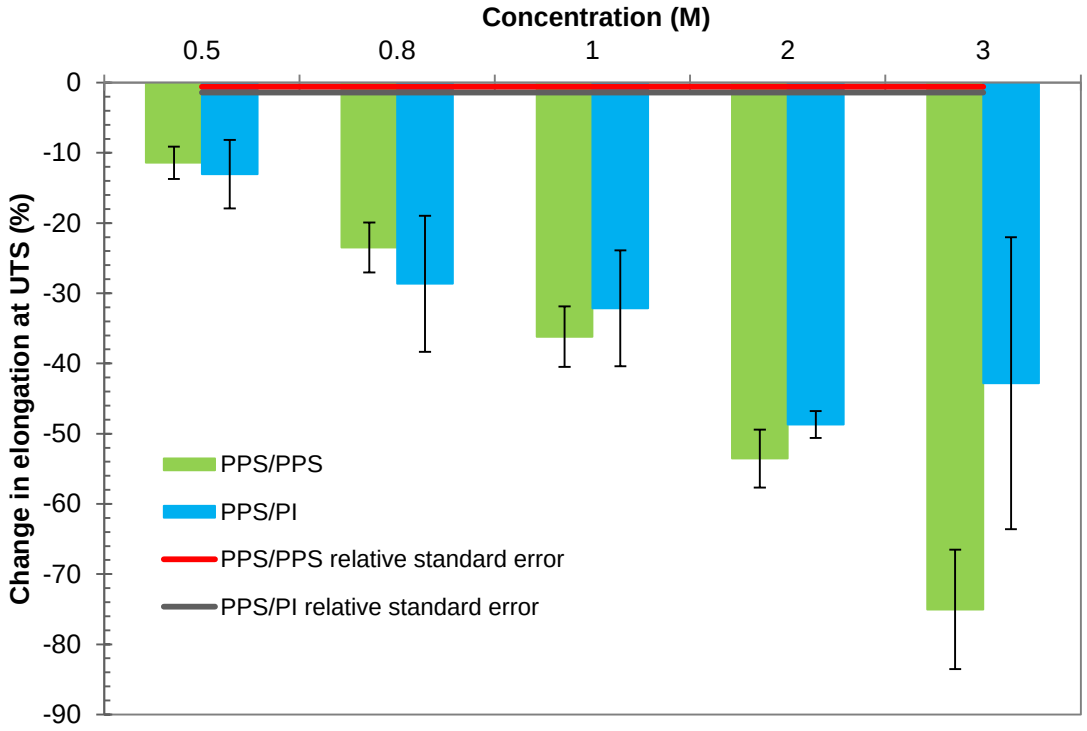

Figure 4-17: Effect of nitric acid exposure for 4 hours at 150°C on PPS/PPS and PPS/PI elongation at maximum tensile strength

EFFECT OF TEMPERATURE

In order to understand the impact of nitric acid exposure on high temperature fabrics throughout the recommended operating range, PPS/PPS and PPS/PI samples were exposed to 1 M nitric acid at four different temperatures. At each temperature set-point PPS/PPS control samples that were submerged in deionised water to be able to exclude any effects that are purely due to increased temperature and moisture.

It can be seen from the results shown in Figure 4-18 that the PPS/PPS samples exposed to water did not experience significant changes in UTS, apart from at the maximum operating temperature of 190°C where a marginally significant increase in strength was exhibited. The significant decrease in UTS of both fabrics when exposed to nitric acid can therefore be attributed to nitric acid attack at the various temperatures that were considered.

The change in the UTS of both PPS/PPS and PPS/PI followed a clear decreasing trend with increasing temperature, with the exception of the data point at 170°C where samples had degraded to a point that no longer allowed tensile strength testing (Figure B-14). Although PI is recommended for operation at high temperature, it can therefore be seen that nitric acid exposure reduces the temperature resistance of the PPS-based fabric, despite PI incorporation. This is in agreement with Klotz and Haug's (2006) statement that at temperatures above 140°C PI is susceptible to acid hydrolysis.

In these acid exposure experiments, decreased elongation was again noted to correspond with the decreased UTS after nitric acid exposure. Similar to the change in the UTS, the change in the elongation also decreased with increasing temperature (Figure B-15). PPS-based fabrics therefore appear to become increasingly brittle when exposed to nitric acid at increasing temperatures.

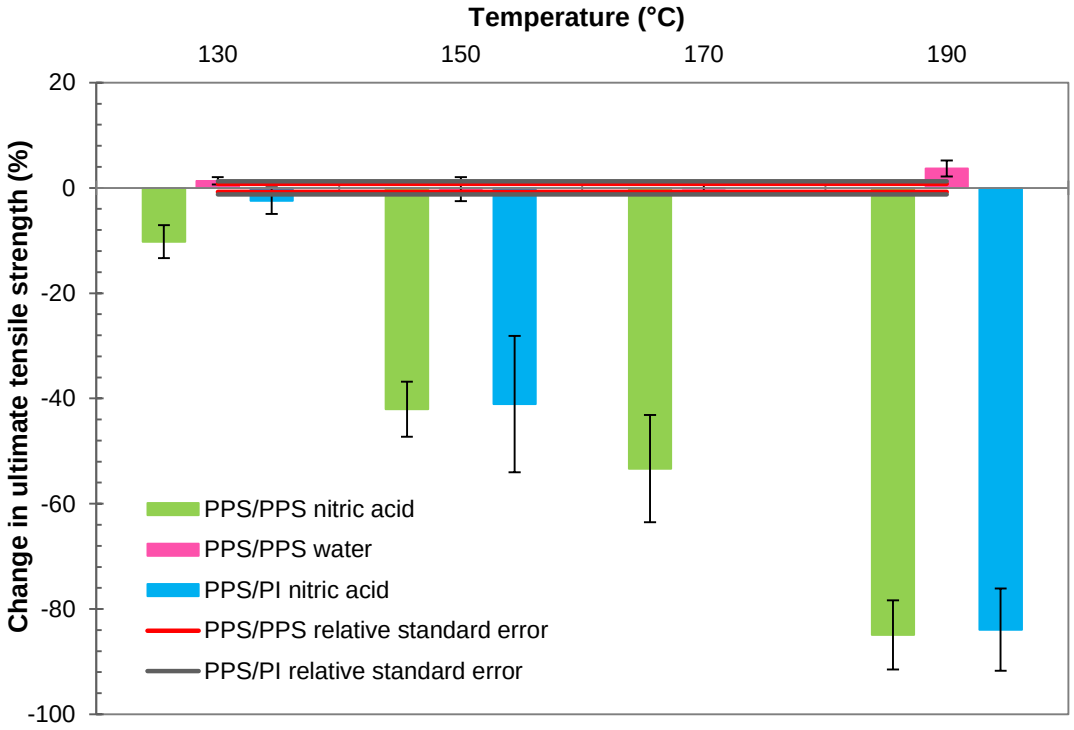

Figure 4-18: Effect of 1 M nitric acid exposure for 4 hours on PPS/PPS and PPS/PI ultimate tensile strength at various temperatures compared to PPS/PPS control samples in water

4.3.3.2 SULPHURIC ACID

An investigation into the impact of sulphuric acid on PPS/PPS and PPS/PI was done in a similar manner to that of nitric acid discussed above.

EXPOSURE TIME

Three PPS/PPS samples per test were exposed to sulphuric acid at the recommended high temperature fabric operating temperature of 150°C for increasing durations. The change in UTS after exposure was found to fluctuate significantly. Different sulphuric acid concentrations were thus considered, and experiments were repeated using PPS/PI samples. It is apparent from Figure 4-19 that the PPS/PPS and PPS/PI UTS increased and decreased with no clear trend related to concentration or exposure time, with large measurement variability observed. Similarly, no trend between increased exposure time or concentration and elongation at UTS was observed. Elongation could be seen to alternatively increase and decrease (Figure B-16) within 13% of the neat fabric elongation, with the exception of PPS/PI after 1 M sulphuric acid exposure which exhibited a significant increase in elongation of 49%. Furthermore, changes in elongation did not correspond with changes in tensile strength. No correlation between mass and ultimate tensile strength change could be seen. Visually, samples could be seen to become pale grey in colour after exposure to sulphuric acid exposure of varying concentrations for 12 hours and 24 hours. No visual change could be observed at lower exposure times.

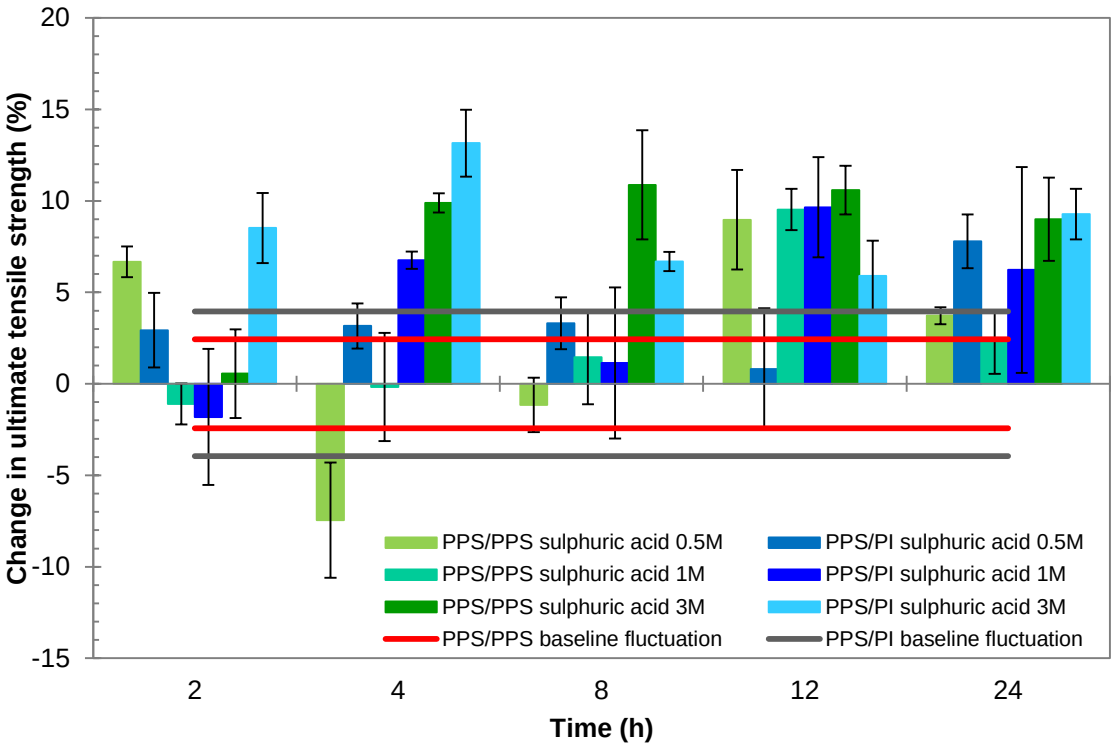

Figure 4-19: Effect of sulphuric acid exposure of various concentrations at 150°C on PPS/PPS and PPS/PI ultimate tensile strength over time

This lack of trend may indicate that PPS/PPS and PPS/PI are not susceptible to acid attack from sulphuric acid, which would corroborate the high strength retention of PPS in sulphuric acid as advertised by Toyobo Co. Ltd. (2005) and reported by Tanthapanichakoon et al. (2006), where significant loss of tensile strength after sulphuric acid exposure was observed only after one year. It is further suggested that this result is analogous to that of Mao et al. (2013), who reported initial increased PPS needle felt tensile strength after exposure to 1000 ppm SO_2 at 200°C before a gradual decrease in strength.

PI, however, has been reported to suffer strength loss after sulphuric acid exposure (Evonik Fibres GmbH, n.d.; Weinrotter & Seidl, 1993). It is suggested that the behaviour of PPS/PI is more closely correlated with that of PPS than PI, since the bulk of the fabric consists of PPS fibre with PI incorporated only in the blended filtration surface. Twelve hours were thus selected as the exposure time for further testing based on test practicality.

EFFECT OF CONCENTRATION

From the results in Figure 4-20 it can be seen that exposing PPS-based fabrics to sulphuric acid of varying concentration at the recommended operating temperature of 150°C results in increasing ultimate tensile strength. PPS/PPS UTS remained relatively constant at an increase of between 9% and 11% from neat samples upon exposure to increasing sulphuric acid concentration. PPS/PI results do not reveal a clear trend with respect to increasing concentration.

Furthermore, neither of the fabrics exhibited a clear trend with respect to changes in elongation after exposure to sulphuric acid solutions with increasing concentration (Figure B-17). The PPS/PPS samples exhibited a marginal increase in elongation after being exposed to a sulphuric acid solution with a concentration of 3 M while insignificant variations were noted at the lower concentrations. The PPS/PI samples also exhibited a marginal increase in elongation after exposure to a 3 M sulphuric acid solution, although a relatively large increase (7.4%) in the elongation was noted after exposure to a 1 M sulphuric acid solution.

Mass changes did not correlate with changes in UTS or elongation of PPS-based fabrics (Figure B-18). PPS/PPS mass increased after sulphuric acid exposure, with the most significant increase of 14% observed after exposure to a sulphuric acid solution of 1 M concentration. This result corroborates the mass increase of PPS after sulphuric

acid exposure reported by Tanthapanichakoon et al. (2006). PPS/PI mass, however, exhibited a trend of decreasing mass with increasing sulphuric acid concentration.

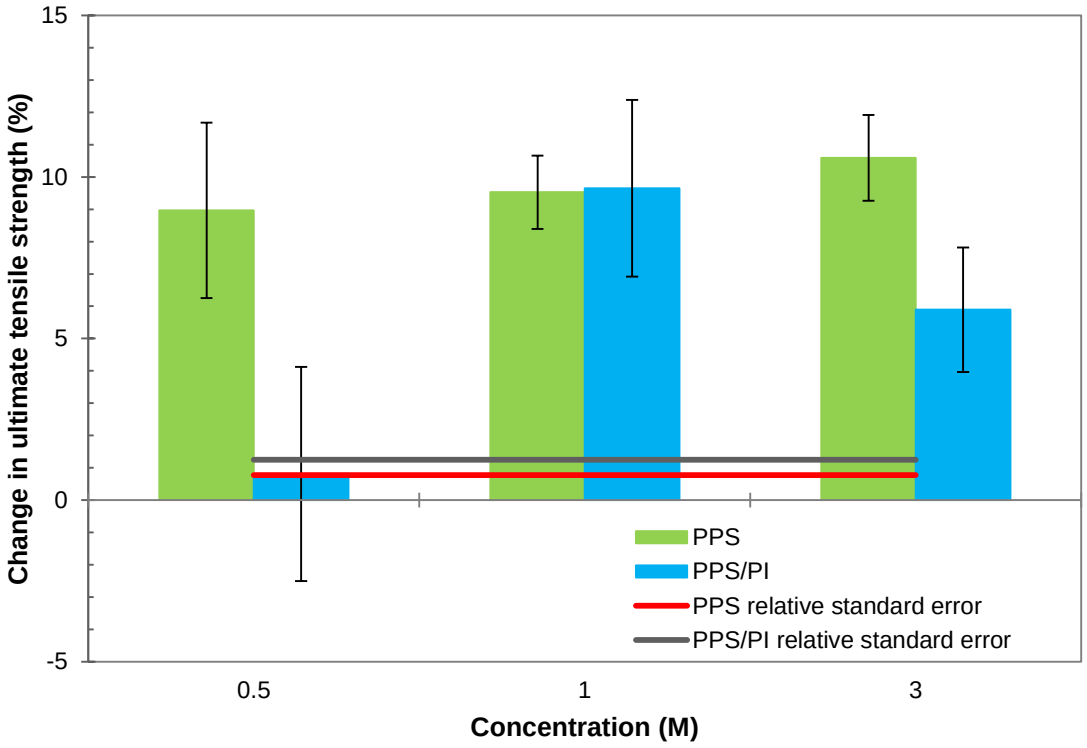

Figure 4-20: Effect of sulphuric acid exposure for 12 hours at 150°C on PPS/PPS and PPS/PI tensile strength at various concentrations

EFFECT OF TEMPERATURE

The results reported in Figure 4-21 reveal that, similar to the results obtained with increasing sulphuric acid concentration, the UTS of both PPS/PPS and PPS/PI increased when exposed to sulphuric acid throughout the operating temperature range of the fabrics. The relative increase in the UTS for both fabrics was significant, except at 170°C.

In terms of elongation at the UTS, PPS/PI elongation increased after sulphuric acid exposure at all temperatures that were considered and reached maximum elongation after acid exposure at 190°C (Figure B-19). Considering the UTS strength increase at 190°C (Figure 4-21), this indicates increased durability of PPS/PI fabric. In contrast, PPS/PPS elongation did not show any change at 130°C and 150°C, but decreased significantly at 170°C and 190°C. Since the UTS of the PPS/PPS fabrics remained constant at 170°C and increased at 190°C, the decrease in the elongation at the UTS

of these fabrics after acid exposure indicates that the fabrics were embrittled after exposure at these conditions.

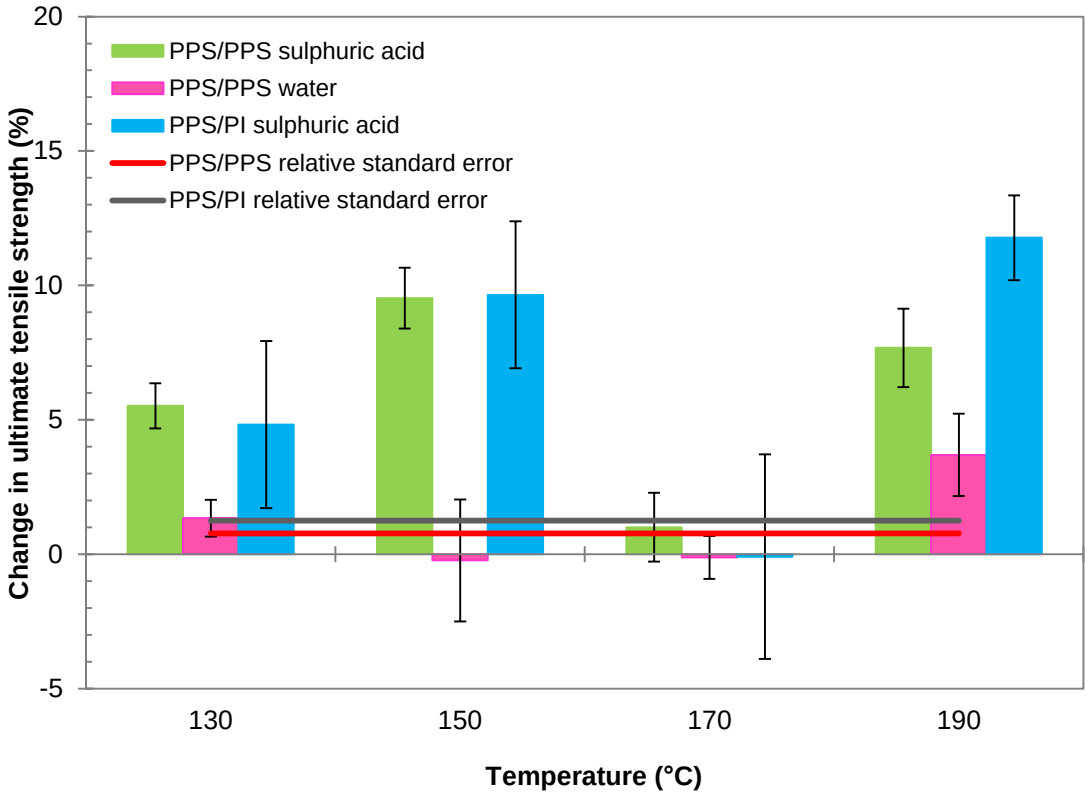

Figure 4-21: Effect of 1 M sulphuric acid exposure for 12 hours on PPS/PPS and PPS/PI tensile strength at various temperatures compared to PPS/PPS control samples in water

4.3.3.3 EFFECT OF COMBINED NITRIC AND SULPHURIC ACID

As with the PAN-based fabrics discussed above, the combined impact of nitric and sulphuric acid on PPS-based fabrics was also studied. The exposure time was set at four hours, based on the extreme degradation of PPS/PPS in nitric acid that was observed at longer exposure times. The exposure temperature was fixed at 150°C.

Both PPS/PPS and PPS/PI showed significant decreasing UTS with increasing concentration, as illustrated in Figure 4-22. While the incorporation of PI seemed to offer a slight benefit when exposed to a solution with 0.5 M concentrations of both acids, exposure at higher concentrations of the mixed acids showed that PPS/PI experienced a greater loss of strength than PPS/PPS. As with nitric acid exposure, exposure to increasing concentrations of the mixed acids had the effect of increasing reduction of elongation at the UTS of both fabrics (Figure B-20). As with UTS, PPS/PI again exhibited greater reduction of elongation at higher concentrations of the mixed

acids than PPS/PPS. This reduction of UTS and elongation implies that both fabrics would be prone to experiencing increased brittle failure at lower applied forces after exposure to the combined nitric and sulphuric acid mixture.

By comparing these results to the degradation by sulphuric acid alone (Figure 4-20), it is clear that the degradation of the PPS-based fabrics in combined nitric and sulphuric acid mixtures was accelerated with the presence of nitric acid. This correlates with the results reported by Tanthapanichakoon et al. (2006), who suggest that the increased degradation of PPS in a mixture of these two acids is due to sulphuric acid acting as a catalyst for the electrophilic aromatic substitution, or nitration, of PPS.

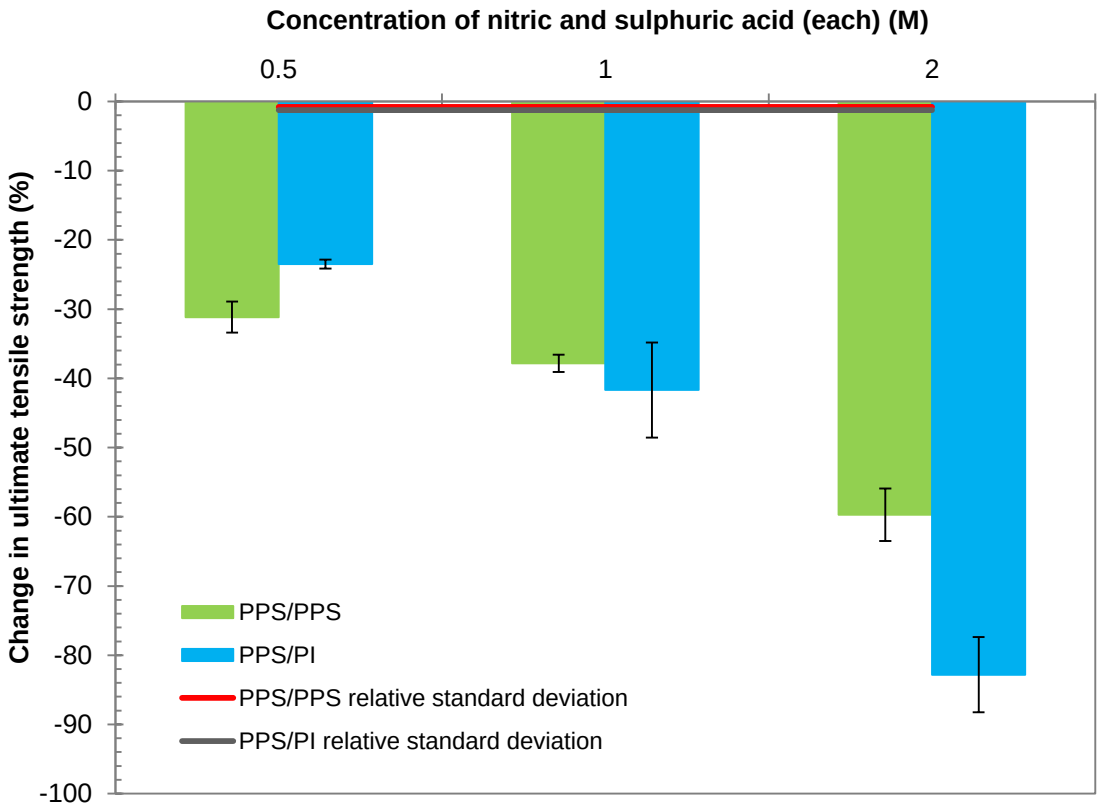

Figure 4-22: Effect of combined nitric and sulphuric acid exposure for 4 hours at 150°C on PPS/PPS and PPS/PI tensile strength at various concentrations

4.3.3.4 SUMMARY OF ACID ATTACK ON HIGH TEMPERATURE FILTRATION FABRIC

To summarise the discussion above, the results of the tensile strength retention at 150°C and four hours exposure time in solutions of increasing concentrations of nitric, sulphuric, and mixed acids are summarised in Table 4-7. Where samples were not tested at the reported concentrations, results were interpolated.

Table 4-7: Strength retention of high temperature fabrics after acid attack

Acid	Fabric type	Tensile Strength Retention (%)			
		Low Concentration (0.5 M)	Medium Concentration (1 M)	High Concentration (2 M)	Average
Nitric acid	PPS/PPS	90	58	42	63
	PPS/PI	82	59	42	61
Sulphuric acid	PPS/PPS	93	100	105	99
	PPS/PI	103	107	126	112
Nitric & sulphuric acids	PPS/PPS	69	62	40	57
	PPS/PI	77	58	17	51

Comparison of the results reveals that the nitric and sulphuric acid mixture was the most aggressive in terms of fabric degradation for both fabric types. However, the acid mixtures were more damaging towards PPS/PI fabric samples, most significantly at high concentrations of 2 M. Nonetheless, nitric acid exposure was found to be the most detrimental to both fabrics, where PPS/PPS showed a marginal strength advantage over PPS/PI.

It is concluded that sulphuric acid exposure does not pose a significant threat to either high temperature fabric. This is further apparent from the results after exposing PPS/PPS and PPS/PI to sulphuric acid solutions of various concentrations for 12 hours (Figure 4-20), where the UTS of both fabrics consistently increased. PI incorporation in PPS showed a consistent strength increase and consequent strength retention benefit after sulphuric acid exposure, which does not correspond with the advertised sensitivity of PI to sulphuric acid attack (Evonik Fibres GmbH, n.d.), or with the low temperature fabric results reported in Table 4-6. This difference may be because PI constitutes only a minor portion of the PPS/PI fabric and degradation after acid exposure is therefore driven by the properties of PPS.

4.4 THERMAL DEGRADATION OF FILTRATION FABRIC YARN

This section reports and discusses the results obtained from the experiments performed according to the procedure described in Section 4.2.4. Whereas the results reported in Section 4.3 relate to the filtration fabrics formed by the combination of the different fibre types in the blended needle felt filtration fabrics, the results reported in this section relate to the impacts of acid attack on the thermal-physical properties of the individual polymeric fibre types.

The results reported below are limited to one sample per experiment and thermal behaviour is reported during heating only, with behaviour during cooling not investigated.

4.4.1 THERMAL DEGRADATION OF PAN

The mass change of PAN yarn while exposed to increasing temperature at a heating rate of 15°C/min in helium is shown in Figure 4-23. The thermal degradation of an unexposed sample is considered as well as samples exposed to 3 M nitric acid or 3 M sulphuric acid at 125°C for 4 hours. DSC results from the same analyses are shown in Figure 4-24.

The onset of weight loss for the unexposed baseline PAN sample was found to occur at approximately 300°C (Figure 4-23). The significant mass loss after this point can be attributed to the release of volatile gases during pyrolysis (Alarifi, et al., 2015). A narrow exothermic peak with onset temperature of 281°C and peak at 310°C can be seen in Figure 4-24. This exothermic peak can be attributed to the cyclisation of the nitrile groups present in PAN at elevated temperatures (Xue, et al., 1996; Karacan, 2012; Al-Attabi, et al., 2017).

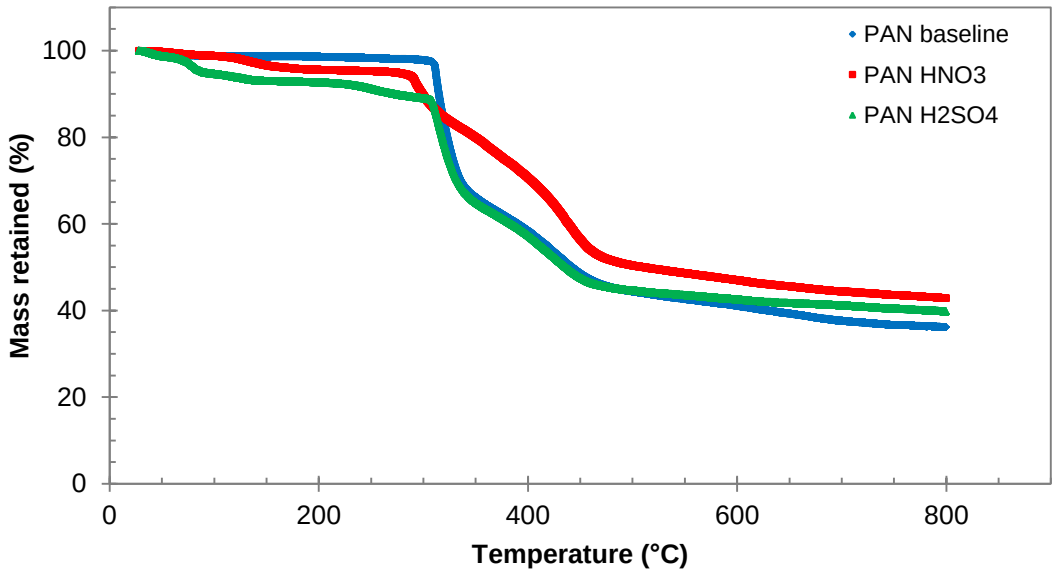

Figure 4-23: Thermogravimetric analysis of PAN yarn at a heating rate of 15°C/min in helium

In comparison, it can be seen from Figure 4-23 and Figure 4-24 that nitric acid exposure affected the pyrolysis and cyclisation reactions of PAN. An initial onset point of a minor thermal degradation event was noted at 115°C, with a second onset point

being present at 286°C that corresponds with the main pyrolysis reaction (Figure 4-23). The rate at which mass loss due to pyrolysis occurred, however, was lower than that of the unexposed PAN sample, and a higher mass retention was found at the end of the TGA temperature program. It is postulated that the minor degradation event was due to the release of residual moisture and nitric acid that was absorbed by the polymer. The DSC thermogram for PAN after nitric acid exposure (Figure 4-24) revealed a broader, less exothermic peak with an earlier onset temperature (260°C) and peak temperature (289°C). This correlates with impurities being present in the sample (Gabbott, et al., 2008), which suggests that the polymer structure could have been altered by reaction with nitric acid during exposure.

After sulphuric acid exposure, the thermal degradation curve of PAN (Figure 4-23) correlated more closely with the baseline curve in terms of degradation rate and the onset temperature of the major pyrolysis process. Furthermore, the onset temperature of the presumed desorption of moisture and acid was lower than that for the nitric acid case at 65°C. Less mass was also retained at the end of the TGA temperature program. It is further evident from the DSC thermogram (Figure 4-24) that while the exothermic peak occurred at the same temperature compared to the unexposed, baseline sample, it again had a reduced height.

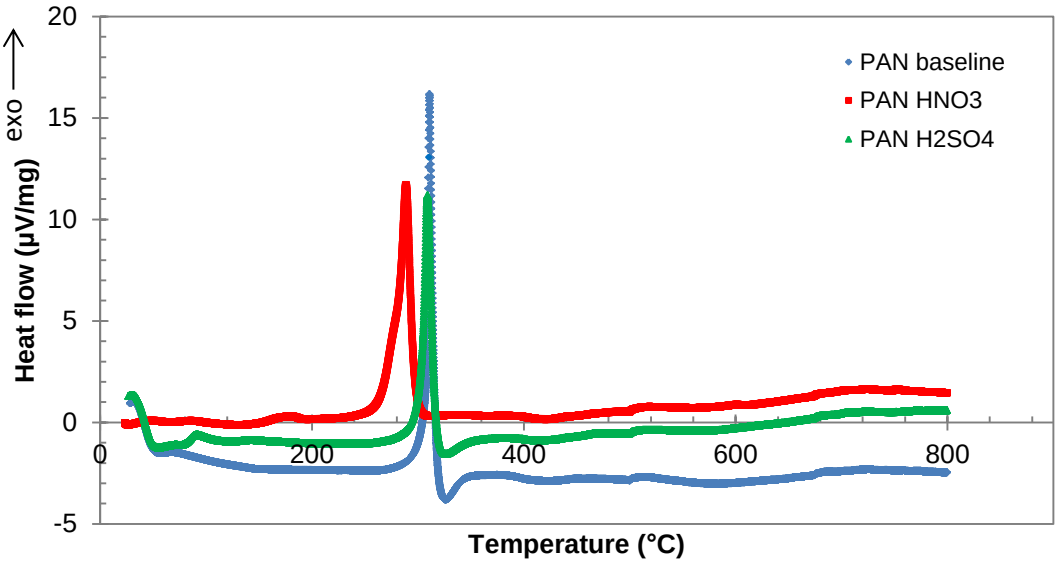

Figure 4-24: DSC thermogram of PAN yarn at a heating rate of 15°C/min in helium

These results reiterate those found when the needle felt filtration fabrics were exposed to sulphuric and nitric acids, as summarised in Table 4-6. Both acids were observed to

have a minor detrimental effect on PAN-based fabric UTS, as verified by the changes in the PAN thermograms. However, strength retention in excess of 95% on average was exhibited by PAN/PAN after nitric or sulphuric acid exposure. Both nitric and sulphuric acids had the effect of increasing the plasticity of needle felt fabrics after acid exposure.

4.4.2 THERMAL DEGRADATION OF PPS

Similar TGA and DSC analyses of PPS yarn were carried out. However, the heating rate of the baseline and nitric acid exposed samples was 15°C/min, while the heating rate for analysis of the sulphuric acid exposed sample was 10°C/min. The higher heating rate of the baseline sample and sample exposed to nitric acid would have the effect of delaying peak thermal degradation (Abu-Bakar & Moinuddin, 2012). Despite this discrepancy, the shapes of the curves provide insight into the changes in PPS thermal behaviour after acid exposure. Although the PPS fibre (yarn) were sourced from a different producer than the fibres used in the needle felt fabric samples, the fibres are rated for the same performance and similar acid exposure behaviour can thus be expected.

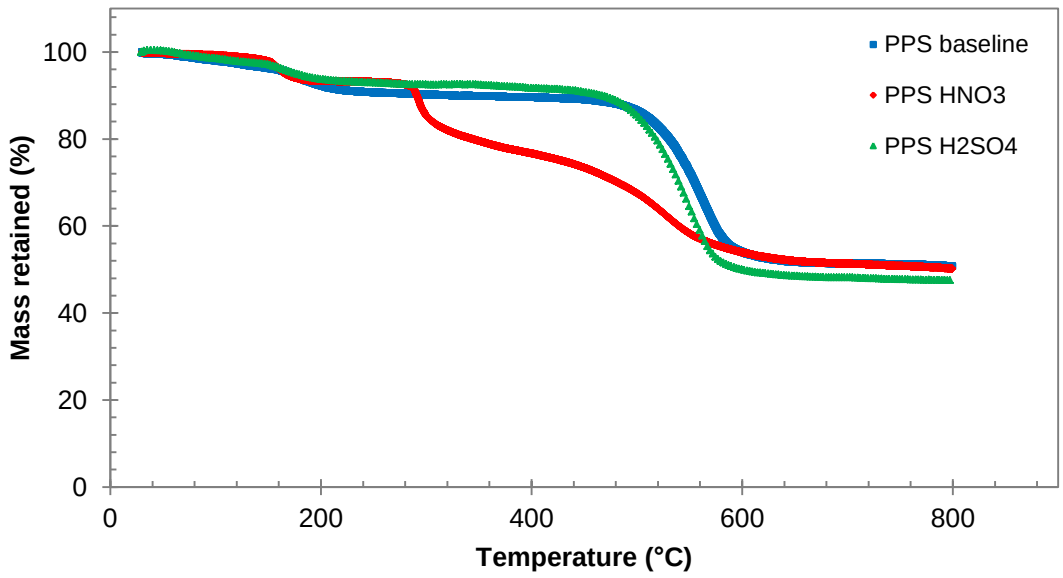

Figure 4-25: Thermogravimetric analysis of PPS yarn in helium at heating rates of 10°C/min (PPS H_2SO_4) and 15°C/min (PPS baseline and PPS HNO_3)

From Figure 4-25 it can be seen that the unexposed, baseline PPS sample exhibited a pyrolysis onset temperature of at 505°C. This result corresponds with the PPS TGA results reported by Deqiang et al. (2013) of maximum PPS weight loss occurring

between 500°C and 600°C for heating rates of 5, 10, 20 and 40°C/min in nitrogen. The result also corresponds reasonably well with the results reported by Li et al. (2002) of the onset of PPS thermal degradation at 490°C at a heating rate of 50°C/min in helium. This confirms that PPS is suitable for use in high temperature baghouse applications. From the DSC thermogram of the unexposed PPS in Figure 4-26 a small endothermic peak at 270°C is visible, which correlates with melting of the polymer. This is reasonably consistent with results reported by Jog et al. (1994) and Nohara et al. (2006) of PPS melting at approximately 280°C.

The thermal degradation of PPS after nitric acid exposure was, however, significantly different from the baseline thermogram. Again, two distinct onset temperatures of mass were observed (Figure 4-25). An initial onset temperature of 150°C was found, followed by a second onset temperature at 280°C, which respectively corresponds with the moisture and acid desorption and pyrolysis reactions. The PPS thermal stability was therefore significantly affected by nitric acid exposure, which corresponds with the results shown in Figure 4-18. Furthermore, the melting temperature was also affected, as it shifted from 270°C to 155°C, while an additional exothermic peak is evident from Figure 4-26 at 293°C. This behaviour implies that the chemical nature of the polymer was affected during nitric acid exposure. Tanthapanichakoon et al. (2006) suggests that this may be due to polyarylene sulfoxide formation and consequent PPS chain scission during nitric acid exposure.

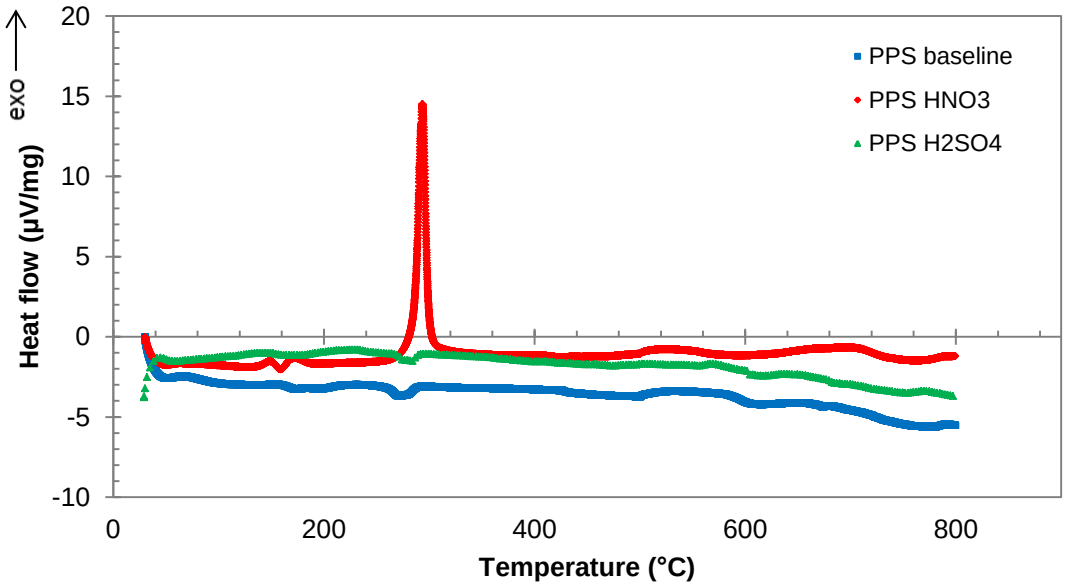

Figure 4-26: DSC thermogram of PPS yarn in helium at heating rates of 10°C/min (PPS H_2SO_4) and 15°C/min (PPS baseline and PPS HNO_3)

After sulphuric acid exposure, the thermal behaviour of PPS was similar to the unexposed baseline sample. Evidently, the onset of the pyrolysis reactions occurred at lower temperature of 485°C (Figure 4-25). This result corroborates the results reported by Cai and Hu (2015) when conducting TGA analysis of PPS needle felt at 10°C/min in air after sulphuric acid exposure, where it was found that the onset of thermal degradation occurred at lower temperatures after acid exposure. The DSC thermogram shown in Figure 4-26 followed an endothermic trend similar to that of the unexposed sample. The onset of pyrolysis reactions may, however, have been delayed should the higher heating rate used for the baseline sample been used. This correlates with the results summarised in Table 4-7, where it was found that the tensile strength of PPS-based fabrics is not significantly affected by sulphuric acid exposure.

4.4.3 THERMAL DEGRADATION OF PI

Similarly, TGA and DSC analyses of PI yarn were conducted. All TGA analyses were performed at a heating rate of 15°C/min. Since PI was only studied in combination with PAN or PPS in the acid exposure tests discussed in Section 4.3, this provides insight into the individual thermal behaviour of the PI polymer used in filtration fabrics. The TGA and DSC results are shown in Figure 4-27 and Figure 4-28 respectively.

The baseline thermal degradation curve of unexposed PI yarn shown in Figure 4-27 confirms PI to be suitable for operation at high temperatures, seeing that the onset of the pyrolysis reactions was found to be 510°C. This thermal behaviour corresponds with Varga et al.'s (2011) report of the onset of PI thermal degradation at 510°C and that of Qiu (2015) of 500°C, both results reported at heating rates of 10°C/min in air. The DSC thermogram shown in Figure 4-28 revealed an initial peak where water loss occurs (Evonik Fibres GmbH, n.d.) before an endothermal plateau and glass transition temperature at 305°C. This is in keeping with the PI glass transition temperature of 307°C to 315°C reported by Shimadzu (2012) at a heating rate of 20°C/min in nitrogen. Carbonisation was experienced within the temperature range considered at temperatures beyond approximately 300°C, during which mass loss can be attributed to non-carbon atoms being expelled as gases, before the onset of graphitisation at higher temperatures (Qiu, 2015).

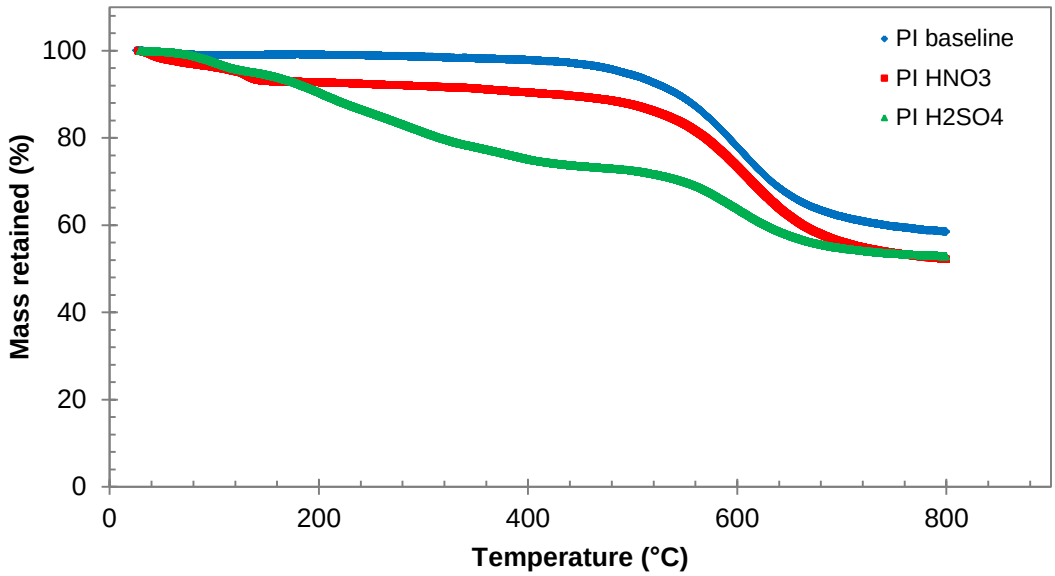

Figure 4-27: Thermogravimetric analysis of PI yarn at a heating rate of 15°C/min in helium

Nitric acid exposure had the effect of introducing an initial onset temperature of minor mass loss at 100°C, prior to a plateau that follows the baseline thermal degradation behaviour as shown in Figure 4-27. The DSC thermogram in Figure 4-28 shows that nitric acid exposure resulted in an initial endothermic peaks at 53°C, which may correspond with the onset of the moisture desorption (Ba, et al., 2009). The exothermic peak at 135°C may be indicative of crystallisation, which would correspond with the improved rigidity of PAN-based fabrics incorporating PI in the filtration surface, as can be seen from Figure 4-5 and Figure 4-6.

Sulphuric acid exposure, however, had a significant effect on the thermal resistance of PI yarn, as shown by the TGA results in Figure 4-27. Virtually immediate, and significant, mass loss was experienced. However, the second-stage reaction event coincided with an onset temperature of 530°C, which was higher than the baseline results. The DSC thermogram shown in Figure 4-28 also had a similar endothermic shape to that of the unexposed baseline sample, although the magnitude of heat flow is approximately double that of the baseline sample. Furthermore, an endothermic peak was observed at 103°C, indicating possible polymer melting.

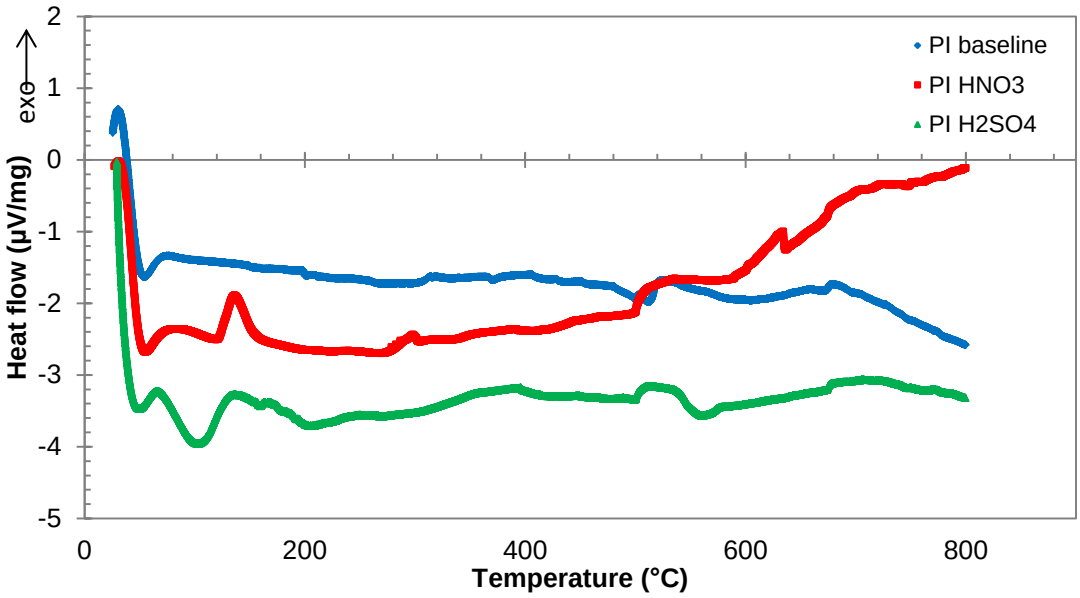

Figure 4-28: DSC thermogram of PI yarn at a heating rate of 15°C/min in helium

The marginal impact of nitric acid and significantly negative impact of sulphuric acid exposure on the PI thermal-physical properties corresponds with the tensile strength results summarised for low temperature fabrics in Table 4-6, but does not correspond with that of high temperature fabrics in Table 4-7. Since the needle felt fabric samples used for tensile strength analysis consisted mainly of the base PAN or PPS fabrics, the individual influence of PI is not easily discernible. It is, however, postulated that the decomposition products of PAN and PPS affect the thermal behaviour of PI.

4.5 CONCLUSIONS OF FABRIC RESISTANCE TO ACID ATTACK AND THERMAL DEGRADATION

For the filtration fabrics and yarns considered in this study at the conditions tested, it is concluded that mixtures of nitric and sulphuric acids caused the most significant degradation of all the filtration fabrics that were considered. The degradation was evident from the negative influence of mixed acid exposure on the tensile strength properties of the fabric filter samples. It is therefore clear that baghouse operating conditions should be maintained at temperatures such as to avoid the occurrence of acid condensation, which can have detrimental effects over extended periods of time.

PAN-based fabrics were found to be more susceptible to degradation by sulphuric acid than nitric acid. In this regard, PI incorporation in low-temperature bags (PAN/PI) offered some tensile strength advantage when exposed to nitric acid or mixtures of nitric and sulphuric acids.

PPS-based fabrics were found to be resistant to acid attack by sulphuric acid, yet highly susceptible to attack by nitric acid. It was found that nitric acid exposure changes the polymer thermal behaviour in terms of an exothermal peak being observed after nitric acid exposure of yarn, which was not present in the unexposed yarn sample. Neither PPS/PPS nor PPS/PI bag filters are therefore suitable for operation in environments where significant nitric acid exposure can be expected. PI incorporation in high temperature fabrics offered a strength benefit with sulphuric acid exposure, although PPS/PPS strength retention in this situation is also high.

PI was shown to be highly susceptible to degradation by sulphuric acid. This was confirmed from the thermal analysis of PI yarn, as well as the detrimental effect on strength that PI incorporation has on PAN-based fabrics exposed to sulphuric acid. When incorporated in PPS-based fabrics, however, a strength increase of fabrics incorporating PI was observed at the conditions tested. It is therefore concluded that the behaviour of PPS-based needle felt filtration fabric in sulphuric acid is driven by PPS and not the minor portion of PI fibre incorporated in the filtration surface of the fabric.

CHAPTER 5: COST-BENEFIT ANALYSIS OF FILTRATION FABRICS

In this chapter, a method to perform a cost-benefit analysis (CBA) specific to comparing the economic merit of fabric filter bag options is proposed.

From the selected literature surveyed in Chapter 2, it is clear that traditional CBA methods for baghouses are suited to establishing overall costs for construction projects and not to making bag fabric selections for existing baghouses. There is, therefore, a need for developing a CBA method that considers the various cost factors associated with baghouse operation with a specific filtration fabric.

The CBA method proposed in this chapter uses life cycle costing (LCC) methods to comparatively evaluate the total costs associated with bag options for application in a baghouse. This method is applied to the incorporation of PI in both low and high temperature bags and conclusions drawn.

5.1 COST MODELLING METHOD

Traditional LCC analysis methods were used to develop a CBA that analyses all costs associated with a filtration fabric selection throughout bag life. A study period was defined, and annual costs were entered as appropriate for each cost category. Annual cost is the sum of all costs for the year in question. Using the net present value (NPV) method, the annual costs were related to the base year when the analysis is performed. For simplicity, the real discount rate is used, allowing inflation to be neglected in the NPV formula. The NPV formula is defined by Equation (5-1) (Maerig & Morris, 2018):

$$NPV = C_t \times \frac{1}{(1+d)^t} \quad \textbf{(5-1)}$$

where:

NPV = present value of the cost in the base year (R)
C_t = cost at time t (R)
d = real discount rate (%)
t = time at which the cost is incurred (years)

5.2 BAG COST FACTORS AND ASSUMPTIONS

As discussed in Chapters 1 and 2, there are four cost elements linked to appropriate bag selection:

- Emissions reduction
- Capital investment
- Bag life
- Pressure drop

These cost drivers and related assumptions for development of the CBA for filtration fabric selection are discussed below. The simplifying assumptions for application of the technical results found in this study are described. The inputs used are based on a typical large, modern baghouse at a South African coal-fired power utility. Detailed inputs and economic parameters used for application of the CBA to this study are described in Appendix C.

5.2.1 EMISSIONS REDUCTION

For purposes of this study, it is assumed that all the fabrics considered are capable of adequately meeting the emissions limits at their relevant installations, should the baghouses be suitably designed and operated. Costs associated with emissions reduction are therefore neglected. The health and social cost of the remaining particulate emissions after abatement is not borne by the bag purchaser and therefore not included in this study.

It must, however, be noted that significant costs can be assigned to emissions. Firstly, emissions excursions can result in boiler unit de-loading in order to remain within legislated emissions limits and consequent loss of income. Fines may also be imposed for emissions excursions, which can be as high as R1 million (Department of Environmental Affairs, 2010). Note that traditional baghouse cost studies do not focus on efficiency as a cost driver since baghouses are typically efficient enough to maintain emissions within legislated limits. However, should emissions limits become stricter as has been the trend in recent years, this may become a consideration in bag selection.

Furthermore, significant costs are associated with the health impact of emissions. These costs are of concern to governmental bodies and are not typically passed on to industry. Methods used for calculating these costs are a topic of debate since data from developed nations are often applied to developing nations and the total mortality and

morbidity numbers do not account for differences in the sources of particulate emissions (domestic coal fires, transportation, etc.) (Farber, 2009; Holland, 2017). However, costs as high as R30 billion (Myllyvirta, 2014) and Int$2.4 billion (Holland, 2017) annually have been estimated. Apart from limitations to current modelling methodologies, the known health impact of particulate emissions and the high associated cost implies that any further reduction in particulate emissions does hold societal value even when extra low emissions levels are not a legislated requirement for industry.

5.2.2 CAPITAL INVESTMENT

For purposes of conducting a CBA which comparatively evaluates filtration fabric selection, investment costs associated with installation, administration and tax are assumed to be the same for all fabric choices and are therefore neglected. The initial capital investment for the bags, however, differs.

Apart from fabric type, bag size and construction affect bag price (Turner, et al., 1987). However, since this study compares bag options for installation in a particular baghouse, it is assumed that all bag options are of the same specification with the only difference being filtration fabric type.

Historically, the relative cost of PI has been significantly higher than PAN or PPS (McKenna & Turner, 1989). Since the materials included in this study consist mainly of the base fabric with PI fibre incorporated only in the filtration surface of the fabric, the cost differential between bags with and without PI incorporation is not as great as when considering 100% PI bags. Market factors affect relative fibre costs, therefore the actual bag costs vary with time. Bags with PI incorporated are, however, consistently more expensive than their counterparts without PI incorporation (Turner, et al., 2002).

The bag prices used in this study for PAN/PAN and PPS/PPS are based on average bag prices quoted by two suppliers for various South African power stations during 2016. Costs are based on 30% South African content and 70% European content and are escalated on this basis and converted to 2018 Rand costs. Costs are normalised for bag size, ensuring indicative pricing suitable for this simplistic comparative study.

Due to market related factors, the same approach has not been followed for the price of PAN/PI and PPS/PI bags. In order to eliminate contractual and market influence on bag pricing, the difference in cost based on fibre prices was used. PAN fibre prices in Euro from 2015 and PPS and PI fibre prices in US Dollar from 2016 were escalated

and converted to 2018 Rand costs. Based on the specified fibre weights per square metre of needle felt fabric the prices of all fabrics considered were calculated. The differences in price between low temperature and high temperature fabric options were then applied to the bag prices of PAN/PAN and PPS/PPS derived above to arrive at the prices for PAN/PI and PPS/PI.

Prices normalised to PAN/PAN for all bags considered in this study are shown in Table 5-1.

Table 5-1: Normalised bag prices

Bag filtration fabric	Relative price
PAN/PAN	R
PAN/PI	1.3R
PPS/PPS	1.9R
PPS/PI	2.1R

5.2.3 BAG LIFE AND STUDY PERIOD

Bag life is a key factor when making bag selections. Although initial capital investment of a particular bag type may be less than an alternative, the useful life of the selected bags ultimately dictates the lifecycle cost of the bags. Bags are deemed to have reached the end of their useful life when failure (due to blinding, mechanical wear or temperature or chemical degradation) limits the operation of the production unit on which the baghouse is installed.

Bag life is a complex variable determined by various factors. During operation bags are exposed to many non-ideal scenarios which affect bag life to varying degrees (Davis, et al., 1990). Accurate bag life prediction is thus difficult and reasonable bag life assumptions require historical knowledge of the operational behaviour of the specific filtration fabric type in the specific application for which it is to be used. Development of an accurate bag life prediction equation taking all elements of fabric degradation into account is beyond the scope of this study.

The major assumption made in the proposed method is that bags are replaced at the end of a predetermined time frame, in year *n*. This defines the study period for the CBA. *n* is defined by the planned outage cycle for the baghouse in question when the

entire bag set[28] is planned for replacement, regardless of condition. Although there are instances where bags operate suitably beyond this time frame, the associated risk of continued operation when an outage opportunity for replacement is not guaranteed makes this a reasonable assumption. The proposed model therefore does life cycle costing for a bag set where the lifetime, equal to *n* years, is predefined.

When bags do not perform adequately throughout the requisite bag life and early replacement is required, capacity losses are suffered. Capacity losses relate to a direct loss of income for power utilities. Losses may be due to capacity reduction in order to maintain pressure drop within the ID fan limits while continuing operation with blinded bags until an outage opportunity is available. Losses may also be due to capacity reduction in order to do on load bag replacement if only a portion of the bags have failed. Losses may be due to temporary unplanned shut-down of the unit in order to replace the entire bag set.

It is assumed that if bag life is predicted to be less than *n* but more than a certain early failure time in years, n_e, then operation continues at reduced capacity until the original planned outage for bag replacement. If bags are predicted to fail before n_e then the unit is temporarily shut-down for an unplanned complete bag replacement. Due to the difficulty in predicting partial bag set failure, on load bag replacement is not catered for in the proposed CBA method. The CBA can, however, be adapted for specific applications where partial bag set replacement can be done on-load and accurate data for predicting partial bag set failure exists.

It is assumed that all bag options are capable of adequately meeting the emissions limits. Costs associated with legal fines for emissions excursions are therefore neglected.

For application of the indicative data developed in this study, it is assumed that bag life is affected only by loss of fabric tenacity due to thermo-chemical degradation and that there is a linear relationship between bag life and strength retention after acid exposure. In reality, bag life is also affected by ash characteristics (Aleksandrov, et al., 2010). The ash cake developed during operation serves to protect the bags from acid attack to varying extents and the strength retention after acid exposure can be expected to be greater than when clean fabric is exposed to acid concentrations in a

[28] A *bag set* is the total quantity of new fabric filter bags required for operation of a specific baghouse. Spare bags for routine replacement of individual bags are included. Spare bags are typically 3% – 5% of the total bag quantity (Patel, 2016).

laboratory. Furthermore, loss of strength is not the only failure mechanism since thermo-chemical exposure may lead to bag shrinkage and changes in permeability.

Ash morphology and electrostatic interactions will also affect the likelihood of the bags blinding and therefore limit bag life (Mukhopadhyay, 2009), however this is considered in the subsequent portion of the CBA and is therefore not double accounted.

For purposes of the crude bag life assumption in this indicative CBA, bag life is calculated based on the simplistic equation described by Equation (5-2).

$$n_a = n \times S_R \quad \textbf{(5-2)}$$

where:

n_a = Actual bag life (years)
n = guarantee bag life (the study period) (years)
S_R = strength retained after acid exposure (%)

n_a can then be used to calculate the outage duration, D_O in hours, according to Equation (5-3), assuming 31 days in a month:

$$D_O = 8\,928 \times (n - n_a) \quad \textbf{(5-3)}$$

It is again cautioned that operational acid attack on filtration fabric will be affected by the nature and amount of ash present on the bags as well as the specific flue gas conditions present in the baghouse. It is therefore unadvisable to draw direct bag life conclusions for specific applications from the acid attack data reported in Chapter 4 of this study without further analysis of the baghouse specific ash properties. However, since the goal of this CBA is to highlight indicative differences between fabric options, the values for S_R found in Table 4-6 for PAN-based fabrics and Table 4-7 for PPS-based fabrics were used. The averages of low, medium and high concentration strength retention were selected. This assumption is deemed reasonable since acid concentrations in flue gas will vary depending on operational parameters. Therefore, in order to draw preliminary conclusions regarding the incorporation of PI in fabrics, it is suitable to use the average strength retention with varying acid concentration to reflect the fabric resistance to the acidic environment considered.

The CBA is heavily reliant on the chosen value of n_e and the allowable load losses for continued operation with failed bags, since capacity reduction is the major cost element

justifying the use of this proposed CBA as opposed to the traditional cost analysis method focusing on bag price only. n_e should be chosen to balance the cost of complete bag set replacement with lost capacity due to continued operation.

5.2.4 PRESSURE DROP AND ID FAN POWER COSTS

Pressure drop is a major cost driver and directly related to bag life. Pressure drop drives electricity consumption and the associated cost. Increasing pressure drop requires increasing electricity to power the ID fan that draws flue gas through the bag house. As discussed in Section 2.2.2, pressure drop is a function of filtration velocity, or the air-to-cloth ratio, to which the baghouse is designed. As bags age, pressure drop is expected to increase steadily. This is reflected by the time dependency of Equation (2-1), Equation (2-2) and Equation (2-3). Bags are, however, required to maintain pressured drop below limits defined by the ID fan for the duration of the planned bag life, *n*. In reality, however, bags may blind before this time due to a variety of factors, as discussed in preceding sections.

Since ID fan power consumption is not solely attributable to baghouse pressure drop and pressure drop is expected to increase throughout bag life, using an absolute pressure drop value is not practical for CBA purposes. Instead, the change in pressure drop due to the bag option selected is assumed to be a constant percentage difference from typical pressure drop throughout bag life. According to simplified fan laws, fan power consumption is linearly related to pressure drop. Fan power consumption, in turn, is linearly related to auxiliary power consumption and consequent electricity cost. The percentage difference in pressure drop is therefore applied as a percentage difference in cost, based on the total expected ID fan electricity cost.

For purposes of this indicative CBA, it is assumed that all bag options are capable of sufficiently maintaining pressure drop within suitable limits for the duration of the study period and that bag blinding as a mechanism of premature bag failure is accounted for by the capacity reduction where reduced bag life due to acidic degradation is applicable.

Based on the results discussed in Chapter 3, however, the electrostatic interactions of the filtration fabrics with ash may offer beneficial ash cake development in some cases, from which it can be hypothesised that a pressure drop benefit may be realised. This benefit would be due to improved ash cake stability, which aids filtration and reduces ash penetration into the fabric volume (Frederick, 1974). It is highlighted that this is an

assumption purely for indicative CBA purposes based only on lab results. It is not reflective of actual operational conditions and further research and in situ testing is required to adequately define this parameter for cost modelling purposes.

Due to the lack of sufficient data to make a reasonable absolute assumption as to the value of the potential pressure drop benefit due to electrostatic interactions, a range of values was assumed and the sensitivity of the CBA to this parameter discussed.

5.3 PROPOSED CBA METHOD FOR FILTER BAG SELECTION

The general form of the proposed CBA method is described in Table 5-2 together with the related formulae.

Table 5-2: Bag CBA method

	Year 1 (***t*** **= 1)**	**Year 2** (***t*** **= 2)**	**…**	**Year *n*** (***t*** **= *n*)**
Bag capital investment	C_{B1}	C_{B2}	…	C_{Bn}
Capacity loss cost	C_{C1}	C_{C2}	…	C_{Cn}
ID fan power cost	C_{ID1}	C_{ID2}	…	C_{IDn}
Total annual cost (TAC)	$C_{B1} + C_{C1} + C_{ID1}$	$C_{B2} + C_{C2} + C_{ID2}$	…	$C_{Bn} + C_{Cn} + C_{IDn}$
NPV	$\frac{TAC_1}{(1+d)^1}$	$\frac{TAC_2}{(1+d)^2}$	…	$\frac{TAC_n}{(1+d)^n}$
Total LCC		$\sum_{t=1}^{n} NPV_t$		

Note that the annual costs entered for years 1 to *n* must only be entered if appropriate for the specific option considered. Based on the assumptions discussed in the preceding section, some cost element entries will be empty for specific applications.

5.3.1 BAG CAPITAL INVESTMENT

Bag capital investment, C_{Bt} in Rand, is the cost of the full bag set. This includes installation costs, delivery, tax, etc. when estimating an absolute cost, but may neglect these additional costs when comparing filtration fabric options if the additional costs can reasonably be assumed to be equal.

C_{Bt} will typically be entered only in year 1 unless bags fail before n_e, in which case bag costs will be entered in the year/s corresponding with replacement of a full bag set during the study period.

5.3.2 CAPACITY LOSS COST

Capacity loss cost, C_{Ct} in Rand, is related to the production loss suffered when capacity must be reduced for continued operation with a failed bag set after n_e or the unit must be shut-down for a full bag replacement before n_e. Either Equation (5-4) or Equation (5-5) apply depending on the scenario.

When bag life > n_e:

$$C_{ct} = L_R \times D_O \times P \quad \textbf{(5-4)}$$

where:
L_R = capacity reduction due to continued operation (MW)
D_O = duration of operation with reduced capacity (h)
P = electricity price (R/MWh)

If this cost spans over more than a year then the cost should be apportioned appropriately. Sustaining a production loss for more than a few months, however, is not a reasonable scenario and n_e will typically be such that this cost only occurs in year n.

When bag life < n_e:

$$C_{ct} = L_T \times D_{BR} \times P \quad \textbf{(5-5)}$$

where:
L_T = total unit capacity (MW)
D_{BR} = duration of outage for bag replacement (h)

This cost will only occur in years when the full bag set fails. If this occurs more than once during the study period, the filtration fabric option is inappropriate for the application.

It is assumed that the units are designed for constant operation. However, should units be designed only for operation for a certain percentage of the day, this factor can be added to reflect that the cost implication is not based on constant operation.

The electricity price, *P*, is assumed to be a simplified constant value. For application of the CBA to specific scenarios this value must be suitably defined according to applicable market factors to adequately reflect the loss of revenue due to capacity reductions. The price, for example, may vary based on the typical demand during the time of year that outage occurs. Furthermore, the cost of operating alternative power sources to replace the lost capacity (such as open cycle gas turbines) should be factored in where baghouse owners have alternative generation options.

5.3.3 ID FAN POWER COST

ID fan power cost, C_{IDt} in Rand, is the potential saving associated with the selection of a certain filtration fabric option. It is defined by Equation (5-6). Where a fabric offers improved pressure drop behaviour, this cost will be included as a cost reduction with negative sign. Since C_{IDt} is a difference in typical power consumption where the ID fan is assumed to operate at 100% load throughout the study period, it cannot be positive as this would represent operation beyond the ID fan limits. In reality, the ID fan will operate at reduced load during certain intervals; however, for cost comparison purposes it is reasonable to use the worst case scenario.

$$C_{IDt} = PD \times L_{ID} \times H \times P \quad \textbf{(5-6)}$$

where:

PD = change in pressure drop (%)

L_{ID} = ID fan operational power consumption (MW)

H = operational hours in a year (h)

Note again that C_{IDt} is not an absolute cost, but is a potential saving that could be realised for certain filtration fabric options. It is assumed that this saving is constant throughout the study period and is therefore included in year 1 to year n. This saving may, however, vary as bags age.

5.4 APPLICATION OF THE PROPOSED CBA METHOD TO FILTRATION FABRICS WITH OPTIONAL PI INCORPORATION

In order to consolidate the technical findings discussed in Chapters 3 and 4, the model described above is applied to different potential operational scenarios for PAN- and PPS-based filtration fabrics for use in low and high temperature baghouses, respectively. Note that results are based on laboratory findings only and cannot be directly applied to actual baghouse operation. The results do, however, provide preliminary indications of under which conditions the incorporation of PI is beneficial or detrimental.

The sensitivity of the CBA to the assumptions made based on the laboratory results is described in order to highlight the importance of considering all cost factors when making bag selections.

5.4.1 CBA RESULTS AND SENSITIVITIES: INCORPORATION OF PI IN PAN-BASED FABRICS

This section reports the results of the application of the proposed CBA to the incorporation of PI in PAN-based filtration fabrics for low temperature baghouses. PAN/PAN and PAN/PI are compared for selection in a particular baghouse under different acidic conditions. Details of all inputs used are described in Table C-1 in Appendix C.

Table 5-3: CBA results for PAN-based fabrics – no pressure drop benefit

Operating Scenario	Total price of Bag Set (R million)	
	PAN/PAN	PAN/PI
No acid exposure	7.62	10.2
Nitric acid exposure	62.0	10.2
Sulphuric acid exposure	52.9	145
Combined nitric and sulphuric acid exposure	140	102

Table 5-3 reports the CBA results when it is assumed that there is no impact on pressure drop due to the electrostatic behaviour of PAN/PAN and PAN/PI. It is apparent that bag costs increase significantly when acidic operating environments are present, due to reduced bag life. Based on the assumptions made in this study, PI incorporation in low temperature fabric offers an advantage in operating scenarios where nitric acid exposure or exposure to both nitric and sulphuric acids prevails. However, when sulphuric acid exposure occurs, PAN/PI is significantly more costly than PAN/PAN and is not an appropriate bag choice.

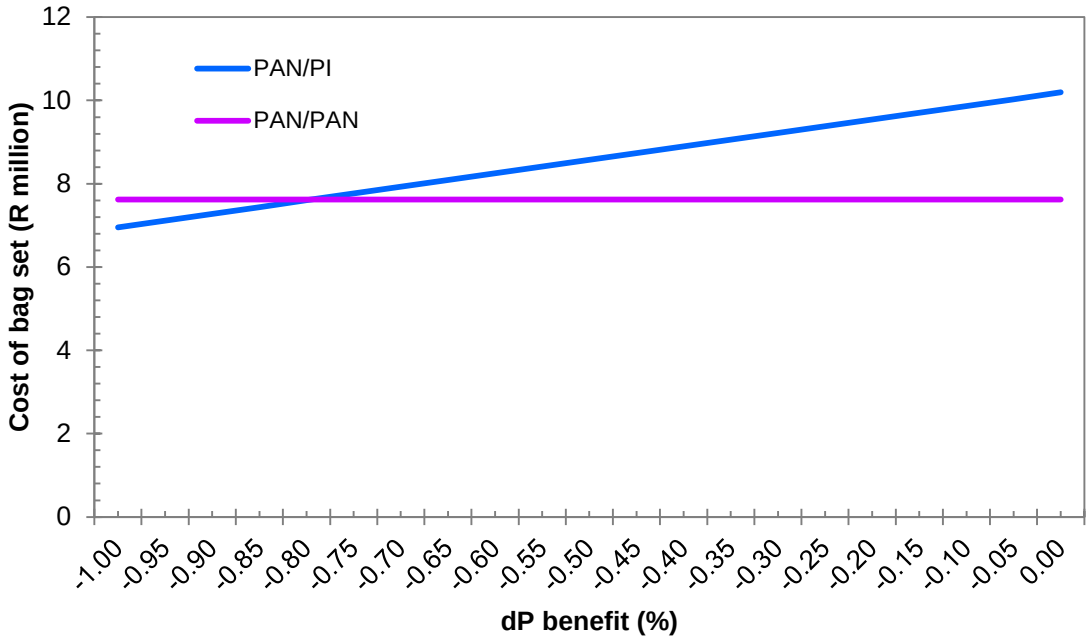

Figure 5-1: CBA sensitivity of low temperature fabrics to pressure drop benefit when no acidic conditions are experienced

The results reported in Table 5-3, however, assume that no pressure drop advantage is realised. Although the potential filtration benefits that may be realised by PI incorporation due to the electrostatic properties of the material was discussed in Chapter 3, further research would be required to accurately quantify this benefit. However, a sensitivity analysis with respect to this parameter was conducted, of which the results are shown in in Figure 5-1. This analysis is based on the assumption that the electrostatic properties of PAN/PAN do not impact pressure drop and the expected baghouse pressure drop is consistently maintained. It is, however, possible that the electrostatic properties of PAN/PAN may be disadvantageous. Nevertheless, it can be seen that if PI incorporation offers a consistent pressure drop reduction of more than 0.79%, the total cost of PAN/PI is less than that of PAN/PAN in conditions where no

acid exposure occurs. It follows that for exposure to nitric acid or to both nitric and sulphuric acids, the cost benefit of PAN/PI over PAN/PAN will become more pronounced if a pressure drop benefit is indeed realised. The chemical degradation of PAN/PI in sulphuric acid is too pronounced for potential pressure drop benefits to meaningfully alter cost.

The additional lifetime cost associated with the use of PAN/PAN in operational environments where significant nitric and combined nitric and sulphuric acid exposure occur is due to the capacity loss suffered as a result of reduced bag life. For nitric acid exposure, PAN/PAN requires load reduction for 2.5 months according to the assumptions used in this study. PAN/PI shows an average strength increase under such conditions and therefore no period of reduced capacity is required (Table 4-6). The sensitivity of the CBA to the required capacity reduction while an outage opportunity for bag replacement is awaited is shown in Figure 5-2, where it is apparent that cost increases rapidly with required capacity reduction. PAN/PAN will only hold a cost benefit over PAN/PI if an unrealistically low load reduction of less than 3 MW is required. Similarly, should a capacity reduction of more than 151MW be required when operating PAN/PAN in environments with sulphuric acid exposure, PAN/PI becomes more cost effective under the assumptions considered in this study. L_R therefore drives the selection of an appropriate n_e when setting up the CBA.

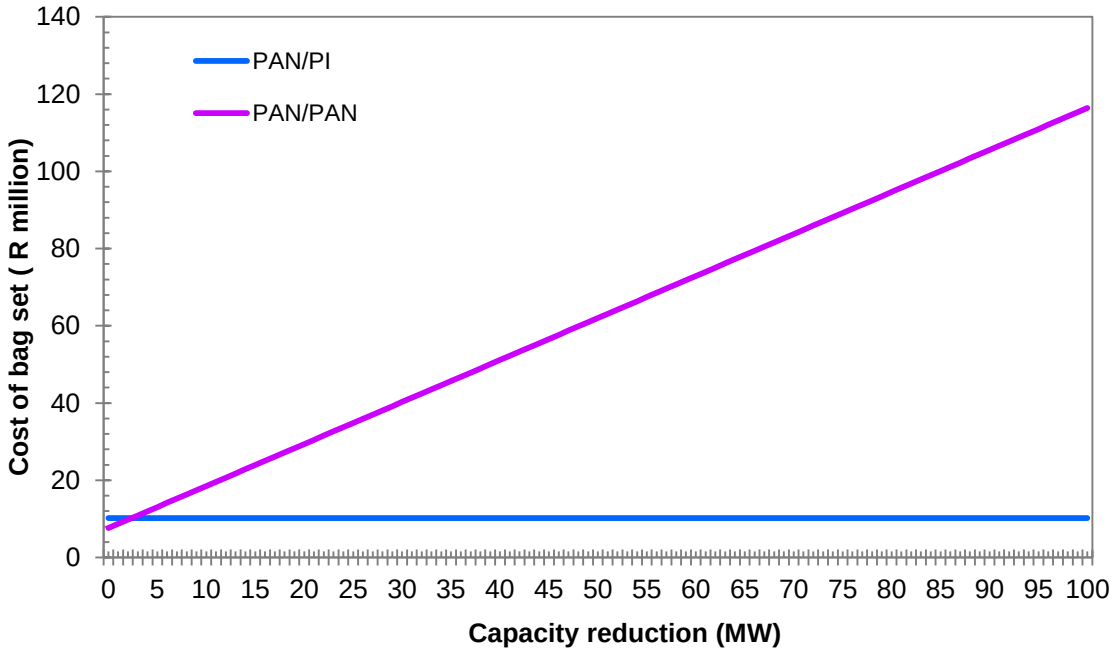

Figure 5-2: CBA sensitivity of low temperature fabric to capacity reduction for continued operation, L_R, after nitric acid exposure

For combined nitric and sulphuric acid exposure, the strength retention of PAN/PAN is such that, according to the assumptions on which this CBA is based, bag life is less than n_e. Therefore, a complete bag set replacement is required during the study period. For cases where full bag set replacement is necessary, cost is sensitive to the outage duration for bag replacement. Figure 5-3 shows that should it be possible to replace the bag set in less than 10 days, PAN/PAN is more cost effective than PAN/PI. Note that PAN/PI also suffers a reduction in strength when exposed to combined nitric and sulphuric acid. The remaining bag life, however, exceeds n_e and therefore only capacity reduction during continued operation is required. This associated cost will, however, increase rapidly with increasing L_R, as discussed above.

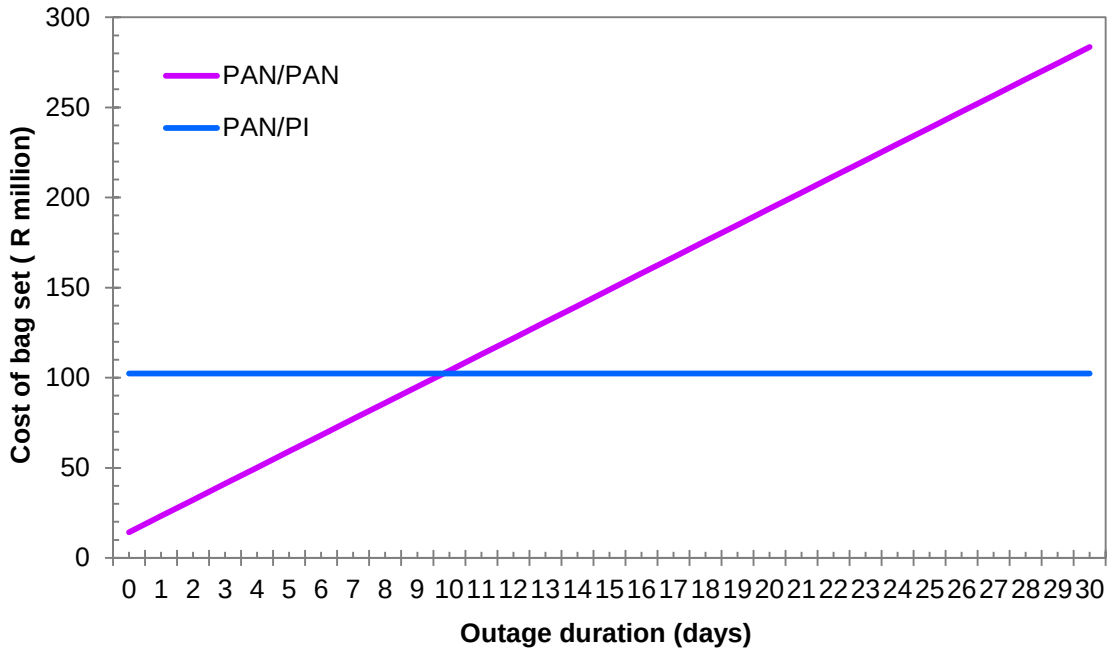

Figure 5-3: CBA sensitivity of low temperature fabrics to outage duration for bag replacement, D_{BR}, after combined nitric and sulphuric acid exposure

5.4.2 CBA RESULTS AND SENSITIVITIES: INCORPORATION OF PI IN PPS-BASED FABRICS

This section discusses the use of the proposed CBA to compare PPS/PPS and PPS/PI for application in high temperature baghouses. The same input parameters defined for low temperature fabrics was used, as described in Appendix C (refer to Table C-1).

The results of the CBA for high temperature fabrics where no potential pressure drop benefit is considered are summarised in Table 5-4. It is evident that PI incorporation in PPS-based fabrics is beneficial in environments where sulphuric acid exposure is

anticipated. This is due to the strength increase of PPS/PI, as reported in Table 4-7. For the other scenarios considered, PPS/PI exhibited marginally poorer strength retention than PPS/PPS. However, since strength retention was similar, costs are driven by initial capital cost.

Table 5-4: CBA results for PPS-based fabrics – no pressure drop benefit

Operating Scenario	Total price of Bag Set (R million)	
	PPS/PPS	PPS/PI
No acid exposure	14.8	16.0
Nitric acid exposure	153	156
Sulphuric acid exposure	24.4	16.0
Combined nitric and sulphuric acid exposure	153.4	156

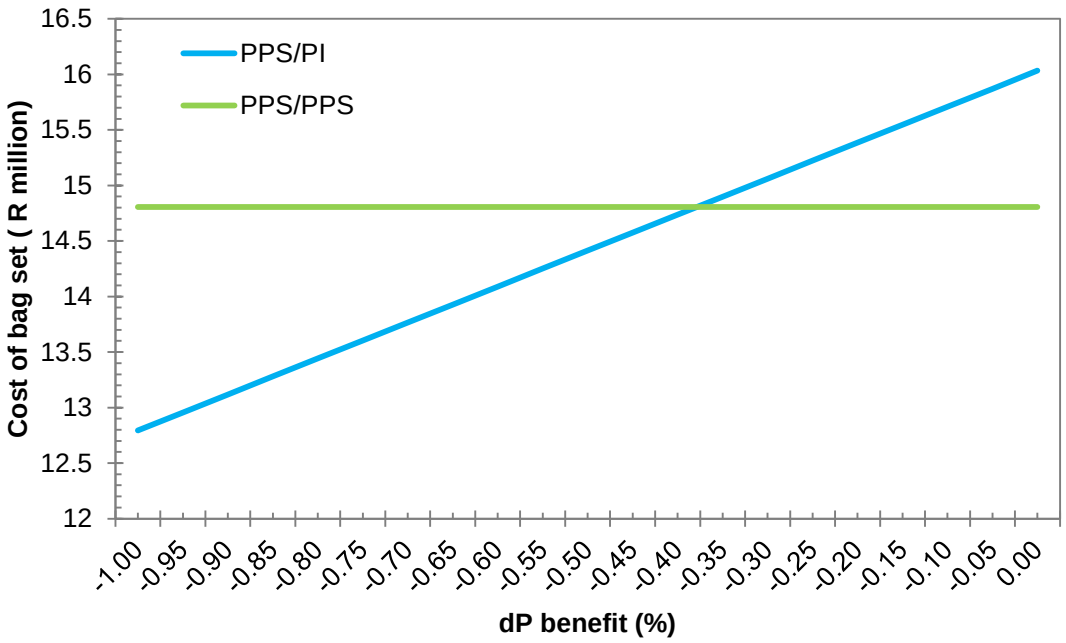

Figure 5-4: CBA sensitivity of low temperature fabrics to pressure drop benefit when no acidic conditions are experienced

The impact of the potential pressure drop benefit that may be realised when incorporating PI in high temperature fabrics due to possible electrostatic interactions as discussed in Chapter 3, are shown in Figure 5-4. It is clear from Figure 5-4 that if a

pressure drop reduction of more than 0.38% is realised, PPS/PI becomes more cost effective than PPS/PPS if no bag degradation due to acid attack is experienced.

It is further clear from Table 5-4 that both fabrics considered are susceptible to severe degradation in environments where nitric and simultaneous nitric and sulphuric acid exposure are anticipated. In these scenarios, with the assumptions considered in this CBA, PPS/PPS and PPS/PI would both fail before n_e and would require an additional set of bags to be purchased and installed during the study period.

In order to highlight the comparative performance of the high temperature fabrics, it was further assumed that a planned outage opportunity is available at n-1 years in the case of only nitric acid exposure. For combined nitric and sulphuric acid exposure, the strength retention of both fabrics is too poor for this assumption to allow meaningful comparison (Table 4-7). When applying this assumption to the CBA for high temperature fabrics exposed to nitric acid, the total cost of PPS/PPS was estimated to be R146 million and that of PPS/PI was R156 million. The influence of L_R in this scenario is shown in Figure 5-5, from which it is apparent that if a capacity reduction of more than 54 MW is required, PPS/PI becomes more attractive than PPS/PPS in terms of cost.

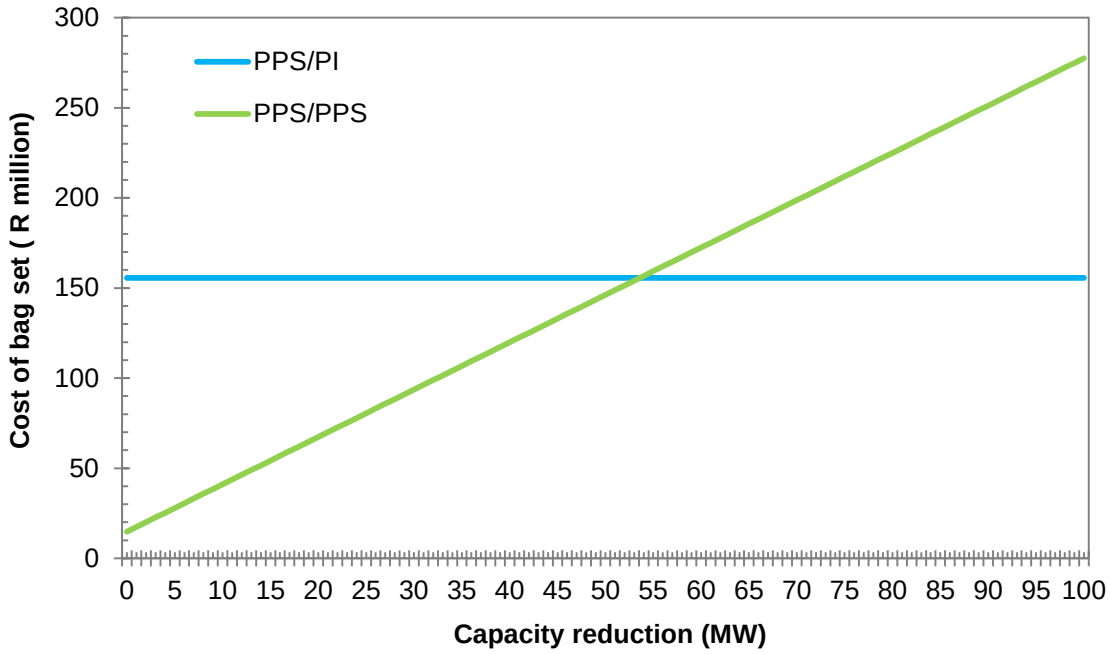

Figure 5-5: CBA sensitivity of high temperature fabrics to capacity reduction for continued operation, L_R, after nitric acid exposure with outage opportunity at n-1 years

5.5 CONCLUSIONS OF CBA OF FILTRATION FABRICS

From the application of the proposed CBA method to the fabrics considered in this study, it can be concluded that costs associated with fabric selection are more significant than initial capital cost only. The CBA method is highly sensitive to input assumptions regarding capacity reduction, required when premature bag failure occurs.

The incorporation of PI in PAN-based fabrics offers a cost advantage when nitric acid or combined nitric and sulphuric acid exposure is experienced. In PPS-based fabrics, PI incorporation offers a cost advantage with respect to conditions where sulphuric acid exposure would prevail. Should PI incorporation allow a pressure drop benefit to be realised, the total cost reduction is projected to be significant.

CHAPTER 6: CONCLUSIONS AND RECOMMENDATIONS

A summary of the main findings of this study, in accordance with the aims and objectives stated in Chapter 1, is presented in this chapter. In addition, recommendations for future work to further develop the findings are made.

6.1 SUMMARY AND CONCLUSIONS

Reducing industrial PM emissions is necessary in order to ensure compliance with legislation as well as to minimise impact on the environment and human health. Baghouses are an attractive option for PM emissions reduction to levels below those dictated by South African legislation, namely the National Environmental Management: Air Quality Act (NEMAQA) of 2004. Appropriate filtration fabric selection for the bags used for PM capture in baghouses is central to cost-effective operation.

This study considered low temperature and high temperature filtration fabrics commonly used in baghouses at South African coal-fired power stations. These fabrics were namely PAN/PAN, PAN/PI, PPS/PPS and PPS/PI. The main aim of the study was to establish whether the incorporation of the more costly PI-blended surface layer is beneficial.

An area of baghouse filtration theory which is not yet well understood is the electrostatic interaction of the filtration fabric with the PM. It is hypothesised that favourable electrostatic interactions may improve filtration velocity and reduce pressure drop. To expand the knowledge on this subject, this study investigated the triboelectric behaviour of the four fabrics considered as well as fabric of 100% PI construction for comparative purposes.

A triboelectric series for the filtration fabrics considered was developed by rubbing fabric samples on a PET reference material as described in Chapter 3. It was found that after triboelectric contact, PI/PI obtains a charge of positive polarity on the filtration surface and the clean gas surface of the fabric. PPS/PPS was found to obtain a highly negative charge on both surfaces. PAN/PAN obtained a negative charge of a lesser magnitude than PPS/PPS on both surfaces. PPS/PI obtained a negative charge on the clean gas surface and positive charge on the filtration surface after triboelectric contact. Similarly, PAN/PI obtained a negative charge on the clean gas surface and positive charge on the filtration surface. It is thus concluded that the PI fibre has the tendency

towards positive charge polarity after triboelectric contact and PAN and PPS have the tendency towards negative charge polarity, where PPS is more negative than PAN. It is further concluded that PI drives the charging behaviour of the fabric when included in a blend with PAN or PPS fibres.

The relative charge dissipation rate of fabrics was also studied. It was found that PPS-based fabrics exhibit the highest charge dissipation rate, followed by PAN based-fabrics and finally by PI fabrics. Comparison of charge dissipation rates with the position of the fabric surfaces on the triboelectric series found no correlation with charge magnitude or polarity. It could, however, be seen that the clean gas surfaces exhibited consistently higher charge dissipation rates than the filtration surfaces. It is suggested that these higher discharge rates are due to the higher surface area exposed to the atmosphere, since the unfinished, woolly clean gas surfaces facilitates the charge dissipation process. Furthermore, blended fabrics exhibited slower charge dissipation rates than the non-blended fabrics.

Further to tests using PET as the reference material, the triboelectric effects of rubbing materials against themselves as a reference were also studied. It was found that PAN develops a negligible charge when rubbed on itself and PPS and PI fluctuate between positive and negative charges of high magnitude.

The interaction of ash with triboelectrically charged fabric was also investigated. It was found that filtration surfaces with negative charge polarity (PAN/PAN and PPS/PPS) interact with ash to a greater extent than those with positive charge polarity. This finding may hold implications for in situ applications as ash cake development could be impacted by electrostatic interactions between the ash and the bag surface. It is suggested that negatively charged fabric surfaces, i.e. the filtration surfaces of PAN/PAN and PPS/PPS, may have a higher propensity towards particulate penetration into the fabric volume and consequent increased pressure drop. PI incorporation in negatively charged PAN- and PPS-based fabrics may therefore offer potential triboelectric benefits, however further research is required to quantify this.

Further to the investigations into differences in triboelectric behaviour of the filtration fabrics with and without PI incorporation, the resistance of the filtration fabrics to acid attack and thermal degradation was studied. Tensile properties after nitric and sulphuric acid exposure were studied throughout the operational temperature ranges of the fabrics.

For PAN/PAN and PAN/PI, it was found that the degradative effect of nitric acid on fabric tensile strength increases with increased temperature within the tested temperature range (95°C - 140°C). Compared to the PAN/PAN results, PAN/PI offered a marginal strength benefit over PAN/PAN after nitric acid exposure.

In sulphuric acid, PAN/PAN showed significant degradation at temperatures beyond the typical operational temperature of 125°C. PAN/PI showed substantial strength reduction at these conditions, which increased with increasing temperature. While both fabrics suffered increasing loss of tensile strength with increased sulphuric acid concentration (up to 3 M), PAN/PI was significantly more susceptible to acid attack from sulphuric acid than PAN/PAN. When exposed to nitric and sulphuric acid mixtures, PAN/PI exhibited better strength retention than PAN/PAN.

PI incorporation in low temperature, PAN-based fabrics therefore offers a tensile strength advantage at the conditions tested after nitric acid, or simultaneous nitric and sulphuric acid exposure, but is not suitable in conditions where sulphuric acid exposure is dominant. PAN/PAN, however, exhibited average strength retention >80% in all acidic conditions studied.

Both high temperature fabrics considered, namely PPS/PPS and PPS/PI, were significantly degraded by nitric acid. The negative effect on tensile strength was seen to increase with increased temperature (between 130°C and 190°C) and concentration (0.5 M – 3 M). The difference in average impact between the fabrics was marginal. DSC analysis revealed that nitric acid exposure changes the thermal behaviour of PPS, with the appearance of an exothermic peak in the DSC thermogram after nitric acid exposure. In contrast, an endothermic peak was observed prior to nitric acid exposure and after sulphuric acid exposure. Furthermore, PPS/PI fabrics were more degraded than PPS/PPS.

Sulphuric acid, however, had only a minor negative impact on PPS-based fabrics, which diminished with increased concentration (up to 3 M). On the other hand, PPS/PI showed a strength benefit, since the tensile strength increased with increasing sulphuric acid concentration. Both fabrics showed an increasing strength trend with increasing temperature, with the exception of insignificant changes at 170°C.

In mixtures of nitric and sulphuric acids, both high temperature fabrics suffered significant strength reduction at the conditions tested. Degradation increased with increasing concentration, and PPS/PI was more affected than PPS/PPS.

It can therefore be concluded that PPS-based, high temperature filtration fabrics are not suitable to operation in environments where exposure to nitric acid, or mixtures of nitric and sulphuric acids, is expected. These fabrics, however, are not sensitive to sulphuric acid attack. PI incorporation in PPS-based fabrics resulted in marginally poorer strength retention after nitric acid and simultaneous nitric and sulphuric acid exposure. After sulphuric acid exposure, however, PI incorporation resulted in increased tensile strength.

Traditional methods for assessing baghouse costs are unsuitable for comparison of bags for use in the same baghouse. A cost benefit analysis method that employs life cycle costing was therefore proposed for use when comparing total costs associated with filtration fabric selection. This method accounts not only for capital costs and bag life as traditional methods do, but includes costs associated with lost production due to early bag failure, as well as pressure drop benefits that may be realised when optimal fabric selections are made. The proposed CBA method was applied to compare the incorporation of PI in low and high temperature fabrics. Since the technical results from this study used to make costing assumptions are based on laboratory results only, the outcomes of the analyses are indicative only.

The CBA method was used for comparison of PAN and PAN/PI for use in a low temperature baghouse. Apart from a base cost analysis where initial capital cost only was considered, three scenarios were considered. Flue gas entering the baghouse was assumed to have either significant levels of nitric acid, sulphuric acid or a mixture of nitric and sulphuric acids. Under the assumptions made in this study, the following cost comparison was found.

When no acid attack is experienced, PI incorporation resulted in an additional cost of 25%. In sulphuric acid conditions, PI incorporation was 64% more expensive than PAN. However, PI incorporation was shown to have a cost advantage of 84% in nitric acid conditions, and 27% in combined nitric and sulphuric acid conditions. Furthermore, should a pressure drop advantage be realised due to the incorporation of PI in the filtration surface of the fabric leading to favourable electrostatic interactions with the ash, the total cost of PAN/PI was reduced. For the conditions considered, PAN/PI is therefore projected, based on the CBA model assumptions, to be more cost effective than PAN in environments where no acid attack is experienced. However, this would only be true if a pressure drop benefit of more than 0.8% is realised.

Similarly, the CBA was used to comparatively evaluate high temperature fabrics. The same acid attack scenarios considered above were applied. It estimated that PI incorporation is 8% more expensive than purchasing PPS only bags when no acid attack is experienced. PI incorporation in PPS is also 2% more expensive when nitric acid or combined nitric and sulphuric acid exposure is experienced. In environments where sulphuric acid attack is experienced, however, PPS/PI is 34% less expensive than PPS. The cost difference between high temperature fabrics is less than for low temperature fabrics, thus was estimated that only if a pressure drop benefit of more than 0.4% can be realised by incorporating PI in the filtration surface, does PPS/PI become more cost effective than PPS.

Costs associated with premature bag failure are significant, and this CBA shows the importance of considering all cost elements when making bag selections. In particular, capacity losses caused by early bag failure and gains due to differences in filtration characteristics, which affect the pressure drop, are significant cost determinants when analysing the total cost related to filtration fabric selection.

6.2 RECOMMENDATIONS

This study was a laboratory based investigation into factors which affect the suitability of specific filtration fabrics for baghouse applications. Recommendations for further work to elaborate on the findings of this study are discussed below.

It is stressed that the results of the CBA to the incorporation of PI in PAN- and PPS-based filtration fabrics were of an exploratory nature only, as the assumptions used for application were based on laboratory investigations. Where the CBA is to be used for fabric selection for a specific baghouse, recommendations for research to improve input assumptions are recommended below. It is further recommended that historical operational data are included in assumptions where available.

The triboelectric properties of polymers in general and polymers used in filtration fabrics in particular are areas which warrant further study. It is recommended that the experiments described in Chapter 3 of this study are repeated using fabric samples from different suppliers. This approach could aid the understanding of electrostatic interactions of polymer types where minor differences in chemical structure exist. It is further recommended that ash charging characteristics are studied to expand the understanding of the mechanism by which ash penetrates negatively charged fabrics.

Furthermore, it is recommended that an experimental set-up be built to simulate fabric filtration and to measure charge development of the filtration materials during pulse cleaning and after ash filtration, when a stable permanent ash layer has formed on the surface. Different ash types could be fed into the laboratory-scale baghouse and the effects on charge development may be studied. Such an experimental setup will allow ash cake development in a similar manner to that experienced in industrial baghouses and parallels between fabric charge and bag permeability during operation can also be drawn. The results from such experiments could aid in developing an improved understanding of the factors affecting bag charge as well as the impact that this has on filtration and pressure drop. This understanding could be extended to the development of better costing assumptions for use in the CBA.

Subsequent to the suggested laboratory-scale experiments, it is recommended that in situ tests are conducted to verify the laboratory results. It is recommended that research is aimed at establishing the absolute pressure drop benefit that may be realised due to favourable electrostatic interactions of different filtration fabrics with ash as well as whether this benefit is constant throughout bag life or fluctuates as bags age. Results could be used to inform CBA assumptions.

To better understand the stability of the selected fabrics when exposed to chemical aggressors, it is recommended that the acid attack experiments described in Chapter 4 are repeated with other acids that may also be present in flue gas, such as hydrochloric acid. Experiments may also be expanded to include alkaline substances. The analyses after exposure should be extended to include permeability and burst strength tests and fabric shrinkage should also be evaluated. Such analyses could be used to further inform CBA assumptions.

It is further recommended that the research be expanded to include acid exposure on fabrics that have a protective ash cake present. This research can include bags in an experimental baghouse casing where ash and simulated flue gas mixtures with varying levels of chemical aggressors and moisture are present. This will not only develop understanding of the stability of the fabric after acid attack that more realistically mimics operation, but various ash types can be used in order to develop a guideline of expected fabric stability based on the typical ash analysis at a specific baghouse. Subsequently, controlled in situ studies can be performed.

Further, thermal degradation studies should be expanded to include investigation of the thermal degradation kinetics of the various fibre types before and after acid exposure.

This would be valuable for lifetime predictions, which could improve input assumptions in the CBA. Furthermore, fibre degradation in gaseous environments present in baghouses should be studied. Air or nitrogen with varying levels of nitrous and sulphurous oxides can be used in thermogravimetric analysis of the polymers used in filtration fabrics in order to evaluate thermal degradation in environments that more closely resemble baghouse operation.

The acid attack and thermal degradation experiments recommended above can be used to draw more realistic bag life assumptions for use in the CBA. It is further recommended that a bag life model including resistance to ash type and chemical and thermal aggressors is developed and verified using historical baghouse data in order to have confidence in costing assumptions.

The CBA can be extended to include more detailed technical input where available. Where accurate bag life predictions can be made, the model may be expanded to allow for partial bag replacement costs. The economic assumptions of the CBA method can also be expanded to consider the full generation fleet of a baghouse owner and not the baghouse in isolation. This expansion would include additional costs for alternative power sources which may need to be activated during capacity loss situations and could include time dependent assumptions for power cost and the discount rate.

REFERENCES

Abu-Bakar, A. & Moinuddin, K., 2012. *Effects of Variation in Heating Rate, Sample Mass and Nitrogen Flow on Chemical Kinetics for Pyrolysis.* Launceston, 18th Australasian Fluid Mechanics Conference.

Adams, C. K., 1987. *Nature's Electricity.* Blue Ridge Summit: Tab Books.

AKSA, 2010. *AKSA Homopolymer Acrylic Fiber - "The Core of Filtration".* [Online] Available at: http://www.aksa.com/en/i-189 [Accessed 28 12 2017].

Alarifi, I. M. et al., 2015. Thermal, Electrical and Surface Hydrophobic Properties of Electrospun Polyacrylonitrile Nanofibers for Structural Health Monitoring. *Materials,* Volume 8, p. 7017–7031.

Al-Attabi, R. et al., 2017. High Efficiency Poly(acrylonitrile) Electrospun Nanofiber Membranes for Airborne Nanomaterials Filtration. *Advanced Engineering Materials.*

Aleksandrov, V., Baranova, R. & Valdberg, A., 2010. Filter materials for bag filters with pulsed regeneration. *Chemical and Petroleum Engineering,* 46(1), pp. 33-39.

Andrabi, S. J. A., Chandra, A., Aslam, M. & Hassan, I., 2012. Influence of Chemical Composition on the Electrical Resistivity of Fly Ash Generated from Indian Coal Based Thermal Power Plants. *Research Journal of Applied Sciences, Engineering and Technology ,* 5(6), pp. 2284-2288.

Ba, C., Langer, J. & Economy, J., 2009. Chemical modification of P84 copolyimide membranes by polyethylenimine for nanofiltration. *Journal of Membrane Science,* Volume 327, pp. 49-58.

Ban, H., Li, T. X., Schaefer, J. & Stencel, J., 1996. Triboelectrostatic separation of unburned carbon from fly ash. *Preprints of Papers, American Chemical Society, Division of Fuel Chemistry,* December.pp. 609-613.

Barca, S., 2011. Energy, property, and the industrial revolution narrative. *Ecological Economics,* 70(7), pp. 1309-1315.

Baytekin, H. et al., 2011. The Mosaic of Surface Charge in Contact Electrification. *Science,* 333(6040), pp. 308-312.

Belo, L. et al., 2014. High-Temperature Conversion of SO2 to SO3: Homogeneous Experiments and Catalytic Effect of Fly Ash from Air and Oxy-fuel Firing. *Energy Fuels,* 28(11), pp. 7243-7251.

Benitez, J., 1993. Fabric Filters. In: *Process Engineering and Design for Air Pollution Control.* Englewood Cliffs: Prentice Hall, pp. 414-439.

Billings, C. E. & Wilder, J., 1970. *Handbook of Fabric Filter Technology,* Washington, D.C.: National Air Pollution Control Administration, U.S. Department of Health, Education and Welfare.

Bowden, P., Neate, M., Curell, B. & Gerakios, M., 2006. *Fabric filters for coal fired power stations.* Cairns, ICESP X .

Brosseau, L. & Berry Ann, R., 2009. *N95 Respirators and Surgical Masks.* [Online] Available at: http://blogs.cdc.gov/niosh-science-blog/2009/10/14/n95/ [Accessed 24 October 2016].

Brown, P. & Cox, C., 2017. *Fibrous Filter Media.* Duxford: Woodhead Publishing.

Bumiller, M., 2012. *Sampling for Particle Size Analysis.* [Online]
Available at:
http://www.horiba.com/fileadmin/uploads/Scientific/Documents/PSA/Webinar_Slides/TR011.pdf
[Accessed 13 April 2018].

Burgo, T. A. d. L. et al., 2011. Electric potential decay on polyethylene: Role of atmospheric water on electric charge build-up and dissipation. *Journal of Electrostatics,* 69(4), pp. 401-409.

Burgo, T. A. L. et al., 2012. Triboelectricity: Macroscopic Charge Patterns Formed by Self-Arraying Ions on Polymer Surfaces. *Langmuir,* Volume 28, pp. 7407-7416.

Burnard, K. et al., 2014. *Emissions Reduction through Upgrade of Coal-Fire Power Plants: Learning from Chinese Experience,* Paris: International Energy Agency.

Cai, W. & Hu, G., 2015. Oxidation degradation of polyphenylene sulfide needle felt at different sulfuric acid dew point temperatures. *High Performance Polymers,* 27(1), pp. 94-99.

Camfil, 2015. *Principles of Filtration.* [Online]
Available at: http://www.camfil.com/Filter-technology/Principles-of-Filtration/
[Accessed 24 October 2016].

Carr, R. C. & Smith, W. B., 1984. Fabric Filter Technology for Utility Coal-Fired Power Plants. *Journal of the Air Pollution Control Association,* 34(1), pp. 79-89.

Charlson, E., Charlson, E., Burkett, S. & Yasuda, H., 1992. Study of the contact electrification of polymers using contact and separation current. *IEEE Transactions on Electrical Insulation,* 27(6), pp. 1144-1151.

Clark, G. & Jacks, D. S., 2007. Coal and the Industrial Revolution, 1700 - 1869. *European Review of Economic History,* 11(1), pp. 39-72.

Clayton, M., 2006. *Selection criteria of PPS and PPS/PI blends for use in power station applications.* Cairns, International Society for Electrostatic Precipitation.

Cook, E., 1971. The Flow of Energy in an Industrial Society. *Scientific American,* 225(3), pp. 134-147.

Davis, R., Kiska, T. & Felix, S., 1990. *A Comparative Evaluation of High-Temperature Pulse-Jet Baghouse Filter Fabrics.* Long Beach, American Society of Mechanical Engineers.

Dennis, R. & Klemm, H., 1979. *Fabric Filter Model Format Change: Volume I - Detailed Technical Report,* Washington D.C.: Environmental Protection Agency.

Dennis, R. & Klemm, H., 1980. Modeling Concepts for Pulse Jet Filtration. *Journal of the Air Pollution Control Association,* 30(1).

Department of Environmental Affairs and Tourism, 2004. *Integrated Environmental Management Information Series: Cost Benefit Analysis,* Pretoria: Department of Environmental Affairs and Tourism.

Department of Environmental Affairs, 2010. *Government Notice - National Environment Management: Air Quality Act (No. 39 of 2004).* Pretoria: The South African Presidency.

Deqiang, C., Jingxian, L., Ning, m. & Baozhi, C., 2013. Study on the Thermal Stability of Polyphenylene Sulfide Filter Media by Non-isothermal Thermogravimetry. *Advanced Materials Research,* Volume 663, pp. 988-992.

Deqiang, C., Jingxian, L., Ning, M. & Baozhi, C., 2013. Study on the Thermal Stability of Polyphenylene Sulfide Filter Media by Non-isothermal Thermogravimetry. *Advanced Materials Research,* Volume 663, pp. 988-992.

Di Blasi, M., Morandi, A. & Popovici, F., 2015. Filter media trends for coal fired boiler bag houses filtration test rig evaluations. *VGB PowerTech,* Volume 11, pp. 64-68.

Diaz, A. & Felix-Navarro, R., 2004. A semi-quantitative tribo-electric series for polymeric materials- the influence of chemical structure and properties. *Journal of Electrostatics ,* Volume 62, pp. 277-290.

Dolan GmbH, 2013. *DOLANIT® Type 12.* [Online]
Available at: http://www.dolan-gmbh.de/en/dolanit-filtration.html
[Accessed 20 March 2018].

Du, B. & Li, J., 2016. Effects of Ambient Temperature on Surface Charge and Flashover of Heat-shrinkable Polymer under Polarity Reversal Voltage. *IEEE Transactions on Dielectrics and Electrical Insulation,* 23(2), pp. 1190-1197.

Ebi, K. L. & McGregor, G., 2008. Climate Change, Tropospheric Ozone and Particulate Matter, and Health Impacts. *Environmental Health Perspectives,* 116(11), pp. 1449-1455.

EMS-Griltech, 2018. *Nexylene®.* [Online]
Available at: https://www.emsgriltech.com/en/products-applications/products/nexylene/
[Accessed 20 March 2018].

Eskom Holdings SOC Ltd, 2017. *Integrated Report,* Sandton: Eskom Holdings SOC Ltd.

Evonik Fibres GmbH, n.d. *P84 Polyimide Fibres Properties, Technical Data and Product Range.* [Online]
Available at: http://www.p84.com/product/p84/en/high-temperature-filtration/
[Accessed 28 12 2017].

Farber, D. A., 2009. Rethinking the Role of Cost-benefit Analysis. *The University of Chicago Law Review,* 76(1355), pp. 1355-1405.

Feng, S. et al., 2016. The health effects of ambient PM2.5 and potential mechanisms. *Ecotoxicology and Environmental Safety,* Volume 128, pp. 67-74.

Frederick, E. R., 1974. Some Effects of Electrostatic Charges In Fabric Filtration. *Journal of the Air Pollution Control Association,* 24(12), pp. 1164-1168.

Frederick, E. R., 1980. Fibres, Electrostatics, and Filtration: A Review of New Technology. *Journal of the Air Polltuion Control Association,* 30(4), pp. 426-431.

Frederick, E. R., 1996. *Utilizing electrical effect in nonaqueous filtration.* Pittsburgh: Filter Media Specification.

Frederick, E. R., 1999. *Triboelectric Property Modification and Selection of Fabrics for Filtration Applications.* United States of America, Patent No. 5,888,274 .

Fuchs, N. & Stechkina, I., 1963. A note on the theory of fibrous aerosol filters. *The Annals of Occupational Hygeine,* 6(Jan-Mar), pp. 27-30.

Gabbott, P. et al., 2008. A Practical Introduction to Differential Scanning Calorimetry. In: P. Gabbott, ed. *Principles and Applications of Thermal Analysis.* Oxford: Blackwell Publishing Ltd.

Gaunt, T. et al., 2012. *Informal Electrification in South Africa: Experience, Challenges and Opportunities,* Cape Town: Sustainable Energy Africa.

Govindsamy, R., 2018. *Typical flue gas constituents at air heater outlet in South African coal fired power stations* [Interview] (20 March 2018).

Greiner, G., Furlong, D., VanOsdell, D. & Hovis, L., 1981. Electrostatic Stimulation of Fabric Filtration. *Journal of the Air Pollution Control Association,* 31(10), pp. 1125-1130.

Greyling, C. J., 1998. *Optimisation of the evaluation methods used on polymeric fibres and fabrics in bag filter plants.* Stellenbosch: Stellenbosch University.

Grobbelaar, H. D., 2006. *Managing bag shrinkage in low temperature fabric filter plants.* Cairns, ICESP X.

Hecen, W., Dehou, J. & Ying, L., 2011. Life Problem Analysis on PPS Filter Application of Bag Dedusters in Coal-Fired Power Plants. *Advanced Materials Research,* Volume 236-238, pp. 2464-2470.

Henniker, J., 1962. Triboelectricity in Polymers. *Nature,* 196(4853), p. 474.

Holgate, C., 2007. Factors and Actors in Climate Change Mitigation:A Tale of Two South African Cities. *Local Environment,* 12(5), pp. 471-484.

Holland, M., 2017. *Health impacts of coal fired power plants in South Africa,* s.l.: Groundwork South Africa.

Humphries, W., Madden, J. & Miceli, M., 1984. The Effect of Particle Precharging on the Performance of a Fabric Filter Collecting Lead Smelter Dust. *Aerosol Science and Technology,* 3(4), pp. 381-395.

Hutton, I. M., 2007. *Handbook of Nonwoven Filter Media.* 1st ed. Oxford: Elsevier.

Ieda, M., Sawa, G. & Shinohara, U., 1967. A decay process of surface electric charges across polyethylene film. *The Japan Society of Applied Physics,* 6(6), pp. 793-794.

Jasti, V. K., 2011. *Electrostatic Charge Generation and Dissipation on Woven Fabrics Treated with Antistatic and Hydrophilic Surface Finishes,* Raleigh: North Carolina State University.

Jeffrey, L., 2005. Characterization of the coal resources of South Africa. *The Journal of The South African Institute of Mining and Metallurgy,* pp. 95-102.

Jog, J., Bulakh, N. & Nadkarni, V., 1994. Crystallization of polyphenylene sulphide. *Bulletin of Materials Science,* 17(6), pp. 1079-1089.

Jonassen, N., 1998. *Electrostatics.* Dordrecht: springer science + business media.

Jung, B., Yoon, J. K., Kim, B. & Rhee, H.-W., 2005. Effect of crystallization and annealing on polyacrylonitrile membranes for ultrafiltration. *Journal of Membrane Science,* 246(1), pp. 67-76.

Karacan, I., 2012. Thermal stabilization of polyacrylonitrile fibres. *Plastics Research Online*.

Kazyuta, V., 2013. Electrostatic Phenomena in Bag Filtration of Industrial Gases. *Steel in Translation,* 43(8), pp. 535-538.

Khean, T. S., 2003. *Studies in Filter Cake Characterisation and Modelling,* Singapore: National University of Singapore.

Khobai, H., Mugano, G. & Le Roux, P., 2017. Exploring the nexus of electricity supply and economic growth in South Africa. *International Journal of Energy Economics and Policy,* 7(4), pp. 240-251.

Klotz, A. & Haug, B., 2006. *Experiences in Bag House Applictions after Coal Fired Boilers.* Cairns, ICESP X.

Koch, M., 2008. *Cake filtration modeling – Analytical cake filtration model and filter medium characterization,* Trondheim: Norwegian University of Science and Technology.

Koehler, J. L. & Leith, D., 1983. Model calibration for pressure drop in a pulse jet cleaned fabric filter. *Atmospheric Environment,* 17(10), pp. 1909-1913.

Koerner, R. M., 1994. *Designing with Geosynthetics.* 3 ed. Upper Saddle River: Prentice Hall.

Kunkel, W., 1950. The Static Electrification of Dust Particles on Dispersion into a Cloud. *Journal of Applied Physics,* Volume 21, pp. 820-832.

Kwetkus, B., 1997. Particle Precharging and Fabric Filtration - Experimental Results of a Corona Precharger. *Journal of Electrostatics,* Volume 40 - 41, pp. 657-662.

Lauer, M., 2008. *Methodology guideline on techno economic assessment (TEA).* Vienna, Joanneum Research.

Lavely, L. L. & Ferguson, A. W., 2003. Power Plant Atmospheric Emissions Control. In: L. F. Drbal, K. L. Westra, P. G. Boston & R. B. Erickson, eds. *Power Plant Engineering.* 6th ed. Boston: Kluwer Academic Publishers, pp. 464-520.

Lee, K. & Liu, B., 1982. Theoretical Study of Aerosol Filtration by Fibrous Filters. *Aerosol Science and Technology,* 1(2), pp. 147-161.

Lian, D. et al., 2016. Enhancing the resistance against oxidation of polyphenylene sulphide fiber via incorporation of nano TiO2-SiO2 and its mechanistic analysis. *Polymer Degradation and Stability,* Volume 129, pp. 77-86.

Liu, C.-y. & Bard, A. J., 2009. Chemical redox reactions induced by cryptoelectrons on PMMA surface. *Journal of the American Chemical Society,* 131(18), pp. 6397-6401.

Liu, J. et al., 2010. *Impact of NOx on Baghouse Filter used for Coal-boiler Smoke.* Chengdu, s.n.

Liu, L., 2010. *Electrostatic Generation and Control on Textiles.,* Raleigh: North Carolina State University.

Liu, L. & Seyam, A. M., 2013. Frictional Electrification on Polymeric Flat Surfaces. *Journal of Engineered Fibers and Fabrics,* 8(1), pp. 126-136.

Li, X.-G., Huang, M.-R., Bai, H. & Yang, Y.-L., 2002. High-Resolution Thermogravimetry of Polyphenylene Sulfide Film under Four Atmospheres. *Journal of Applied Polymer Science,* Volume 83, pp. 2053-2059.

Lloyd, S., 1987. The Control of Air Pollution at South African Coal-Fired Power Stations. *Clean Air Journal,* 7(4), pp. 20-24.

Lowell, J. & Rose-Innes, A., 1980. Contact electrification. *Advances in Physics,* 29(6), pp. 947-1023.

Lupión, M., Gutiérrez Ortiz, F. J., Navarrete, B. & Cortés, V. J., 2010. Assessment performance of high-temperature filtering elements. *Fuel,* Issue 89, pp. 848-854.

Maerig, T. & Morris, L., 2018. *Life Cycle Cost Analysis Handbook.* 2nd ed. Juneau: State of Alaska - Department of Education & Early Development.

Maity, S. & Singha, K., 2012. Structure-Property Relationships of Needle-Punched Nonwoven Fabric. *Frontiers in Science,* 2(6), pp. 226-234.

Mao, N., Chang, D. Q., Liu, J. X. & Sun, X., 2013. Experimental study on the durability performance of PPS filter media. *Applied Mechanics and Materials,* Volume 300-301, pp. 1077-1080.

Margolis, J. M., 1985. *Engineering Thermoplastics: Properties and Applications.* 8 ed. New York, Inc.: Marcel Dekker.

Marier, P. & Dibbs, H., 1974. The catalytic conversion of SO2 to SO3 by fly ash and the capture of SO2 and SO3 by CaO and MgO. *Thermochimica Acta,* 8(1), pp. 155-165.

Markandya, A. & Wilkinson, P., 2007. Electricity generation and health. *Energy and Health,* 370(2), pp. 979-990.

McCarty, L. S. & Whitesides, G. M., 2008. Electrostatic Charging Due to Separation of Ions at Interfaces: Contact Electrification of Ionic Electrets. *Angewandte Chemie,* 47(12), pp. 2188-2207.

McKenna, J. D., 2013. *Key Issues When Selecting Fabric Filter Bags to Achieve Optimum Bag Life.* Roanoke, McIlvaine Company Hot Topic Hour.

McKenna, J. D. & Turner, J. H., 1989. *Fabric Filter-Baghouses I, Theory, Design, and Selection..* 1st ed. Roanoke: ETS.

McKenna, J., Mycock, J. & Lipscomb, W., 1974. Performance and Cost Comparisons between Fabric Filters and Alternative Particulate Control Technologies. *Journal of the Air Pollution Control Association,* 24(12), pp. 1144-1148.

Mekishev, G., Yovcheva, T., Gentcheva, E. & SR, N., 2005. Study of electrets stored at pressures lower than atmospheric. *Journal of Electrostatics,* 63(11), pp. 1009-1015.

Mirasgedis, S. et al., 2008. Environmental damage costs from airborne pollution of industrial activities in the greater Athens, Greece area and the resulting benefits from the introduction of BAT. *Environmental Impact Assessment Review,* Volume 28, pp. 39-56.

Mishra, A., 1982. Studies of polymer electrets III Charge decay behavior in polar polymer homoelectrets. *Journal of Applied Polymer Science,* 27(6), p. 1967–1975.

Morton, W. E. & Hearle, J. W. S., 2008. *Physical Properties of Textile Fibres.* 4 ed. Cambridge: Woodhead Publishing Ltd.

Mukhopadhyay, A., 2009. Pulse-jet filtration: An effective way to control industrial pollution Part I: Theory, selection and design of pulse-jet filter. *Textile Progress,* 41(4), pp. 195-315.

Mukhopadhyay, A. & Choudhary, A. K., 2013. Performance of Filter Media as Function of Fibre Fineness in Pulse Jet Filtration System. *Textiles and Light Industrial Science and Technology,* 2(1), pp. 13-26.

Mycock, J., 1999. Pick the right baghouse material. *Power Engineering*, July, pp. 43-45.

Myllyvirta, L., 2014. *Health impacts and social costs of Eskom's proposed non-compliance with South Africa's air emission standards,* Exeter: Greenpeace International.

Neundorfer, 2016. *Baghouse Knowledge Base Lesson 4: Fabric Filter Material.* [Online] Available at: http://www.neundorfer.com/wp-content/uploads/2016/05/Baghouse-KnowledgeBase-04-Fabric-Filter-Material.pdf
[Accessed 20 October 2016].

Neundorfer, 2016. *Introduction to Baghouse / Fabric Filters.* [Online] Available at: http://www.neundorfer.com/knowledgebase-posts/fabric-filters/
[Accessed 25 August 2016].

Neundorfer, 2018. *How Boiler Performance Impacts ESP.* [Online] Available at: http://www.neundorfer.com/knowledgebase-posts/how-boiler-

performance-impacts-esp/
[Accessed 25 October 2018].

Nguyen, H., Morrison, A. L. & Nelson, P. F., 2008. *Analysis of Pollution Control Costs in Coal Based Electricity Generation,* Pullenvale: Cooperative Research Centre for Coal in Sustainable Development.

Nohara, L. B. et al., 2006. Study of crystallization behavior of poly(phenylene sulfide). *Polímeros,* 16(2), pp. 104-110.

Pakravan, H., Jamshidi, M., Latifi, M. & Pacheco-Torgal, F., 2012. Influence of Acrylic Fibers Geometry on the Mechanical Performance of Fiber-Cement Composites. *Journal of Applied Polymer Science,* 125(4), p. 3050–3057.

Park, C. H., Park, J. K., Jeon, H. S. & Chun, B. C., 2008. Triboelectric series and charging properties of plastics using the designed vertical-reciprocation charger. *Journal of Electrostatics,* 66(11-12), pp. 578-583.

Patel, E., 2016. *Fabric Filter Plant Bag Standard,* Sandton: Eskom.

Pelucchi, C. et al., 2009. Long-term particulate matter exposure and mortality: a review of European epidemiological studies. *BMC Public Health,* 9(453).

Pesendorfer, F., 2014. *Triboelectric Measurement,* Schorfling am Attersee: Evonik Fibres GmbH.

Pesendorfer, F., 2015. *Triboelectric Measurement,* Schoerfling am Attersee: Evonik Fibres GmbH.

Pesendorfer, F., 2016. *Results of the Triboelectric Measurement: Iron Oxide Fe2O3 Dust,* Schoerfling am Attersee: Evonik Industries.

Piperno, S. et al., 2012. Absorption vs. redox reduction of Pd2+ and Cu2+ on triboelectrically and naturally charged dielectric polymers. *Physical Chemistry Chemical Physics,* 14(16), pp. 5551-5557.

Popovici, F., 2010. Filtration with high-efficiency fibres in coal fired boiler applications. *VGB Powertech International Journal for Electricity and Heat Generation,* Issue 4, pp. 89-92.

Purchas, D. B. & Sutherland, K., 2002. *Handbook of Filter Media.* 2nd ed. Oxford: Elsevier .

Qiu, S., 2015. *Preparation and Characterization of Matrimid/P84 Blend Films.* Manhattan: Kansas State University.

Ramer, E. & Richards, H., 1968. Correlation of the Electrical Resistivities of Fabrics With Their Ability to Develop and to Hold Electrostatic Charges. *Textile Research Journal,* 38(1), pp. 28-35.

Rampiar, R., 2018. *Eskom SOx and NOx emissions* [Interview] (20 March 2018).

Rathwallner, G., 2008. Saving money in the baghouse. *World Cement*, April.

Rathwallner, G., 2009. *Filter media for coal fired boilers: suitable filter bag materials for different flue gas cleaning configurations.* Bangkok, PowerGen Asia.

Rathwallner, G., 2009. Troubleshooting frequent baghouse operating problems. *World Cement*, November.

Rathwallner, G., 2010. *Filter felts – a key component of bag houses.* New-Delhi, Filtrex Asia.

Ruhl, C. et al., 2012. Economic development and the demand for energy: A historical perspective on the next 20 years. *Energy Policy,* Volume 50, pp. 109-116.

Sakaguchi, M., Makino, M., Ohura, T. & Iwata, T., 2014. Contact electrification of polymers due to electron transfer among mechano anions, mechano cations and mechano radicals. *Journal of Electrostatics,* Volume 72, pp. 412-416.

Saleem, M., Khan, R. U., Tahir, M. S. & Krammer, G., 2011. Experimental study of cake formation on heat treated and membrane coated needle felts in a pilot scale pulse jet bag filter using optical in-situ cake height measurement. *Powder Technology,* Volume 214, pp. 388-399.

Saleem, M., Krammer, G. & Tahir, M. S., 2012. The effect of operating conditions on resistance parameters of filter media and limestone dust cake for uniformly loaded needle felts in a pilot scale test facility atambient conditions. *Powder Technology,* Volume 228, pp. 100-107.

Sasol, 2003. *PURAL/CATAPAL.* [Online]
Available at: http://www.sasoltechdata.com/tds/PURAL_CATAPAL.pdf
[Accessed 13 April 2018].

Sharma, R. et al., 2003. Effect of Ambient Relative Humidity and Surface Modification on the Charge Decay Properties of Polymer Powders in Powder Coating. *IEEE transactions on industry applications,* 39(1), pp. 87-95.

Shimadzu, 2012. *Application Data Book: Polymer and Electronic Material.* 2 ed. Kyoto: Shimadzu Corporation.

Sipes, J., 2011. *Basics of Air Filtration,* Suwanee: Price Industries.

Sloat, D. G., Gaikwad, R. P. & Chang, R. L., 1993. The Potential of Pulse-Jet Baghouses for Utility Boilers Part 3: Comparative Economics of Pulse-Jet Baghouse, Precipitators and Reverse-Gas Baghouses. *Air & Waste,* 43(1), pp. 120-128.

Śmigiel-Kamińska, D., 2014. Damaging effect of corrosive substances on textile products and fibres in the view of forensic analyses. *Forensic Practice,* 284(2).

Soong, Y., Schoffstall, M. R., Irdi, G. A. & Link, T. A., 1999. *Triboelectric separation of fly ash.* Kentucky, Center for Applied Energy Research, University of Kentucky.

Srivani, T., n.d. *Yarn numbering and sewing threads.* [Online]
Available at: https://www.scribd.com/doc/15571087/Yarn-Numbering-and-Sewing-Threads
[Accessed 26 April 2018].

Sterner, T. & Persson, U. M., 2008. An Even Sterner Review: Introducing Relative Prices into the Discounting Debate. *Review of Environmental Economics and Policy,* 2(1), pp. 61-76.

Tanthapanichakoon, W. et al., 2007. Degradation of bag-filter non-woven fabrics by nitric oxide at high temperatures. *Advanced Powder Technology,* 18(3), pp. 349-354.

Tanthapanichakoon, W. et al., 2006. Degradation of semi-crystalline PPS bag-filter materials by No and O2 at high temperature. *Polymer Degradation and Stability,* Issue 91, pp. 1637-1644.

Tanthapanichakoon, W. et al., 2006. Mechanical degradation of filter polymer materials: Polyphenylene sulfide. *Polymer Degradation and Stability,* Issue 91, pp. 2614-2621.

Thankur, R., Das, D. & Das, A., 2013. Electret air filters. *Separation & Purification Reviews,* Volume 42, pp. 87-129.

Themmel, W., 2006. It's in the baghouse. *World Cement*, October.

Topkin, J., 2000. *Bag Filter Research 2000 - New Technologies,* Johannesburg: Eskom Resources and Strategy Research Division.

Toray Industries, Inc, 2018. *Torcon: Polyphenylene Sulfide (PPS) Fiber.* [Online]
Available at: http://www.toray.com/products/fibers/fib_0080.html
[Accessed 20 March 2018].

Toyobo Co., Ltd., 2005. *Procon® Heat Chemical Resistant Fiber.* [Online]
Available at: http://www.toyobo-global.com/seihin/fb/procon/
[Accessed 19 December 2017].

Turner, J. H. et al., 2002. Baghouses and Filters. In: D. C. Mussatti, ed. *EPA Air Pollution Control Cost Manual.* Research Triangle Park: United States Environmental Protection Agency, pp. 564-622.

Turner, J. H., McKenna, J. D. & Vatavuk, W. M., 1998. Chapter 1: Baghouses and Filters. In: U. E. P. Agency, ed. *Particulate Matter Controls.* Durham: US Environmental Protection Agency, pp. 1-55.

Turner, J. H., McKenna, J. D. & Vatavuk, W. M., 1998. *Particulate Matter Controls,* Durham: U.S. Environmental Protection Agency.

Turner, J. H. et al., 1987. Sizing and Costing of fabric Filters Part II: Costing Considerations. *JAPCA,* 37(9), pp. 1105-1112.

United States Environmental Protection Agency, 2016. *Six Common Pollutants - Particulate Matter - Health.* [Online]
Available at: https://www3.epa.gov/pm/health.html
[Accessed 18 May 2016].

Vanherck, K., Koeckelberghs, G. & Vankelecom, I. F., 2013. Crosslinking polyimides for membrane applications: A review. *Progress in Polymer Science,* Volume 38, pp. 874-896.

Varga, K. et al., 2011. Thermal and sorption study of flame-resistant fibers. *Lenzinger Berichte,* Volume 89, pp. 50-59.

Weber, C., Altenhofen, U. & Zahn, H., 1988. Basic studies on the stability of filtration fabrics - Part I: The effects of sulphur dioxide and hitrogen oxides on polyacrylonitrile. *Textile Research Journal,* pp. 207-514.

Wedman, E. I. J. & Gore, W. L., 2010. *A Practical Guide to Filter Media Failure Analysis.* Rosemont, Powder & Bulk Solids Conference and Exhibition.

Weinrotter, K. & Seidl, S., 1993. High-Performance Polyimide Fibres. In: M. Lewin & J. Preston, eds. *Handbook of Fiber Science and Technology: Volume III.* New York: Marcel Dekker, Inc., pp. 179-204.

Williams, M. W., 2012. Triboelectric charging of insulating polymers - some new perspectives. *AIP Advances,* 2(1).

Williams, M. W., 2012. What creates static electricity?. *American Scientist,* Volume 100, pp. 316-323.

World Health Organization, 2013. *Health effects of particulate matter: Policy implications for countries in eastern Europe, Caucasus and central Asia,* Copenhagen: World Health Organization - Europe.

Wu, Z., 2001. *Air pollution control costs for coal-fired power stations,* London: IEA Clean Coal Centre.

Xing, J., Ni, Q.-Q., Deng, B. & Liu, Q., 2016. Morphology and properties of polyphenylene sulfide (PPS)/polyvinylidene fluoride (PVDF) polymer alloys by melt blending. *Composites Science and Technology,* Volume 134, pp. 184-190.

Xing, J., Xu, Z. & Deng, B., 2018. Enhanced Oxidation Resistance of Polyphenylene Sulfide Composites Based on Montmorillonite Modified by Benzimidazolium Salt. *Polymers,* 10(83).

Xue, T. J., McKinney, M. A. & Wilkie, C. A., 1996. The thermal degradation of polyacrylonitrile. *Polymer Degradation and Stability,* 58(1-2), pp. 193-202.

Yan, K., 2009. *Electrostatic Precipitation.* Hangzhou: Zhejiang University Press.

Yiğit, M., Seçkin, T., Köytepe, S. & Çetinkaya, E., 2007. Synthesis and Characterization of Polyimides Prepared from Optically Active (R,R) and (S,S)-1,3-bis(p-N,N´-dimethylaminobenzyl)-perhydrobenzimidazol-2-thion. *Turkish Journal of Chemistry,* 31(2), pp. 113-124.

Zevenhoven, R. & Kilpinen, P., 2001. Chapter 2: Flue gases and fuel gases. In: *Control of Pollutants in Flue Gases and Fuel Gases.* 1st ed. Espoo/Turku: Helsinki University of Technology.

Zhang, L., Xu, Z. & Chen, G., 2008. Decay of Electric Charge on Corona Charged Polyethylene. *Journal of Physics: Conference Series,* 142(1).

Zhang, Q., Li, S., Li, W. & Zhang, S., 2007. Synthesis and properties of novel organosoluble polyimides derived from 1,4-bis[4-(3,4-dicarboxylphenoxy)]triptycene dianhydride and various aromatic diamines. *Polymer,* 48(21), pp. 6246-6253.

Zhu, S., Xu, Y., Huang, C. & Jin, X., 2018. Triboelectric Effect of Polytetrafluoroethylene Fibers to Improve the Filtration Performance of Air-Purified Materials. *Journal of Engineered Fibers and Fabrics,* 13(1), pp. 60-71.

APPENDIX A: TRIBOELECTRIC BEHAVIOUR OF FILTRATION FABRICS

A.1 REPEATABILITY OF CHARGE BEHAVIOUR

Where average data were reported in Chapter 3, results of all triboelectric tests are included in this appendix.

As an introduction to the results reported in subsequent sections of this Appendix, averaged data are reported in Table A-1, representing four samples per set. Of particular importance in this table are the standard deviation and the change thereof between measurement intervals. The significant standard deviation reported is in keeping with the irreproducibility of triboelectric tests reported in literature (Charlson, et al., 1992; Diaz & Felix-Navarro, 2004; Hutton, 2007), theorised to be due to the impact of the environment on discharge behaviour (Ramer & Richards, 1968; Frederick, 1974; Mishra, 1982).

The rows labelled ‘change in standard deviation during discharge’ report the percentage change in standard deviation from the standard deviation of the initial rubbed charge measurement. This behaviour highlights that although the standard deviation itself is substantial (with the exception of the initial charge prior to triboelectric contact which is, in itself, insignificant), the standard deviation shows very low variation between measurements. This implies that while the charge magnitude varies between samples, the charge dissipation characteristics are constant. The average curves shown in Figure 3-10 can therefore be considered to be representative of the discharge characteristics of the fabrics.

Note that the initial fabric charge is not zero, despite discharging prior to testing, due to charges imparted on the fabric samples during handling in the experimental setup.

It can be further noted that the variation in standard deviation typically increases with charge dissipation time, although deviation remains below 1%. It is hypothesised that this increase in variation is indicative of the impact of environmental factors on charge decay: where more time is allowed for charge decay the discharge characteristics of individual specimens show greater variation due to changes in localised atmospheric conditions.

Results of the triboelectric characterisation tests repeated for four samples per fabric type are subsequently reported and discussed.

Table A-1: Average discharge characteristics of selected filtration fabrics

Material			Initial charge	Rubbed charge	30 sec discharge	60 sec discharge	90 sec discharge	120 sec discharge	150 sec discharge	180 sec discharge
PAN/PAN	clean gas surface	Average (kV)	-0.07	-12.78	-11.00	-9.85	-9.15	-8.53	-8.15	-7.78
		Standard deviation (kV)	0.06	1.26	1.13	1.04	0.96	0.85	0.87	0.85
		Change in standard deviation during discharge (%)			-0.10	-0.17	-0.24	-0.33	-0.31	-0.33
PAN/PAN	filtration surface	Average (kV)	-0.22	-11.88	-10.53	-9.73	-9.23	-8.83	-8.48	-8.20
		Standard deviation (kV)	0.10	4.69	4.97	4.68	4.32	4.01	3.81	3.57
		Change in standard deviation during discharge (%)			0.06	0.00	-0.08	-0.14	-0.19	-0.24
PPS/PPS	clean gas surface	Average (kV)	-0.30	-13.70	-8.78	-7.50	-5.75	-5.28	-4.95	-4.73
		Standard deviation (kV)	0.08	5.29	4.27	3.52	1.87	1.63	1.47	1.37
		Change in standard deviation during discharge (%)			-0.19	-0.33	-0.65	-0.69	-0.72	-0.74
PPS/PPS	filtration surface	Average (kV)	-0.38	-12.80	-11.00	-9.90	-9.20	-8.50	-8.20	-7.80
		Standard deviation (kV)	0.24	1.30	1.10	1.00	1.00	0.80	0.90	0.80
		Change in standard deviation during discharge (%)			-0.15	-0.23	-0.23	-0.38	-0.31	-0.38
PI/PI	clean gas surface	Average (kV)	-0.15	19.60	17.40	15.90	14.68	13.95	13.33	12.78
		Standard deviation (kV)	0.07	3.08	3.18	3.00	2.85	2.78	2.62	2.54
		Change in standard deviation during discharge (%)			0.03	-0.03	-0.08	-0.10	-0.15	-0.18
PI/PI	filtration surface	Average (kV)	-0.03	14.82	13.40	12.62	12.06	11.68	11.34	11.04
		Standard deviation (kV)	0.14	3.39	2.50	2.47	2.42	2.47	2.49	2.53
		Change in standard deviation during discharge (%)			-0.26	-0.27	-0.28	-0.27	-0.27	-0.25
PAN/PI	clean gas surface	Average (kV)	-0.11	-7.57	-7.03	-6.53	-6.17	-5.83	-5.63	-5.40
		Standard deviation (kV)	0.08	2.18	1.87	1.60	1.43	1.30	1.17	1.12

Material		Initial charge	Rubbed charge	30 sec discharge	60 sec discharge	90 sec discharge	120 sec discharge	150 sec discharge	180 sec discharge
	Change in standard deviation during discharge (%)			-0.14	-0.27	-0.34	-0.40	-0.46	-0.48
PAN/PI filtration surface	Average (kV)	0.10	9.93	9.38	8.93	8.58	8.35	8.08	7.88
	Standard deviation (kV)	0.23	2.02	1.84	1.69	1.50	1.44	1.36	1.29
	Change in standard deviation during discharge (%)			-0.08	-0.16	-0.26	-0.29	-0.32	-0.36
PPS/PI clean gas surface	Average (kV)	-0.17	-13.98	-9.63	-8.20	-7.53	-7.05	-6.18	-5.98
	Standard deviation (kV)	0.09	1.90	2.26	2.25	2.12	2.00	1.42	1.36
	Change in standard deviation during discharge (%)			0.19	0.18	0.11	0.05	-0.25	-0.28
PPS/PI filtration surface	Average (kV)	0.04	11.50	6.98	6.03	5.55	5.18	4.90	4.68
	Standard deviation (kV)	0.05	0.50	1.09	0.83	0.68	0.59	0.55	0.55
	Change in standard deviation during discharge (%)			1.18	0.67	0.36	0.19	0.10	0.11

A.2 DISCHARGE BEHAVIOUR OF PAN/PAN

Figure A-1 describes results of multiple PAN/PAN discharge characteristics tests. Clean gas surface tests were conducted at an average temperature of 20 ± 0.29°C relative humidity of 34 ± 1.5% and filtration surface tests at 20 ± 0.16°C and 33 ± 0.38%.

For *clean gas surface test 1* and *filtration surface test 2*, many loose fibres were observed on the rubbed material surface. It is surmised that the initial rapid discharge was due to fibre contact aiding rapid discharge since temperature and humidity did not change significantly.

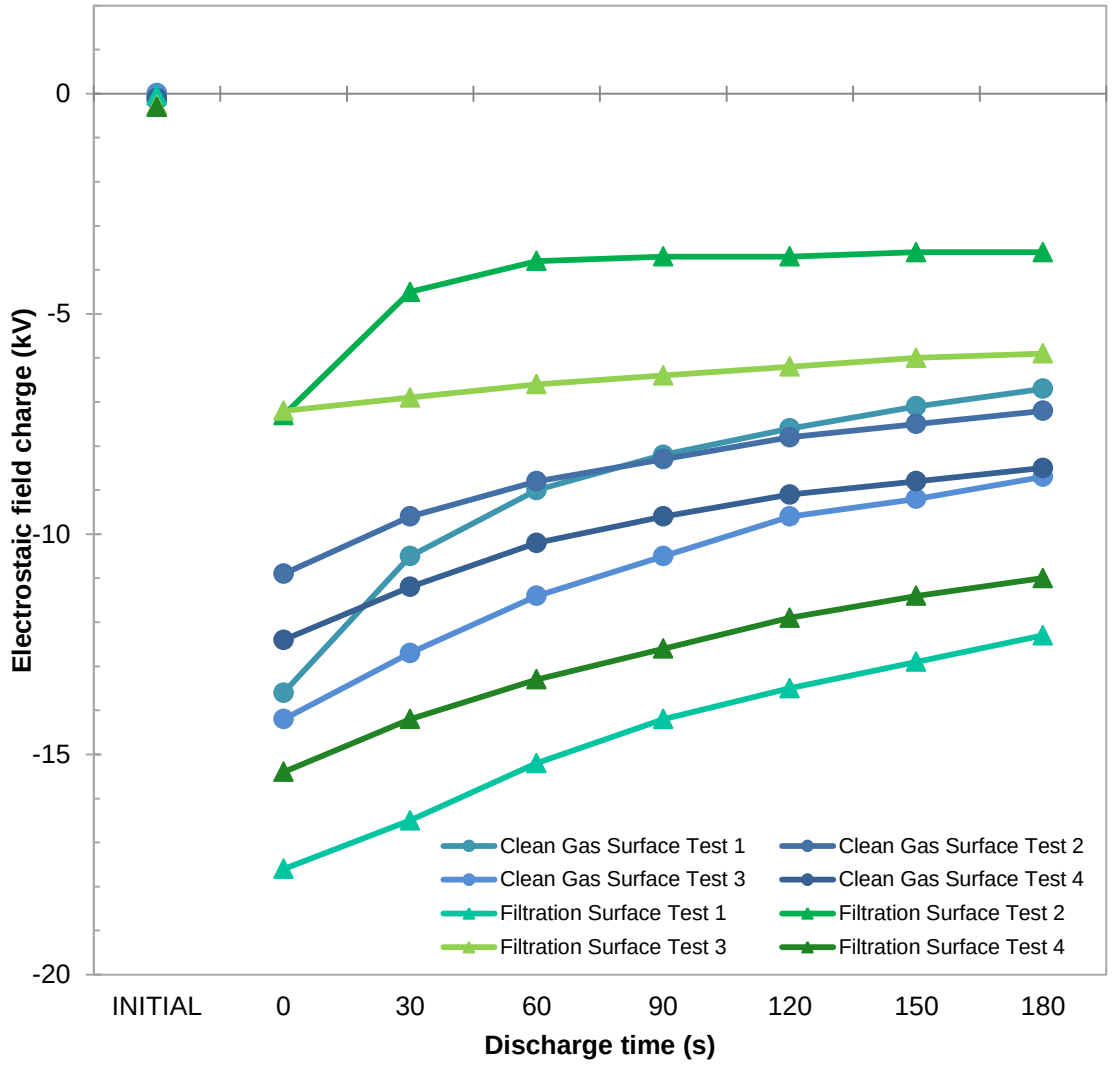

Figure A-1: Discharge characteristics of PAN/PAN when triboelectrically charged with PET

A.3 DISCHARGE BEHAVIOUR OF PPS/PPS

Figure A-2 illustrates the discharge behaviour of PPS/PPS. Clean gas surface tests were conducted at an ambient temperature of 20 ± 0.22°C and relative humidity of 44 ± 0.64%. Filtration surface tests were conducted at 20 ± 0.07°C and 33 ± 0.30%, with the exception of *filtration surface: higher humidity*, which was conducted at 20°C and 44% relative humidity.

It was noticed that throughout a test day charge magnitude tended to increase. It is therefore possible that charge was accumulating on the apparatus and that the reason for the lower charge magnitude of *filtration surface: higher humidity* is that it was completed earlier in a test day.

Since the electrostatic field meter could only measure between the range of ±22 kV, the charged values for *filtration surface tests 1, 3* and *4* have been extrapolated using the least squares best fit method.

As with the PAN/PAN results, long fibres were observed to loosen from the sample surface. During *clean gas surface 4* such a fibre was attracted to the field meter and caused rapid discharge at the 60 second discharge interval.

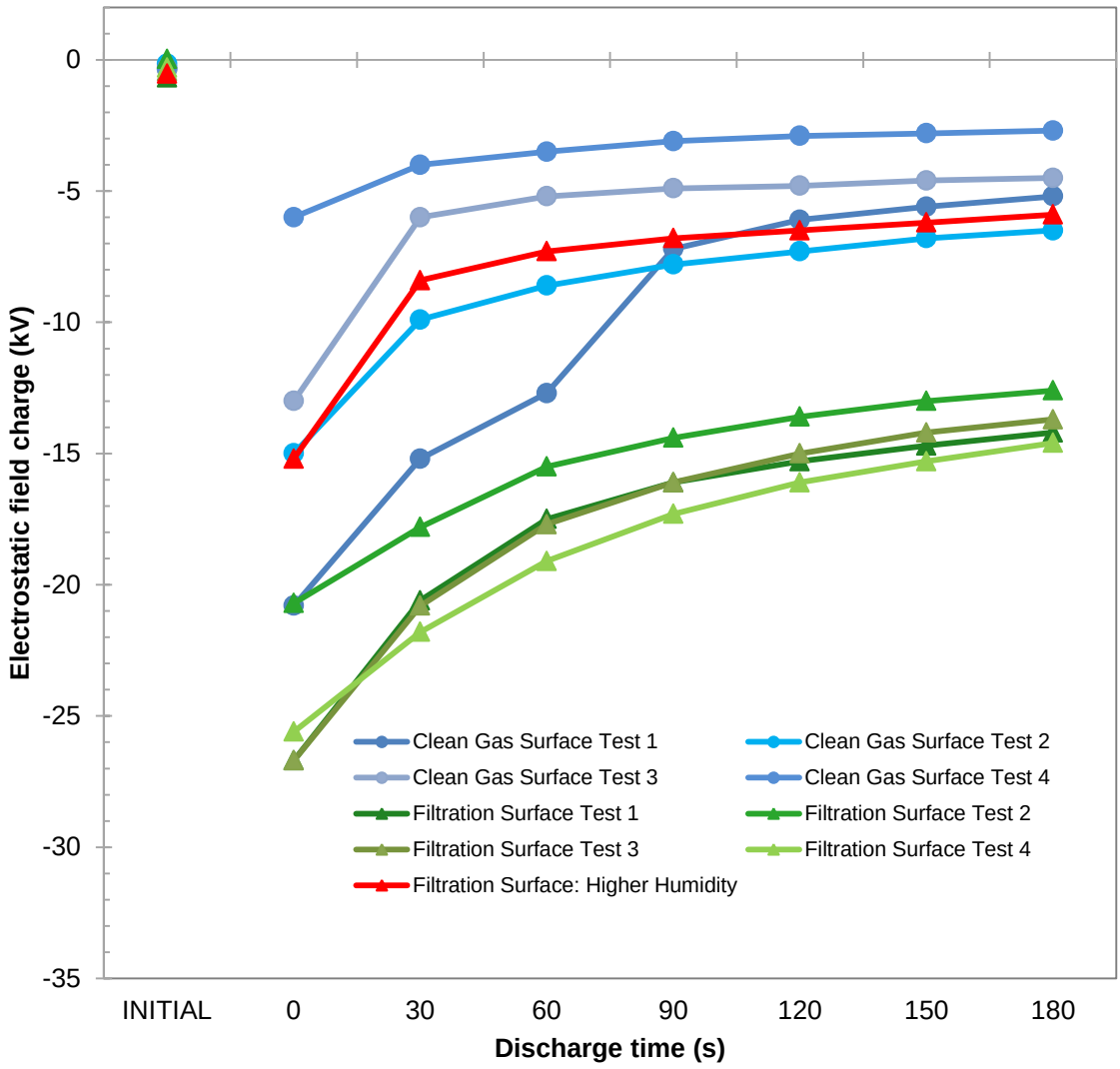

Figure A-2: Discharge characteristics of PPS/PPS when charged with a PET reference wheel

A.4 DISCHARGE BEHAVIOUR OF PI/PI

Figure A-4 describes the discharge behaviour of PI/PI. Clean gas surface tests were conducted at 21 ± 0.05°C and 34 ± 0.61% relative humidity, while filtration surface tests were conducted at 21 ± 0.12°C and 35 ± 4.6% relative humidity.

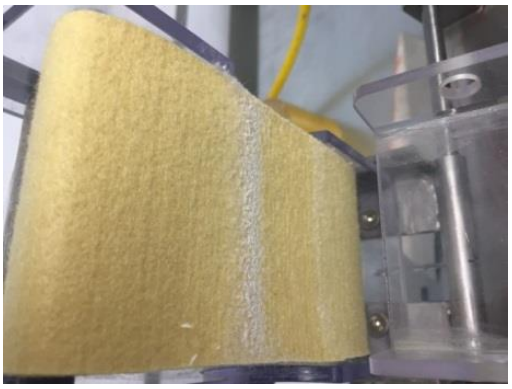

Figure A-3: PAN residue on PI/PI sample

A white substance was observed on the surface of the PI/PI samples, as can be seen in Figure A-3. Chemical analysis of the substance revealed it to be PAN. It is theorised that the previous PAN/PAN samples tested on the same PET wheel deposited this powdery substance on the surface of the reference wheel. For purposes of discharge characteristics, however, it is not supposed that this had a marked impact as PAN is known to be highly negative and highly positive PI/PI results were observed.

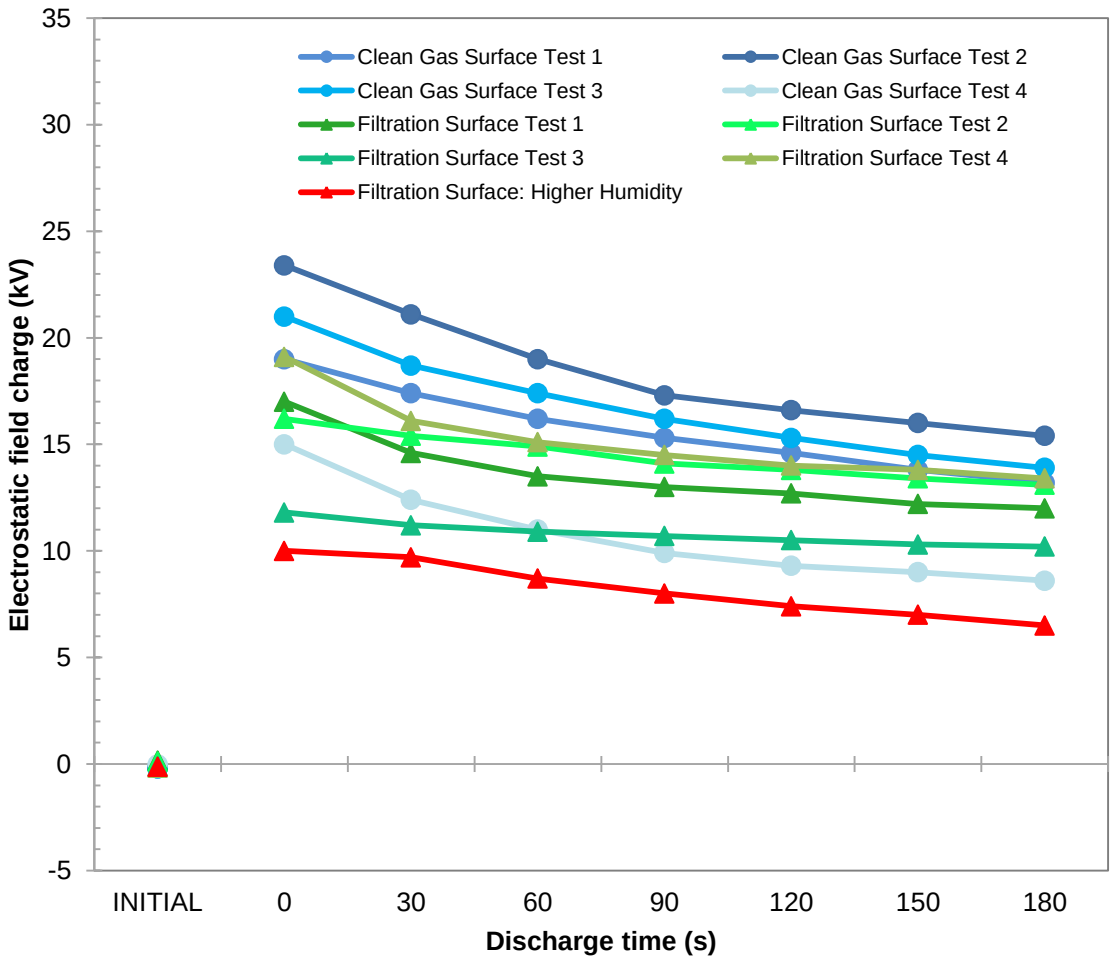

Figure A-4: Discharge characteristics of PI/PI when charged with a PET reference wheel

A.5 DISCHARGE BEHAVIOUR OF PAN/PI

The discharge behaviour of PAN/PI is illustrated by Figure A-5. Clean gas surface tests were conducted at an ambient temperature of 21 ± 0.05°C and 32 ± 0.24% relative humidity. Note that unlike other tests where four repeats were considered, only three clean gas surface repeats were conducted. Filtration surface tests were conducted at 21 ± 0.08°C and 32 ± 0.11% relative humidity.

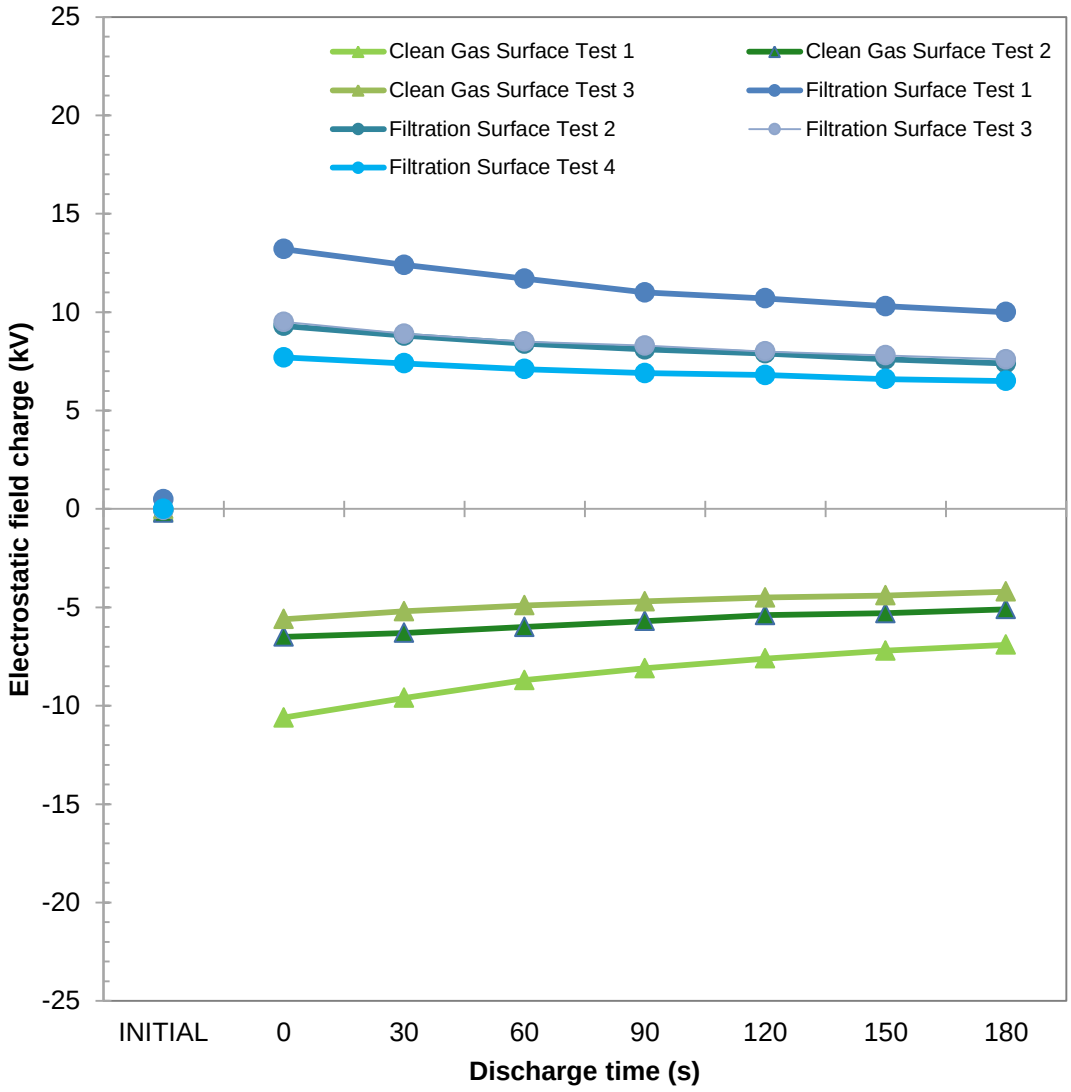

Figure A-5: Discharge characteristics of PAN/PI when charged with a PET reference wheel

A.6 DISCHARGE BEHAVIOUR OF PPS/PI

Figure A-6 describes the discharge behaviour of PPS/PI. Clean gas surface tests were conducted at 20 ± 0.31°C and relative humidity of 43 ± 0.84%, while filtration surface tests were conducted at 20 ± 0.10°C and 43 ± 0.23% relative humidity.

As with previous tests, loose fibres were observed after triboelectric contact. It is surmised that during *clean gas surface test 2* such a fibre touched the test frame at 150 sec discharge, resulting in a sudden charge decrease that does not fit with the trend observed for other tests.

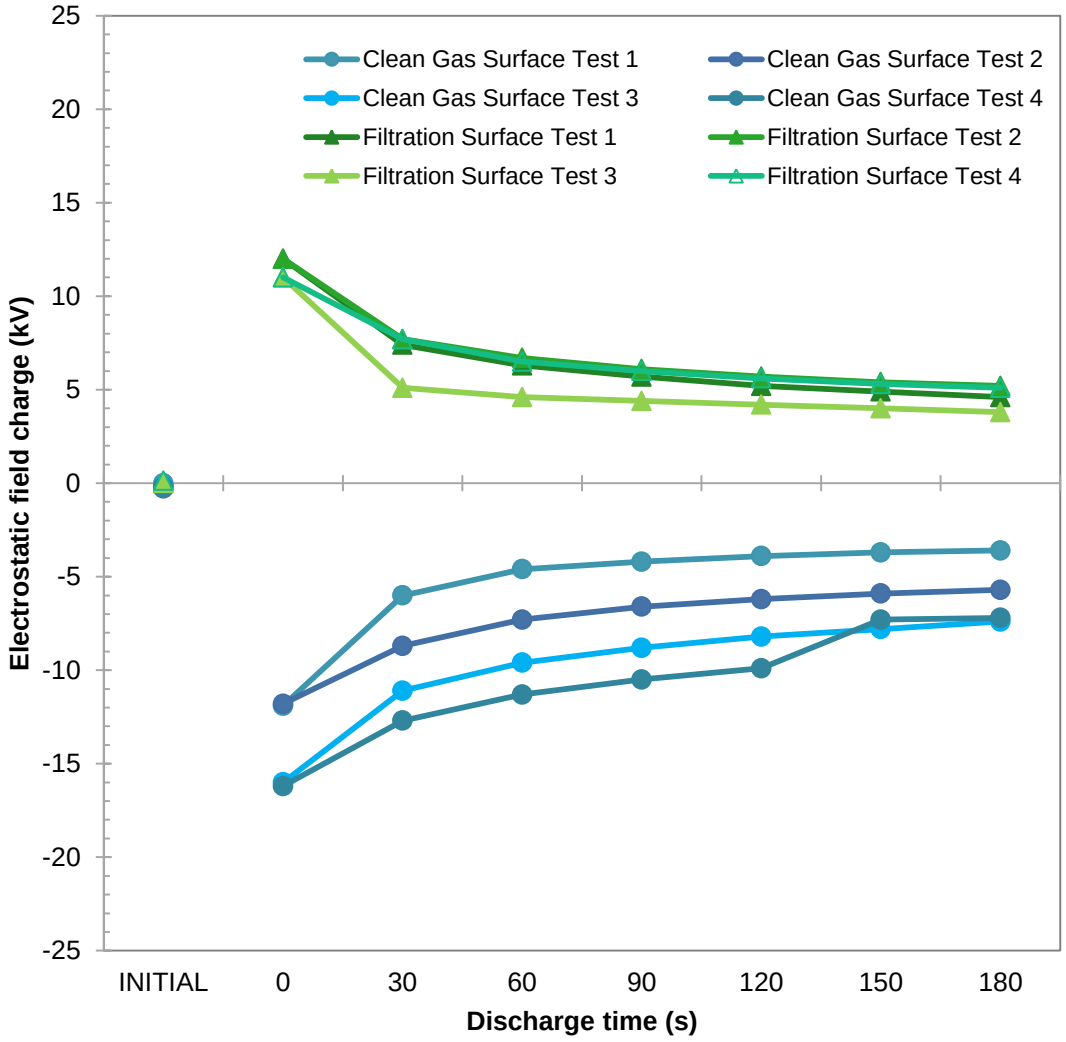

Figure A-6: Discharge characteristics of PPS/PI when charged with a PET reference wheel

A.7 DISCHARGE CHARACTERISTIC MODELS

Table A-2 describes the discharge characteristic models which consider the incremental charge dissipation of the filtration fabrics.

Table A-2: Discharge characteristic models of selected filtration fabrics

Material	Discharge characteristics – Best data fit	Curve type	R^2	Discharge characteristics - Exponential decay	R^2
PAN/PAN clean gas surface	$-0.00331439x^4 + 0.075947\,x^3 - 0.692708\,x^2 + 3.37089\,x - 15.525$	quartic	0.999798	$-13.2981e^{-0.0850944x}$	0.998619
PAN/PAN filtration surface	$-0.00420455x^4 + 0.0875505\,x^3 - 0.699583\,x^2 + 2.90152\,x - 14.1657$	quartic	0.999996	$-12.1313e^{-0.0616427x}$	0.999123
PPS/PPS clean gas surface	$-0.0245265x^4 + 0.473674\,x^3 - 3.46146\,x^2 + 11.9796\,x - 22.5964$	quartic	0.992738	$-15.3139e^{-0.21149x}$	0.985303
PPS/PPS filtration surface	$2.58706\log x - 12.7793$	logarithmic	0.999968	$-13.3165e^{-0.0847599x}$	0.998619
PI/PI clean gas surface	$-0.022222\,x^3 + 0.428869\,x^2 - 3.30069\,x + 22.4893$	cubic	0.999817	$20.3752e^{-0.0731258x}$	0.999194
PI/PI filtration surface	$0.00401515x^4 - 0.0859091\,x^3 + 0.704167\,x^2 - 2.91762\,x + 17.1657$	quartic	0.999881	$14.9947e^{-0.0482253x}$	0.99937
PAN/PI clean gas surface	$1.13662\log(0.00114884x)$	logarithmic	0.99982	$-7.88776e^{-0.05748x}$	0.999786
PAN/PI filtration surface	$-1.06272\log(0.0000801739)$	logarithmic	0.999939	$10.1543e^{-0.0385745x}$	0.999867
PPS/PI clean gas surface	$-0.036553x^4 + 0.679293\,x^3 - 4.57708x^2 + 13.8517\,x - 23.8893$	quartic	0.999728	$-14.6025e^{-0.151696x}$	0.98938
PPS/PI filtration surface	$0.0375x^4 - 0.708333\,x^3 + 4.83958x^2 - 14.4682\,x + 21.7643$	quartic	0.99718	$11.6701e^{-0.165247x}$	0.977193

APPENDIX B: EFFECTS OF ACID ATTACK ON FILTRATION FABRICS

Supporting data relating to the discussion in Chapter 4 are presented below.

B.1 EFFECT OF ACID ATTACK ON LOW TEMPERATURE FABRICS

Figure B-1: Degraded PAN/PAN tensile samples after 0.8 M nitric acid exposure at 125°C for 8 hours (left) and 24 hours (right)

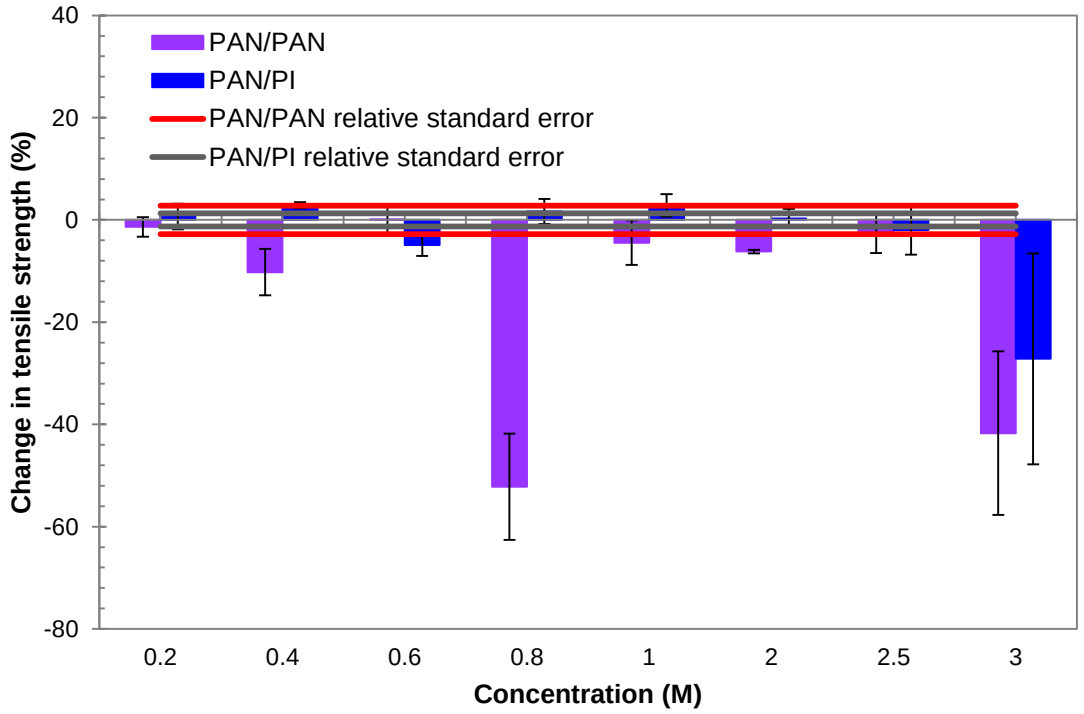

Figure B-2: Effect of nitric acid on PAN/PAN and PAN/PI tensile strength after 4 hours at 125°C

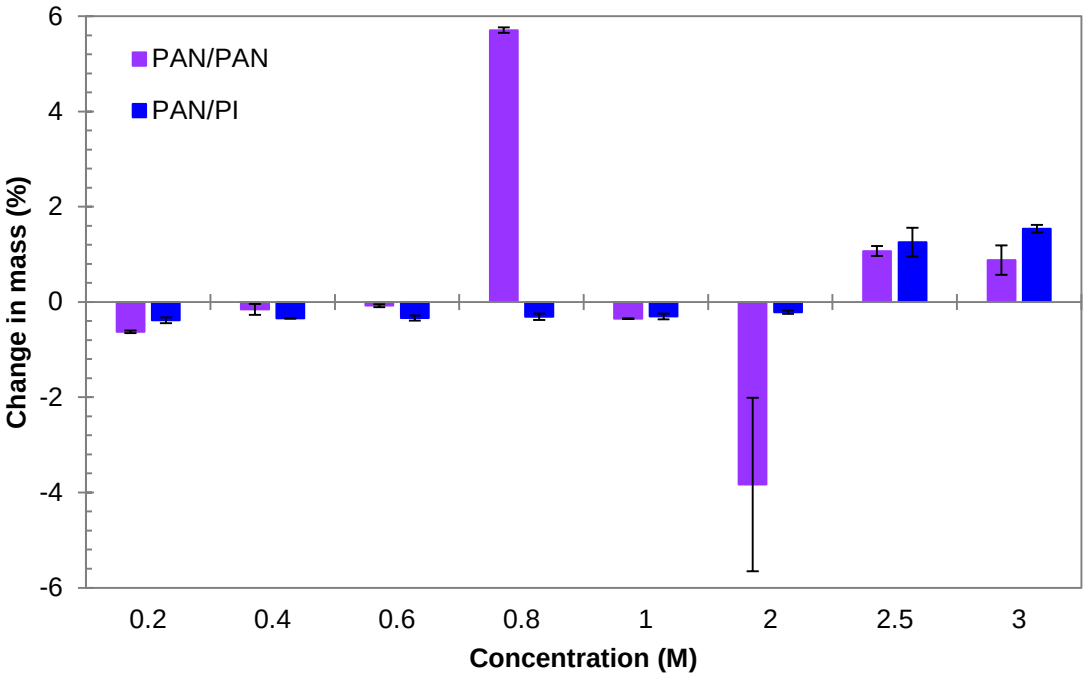

Figure B-3: Effect of nitric acid exposure for 4 hours at 125°C on PAN/PAN and PAN/PI mass

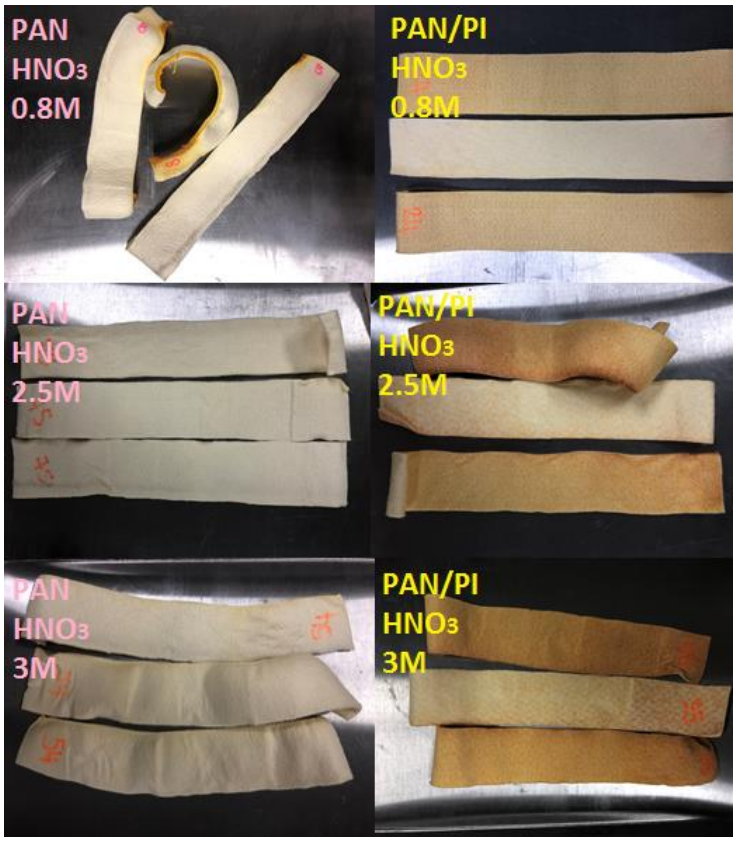

Figure B-4: Photographs of PAN/PAN (left) and PAN/PI (right) after exposure to nitric acid for 4 hours at 125°C

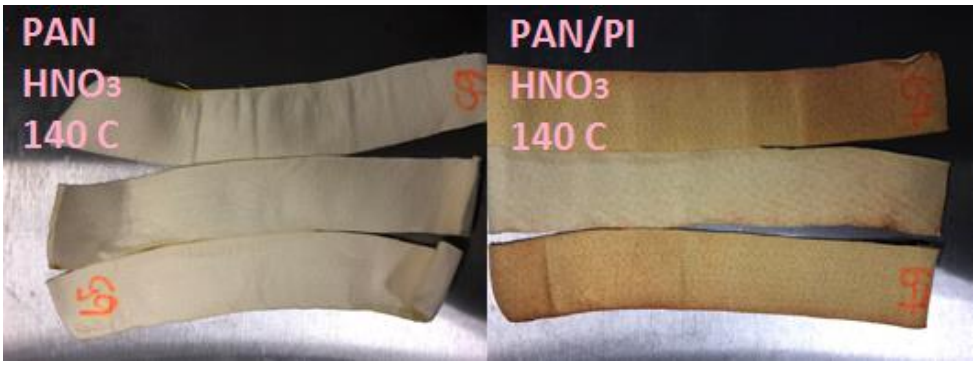

Figure B-5: Photographs of PAN/PAN (left) and PAN/PI (right) after exposure to 2 M nitric acid for 4 hours at 140°C

Figure B-6: Degraded PAN/PAN tensile samples after sulphuric acid exposure at 125°C for 12 hours (left) and 24 hours (right)

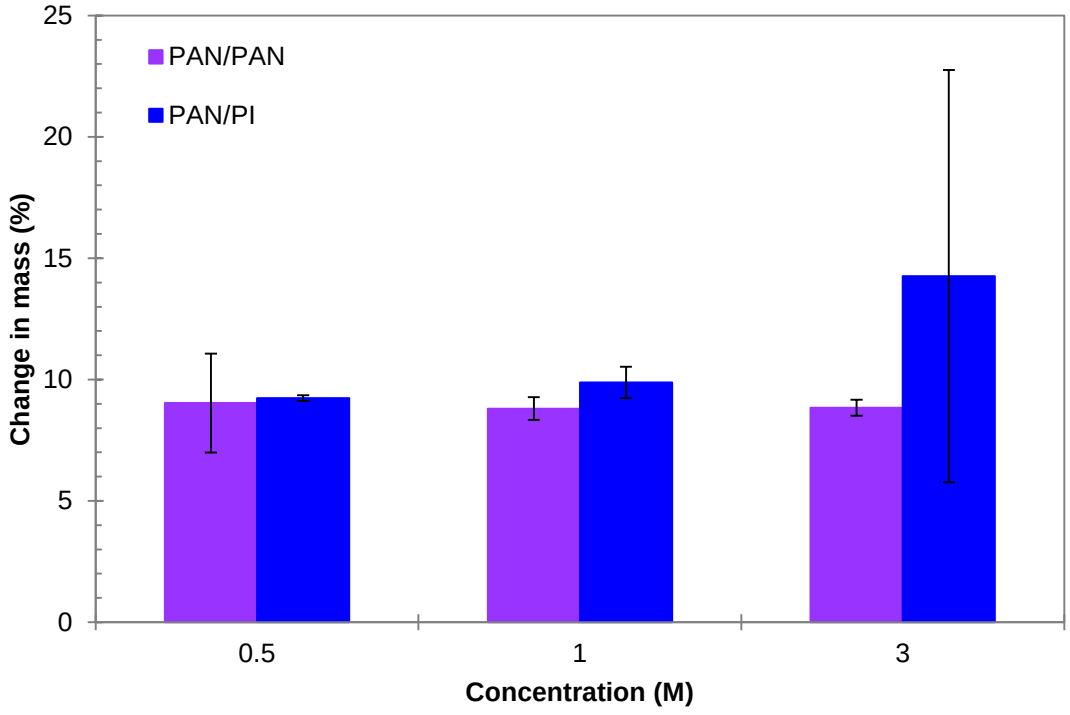

Figure B-7: Effect of sulphuric acid exposure for 8 hours at 125°C on PAN/PAN and PAN/PI mass

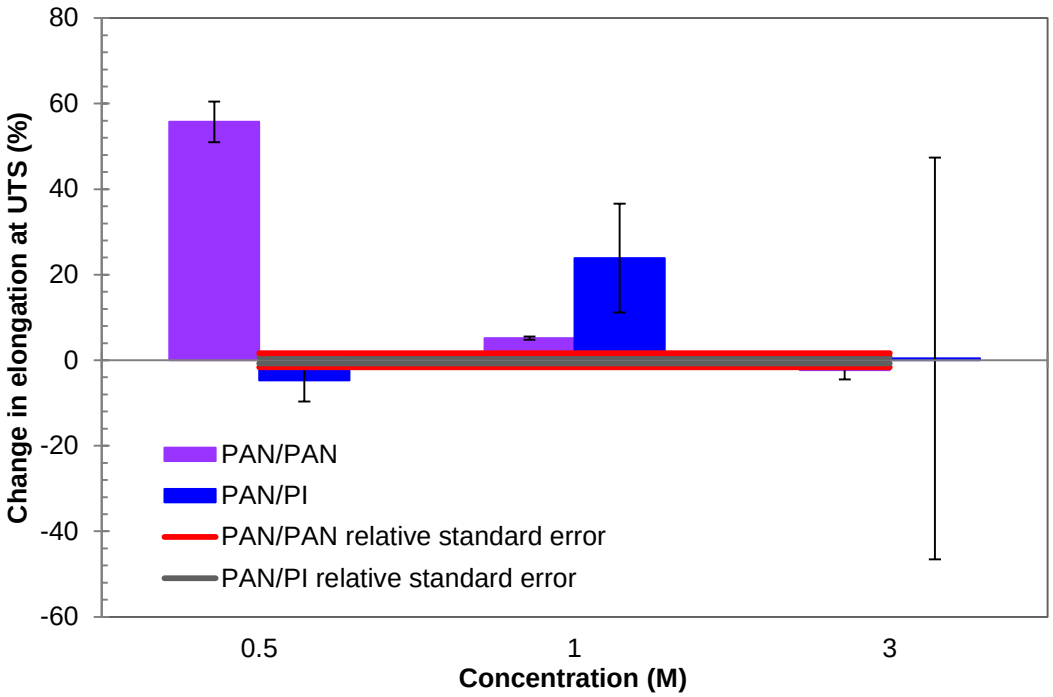

Figure B-8: Effect of sulphuric acid exposure for 8 hours at 125°C on PAN/PAN and PAN/PI elongation at ultimate tensile strength

Figure B-9: PAN/PAN after 0.5 M sulphuric acid exposure for 8 hours at 125°C

Figure B-10: PAN/PI after 0.5 M, 1 M and 3 M sulphuric acid exposure for 8 hours at 125°C

Figure B-11: Photographs of PAN/PAN (left) and PAN/PI (right) after exposure to 1 M sulphuric acid for 8 hours at 140°C

B.2 EFFECT OF ACID ATTACK ON HIGH TEMPERATURE FABRICS

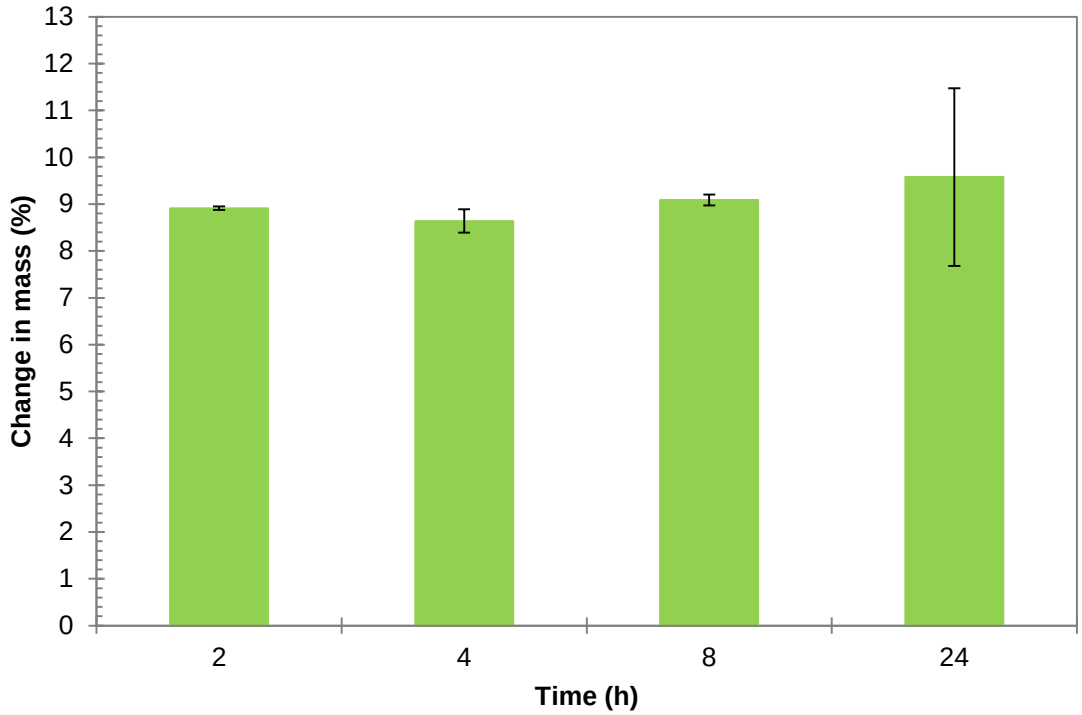

Figure B-12: Effect of 0.8 M nitric acid exposure at 150°C on PPS/PPS mass

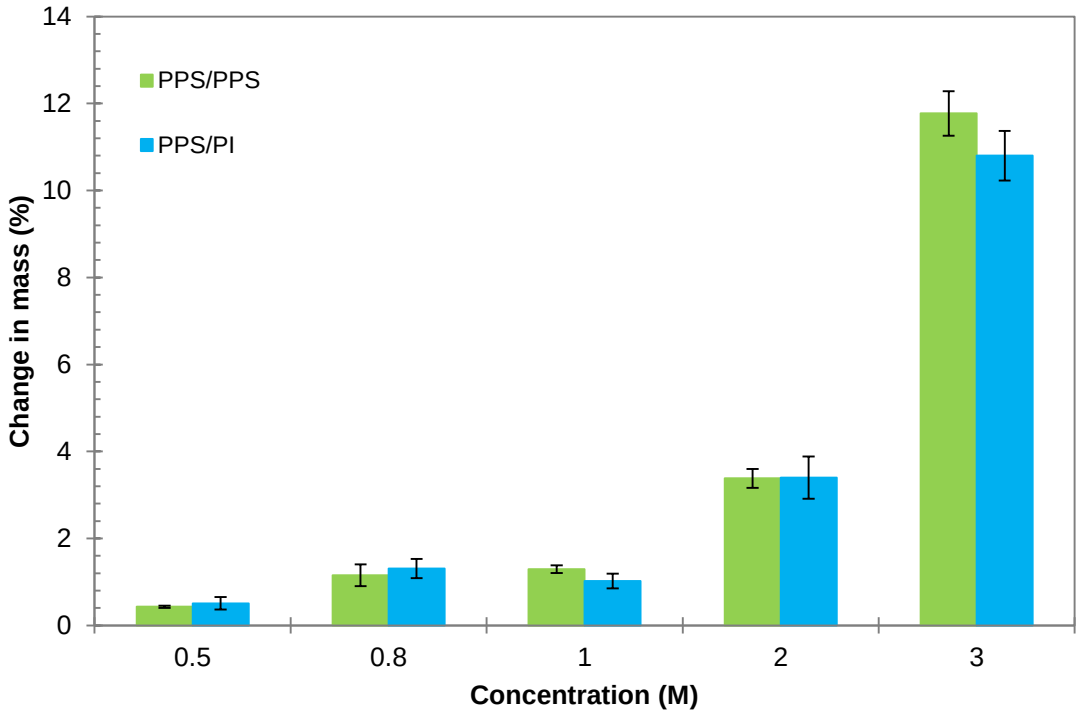

Figure B-13: Effect of nitric acid exposure for 4 hours at 150°C on PPS/PPS and PPS/PI mass

Figure B-14: High temperature fabric after 1 M nitric acid exposure for 4 hours at various temperatures

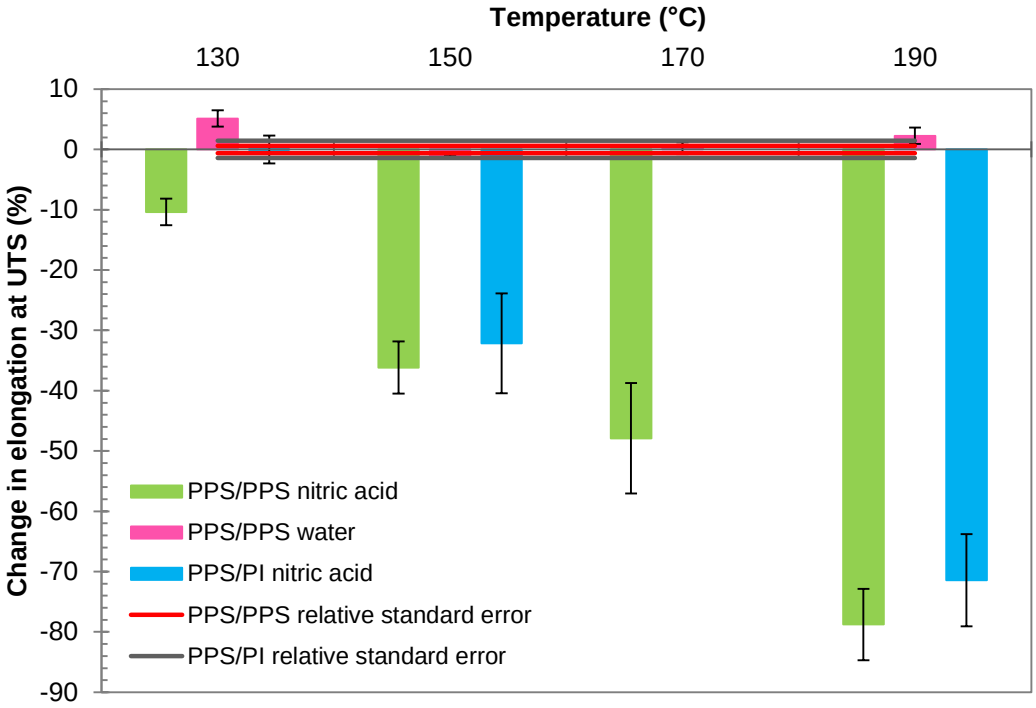

Figure B-15: Effect of 1 M nitric acid exposure on PPS/PPS and PPS/PI elongation at ultimate tensile strength at various temperatures compared to PPS/PPS control samples in water

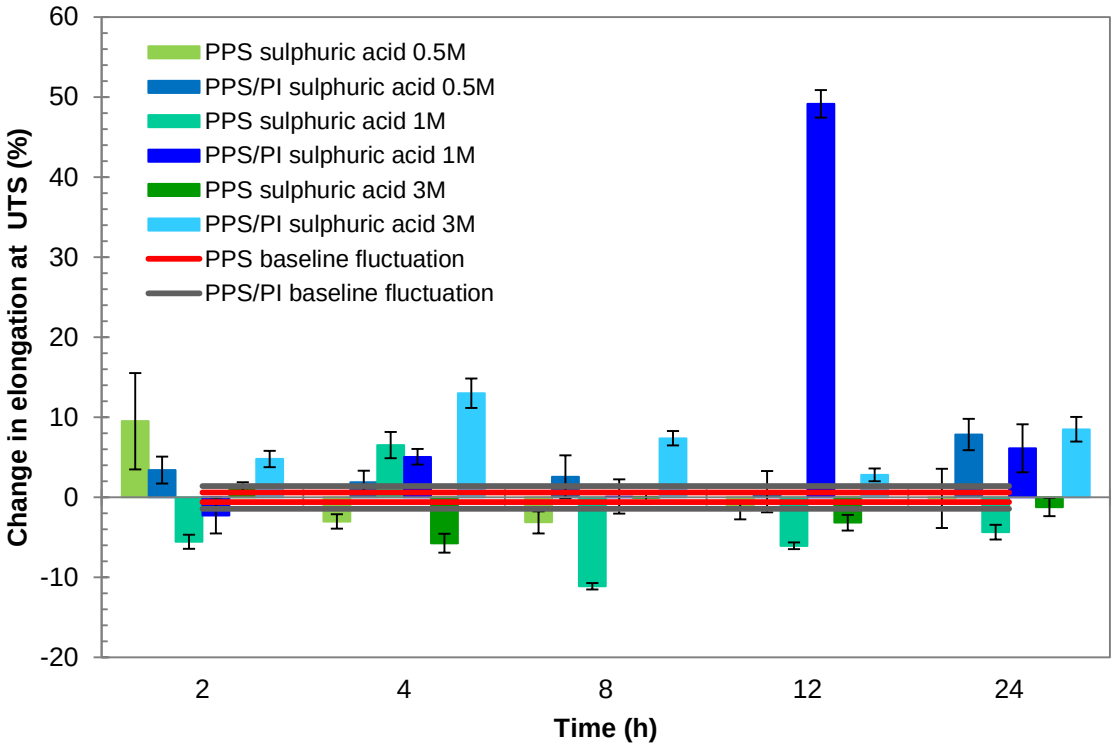

Figure B-16: Effect of sulphuric acid exposure of various concentrations at 150°C on PPS/PPS and PPS/PI ultimate tensile strength over time

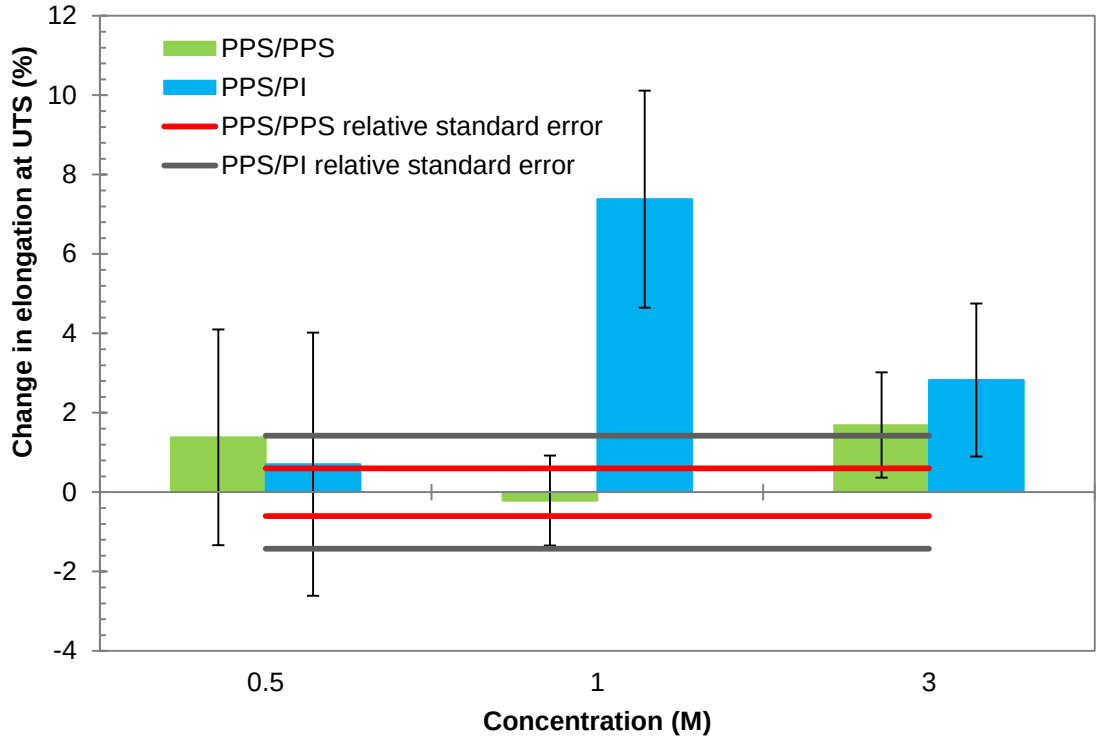

Figure B-17: Effect of sulphuric acid exposure for 12 hours at 150°C on PPS/PPS and PPS/PI elongation at ultimate tensile strength at various concentrations

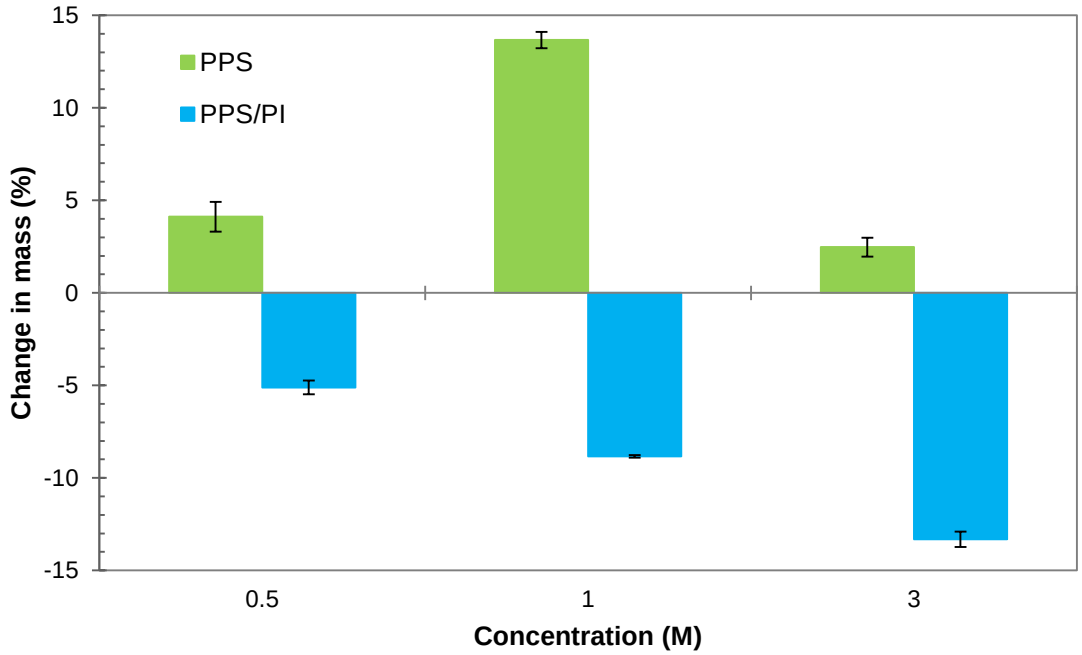

Figure B-18: Effect of sulphuric acid exposure for 12 hours at 150°C on PPS/PPS and PPS/PI mass

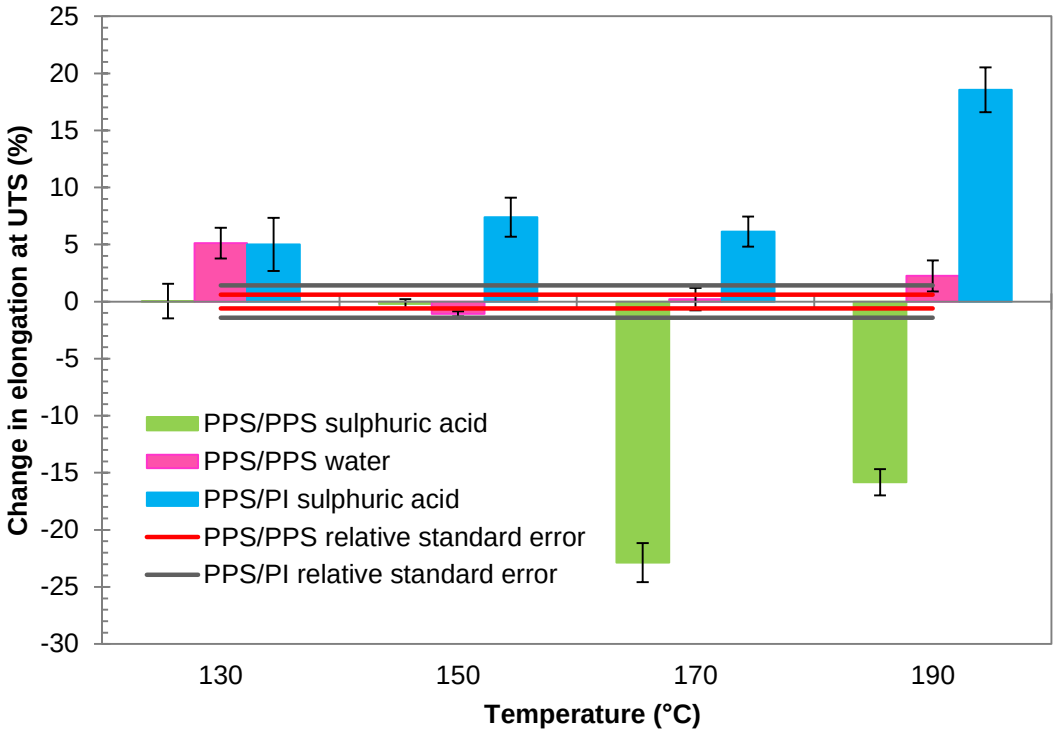

Figure B-19: Effect of 1 M sulphuric acid exposure for 12 hours on PPS/PPS and PPS/PI elongation at ultimate tensile strength compared to PPS/PPS control samples in water

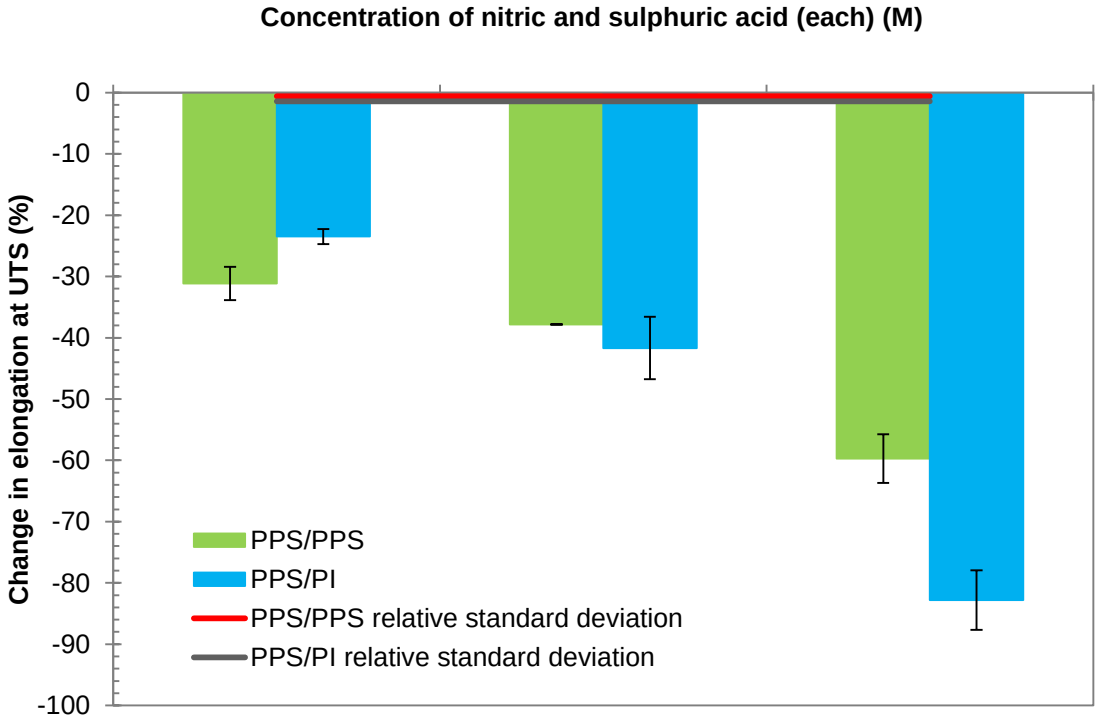

Figure B-20: Effect of combined nitric and sulphuric acid exposure for 4 hours at 150°C on PPS/PPS and PPS/PI elongation at ultimate tensile strength

APPENDIX C: INPUTS TO CBA

The inputs used for the application of the proposed CBA to low and high temperature fabrics in Chapter 5 are defined in Table C-1. They reflect a typical large, modern pulse jet baghouse at a South Africa coal-fired power station.

Table C-1: Inputs to CBA

Parameter	Unit	Value
n	years	4
n_e	years	3.5
L_R	MW	50
L_T	MW	600
P	R/MWh	770
D_{BR}	days	14
Number of bags in baghouse	-	20 160
PAN/PAN bag price	R	405.81
PAN/PI bag price	R	542.48
PPS/PPS bag price	R	787.99
PPS/PI bag price	R	853.32
Real discount rate	%	7.3
South African annual escalation	%	5.4
European annual escalation	%	1.3
United States annual escalation	%	2.9
€/ZAR exchange rate June 2016	-	16.71
€/ZAR exchange rate September 2018	-	17.69
USD/ZAR exchange rate September 2018	-	15.04